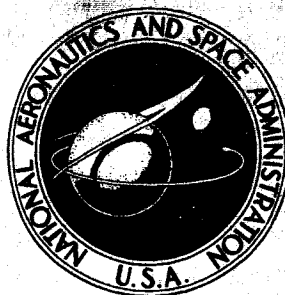


**NASA CONTRACTOR
REPORT**



NASA CR-968

NASA CR-968

GPO PRICE \$ _____

CFSTI PRICE(S) \$ _____

Hard copy (HC) _____

Microfiche (MF) _____

ff 653 July 65

**A STUDY OF THE CRITICAL
COMPUTATIONAL PROBLEMS
ASSOCIATED WITH STRAPDOWN
INERTIAL NAVIGATION SYSTEMS**

Prepared by
UNITED AIRCRAFT CORPORATION
Farmington, Conn.
for Electronics Research Center

FACILITY FORM 602

868-21652

(ACCESSION NUMBER)

(THRU)

(PAGES)

(CODE)

(NASA CR OR TMX OR AD NUMBER)

(CATEGORY)

A STUDY OF THE CRITICAL COMPUTATIONAL PROBLEMS
ASSOCIATED WITH STRAPDOWN INERTIAL
NAVIGATION SYSTEMS

Distribution of this report is provided in the interest of information exchange. Responsibility for the contents resides in the author or organization that prepared it.

Issued by Originator as Report No. SCR 328-I

Prepared under Contract No. NAS 12-91 by
UNITED AIRCRAFT CORPORATION
Farmington, Conn.

for Electronics Research Center

NATIONAL AERONAUTICS AND SPACE ADMINISTRATION

For sale by the Clearinghouse for Federal Scientific and Technical Information
Springfield, Virginia 22151 - CFSTI price \$3.00

FOREWORD

This final report was prepared by United Aircraft Corporate Systems Center for NASA Electronics Research Center as fulfillment of Contract No. NAS 12-91. The work described in this report was initiated by United Aircraft Corporate Systems Center under a company funded research program and extended and documented herein for NASA Electronics Research Center under the above-referenced contract. The principle goals of the contract are: (1) to develop analytical models of the computational errors associated with the computational process of strapdown inertial navigators and (2) by using these models, to establish the computational requirements of strapdown navigators for the various phases of flight of typical missions. This report is divided into two volumes. The first volume describes the analytical models of the computational errors of strapdown navigators and reports upon specific hardware application studies and computational requirements. The second volume* describes in detail the digital computer program developed under this program that permits rapid evaluation of strapdown associated computational errors for restrained sensor systems.

* CR-86022

TABLE OF CONTENTS

<u>Section</u>	<u>Page</u>
I. SUMMARY	I-1
II. INTRODUCTION	II-1
A. Commonality of Sensor Mechanizations	II-3
B. Study Objectives and Report Organization	II-6
III. FUNCTIONAL EVALUATION OF COMPUTATIONAL REQUIREMENTS	III-1
A. Position Computations	III-1
B. Accelerometer Data Coordinate Transformation	III-3
1. Restrained Accelerometer System	III-3
2. Free Accelerometer System	III-5
C. Attitude Computations	III-8
1. Free Gyro System	III-8
2. Restrained Gyro System	III-9
D. Summary of Parameters Affecting Computational Accuracy	III-12
IV. COMPUTATIONAL ERROR ANALYSIS	IV-1
A. Restrained Gyro Attitude Reference System	IV-1
1. Discrete Motions	IV-7
2. Vibratory Motions	IV-24
3. Sensor Associated Errors	IV-28
B. Free Gyro Attitude Reference System	IV-31
C. Free Accelerometer Reference System	IV-37
D. Restrained Accelerometer Reference System	IV-38
1. Uncertainty in Accelerometer Input Axis Orientation	IV-39
2. Size Effect	IV-40
E. Position Computation	IV-44
1. Boost and Injection	IV-44
2. Orbital Navigation	IV-46
V. HARDWARE APPLICATION STUDIES	V-1
A. Shifting Dynamic Range	V-1
1. Gyro Sensor Loop	V-2
2. Accelerometer Sensor Loop	V-4
3. Strapdown Computational Process	V-4

TABLE OF CONTENTS (Continued)

<u>Section</u>	<u>Page</u>
B. Sequential Sensor Sampling and Resynchronization	V-5
C. Redundancy	V-13
1. Reliability	V-13
2. Performance	V-19
3. Failure Detection	V-23
VI COMPUTATIONAL REQUIREMENT STUDY	VI-1
A. System Error Analysis	VI-1
B. Flight Environments	VI-5
C. Analysis Results	VI-8
VII LIST OF SYMBOLS	VII-1
VIII REFERENCES	VIII-1
APPENDICES	
A. Strapdown Inertial Sensors and Sensor Loops	
B. Kinematic Equations and Algorithms	
C. Closed Form Solution for Angular Motions	
D. Development of the Computational Attitude Error Parameter	
E. Analysis of Coning Motion	
F. Truncation Error Models for Random Vibratory Angular Motions	
G. Derivation of Sensor Associated Error Models	

LIST OF ILLUSTRATIONS

<u>Figure</u>	<u>Page</u>
I-1 Regions of Error for Restrained Gyro Attitude Computations . .	I-5
II-1 Comparison of Strapdown and Gimballed Navigation Systems . .	II-2
III-1 Restrained Gyro and Attitude Computer Bandwidth Relationship .	III-11
IV-1 Computer Error Analysis Digital Program for Restrained Gyro Attitude Computations	IV-2
IV-2 Computational Process Design Procedure	IV-3
IV-3 Characteristics of the Attitude Error Matrix Truncation Error for Restrained Gyros	IV-5
IV-4 Regions of Error for Restrained Gyro Attitude Computation. . .	IV-6
IV-5 Control of Computational Error	IV-8
IV-6 Attitude Errors for Constant Rates of Vehicle Rotation	IV-11
IV-7 Attitude Error for Two Out-of-Phase Vehicle Sinusoidal Oscillations (Coning)	IV-12
IV-8 Truncation Errors for Sinusoidal Vehicle Oscillations	IV-13
IV-9 Combined Truncation and Round-Off Error for Coning Rotations	IV-14
IV-10 Effect of Quantization on Computational Error for Coning Motion ($\Theta = 0.096$ rad)	IV-15
IV-11 Deviation Factors vs. Sampling Frequency Parameter for Fourth Order Runge-Kutta	IV-18
IV-12 Attitude Round-Off Error as a Function of Word Length for Calculating Incremental Changes in Direction Cosines . . .	IV-20
IV-13 Quantization Error for Coning Motion	IV-22
IV-14 Truncation Error Comparison of Incremental (DDA) and Whole Number (DDP) Computers	IV-23
IV-15 Comparison of the Analytical and Simulation Results for Single Axis Random Motion	IV-26
IV-16 Error Characteristics of Trigonometric Approximations. . . .	IV-33
IV-17 Effect of Word Length on Trigonometric Computational Errors	IV-34

LIST OF ILLUSTRATIONS (continued)

<u>Figure</u>	<u>Page</u>
IV-18 Computer Square Root Routine Errors vs. Computer Word Length	IV-35
IV-19 Restrained Accelerometer Size Effect Error	IV-42
IV-20 Boost Cutoff Injection Position Computer Error	IV-45
IV-21 Boost Cutoff Injection Altitude Computer	IV-45
IV-22 Boost Cutoff Velocity Computer Error	IV-45
IV-23 Orbital PTL Computer Error Summary ($\Delta t = 5$ seconds) . . .	IV-47
IV-24 Orbital PTL Computer Error Summary ($\Delta t = 20$ seconds) . . .	IV-47
IV-25 Orbital PTL Computer Error Summary ($\Delta t = 60$ seconds) . . .	IV-47
IV-26 Effect of Integration Interval on Orbital Position Error	IV-48
IV-27 Effect of Integration Interval on Orbital PTL Error	IV-48
V-1 Computational Error with Resynchronization of Asynchronized Gyro Samplings	V-10
V-2 Sensor Data Resynchronization Error for Coning Motion	V-11
V-3 Redundant Gyro Configuration Functional Schematic	V-16
V-4 Effect of Redundancy on Probability of Mission Success	V-18
V-5 Effect of MTBF on Probability of Success	V-20
V-6 Redundant Gyro Equations and Sensor Arrangements	V-21
VI-1 Navigation System Information Error Model.	VI-3
VI-2 Atmospheric Induced Angular Motion	VI-6
VI-3 Linear Power Spectral Density	VI-7
VI-4 Angular Power Spectral Density	VI-9
VI-5 Injection Errors Due to Attitude Computation Truncation Errors	VI-32
VI-6 Injection Errors Due to Attitude Computation Round Off Errors	VI-33
VI-7 Coordinate Conversion Computational Error	VI-34
VI-8 Attitude Computation Truncation Errors (For Postulated Coning Motion).	VI-36

LIST OF TABLES

<u>Table</u>	<u>Page</u>
I-I Strapdown Inertial Sensor Classification	I-3
I-II Parameters Affecting Strapdown Computational Accuracy	I-4
III-I Definition of Terms	III-2
III-II Free Pendulous Gyro Accelerometer Coordinate Transformation Process	III-7
III-III Typical Attitude Matrix Computational Process for Free Gyros . .	III-10
III-IV Parameter Affecting Strapdown Computational Accuracy	III-13
IV-I Attitude Computational Error Summary	IV-10
IV-II Computational Truncation Error for Angular Vibration Motion About an Axis of Rotation Fixed with Respect to the Vehicle . .	IV-25
IV-III Computational Error for Random Vibratory Coning Motion	IV-27
IV-IV Number of Iterations for Convergence	IV-36
V-I Summary of Resynchronization Data	V-12
V-II Nondimensional Failure Rate Analysis Summary	V-14
V-III Redundant Sensor Performance Summary	V-23
VI-I Summary of Computational Characteristics for Simulation Runs	VI-8
VI-II Definition of Error Sources	VI-11
VI-III Error Summary for Configuration 1	VI-12
VI-IV Error Summary for Configuration 2	VI-17
VI-V Error Summary for Configuration 3	VI-22
VI-VI Error Summary for Configuration 4	VI-27

I. SUMMARY

This report presents a detailed and comprehensive evaluation of the computational processes of strapdown inertial navigators; the computational requirements and error sources are defined and analytic models of the computational errors are developed. The analytic computational error models were developed with the aid of detailed digital simulations of the flight environment, the strapdown inertial sensors, the computer hardware and the numerical processes. The strapdown computational processes investigated were the determination of attitude, the resolution of accelerometer data into the inertial frame and the computation of position.

The design and performance evaluation of the strapdown computational process is shown to be simplified by its separation from specific sensor mechanizations. All strapdown sensor mechanizations can be placed into two classes. Class 1 contains those sensors whose input axes are restrained relative to the vehicle and Class 2 contains those sensors whose input axes are free of vehicle orientation. The computational process for all sensor mechanizations within a class are identical. Table I-I lists the sensors of each class that are currently being investigated in the guidance industry. Within each class only a description of the sensor loops' digital information output (frequency response, frequency of data availability and resolution or quantization) is required to evaluate its effect on computational accuracy.

For each class of sensor mechanization, the critical computational problems have been isolated and each computational error source and its characteristics have been separated from the total system error. Table I-II lists the parameters that have been determined to effect computational accuracy. Their effect on computational accuracy is precisely described by analytic models that have been developed for linear and angular environments, both discrete and random. These computational error models permit the performance evaluation of strapdown computational processes to be accomplished for any arbitrary set of mission requirements and environments without employing additional digital simulations of the strapdown system.

The critical computational problems associated with strapdown inertial navigators are defined and discussed in the main body of this report. Substantiating data and mathematical derivations are presented in appendices A through G.

The attitude computational error associated with the numerical integration of the angular kinematic equations necessary with restrained gyros is characterized by four distinct regions of error as shown in Figure I-1:

- (1) Round-off - the error is inversely proportional to computer word length
- (2) Quantization - the error is proportional to gyro output pulse weight
- (3) Truncation - the slope is proportional to the order of the numerical integration scheme
- (4) Bandwidth limited - the region in which the computational frequency is less than the angular motion frequency.

Of primary importance for a restrained gyro attitude reference system is the development of a gyro data processing technique that eliminates the interrelated problems of commutativity and sensor quantization and permits the use of any order integration scheme to minimize the truncation error. Such a scheme is developed herein.

The individual strapdown inertial sensor loops are coupled only in the digital data processing; therefore, an investigation has been made of the following sensor utilization techniques, which significantly enhance the strapdown navigator's mission flexibility, accuracy and reliability for small increases in the computational requirements:

- (1) Shifting of the dynamic operating range of torque-rebalanced sensors as a function of environment to improve performance and reduce power during periods of low level environments.
- (2) Staggering the sampling of the sensors in time and performing resynchronization within the computer to reduce the weight of the interface electronics between the sensors and the computer.
- (3) Using a single gyro properly oriented relative to a basic triad of gyros to achieve the same reliability as obtainable with a completely redundant sensor package.

Utilizing the developed analytical models of the computational errors, a digital computer program (described in Volume II* of this report) has been developed that permits the evaluation of the effect that a computational process has upon attitude, velocity and position accuracy. Evaluated in this program are the computational functions of the attitude determination process and the coordinate resolution of accelerometer data for restrained sensor systems. This program has been utilized to parametrically define computational requirements in terms of performance for a boost-parking orbit, injection and coast-translunar injection mission. This study indicates the trends of computational requirements with variations in required accuracy.

* CR-86022

TABLE I-I

STRAPDOWN INERTIAL SENSOR CLASSIFICATION

	RESTRAINED SENSORS	FREE SENSORS
ANGULAR MOTION SENSORS (GYROS)	<ul style="list-style-type: none">• RATE OR RATE INTEGRATING GYROS• SINGLE AXIS PLATFORMS• RESTRAINED PENDULOUS INTEGRATING GYRO ACCELEROMETERS• "PAIRED ACCELEROMETERS"	<ul style="list-style-type: none">• FREE GYROS
LINEAR MOTION SENSORS (ACCELEROMETERS)	<ul style="list-style-type: none">• FORCE OR TORQUE RE-BALANCED ACCELERO-METERS• RESTRAINED PENDULOUS INTEGRATING GYRO ACCELEROMETERS• FREE GYRO CENTERING FORCE MEASUREMENTS	<ul style="list-style-type: none">• FREE PENDULOUS GYRO ACCELEROMETERS

TABLE I-II
PARAMETERS AFFECTING STRAPDOWN COMPUTATIONAL ACCURACY

- Vehicle Angular & Linear Motion
 - Amplitude
 - Frequency
 - Phase
- Sensor Loop Characteristics
 - Bandwidth
 - Data Rate
 - Quantization
- Computer Hardware
 - Word Length
 - Speed
- Computational Algorithms
 - Sensor Data Processing or Filtering^{*}
 - Order of Numerical Integration Schemes
 - Order of Transcendental Approximations
 - Frequency of Solution

* Extraction of angular rate or specific force from their respective integrals provided by the inertial sensors

APPENDIX F

TRUNCATION ERROR MODELS FOR RANDOM VIBRATORY

ANGULAR MOTIONS

An actual flight environment will consist of low frequency deterministic motions superimposed on a random background of vibratory motions; therefore, the computational errors introduced by vibratory motions must also be considered.

As described in Section IV A the attitude matrix computational truncation error for the input of a single systematic motion can be described in terms of an angular drift rate whose magnitude is a function of the computer and integration processes. For a sinusoidal input, the truncation error can be described by the following equation

$$\dot{C} = f_c k \beta^b \sin^d \left(\frac{\pi f}{2 f_c} \right) \quad (F-1)$$

where k , b the angular amplitude exponent, and d , the frequency ratio exponent, are dependent upon the order of the integration scheme; f_c is the number of integrations performed per second, while f and β are the frequency and amplitude of the sinusoidal motion. Table IV-I lists these coefficients.

Digital simulations have shown that the attitude computations possess the property of superposition such that equation (F-1) can be expanded to describe multiple, simultaneous sinusoidal inputs about an axis of rotation fixed with respect to the sensor package:

$$\dot{C} = k f_c \sum_{\eta=1}^m \beta_{\eta}^b \sin^d \left(\frac{\pi f_{\eta}}{2 f_c} \right) \quad (F-2)$$

Because of the superposition property, the attitude error for an angular random environment of fixed spacial orientation described by an angular rate power spectral density over a frequency range can be analytically derived in closed form. The derivation and the comparison of it with the results of digital simulations follows.

Equation (F-1) can be written in terms of the maximum rate amplitude rather than maximum angular amplitude for a sinusoidal oscillation at frequency, f_i :

$$\dot{\bar{C}}(f_i) = \frac{k f_c \dot{\beta}^b}{(2\pi f_i)^b} \sin^d \left(\frac{\pi f_i}{2 f_c} \right) \quad (F-3)$$

The maximum angular rate amplitude at a frequency f_i can be estimated from the power spectral density describing the random angular motion, ϕ , by

$$\dot{\beta}^2(f_i) = 2\phi(f_i) \Delta f \quad (F-4)$$

Substituting equation (F-4) into (F-3) yields

$$\dot{\bar{C}}(f_i) = \frac{f_c k}{(2\pi f_i)^b} [2\phi(f_i)\Delta f]^{\frac{b}{2}} \sin^d \left(\frac{\pi f_i}{2 f_c} \right) \quad (F-5)$$

For rectangular, 2nd order Runge-Kutta and 4th order Runge-Kutta this equation becomes

$$\dot{\bar{C}}_R(f_i) = \frac{f_c k_R}{2\pi^2 f_i^2} \phi(f_i) \Delta f \sin^2 \left(\frac{\pi f_i}{2 f_c} \right) \quad k_R = .117 \quad (F-6)$$

$$\dot{\bar{C}}_2(f_i) = \frac{f_c k_2}{4\pi^4 f_i^4} \phi^2(f_i) (\Delta f)^2 \sin^4 \left(\frac{\pi f_i}{2 f_c} \right) \quad k_2 = .1 \quad (F-7)$$

$$\dot{\bar{C}}_4(f_i) = \frac{f_c k_4}{4\pi^4 f_i^4} \phi^2(f_i) (\Delta f)^2 \sin^6 \left(\frac{\pi f_i}{2 f_c} \right) \quad k_4 = .05 \quad (F-8)$$

Replacing the summation process of equation (F-2) by an integration process over all frequencies, the total error for the rectangular integration becomes

$$\bar{C}_R = \frac{f_c k_R}{2\pi^2} \int_0^{f_o} \frac{\phi(f)}{f^2} \sin^2 \left(\frac{\pi f}{2f_c} \right) df \quad (F-9)$$

By a change in the integration variable ($\tau = \pi f / 2f_c$), this equation can be simplified to

$$\bar{C}_R = \frac{k_R}{4\pi} \int_0^{\frac{\pi f_o}{2f_c}} \phi \left(\frac{2f_c \tau}{\pi} \right) \frac{\sin^2 \tau}{\tau^2} d\tau \quad (F-10)$$

By the same change in the variable (Δf to ΔZ), the errors for the 2nd and 4th order integration processes at frequency f_i , (Equations F-7 and F-8) become

$$\dot{C}_2 \left(\frac{2f_c \tau_i}{\pi} \right) = \frac{k_2}{16 f_c \pi^2} \phi^2 \left(\frac{2f_c \tau_i}{\pi} \right) \frac{\sin^4(\tau_i)}{\tau_i^4} (\Delta \tau)^2 \quad (F-11)$$

$$\dot{C}_4 \left(\frac{2f_c \tau_i}{\pi} \right) = \frac{k_4}{16 f_c \pi^2} \phi^2 \left(\frac{2f_c \tau_i}{\pi} \right) \frac{\sin^6(\tau_i)}{\tau_i^4} (\Delta \tau)^2 \quad (F-12)$$

The summation process for the total computational error (Equation F-2) can then be expressed as

$$\bar{C}_2 = \frac{k_2}{16 f_c \pi^2} \sum_{i=1}^n \left[\phi \left(\frac{2f_c \tau_i}{\pi} \right) \frac{\sin^2(\tau_i)}{\tau_i^2} \Delta \tau \right]^2 \quad (F-13)$$

$$\bar{C}_4 = \frac{k_4}{16 f_c \pi^2} \sum_{i=1}^n \left[\phi \left(\frac{2f_c \tau_i}{\pi} \right) \frac{\sin^3(\tau_i)}{\tau_i^2} \Delta \tau \right]^2 \quad (F-14)$$

These expressions can also be expressed as a double summation, that is functionally

$$\bar{C} = \sum_{i=1}^n g_i^2 = \sum_{i=1}^n \sum_{j=1}^n g_i g_j \Delta \tau_i \Delta \tau_j \delta_{ij}; \delta_{ij} = \begin{cases} 0, & i \neq j \\ 1, & i = j \end{cases} \quad (F-15)$$

Functionally, this double summation behaves like a double integral with the variables of integration related by a delta function. The error equations (based upon functional analysis) can then be expressed as

$$\bar{C}_2 = \frac{k_2}{16\pi^2 f_c} \iint \phi\left(\frac{2f_c u}{\pi}\right) \frac{\sin^2 u}{u^2} \phi\left(\frac{2f_c v}{\pi}\right) \frac{\sin^2 v}{v^2} \delta(v-u) dv du \quad (F-16)$$

$$\bar{C}_4 = \frac{k_4}{16\pi^2 f_c} \iint \phi\left(\frac{2f_c u}{\pi}\right) \frac{\sin^3 u}{u^2} \phi\left(\frac{2f_c v}{\pi}\right) \frac{\sin^3 v}{v^2} \delta(v-u) dv du \quad (F-17)$$

with this assumption validated by the favorable agreement between this model and the simulation results to be presented below.

Integrating first with respect to (v), the above equations have value only at (v) equal to (u) and by definition of the delta function,

$$x(u) = \int \delta(v-u) x(v) dv \quad (F-18)$$

become

$$\bar{C}_2 = \frac{k_2}{16\pi^2 f_c} \int_0^{\frac{\pi f_o}{2f_c}} \phi^2\left(\frac{2f_c u}{\pi}\right) \frac{\sin^4(u)}{u^4} du \quad (F-19)$$

$$\bar{C}_4 = \frac{k_4}{16\pi^2 f_c} \int_0^{\frac{\pi f_o}{2f_c}} \phi^2\left(\frac{2f_c u}{\pi}\right) \frac{\sin^6(u)}{u^4} du \quad (F-20)$$

In applying equations (F-10), (F-19), and (F-20), the power spectral density input to the computer is that passed on to it by the gyro

$$\Phi(f) = |G_g(f)|^2 \cdot |G_s(f)|^2 \Phi'(f) \quad (F-21)$$

where G_g is the gyro transfer function, G_s is the sensor package transfer function and $\Phi'(f)$ is the power spectral density at the sensor package mounting base.

In general the integrals involved in the above equations must be evaluated numerically. Figure F-1 evaluates the integrals of the above equations for the cases in which the power spectral density is constant over the entire frequency range.

The digital simulations used in verifying these results were made by approximating power spectral densities with multiple discrete sinusoids applied simultaneously. The discrete frequencies were chosen from a table of random numbers after first assuming a band limited power spectral density. The spectrum was then divided into sub-bands, each containing one of the discrete frequencies, and the amplitude of each of the approximating sinusoids was determined by equating the power content to that in the sub-bands containing them. Runs were made for several sets of approximating sinusoids with power spectral density band limited to 50 and 100 cps (f_o). The magnitude of the power spectral density employed were 0.55 and 1.1 (rads/sec)²/cps, extremely large values compared to flight values. A large magnitude was selected in order to emphasize the truncation error relative to the round-off error. Frequency ranges of 50 and 100 cps motion input were selected as being typical of the bandwidth of restrained gyros. Figures F-2 and F-3 present the analytical results and simulation data for comparison.

Figure F-2 displays the computational error for a fixed angular environment as the order of the integration scheme and the frequency with which the equations are solved are varied. Figure F-3 displays the computational error for a fixed integration scheme, 2nd order, as the magnitude and frequency range of the angular environment and the computational frequency are varied. Both figures demonstrate good agreement (slopes and relative magnitude between error curves) between the theoretical and simulation results for all cases in which the computational frequency (f_c) is higher than the upper frequency limit of the vibratory input (f_o). The principal difference between the theoretical and simulation results for $f_c > f_o$ is a constant factor in the truncation region: 2.5 for the 4th order scheme; 3.5 for the 2nd order scheme and 3.3 for the rectangular process. Figures F-4 and F-5 display the same results as contained in Figures F-2 and F-3 but with the theoretical results multiplied by the cited constants at all frequencies in the truncation region. In these figures, the agreement between theoretical and simulation results discussed above is readily apparent.

Additional comparison of the theoretical and simulation results with regard to the exponents of the computational frequency, the amplitude and the frequency bandwidth

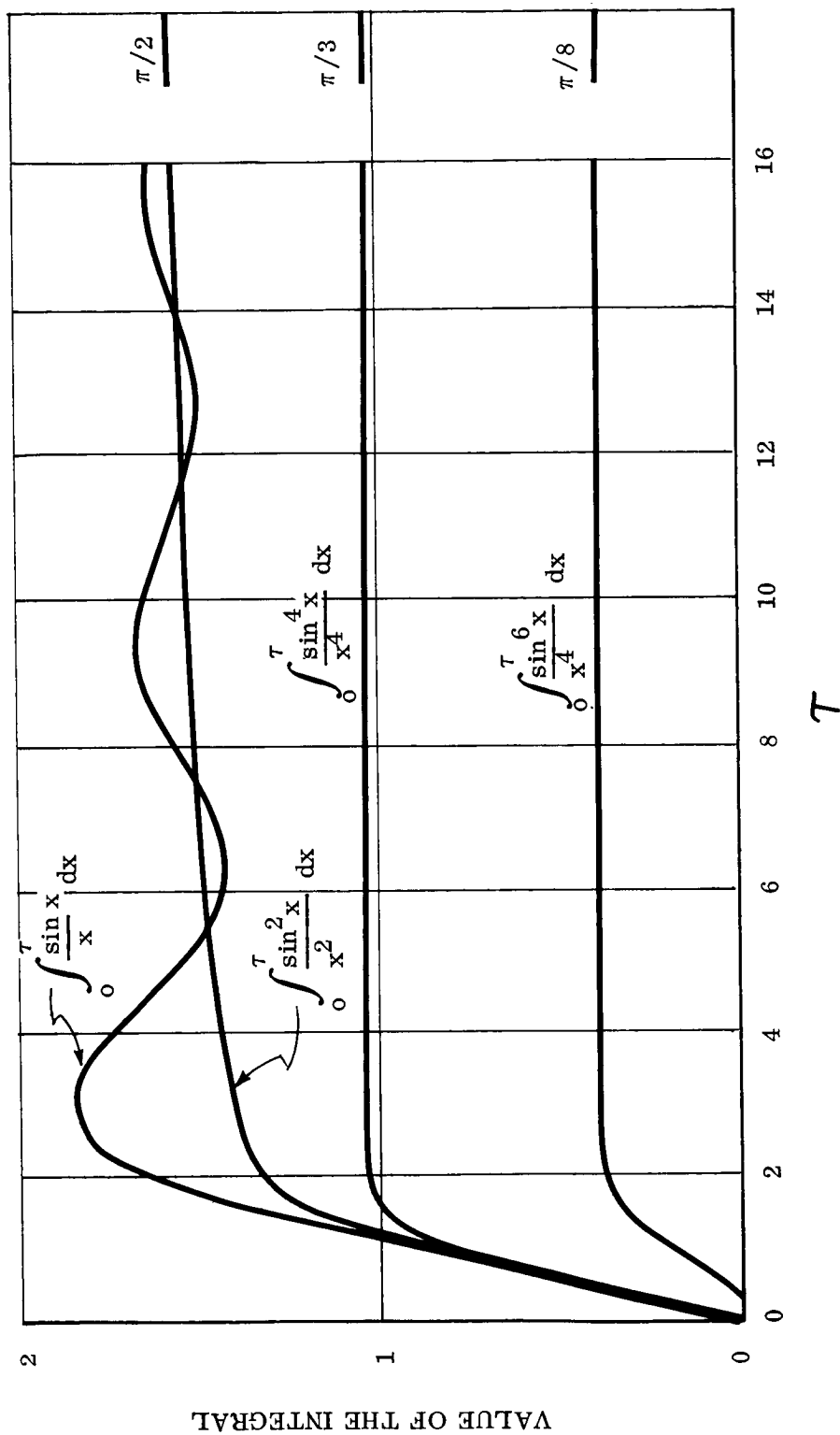
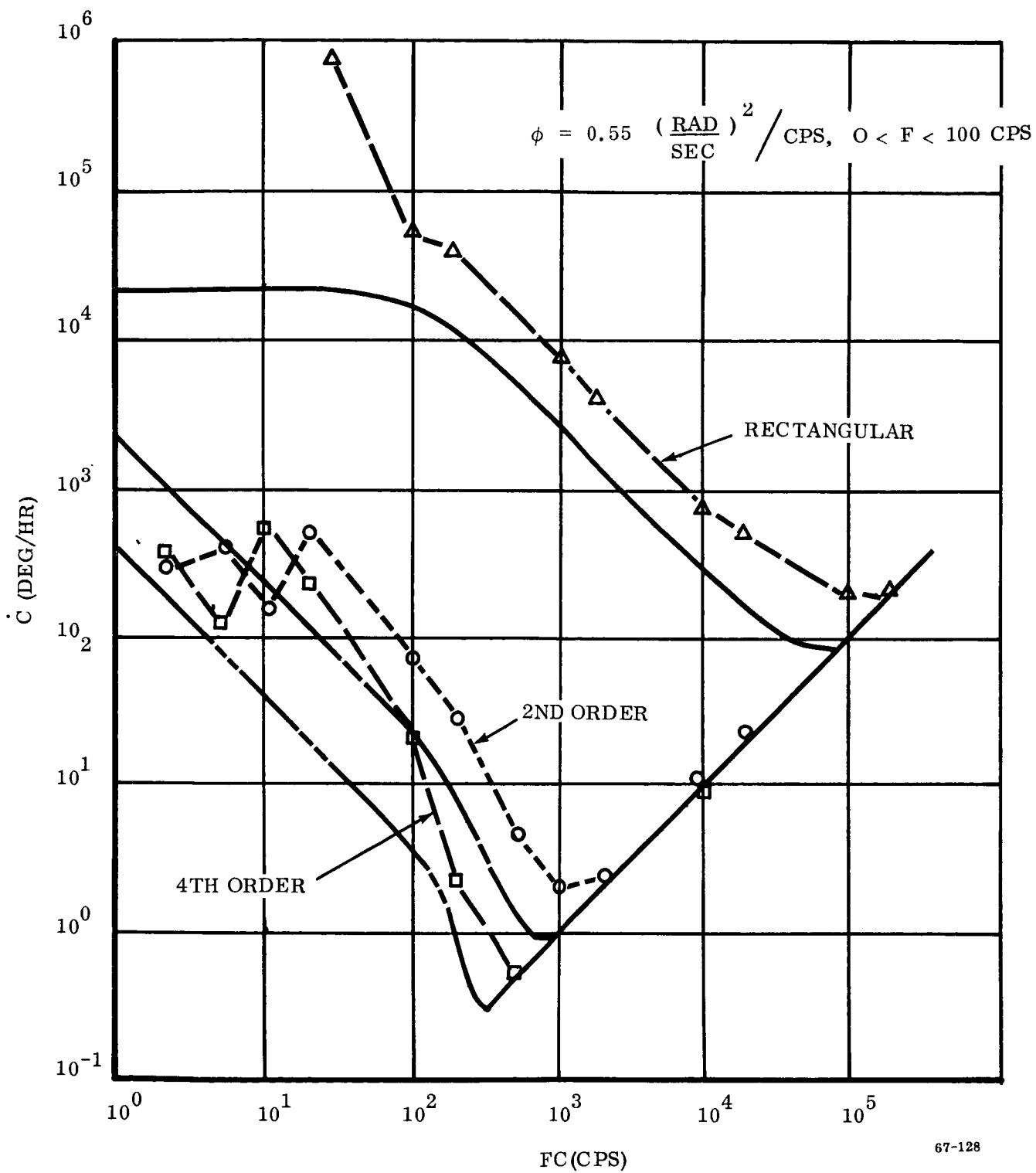


Figure F-1 Numerical Evaluation of Integrals



67-128

Figure F-2 Comparison of Theoretical and Simulation Results for Single Axis Random Motion

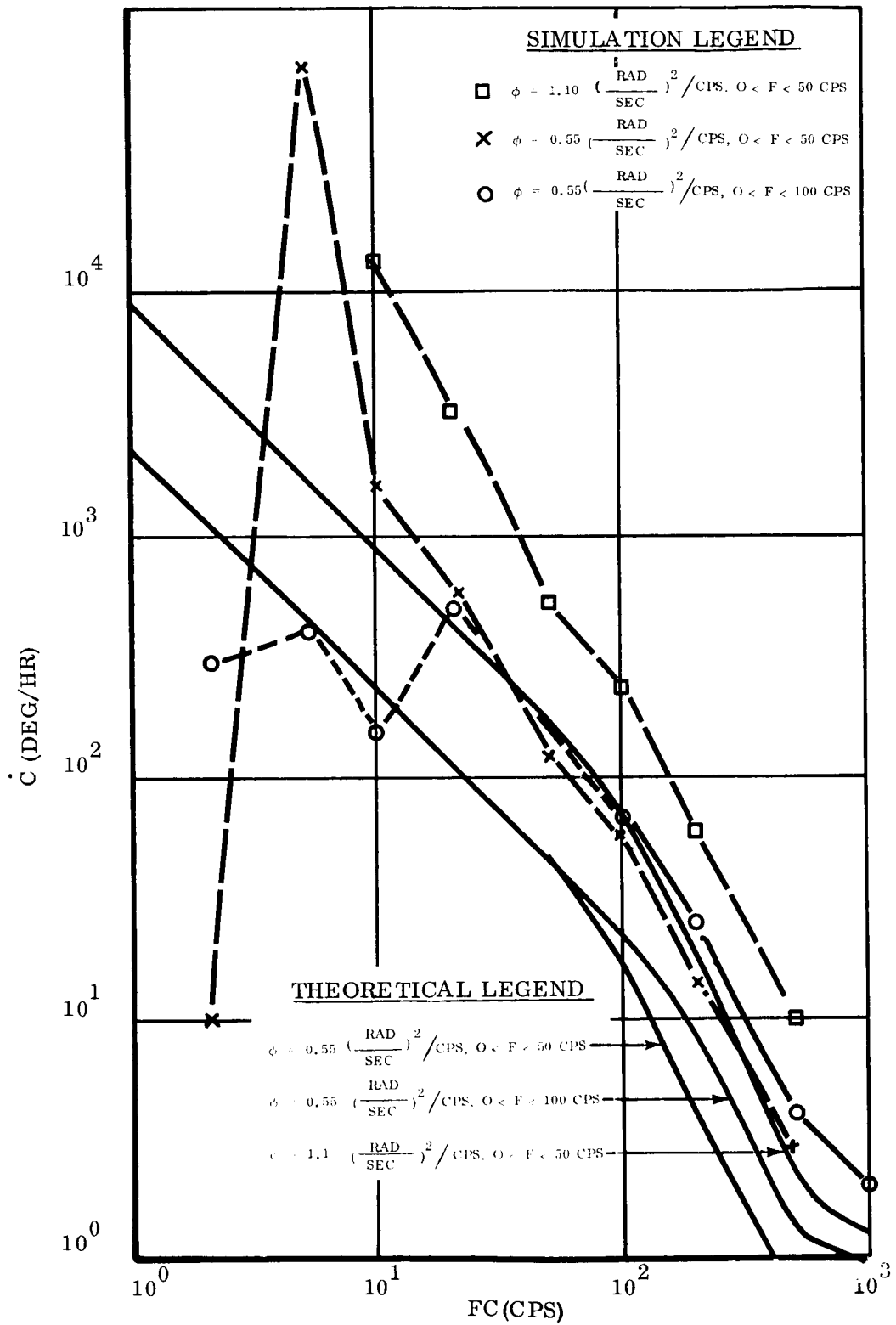
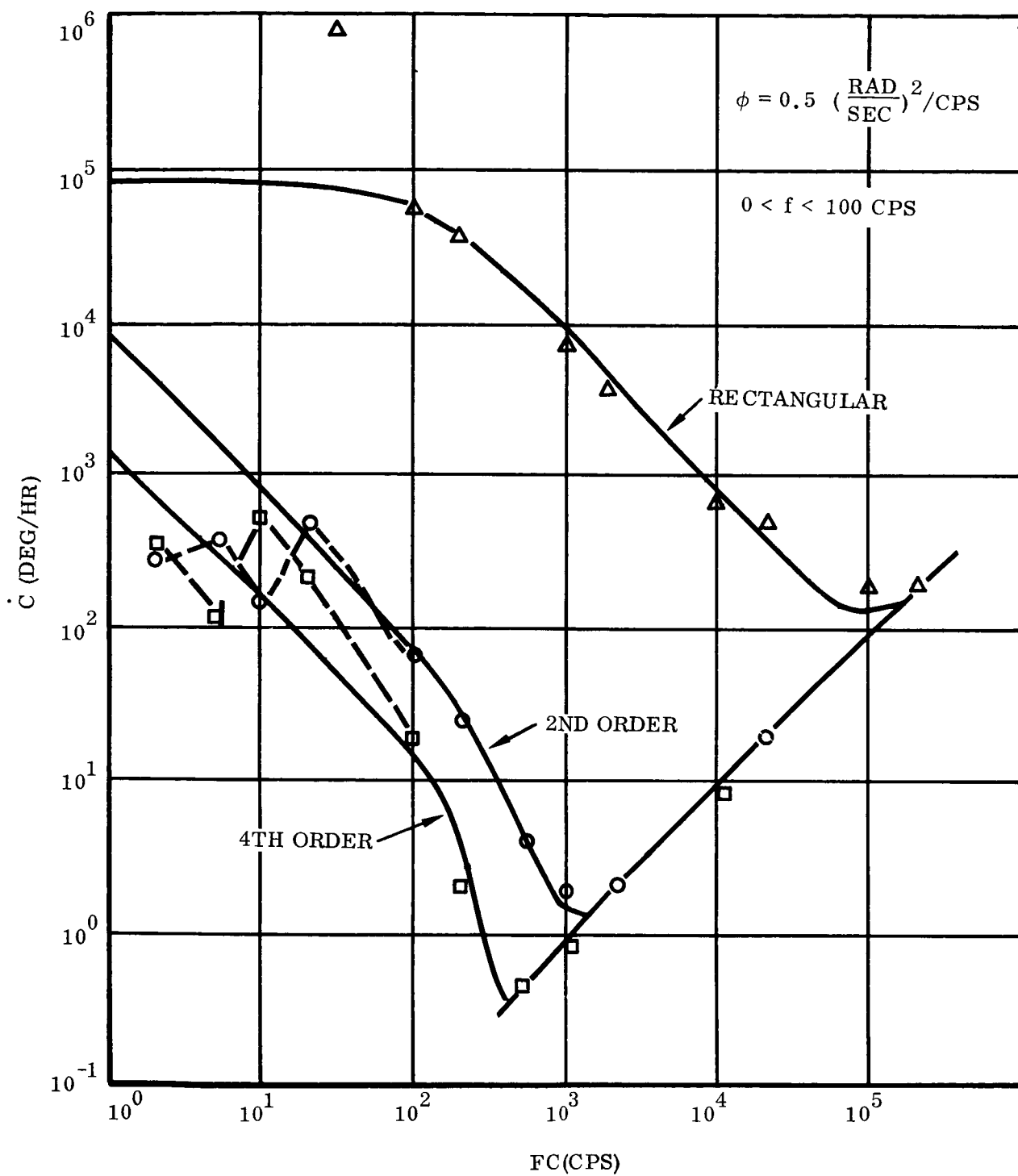


Figure F-3 Comparison of Theoretical and Simulation Results for Single Axis Random Motion



67-127

Figure F-4 Comparison of Adjusted Theoretical and Simulation Results for Single Axis Random Motion

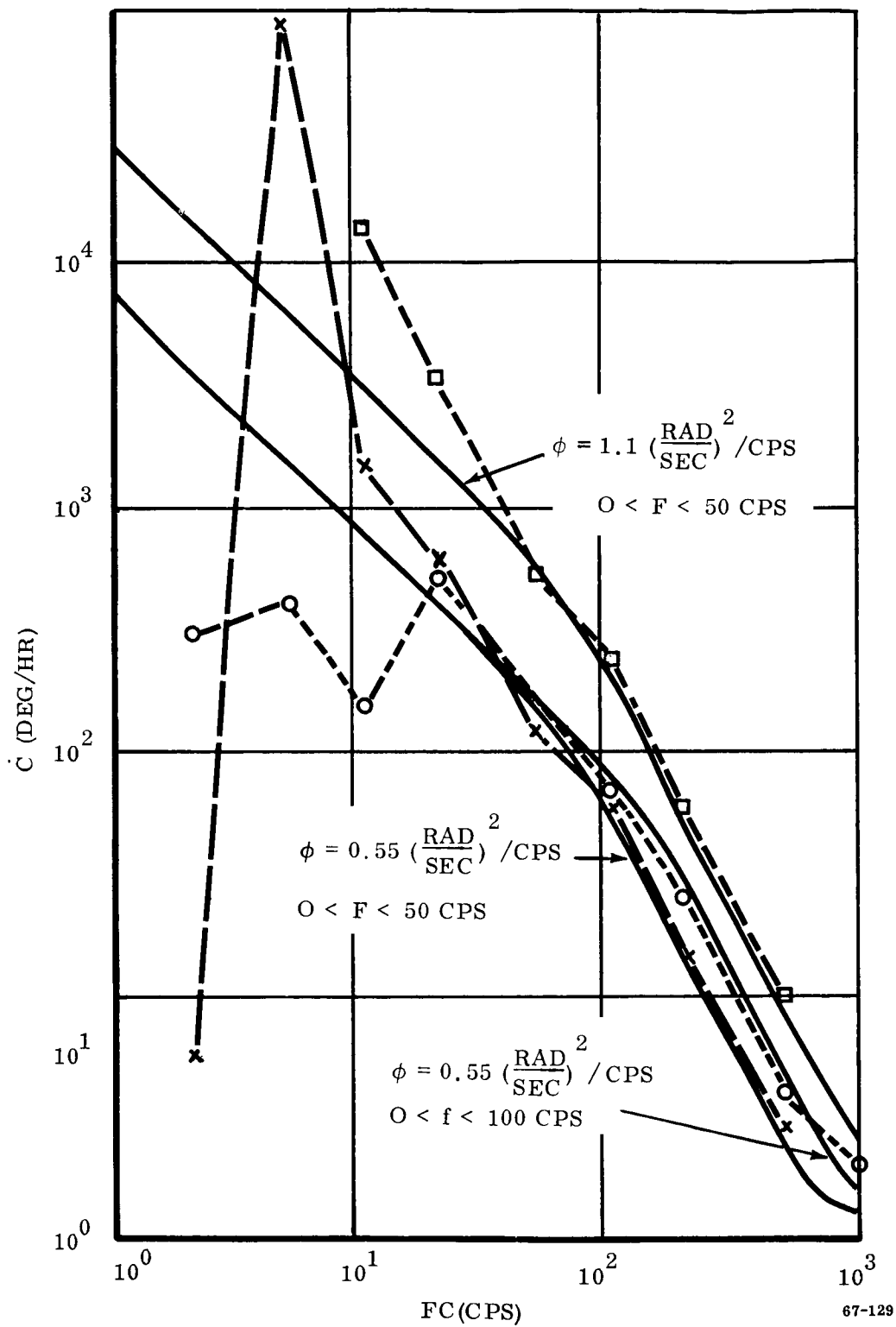


Figure F-5 Comparison of Adjusted Theoretical and Simulation Results for Single Axis Random Motion

of the vibratory input are presented in Tables F-I and F-II. Table F-I presents the theoretical model asymptotic limits for the computational frequency both higher and lower than the maximum vibratory input frequency as simplified for the special case of constant power spectral density (ϕ) investigated. Table F-II compares the theoretical and simulation results for the exponents of f_c , ϕ , and f_0 . As would be expected from the prior visual inspection of Figures F-4 and F-5, good agreement is obtained in the region of $f_c > .1 f_0$, which is the principal frequency region of concern in the design of the computational process. More precise evaluation of the exponents than is presented via digital simulations would require additional runs.

Two possible explanations of the failure of the theoretical model for $f_c < .1 f_0$ are: (1) the lack of a complete error model for discrete sinusoidal inputs for $f_c < f_0$ as has been noted for the rectangular integration process (Section IV.A.1) or (2) the failure of the superposition characteristics in this region that has been assumed and verified for $f_c > f_0$.

A similar analysis was performed for coning motion in a random environment. In this analysis a worst case was assumed, i.e., that of identical power spectral densities, $\phi(f)$, of the vibrations on both axes with a ninety degree phase shift at all frequencies. In practice, coning if it occurs, will occur at discrete frequencies or in a narrow frequency region in which a vibratory coupling mechanism occurs, i.e., control systems, structure or sensor housing transmissibility breakdown. For coning caused by discrete inputs the drift rate in the truncation region ($f_0/f_c < .8$) may be expressed as

$$\dot{C}(f) = k \beta^2 (f) f^a f_c^{1-a} \quad (F-22)$$

where k and a are functions of the integration scheme. With $\beta = \dot{\beta}/2\pi f$ and using equation (F-4), this becomes

$$\dot{C}(f) = \frac{k}{2\pi^2} \phi(f) f^{a-2} f_c^{1-a} \Delta f \quad (F-23)$$

In a similar fashion as before

$$\overline{\dot{C}} = \frac{k}{2\pi^2} \frac{1}{f_c^{a-1}} \int_0^{.8f_c} \phi(f) f^{a-2} df \quad (F-24)$$

For frequencies of input above $f_0/f_c > .8$, the drift rate becomes independent of the integration scheme

TABLE F-I

COMPUTATIONAL TRUNCATION ERROR FOR CONSTANT ANGULAR POWER
SPECTRAL DENSITY

Integration Scheme	<u>Computational Frequency Region</u>	
	$\frac{f_o}{f_c} < 1$	$\frac{f_o}{f_c} > 1$
Rectangular	<u>Theoretical Model Equations</u>	
	$\bar{C} = \frac{k_R}{8} \frac{f_o}{f_c} \phi$	$\frac{k_R}{8} \phi$
	$\bar{C} = \frac{k_2}{32\pi} \phi^2 \frac{f_o}{f_c^2}$	$\frac{k_2}{48\pi} \phi^2 \frac{1}{f_c}$
4th Order	$\bar{C} = \frac{k_4\pi}{384} \phi^2 \frac{f_o^3}{f_c^4}$	$\frac{k_4}{128\pi} \phi^2 \frac{1}{f_c}$

TABLE F-II

COMPARISON OF THEORETICAL & SIMULATION RESULTS FOR
SINGLE AXIS RANDOM MOTION

(a) Exponent of Computational Frequency

Integration Scheme	Computational Frequency Region			
	$f_c > f_o$		$f_c < f_o$	
	Theoretical Exponent	Simulation Exponent (1)	Theoretical Exponent	Simulation Exponent (2)
1st order	-1	-1	0	-
2nd order	-2	-2	-1	-1.2 to -1.9
4th order	-4	-3.7	-1	-1.3

(b) Exponent of Amplitude (ϕ) and Frequency Band (f_o)
of the Random Motion for Second Order Integration

Error Amplitude Ratio	Computational Frequency Region			
	$f_c > f_o$		$f_c < f_o$	
	Theoretical Exponent	Simulation Exponent (1)	Theoretical Exponent	Simulation Exponent (2)
Exponent of f_o $\frac{\dot{C}(\Phi = 0.55, f_o = 50)}{\dot{C}(\Phi = 0.55, f_o = 100)}$	1	.9	0	0
Exponent of ϕ $\frac{\dot{C}(\Phi = 1.1, f_o = 50)}{\dot{C}(\Phi = 0.55, f_o = 50)}$	2	2	2	2

(1) Not including the transition region from truncation to roundoff

(2) $.1 f_o < f_c < f_o$

$$\dot{C}(f) = \frac{65}{\pi} \frac{\beta^2(f)}{f} \quad (F-25)$$

Again approximating the rate amplitude in terms of the power spectral density, total drift rate is

$$\bar{C} = \frac{130}{\pi} \int_{.8f_c}^f \frac{\phi(f)}{f} df \quad (F-26)$$

These equations are summarized for three integration schemes in Table F-III. As before, the power spectral density in the above equations is that of the environment as seen by the computer after it is modified by gyro and sensor package transfer functions.

TABLE F-III

COMPUTATIONAL ERROR FOR RANDOM VIBRATORY CONING MOTION

Integration Scheme	$f_o/f_c < .8$	$f_o/f_c > .8$
Rectangular	$\bar{C} = \frac{327}{2\pi^2} \frac{1}{f_c} \int_0^{.8f} \phi(f) df$	$\bar{C} = \frac{730}{\pi^2} \int_{.8f_c}^{f_o} \frac{\phi(f)}{f} df$
2nd order RK	$\bar{C} = \frac{408}{2\pi^2} \frac{1}{f_c} \int_0^{.8f} f \phi(f) df$	
4th order RK	$\bar{C} = \frac{646}{2\pi^2} \frac{1}{f_c} \int_0^{.8f} f^3 \phi(f) df$	

APPENDIX G

DERIVATION OF SENSOR ASSOCIATED ERROR MODELS

A. Introduction

Several error sources in a strapdown system are associated with the sensors that produce a distortion of the vehicle motion information that is passed on to the computer. These error sources must be treated on a system basis and they must reflect the impact they have upon the error induced in the knowledge of attitude by the computer processing erroneous data. Three such error sources, finite gyro bandwidth, unmatched gyro loop frequency response and gyro output axis acceleration sensitivity, are discussed in this appendix and analytic models of the errors produced by each are derived.

B. Strapdown System Navigation Errors due to the Finite Bandwidth of the Gyros

The finite bandwidth characteristics of the strapdown gyros cause two navigator errors. First is the attenuation, beyond the bandwidth of the gyro, of the random angular environment applied to the sensor package which represents true angular motion of the accelerometer input axes that should be followed by the gyros in order to correctly resolve the accelerometer outputs into the inertial frame. Second is the error induced if vehicle coning motion occurs at frequencies beyond the bandwidth of the gyros. The two sinusoidal rate components will be attenuated by the gyro loops and not seen by the computer while the constant rate component (zero frequency) will be passed on to the computer. This will result in a drift rate of the attitude reference equal to the value of the constant rate component. In either case, the attitude computational process, even if it were perfect, cannot undo the error that has been created. A method of evaluating the gyro amplitude attenuation errors has been developed and is presented.

The mean square angular amplitude of the sensor package and hence of the accelerometer's input axis in the presence of an ergodic random angular environment that is defined by a power spectral density of angular rate is

$$\bar{\theta}^2 = \frac{1}{2\pi} \int_{-\infty}^{\infty} \frac{|G_s(j\omega)|^2}{(j\omega)^2} \phi(j\omega) d\omega \quad (G-1)$$

where G_s is the structural transfer function between the gyros and the sensor package's mounting surface in the vehicle and ϕ is the random angular rate power spectral density at the mounting surface.

Because the gyros have a finite frequency range over which the input rate is perfectly followed, the motion of the accelerometer's input axis over all frequencies will not be precisely described by the gyro's output. Symbolizing the gyro's transfer function by G_g , if the probability density function of ϕ is odd the maximum mean square angular error in the system's knowledge of attitude due to the bandwidth limitation of the gyro is

$$\epsilon_{\theta}^2 = \frac{1}{2\pi} \int_{-\infty}^{\infty} [1 - G_g(j\omega)]^2 \frac{|G_s(j\omega)|^2}{(j\omega)^2} \phi(j\omega) d\omega \quad (G-2)$$

This mean square angular error is an uncertainty in knowledge of the angular orientation of the accelerometer's input axis and as a result contributes an error in the transformation of the accelerometer outputs from the vehicle to the inertial computational frame during the thrusting phases. This error has components along the pitch and yaw vehicle axes of magnitude:

$$\Delta F = F \cdot \epsilon_{\theta}^2 \quad (G-3)$$

where F is the applied specific force and ΔF the resulting error.

If we consider, as an example, an angular vibratory input that has a significant amplitude that extends over a frequency band that is much wider than the gyro bandwidth, the previous equation (G-2) can be approximated by

$$\epsilon_{\theta}^2 = \frac{1}{\pi} \int_{\omega_{bw}}^{\infty} \frac{|G_s(j\omega)|^2}{(j\omega)^2} \phi(j\omega) d\omega \quad (G-4)$$

in which the input environment is integrated over the range from the gyro bandwidth (ω_{bw}) to infinity. Note that the integration from minus to plus infinity was first replaced by twice the integral from zero to infinity. If we further assume that the sensor package has a transmissibility of unity, equation (G-4) becomes

$$\epsilon_{\theta}^2 = \frac{1}{\pi} \int_{\omega_{bw}}^{\infty} \frac{\phi(j\omega)}{(j\omega)^2} d\omega \quad (G-5)$$

Considering a constant power spectral density whose probability density function is odd and evaluating the above integral yields

$$\frac{-2}{\epsilon_0} = \frac{-\phi}{\pi} \frac{1}{\omega} \Bigg|_{\omega_{bw}}^{\infty} = \frac{\phi}{\pi \omega_{bw}} = \frac{\phi}{2 \pi^2 f_{bw}} \quad (G-6)$$

For gyro bandwidths between 50 and 100 cps, the order of present designs, the difference between a power spectral density integrated over a range from the gyro bandwidth to 500, to 1000 or 2000 cps is negligible. To indicate the magnitude of maximum errors that can occur, Figure G-1 shows the mean angular error as a function of power spectral density amplitude and gyro bandwidth. To be compatible with knowledge of the electrical and mechanical uncertainty in knowledge of the orientation of the sensor input axes, this gyro bandwidth produced error should be of the order of 1 to 10 arc seconds depending upon the particular mission and operational procedure under consideration.

To this point, the random angular motion has been assumed to be characterized by an angular motion whose mean amplitude is zero and whose integrated effects produce individual gyro outputs whose mean value of angular rate is zero. The zero mean angular amplitude is a reasonable assumption as the sensor package is rigidly attached to the vehicle. Whether the mean value of the gyro rate output is zero or some value other than zero, depends upon the spatial orientation of the axis of rotation of the random angular input with time. If the random angular axis of rotation moves with respect to the sensor package with time, it can cause a gyro input axis to describe closed contours in space such that the mean of the gyro output is other than zero.

A classical example of this motion is coning motion in which two out-of-phase sinusoidal motions about two orthogonal axes causes an axis orthogonal to the two to describe a cone in space.

For "coning" motions beyond the gyro bandwidth, the drift rate of the attitude reference due to the finite gyro bandwidth would be

$$\omega(\text{drift rate}) = \frac{1}{8 \pi^2} \int_{\omega_{bw}}^{\infty} [1 - G_g(j \omega)]^2 \cdot |G_s(j \omega)|^2 \phi(j \omega) \ln \omega d\omega \quad (G-7)$$

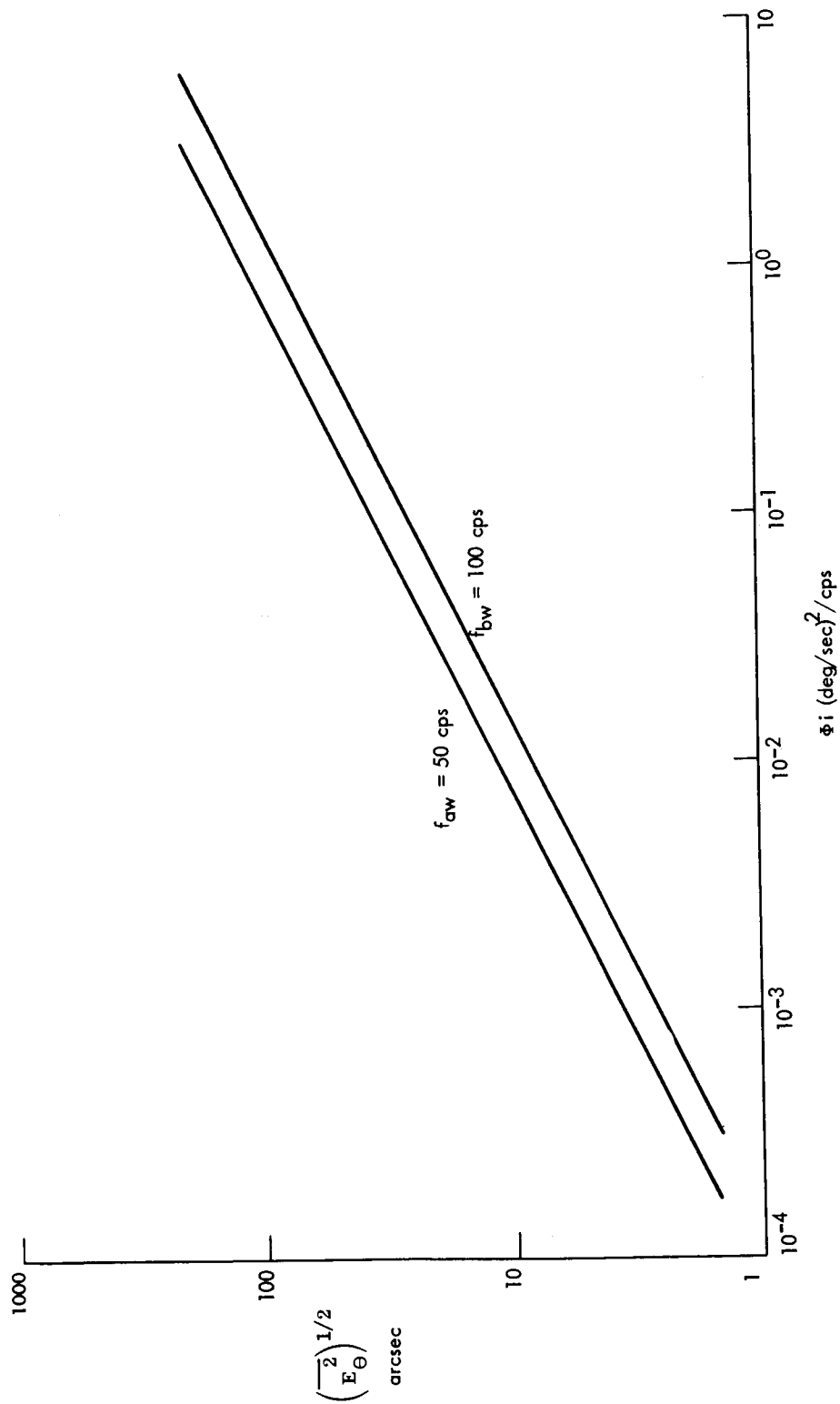


Figure G-1 Angular Uncertainty In Accelerometer Orientation Due To Finite Gyro Bandwidth

where G_g is the gyro transfer function, G_s the sensor package structural transfer function, ϕ the power spectral density at the sensor package mounting point. This equation was derived from the basic coning equation describing the magnitude of the constant rate component developed in Appendix F

$$\omega(f_i) = \frac{\dot{\theta}_i^2(f_i)}{4\pi f_i} \quad (G-8)$$

where

$$\dot{\theta}_i^2(f_i) = \lim_{\Delta f \rightarrow 0} \int_{f_i - \Delta f}^{f_i + \Delta f} \phi(f) df \quad (G-9)$$

C. Unmatched Gyro Loop Transfer Functions

An analysis of the response of a triad of gyros in which each of the gyro loops has a slightly different transfer function indicates that in the presence of an applied sinusoidal angular rate, whose axis of rotation is fixed relative to the sensor package and has components on two or more input axes, an erroneous signal is created. This erroneous output of the attitude reference sensors, even when processed in a perfect computer, results in a constant drift of the computational reference frame. The drift rate is a function of the amplitude and spatial orientation of the applied rate and the phase difference of the gyro loop transfer functions between the gyros of the triad.

The effects to be described are presented for a two dimensional attitude reference since the results are easily generalized to the case of three dimensions. This appendix will consider a pair of gyro loops which sense rates in the x, y body plane. Let these two gyro loops have slightly different transfer functions as illustrated in Figure G-2. The difference in the amplitude response of the two loops is some $\epsilon(f)$ and in the phase response some $\delta(f)$.

The remainder of this discussion will be concerned with the response at a single frequency; therefore, for brevity of notation, the frequency dependency of ϵ and δ will be dropped. It is, however, necessary that the frequency dependency of these terms be included when performing an error analysis.

If a sinusoidal rate of the form $\omega = \alpha \sin \beta t$ is applied to the gyros in the x, y plane along an axis whose orientation is fixed in space (see Figure G-3), the difference in the transfer functions will produce a distortion of the applied motion.

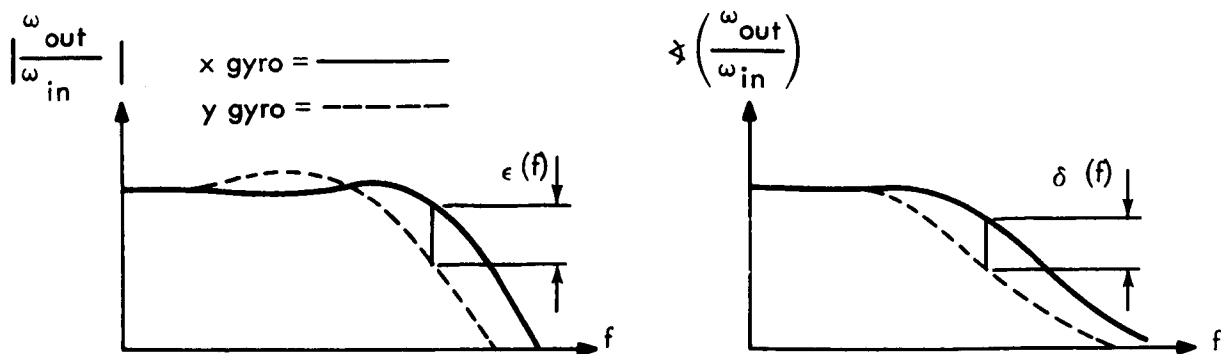


Figure G-2 Postulated Differences in Gyro Transfer Functions

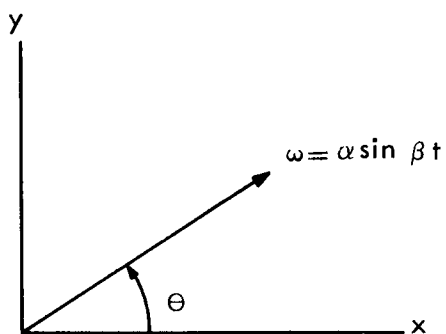


Figure G-3 Geometry of the Angular Rate Experienced by the IMU

The applied rate vector may be resolved along the two input axes and expressed as:

$$\underline{\omega} = \begin{bmatrix} \alpha \cos \theta \sin \beta t \\ \alpha \sin \theta \sin \beta t \\ 0 \end{bmatrix} \quad (G-10)$$

1. The Effect of Differences in Amplitude Response

In the case where the amplitude response of the two loops differs, the indicated rate is a distorted version of the applied rate and may be represented as:

$$\omega' = \begin{bmatrix} (1 + \epsilon) \alpha \cos \theta \sin \beta t \\ \alpha \sin \theta \sin \beta t \\ 0 \end{bmatrix} \quad (G-11)$$

This may be written in polar form, dropping second order terms in ϵ as:

$$\omega' = \alpha (1 + \epsilon \cos^2 \theta) \sin \beta t \angle \left(\tan^{-1} [(1 - \epsilon) \tan \theta] \right) \quad (G-12)$$

This is shown in Figure G-4.

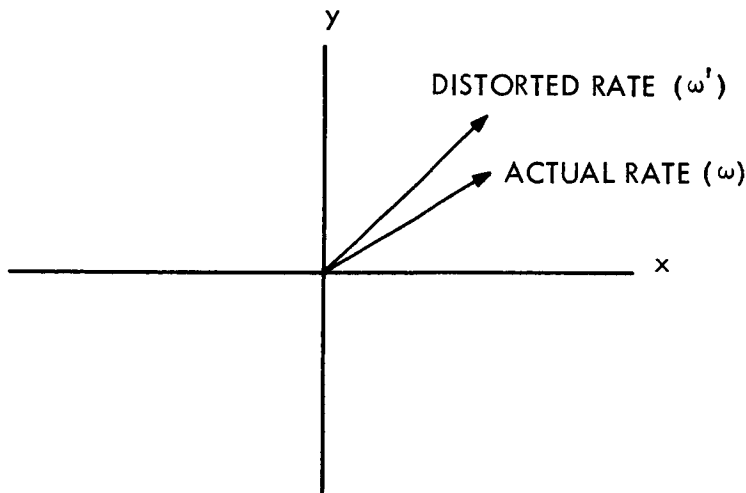


Figure G-4 Distortion of the Original Motion Due to the Difference in Amplitude Response

In this form it is easy to see that the effect of the different amplitude responses is to change the magnitude and spatial orientation of the applied rate. Both the true and distorted motion, however, cause the body to return to its initial orientation periodically such that the error introduced into the computational frame is also periodic and bounded.

2. The Effect of Differences in Phase Response

The difference, δ , between the phase of the transfer functions of the two gyros will also cause the gyros to distort the applied rate. In this case the indicated rate will be:

$$\omega' = \begin{bmatrix} \alpha' \cos \theta \sin \beta t \\ \alpha' \sin \theta \sin (\beta t + \delta) \\ 0 \end{bmatrix} \quad (G-13)$$

where α' equals the applied rate (α) times the mean amplitude response of the loops at the frequency of interest. The above equation may be written as:

$$\omega' = \begin{bmatrix} \alpha' (\cos \theta - \cos \theta \sin \delta) \sin \beta t \\ \alpha' \sin \theta \cos \delta \sin \beta t \\ 0 \end{bmatrix} + \begin{bmatrix} \alpha' \cos \theta \sin \delta \sin \beta t \\ \alpha' \sin \theta \sin \delta \cos \beta t \\ 0 \end{bmatrix} \quad (G-14)$$

The first term in this expression is an effect identical to that produced by the difference in amplitude response and introduces a periodic, but bounded, error in the computational reference. The second term, however, describes a constant rate vector of magnitude $\alpha' \sin \theta \sin \delta$ rotating in the x, y plane at a rate β (See Figure G-5).

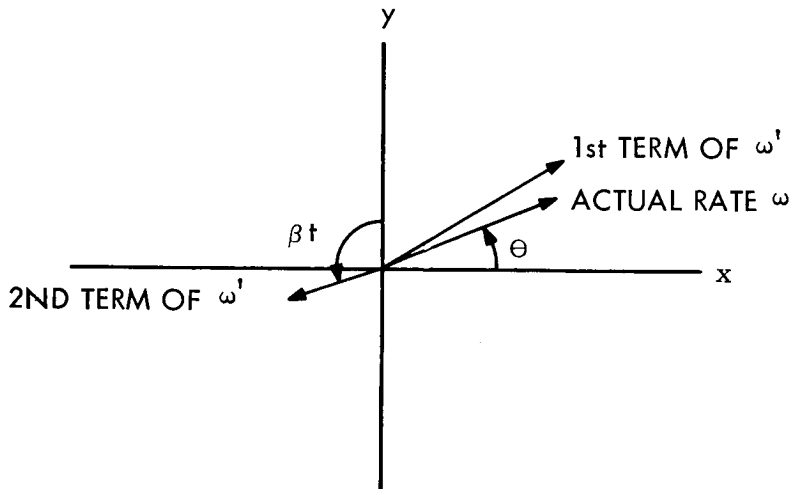


Figure G-5 Component of ω Introduced by the Differences in Phase Response

A closed form solution of attitude equation $[\frac{d}{dt}(T_b^I) = T_b^I \Omega]$ for this type of motion shows that this will produce a constant drift of the computational frame (developed in Appendix C) given by:

$$D.R. = \frac{1}{2} \frac{(\alpha' \sin \delta)^2 \sin \Theta \cos \Theta}{\beta} \quad (G-15)$$

D. Gyro Output Axis Acceleration Sensitivity

A strapdown unit using single degree of freedom of gyros, when subjected to a sinusoidal angular rate about an axis that projects a component on the input axis of one gyro and the output axis of another gyro, outputs an erroneous angular rate vector. This leads to a divergent error in the knowledge of attitude even with a perfect attitude computational process. This is due to the sensitivity of single-degree-of-freedom gyros to accelerations about the output axis. It is shown that this drift rate in the knowledge of attitude is proportional to both the square of the amplitude of the sinusoidal rate and the gyro's inertia to momentum ratio; the drift rate is independent of the frequency of the input motion up to the bandwidth of the gyro.

Consider as an example, a strapdown unit in which the three gyros are mounted as shown in Figure G-6; the input axes defining an orthogonal triad while the output axes are such that two of them are parallel and the third perpendicular to these two.

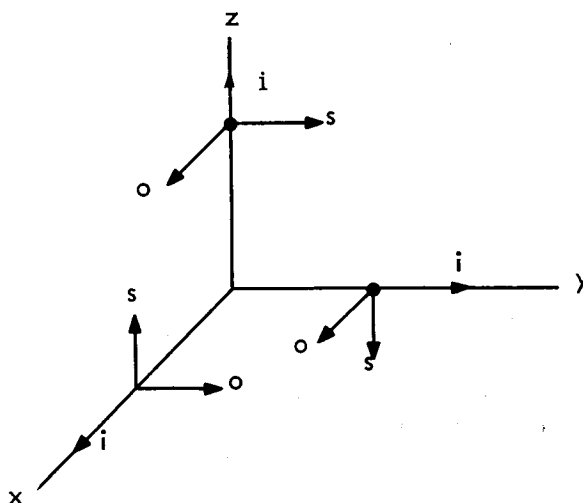


Figure G-6 Typical Configuration of Gyros in an Inertial Unit

Now consider what happens if an arbitrary variable amplitude angular rate with a fixed orientation in the body frame is applied to this triad of gyros. For convenience of computation let this rate be applied along the y body axis:

$$\omega_b = \begin{bmatrix} 0 \\ \omega_y \\ 0 \end{bmatrix} \quad (G-16)$$

The y gyro will of course indicate this rate; however, note that this rate also appears along the output axis of the x gyro. As seen from the gyro block diagram (Figure G-7), this causes the x gyro to indicate to the computer, an equivalent rate about the x axis of:

$$\left(I_{o/H} \right) \dot{\omega}_y \quad (G-17)$$

Hence for a vehicle motion described by:

$$\omega_b = \begin{bmatrix} 0 \\ \omega_y \\ 0 \end{bmatrix} \quad (G-18)$$

the gyro outputs indicate a different motion:

$$\omega'_b = \begin{bmatrix} \left(I_{o/H} \right) \dot{\omega}_y \\ \omega_y \\ 0 \end{bmatrix} \quad (G-19)$$

This effect is absent for rates applied about the z body axis since (as seen in Figure G-5) none of the gyro output axes are parallel to this axis. For rates applied about the x body axis, however, the magnitude of the erroneous output is increased by a factor of $\sqrt{2}$ since both the y and z gyros have output axes parallel to the x body axis.

For the case of a sinusoidal rate applied to the unit (perhaps by control system) limit cycles or vibration), ω_y can be expressed as

$$\omega_y = \alpha \sin \beta t \quad (G-20)$$

$$\omega_{\text{INDICATED}} = \frac{K_{SF} K_F G(S) H}{I_0 S^2 + fS + K_T K_F G(S)} \left(\frac{\omega_0 I_0 S}{H} + \omega_I \right)$$

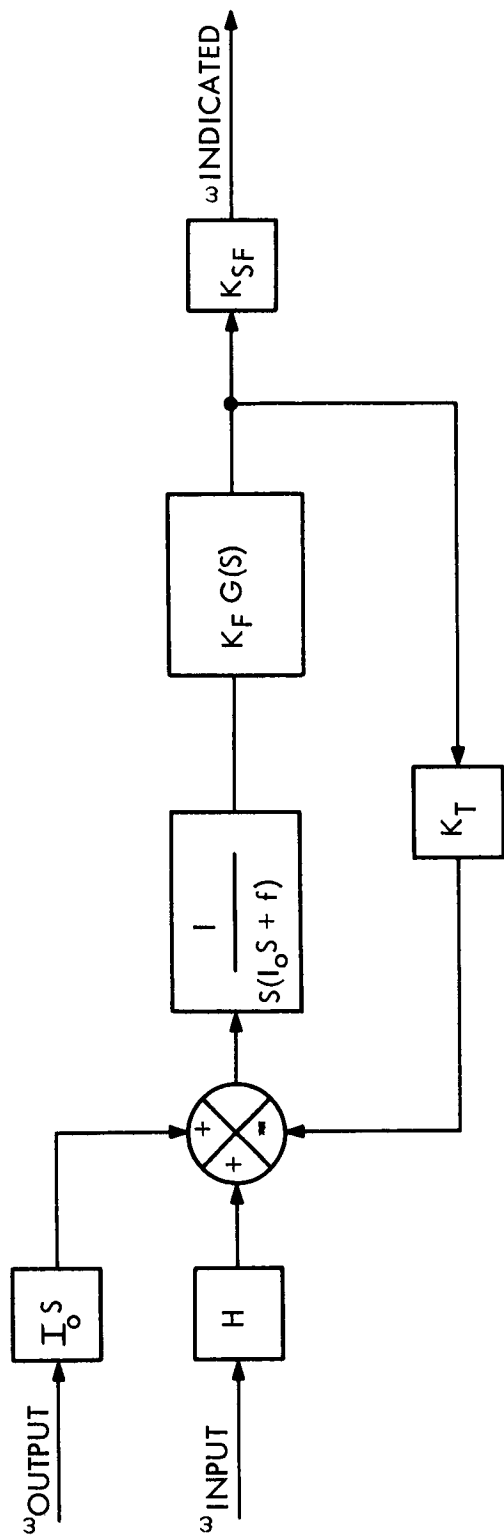


Figure G-7 Gyro Loop Block Diagram

and the true angular rate experienced by the vehicle is therefore:

$$\omega_b = \begin{bmatrix} 0 \\ \alpha \sin \beta t \\ 0 \end{bmatrix} \quad (G-21)$$

The unit, however, indicates an angular rate of:

$$\omega_b = \begin{bmatrix} \left(\frac{I_o}{H} \right) \alpha \beta \cos \beta t \\ \alpha \sin \beta t \\ 0 \end{bmatrix} \quad (G-22)$$

for all frequencies of the ω_y sinusoid less than the gyro bandwidth.

The independence of the frequency of the motion extends to the gyro bandwidth beyond which it is attenuated at a rate of 20 to 40 d.b. per decade depending upon the loop design.

This erroneous rate (one of the class of coning motions considered in Appendix E) causes a constant drift rate of the inertial reference. The magnitude of the drift rate is equal to the solid angle described by the z body axis if it were in fact to be subjected to the erroneous rate. As shown in Appendix E, the drift rate is:

$$DR = \frac{1}{2} \frac{I_o}{H} \alpha^2 \text{ rad/sec} \quad (G-23)$$

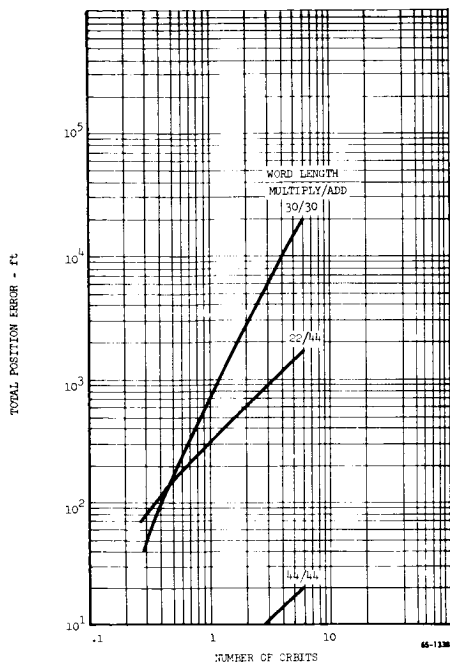


Figure IV-23 Orbital PTL Computer Error Summary ($\Delta t = 5$ seconds)

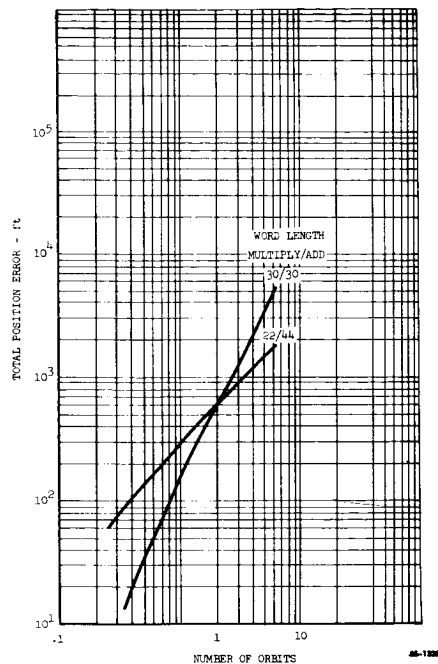


Figure IV-24 Orbital PTL Computer Error Summary ($\Delta t = 20$ seconds)

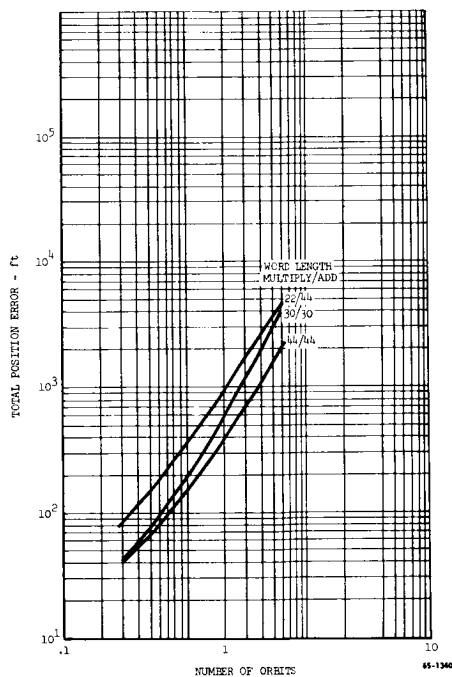


Figure IV-25 Orbital PTL Computer Error Summary ($\Delta t = 60$ seconds)

former group, the error is predominately truncation error; for the latter computer, it is predominately round-off error. Figure IV-26 replots the preceding data (plus other data points not presented) as a function of integration time intervals for position errors at the end of the first and sixth orbits. At the smaller integration intervals, the round-off error dominates; at larger intervals, the truncation error is largest.

The effect of computer word length on the truncation and round-off processes can also be seen in Figure IV-27 where the equivalent position error per integration step is plotted as a function of the integration step interval. For the 30/30 computer, the error is independent of integration interval below an integration interval of 30 seconds. This is characteristic of round-off error; beyond 30 seconds, the error undergoes a transition to truncation. For the 22/44 and 44/44 computer, the range investigated covers the regions in which truncation is the predominate error.

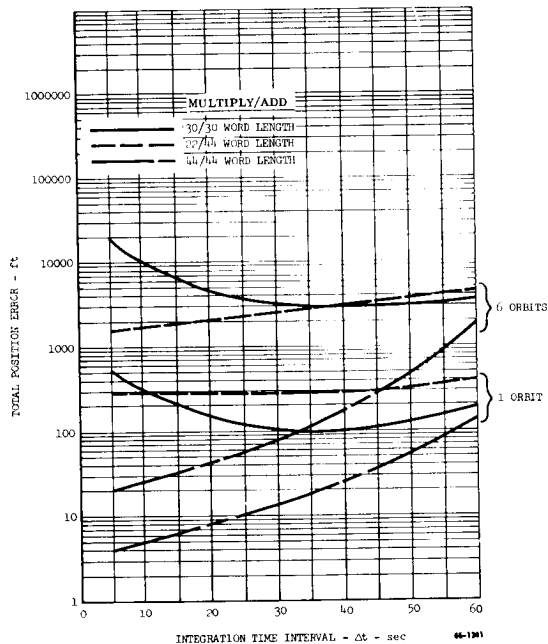


Figure IV-26 Effect of Integration Interval on Orbital Position Error

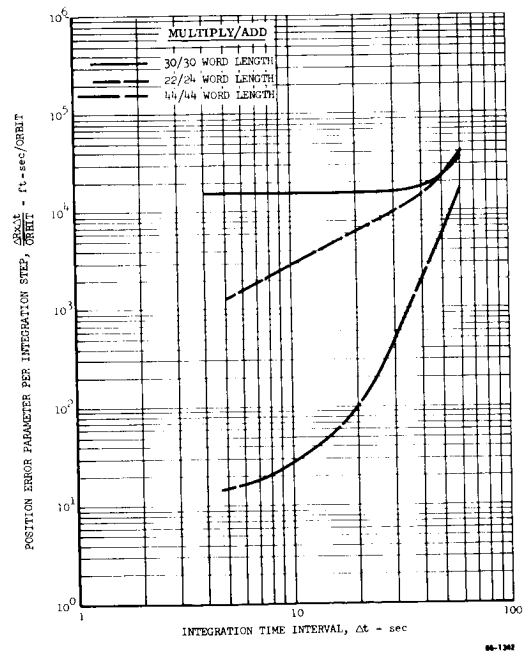


Figure IV-27 Effect of Integration Interval on Orbit PTL Error

V. HARDWARE APPLICATION STUDIES

A strapdown navigator, as inspected from the computational point of view, consists of inertial sensors that measure components of linear and angular motion which are coordinated by the computational process to define the complete system motion in a vectorial sense. With the coupling of the inertial sensors occurring only in the computer, the sensor loops are essentially independent. This allows certain concepts to be implemented on the sensor level that are not required, are not necessary or not permitted in a gimballed system. The application of these concepts on a sensor level will result in maximizing the mission capability of strapdown navigators. The following areas have been considered and are discussed in this section. The additional computational requirements to implement these concepts are outlined and are shown to be small.

1. The shifting of the dynamic operating range of torque-rebalanced sensors as a function of the level of environment during each phase of flight (boost, free-flight, midcourse corrections and terminal corrections, etc.) to improve performance and reduce power during periods of low environments.

2. The asynchronous sampling of restrained gyros and their data resynchronization by a general purpose computer to reduce the weight of the interface electronics between the sensors and computer that are required to store the pulse sum from each sensor until the computer requires the data.

3. Applying redundancy at the sensor level rather than at the inertial measurement unit level to improve system reliability. (Employing redundancy on a sensor level as opposed to a system level results in the same reliability, but requires fewer sensors and thus less weight, or conversely, higher reliability for the same weight).

A. Shifting Dynamic Range

A strapdown inertial navigator must always be designed to perform to a desired level of accuracy under the most severe linear and angular environments anticipated during flight. This includes the scaling of the maximum output from inertial sensors and the scaling of the computer word length and its computational rate for the maximum linear and angular motions. For multiple level environment missions, rescaling of the strapdown inertial navigator for the different environments will permit the achievement of either improved performance or lower power during the periods of low level environments. This may result in a decrease of the overall vehicle weight from the system's standpoint because propellant weight in future midcourse or terminal maneuvers will be saved due to the increased navigational accuracy and the decrease in power will reduce the weight of the device used to store or generate power for the strapdown navigator. The techniques, requirements and trade-offs for shifting the dynamic range of re-

strained torque rebalanced inertial sensor loops and a general purpose computer are discussed in the following sections.

1. Gyro Sensor Loop

A restrained, torque-rebalanced sensor loop consists of the gyro and its permanent magnet torquer and control electronics that supply the correct amount of current to the torquer to counteract the torque produced by the angular rate along the gyro's input axis. The magnitude of the maximum current, i , required is proportional to the product of the maximum value of angular rate, ω , and the angular momentum of the rotor, H :

$$i = kH\omega$$

Typical torque rebalanced electronics however do not vary the magnitude of the retorquing current in proportion to the applied rate because it is very difficult to maintain an accurate value of current over a large dynamic range. Rather, a single precisely controlled level of current is employed. The time over which the current is applied is modulated, alternating between plus and minus, so as to maintain the integral of current over time equal to the integral of the torque created by angular rate over time:

$$\int i dt = \int kH\omega dt$$

Several examples of these schemes are presented in Appendix A.

The two variables that can be used to readily change the scaling of the gyro loop's dynamic range in flight are: (1) the magnitude of the level of current used in rebalancing the gyro loop and (2) the magnitude of the rotor's angular momentum achieved by varying the rotor speed. The variations and trade-offs in power, performance and maximum rate capability can be observed in terms of ratios or percentage changes referenced against a gyro operating at a given set of conditions denoted by a superscript one. Linear relationships between power, performance and maximum angular rate are presented below. Nonlinearities have not been considered because their behavior is not general but rather is associated with particular designs and the components selected to implement the design concept.

Rotor Power - A majority of gyro spin motors operate at nearly constant current such that the voltage hence the power is proportional to the rotor speed (α)

$$\frac{(\text{Power})_{\text{Rotor}}^1}{(\text{Power})_{\text{Rotor}}^0} = \frac{H^1}{H^0} = \frac{\alpha^1}{\alpha^0}$$

Retorquing Power - The retorquing power is proportional to the square of the current, thus it is proportional to the square of the change in angular momentum and maximum angular rate

$$\frac{(\text{Power})_{\text{Retorquing}}^1}{(\text{Power})_{\text{Retorquing}}^0} = \left(\frac{W_{\text{Max}}^1}{W_{\text{Max}}^0} \right)^2 \times \left(\frac{H^1}{H^0} \right)^2$$

For most torquer designs there is a maximum power input after which the torquer efficiency decreases and the relationship becomes highly non-linear.

Gyro Bias and Mass Unbalance - The gyro bias and unbalance error coefficients are inversely proportional to the rotor's angular momentum and are independent of the retorquing electronics

$$\frac{B_{\text{gyro}}^1}{B_{\text{gyro}}^0} = \frac{U^1}{U^0} = \frac{H^0}{H^1} = \frac{(\text{Power})_{\text{Rotor}}^0}{(\text{Power})_{\text{Rotor}}^1}$$

Retorquing Electronics Bias - The equivalent bias error in the retorquing electronics is due to differences in the magnitude of the plus and minus current levels over the basic pulsing limit cycle period (Appendix A). Over reasonable ranges of current variation, the difference between the two levels of current for most designs is proportional to the absolute value of current level

$$\frac{B_{\text{electronics}}^1}{B_{\text{electronics}}^0} = \frac{i_{\text{max}}^1}{i_{\text{max}}^0} = \frac{(\text{Power})_{\text{retorquing}}^1}{(\text{Power})_{\text{retorquing}}^0}$$

Sensor Loop Scale Factor - The scale factor error of the gyro and the retorquing electronics are essentially independent of the variation in angular momentum and retorquing current level.

The most severe environments for which strapdown navigators must be designed occur during periods of thrusting. For the gyros, there may also be periods of desired high angular rates during nonthrusting phases of flight. For the more serene environments, the above equations demonstrate one of the following:

1. Improved sensor loop performance is obtained with lower power by reducing the retorquing current level to a value that will handle anticipated rate environments.

2. A further improved sensor loop performance is obtained for the same power by reducing the retorquing current while increasing the angular momentum of the rotor by the amount of power deleted from the retorquing process.

In order to change the retorquing current level or wheel speed, the strapdown inertial navigator's computer must be able to control switching functions external to the computer; the computer must be able to change conditions from one precise condition to another precise known condition. To change gyro wheel speed, the computer must control changes in the power supply's rotor speed excitation frequency. To change retorquing current level over wide dynamic ranges, it is necessary to be able to select different resistors or their equivalent in the current level control circuitry.

In order to change gyro rotor speed with minimum system error, it is necessary that the angular rates at the time of switching be small in order to minimize the error associated with the uncertainty in gyro scale factor during the transient spin up and spin down period, which is in the order of ten to twenty seconds. The alternative to using low rates during the transient period is to use stellar observations to correct the attitude inertial reference after the change in wheel speed has been accomplished. In contrast, the change in retorquing current levels can be made in less than a millisecond.

2. Accelerometer Sensor Loop

The pulse torquing rebalancing concepts applied to accelerometers are identical to those used in the gyro sensor loops. In the accelerometer loop, the pendulousity, the pendulous mass times the moment arm, cannot be varied as is the angular momentum in the gyro. Therefore, the only item that can be used to change accelerometer dynamic range is the retorquing current level. The retorquing power required is again proportional to the square of the maximum level of acceleration that the loop must measure. For the accelerometer loops, the electronic equivalent bias is proportional to the maximum acceleration (current) level and the scale factor of the entire loop is insensitive to the maximum acceleration (current) level. The change of levels is accomplished quite rapidly and accurately during nonthrusting phases.

3. Strapdown Computational Process

The shifting of the dynamic range of the attitude and position computational processes in a general purpose computer for serene space environments requires only the decreasing of the computational frequency (the increasing of the size of

the integration interval). The computational frequency is reduced so as to place the errors created by the attitude and position computational processes in the transition region between round-off and truncation for the lower environmental levels. (The same design philosophy is also used in the design of the computational processes for the environment encountered during all flight phases including boost.) This simple change in the computational frequency lowers the computational error from that occurring during periods of high level environment flight that use the same computer word length. The lower computational frequency also reduces the duty cycle of the computer that in turn reduces the average power required to operate, access and read the memory. Using longer computer word lengths or its equivalent, double precision computations, and higher order integration schemes to further reduce the attitude and position computational errors is usually not necessary; the lowering of the attitude computational frequency is sufficient to maintain the computational error below the gyro errors even when the latter are rescaled to improve performance. In order to accommodate the change in sensor scaling, discussed in the previous section, the computational process must simply select a new set of sensor compensation terms (scale factor, bias and for thrusting, unbalance) from its data memory.

The additional computational functions to change the scaling of the navigator are negligible compared to the basic computational routines. A few program instructions are required to implement the logic decisions as to when the dynamic range is to be changed. A few data memory locations are required to store the additional sensor compensation coefficients.

B. Sequential Sensor Sampling and Resynchronization

A strapdown sensor unit operating in conjunction with a general purpose computer requires an interface unit which stores or holds the output from each sensor until the computer is able to accept the data. To provide synchronized sensor data, which is of primary importance for restrained sensors, a holding register for each sensor is required in the interface module. The availability of holding registers permits shifting of the data from all sensors into the interface module on the occurrence of a single synchronizing pulse and the reading of the data from the interface module by the computer in a sequential manner through a single input/output channel.

If sensor data were not transferred simultaneously from the sensor to the interface module, but rather sequentially, only one common holding register would be required. This would substantially reduce the number of components, size and weight of the interface module. However, computer logic would then have to provide a means of resynchronizing the sensor data prior to processing in the manner discussed in Appendix B. If the resynchronization is neglected, the re-

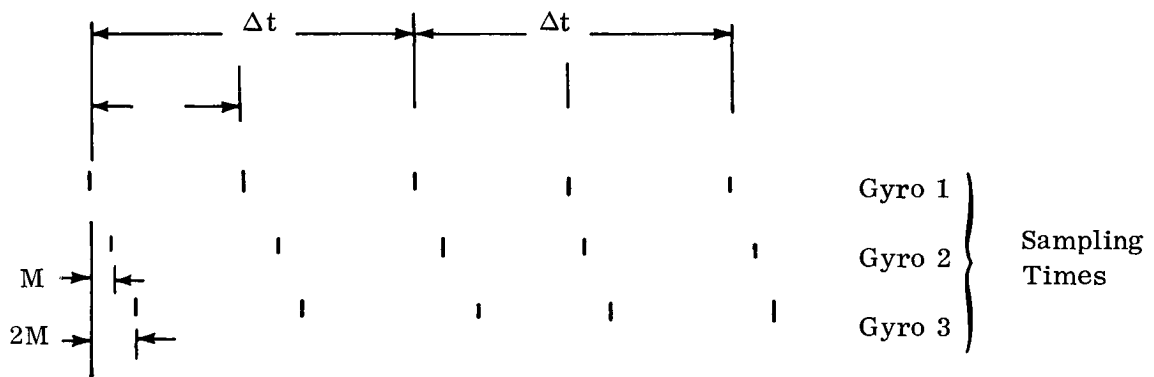
sulting error due to the phase shifted data will behave in an identical manner to that due to sensor quantization. The strapdown attitude computational process has been examined to determine the characteristics of the data resynchronization process.

The strapdown attitude computational process must numerically integrate nine differential equations

$$d/dt [T] = [T] [\Omega]$$

where $[T]$ is the 3×3 direction cosine attitude matrix defining the transformation from the rotating to a fixed coordinate system, and where $[\Omega]$ is a skew-symmetric matrix whose elements are components of angular rate measured in the rotating frame (see Appendix B). To numerically integrate these equations, measurements of components of angular rate are required at particular points within the integration interval. Techniques to extract rates accurately from three gyro outputs have been developed and discussed in Section IV. Such a scheme for synchronized (in time) sampling of the triad of gyros that yields rate estimate accuracy compatible with a 4th order Runge-Kutta algorithm has been developed.

If the acceptable computational accuracy could be obtained with the gyro outputs available asynchronous in time, the number of static registers for the gyros could be reduced from three to one. A schematic of the time of sensor data availability and integration intervals for a fourth order integration process with asynchronous sampling is

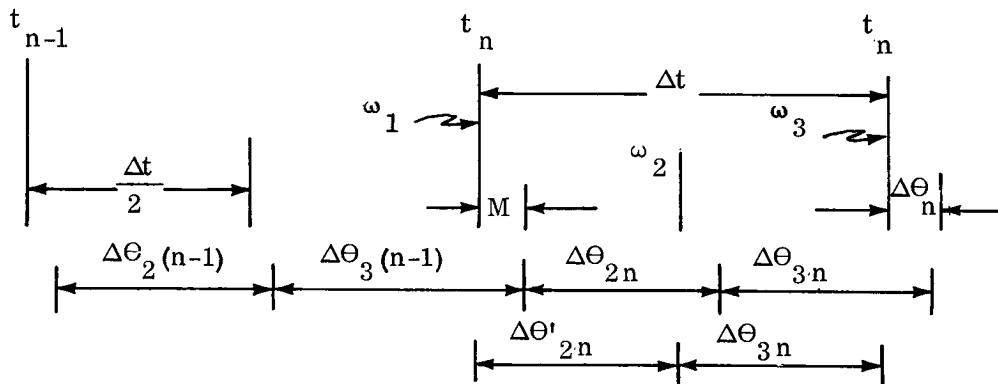


This figure shows the sampling of the gyros displaced by a time increment M , to be used in an integration interval of size Δt . For a 4th order integration process it is necessary that estimates of the components of angular rate at the beginning, midpoint and end of the integration interval be formulated (as before with synchronous

outputs) with accuracy sufficient to preserve the accuracy of the fourth order integration process.

One way to approach the problem is to use the gyro data samplings that are unsynchronized with respect to the integration interval to estimate the gyro outputs that would have been obtained if the gyros were sampled at the midpoint and end of the integration interval. These estimated gyro outputs can then be processed to extract rates by the aforementioned gyro data processing equations.

Such a resynchronization process is schematically described below. The time relationship between the integration process, the sampled gyro outputs ($\Delta\theta$) of the i^{th} sensor and the estimate of the gyro outputs ($\Delta\theta'$) that would have been obtained if the sensor had been sampled synchronously in time with the integration process are also shown.



The equations and process for obtaining the synchronized gyro estimates are:

Given: Gyro outputs every $h/2$ period of time that lag the beginning and midpoint of the integration interval by M time period.

Derive: Estimates of gyro outputs over the first and second half of the integration intervals to be used with the standard rate extraction equations.

Procedures:

1. Describe Θ as a second order polynomial in time over the time period of $\Delta\Theta_{2n}$ and $\Delta\Theta_{3n}$

$$\Theta_n(t) = a_n t + b_n t^2$$

$$a_n = \frac{1}{h} (3\Delta\Theta_{2n} - \Delta\Theta_{3n})$$

$$b_n = \frac{1}{h^2} (\Delta\Theta_{3n} - \Delta\Theta_{2n})$$

2. Estimate the gyro outputs during the first and second halves of the integration interval

$$\Delta\Theta'_{2n} = \Theta_n \Big|_0^{h/2-M} + \Delta\Theta_{n-1}^*$$

$$\Delta\Theta'_{3n} = \Theta_n \Big|_{n/2-M}^h$$

$$\Delta\Theta_n^* = \Theta_n \Big|_{h-M}^h$$

In initiating the process, $\Delta\Theta_{n-1}$ can be assumed to be

$$\Delta\Theta_{n-1}^* = a_n \cdot M$$

3. Apply present rate extraction equation (presented by Appendix B) utilizing

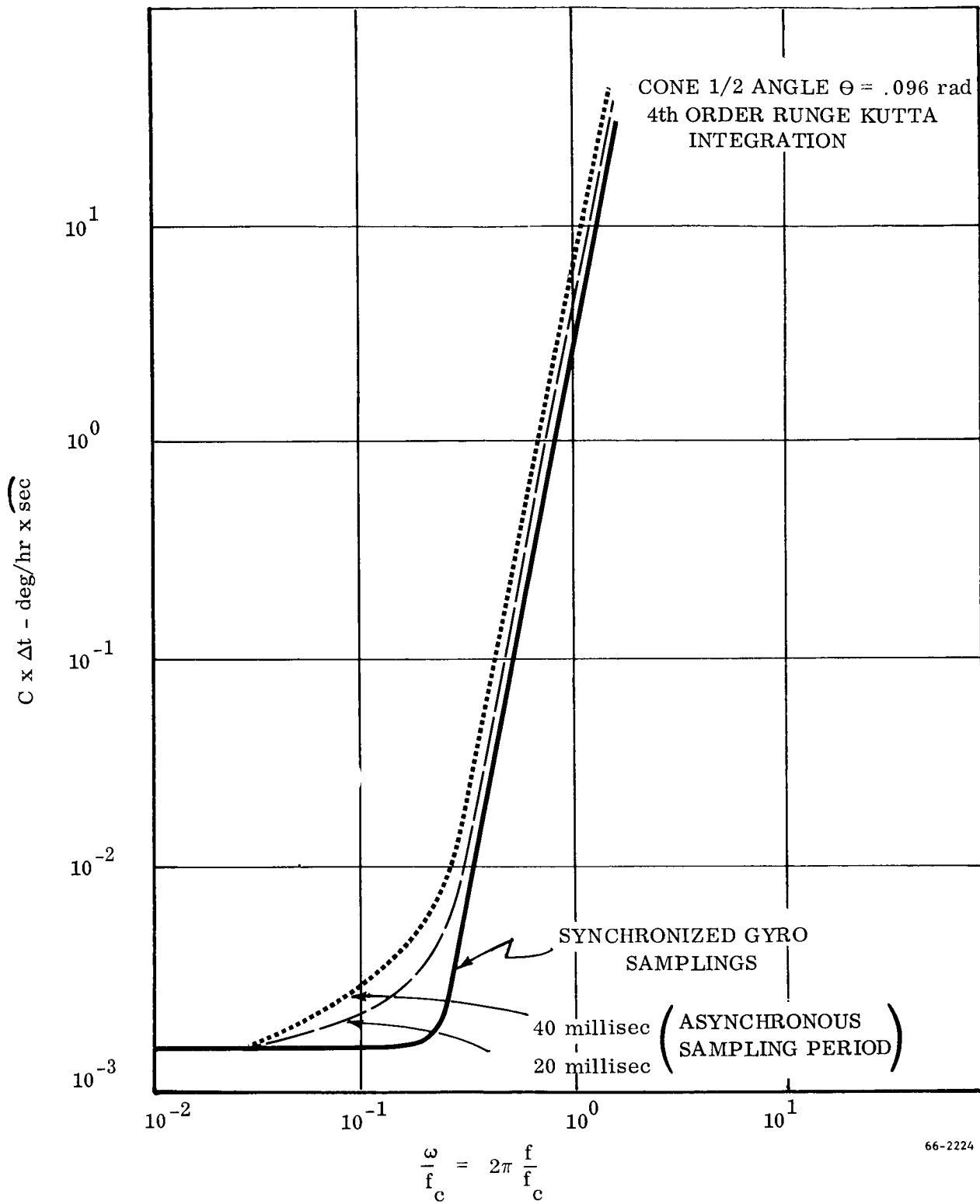
$$\Delta\Theta'_{2n} \text{ and } \Delta\Theta_{3n}$$

4. Repeat for the other two gyros.

Digital simulations have been run to evaluate this process and have demonstrated accuracies compatible with the fourth order integration algorithm employed. A coning type motion was used in these simulations since it represents one of the most difficult motions for the computer to follow. The errors introduced by the asynchronous sampling were small and it was necessary to use rather

large delay times ($M = 20$ and 40 millisecc) to separate it from the normal truncation errors. Figure V-1 presents the total computational error for the employed coning motion. The two cases run with the resynchronization of asynchronized gyro samplings using the aforementioned resynchronization process can be compared with the case of synchronous gyro samplings. The principle effects of resynchronizing asynchronous samplings is to modify the transition region from round-off to truncation and to increase the truncation error by a constant factor. It is seen from Figure V-1 that the resynchronization error is a function of the fifth power of the frequency ratio (the same as the truncation error). Figure V-2 presents the additional error introduced above the truncation error by the resynchronization process. This figure was obtained by subtracting from the 20 millisecond asynchronized sampling curve the synchronized sampling error curve of Figure V-1. Also shown are data for two different amplitudes of vehicle motion. The data of Figure V-2 demonstrate that the error in resynchronization is proportional to the square of the angular motion amplitude. Table V-I tabulates the resynchronization errors for the two different asynchronization time intervals employed. It is shown in this table that the resynchronization error is directly proportional to the magnitudes of the asynchronization period. These results can be analytically described by the following error model

$$\text{Drift rate} - KM \Theta^2 (f/f_c)^5$$



66-2224

Figure V-1 Computational Error with Resynchronization of Asynchronous Gyro Samplings

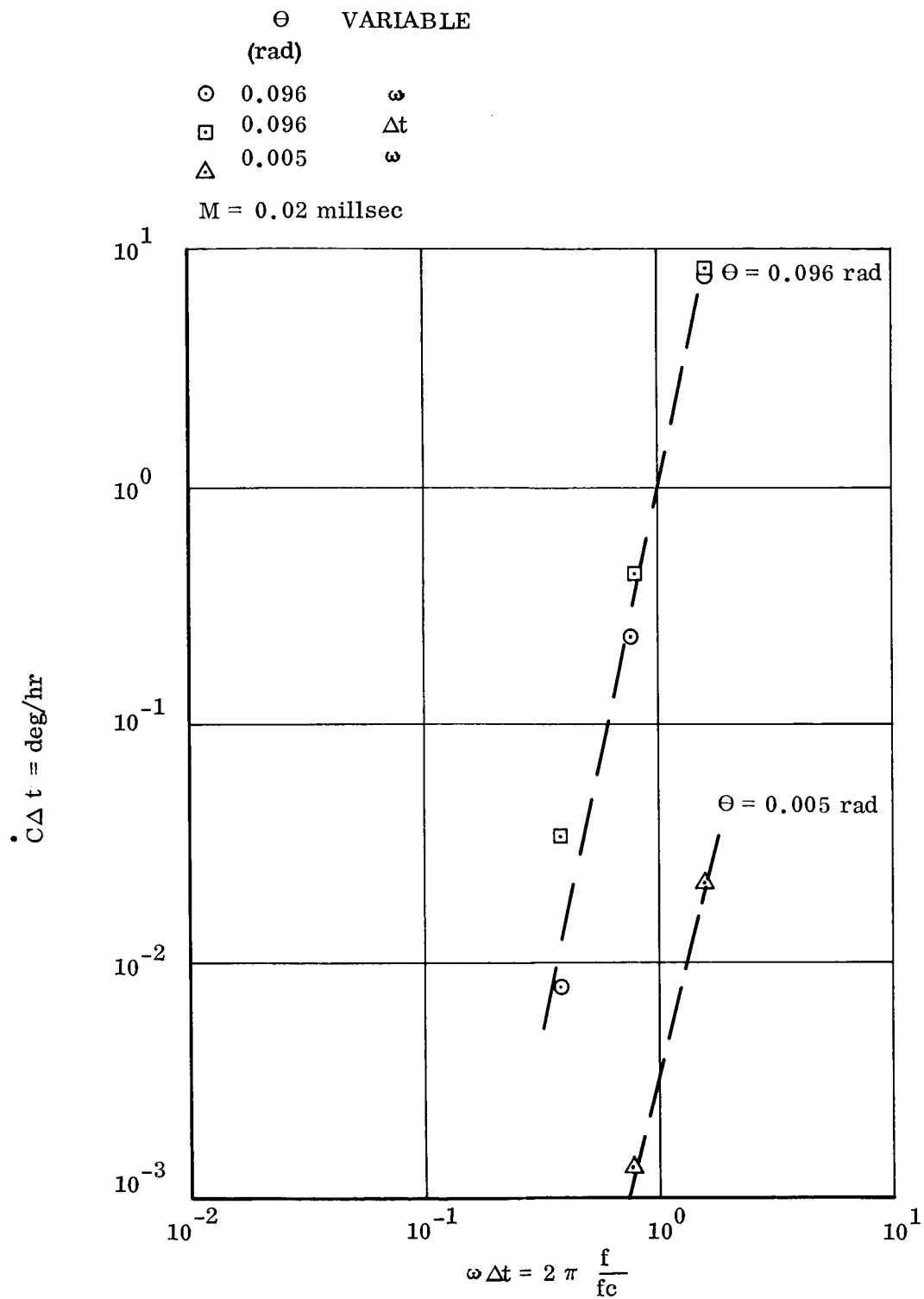


Figure V-2 Sensor Data Resynchronization Error for Coning Motion

TABLE V-I

SUMMARY OF RESYNCHRONIZATION DATA

Θ (rad/cps)	Δt (sec)	ω (rad/sec)	$\omega \Delta t$	Resynchronization Error	
				arc sec/step for M = 0.02 sec	arc sec/step for M = 0.04 sec
0.096	1	1.57	1.57	7.68×10	1.42×10^1
	1	0.785	0.785	2.36×10^{-1}	4.35×10^{-1}
	1	0.392	0.392	7.66×10^{-3}	1.92×10^{-2}
	0.5	1.57	0.785	4.33×10^{-1}	7.75×10^{-1}
	0.25	1.57	0.396	3.07×10^{-2}	----
0.005	1	1.57	1.57	2.13×10^{-2}	4.26×10^{-2}
	1	0.785	0.785	1.37×10^{-3}	3.48×10^{-3}

C. Redundancy

Physical redundancy is an effective means of extending space guidance system reliability design goals to levels that are not attainable with state-of-the-art technology. Therefore, redundancy may be considered as a stop gap, achieved at the expense of other system parameters, to strengthen the weakest links of the guidance system until advanced technology can provide critical items with improved reliability characteristics so as to negate the need for redundancy. The implementation of a redundant guidance configuration requires that certain basic technological ideas be considered. Among these are:

1. A decision defining the type of redundancy to be used and the level at which redundancy is to be established.
2. The ability to detect failure and to correct the malfunction by switching to a redundant unit without permanent loss of the entire system.
3. The trade-offs of system performance, computer requirements, weight, power, volume, etc., associated with redundancy.

The following paragraphs examine the above considerations as related to the inertial sensors of a strapdown navigator for extended duration space mission applications. It is assumed that the strapdown navigator will be used in conjunction with and receive support from additional spaceborne sensors to provide the basic data needed for navigation, guidance and control functions for these missions. The availability of data external to the inertial navigator will be shown to be critical to isolate "failures" caused by the inertial sensors being out of performance specification. However, physical failures can be detected completely within the inertial navigator. The following sections discuss reliability factors, performance, and failure detection functions.

1. Reliability

The failure rate of a system is a measure of the anticipated reliability of the unit when operating under an environment and duty cycle specified for a particular mission. Failure rate estimates are obtained by summing the failure rates of the piece parts that comprise the system. The failure rate of several strapdown sensor package designs of the restrained sensor class for a fairly broad range of missions have been averaged to obtain a representative nondimensionalized failure rate breakdown at the subsystem level assuming that all subsystems are continuously operating. This breakdown is shown in Table V-II. The data presented is a good example of the reliability apportionment attained between the subassemblies of the strapdown sensor

TABLE V-II

NONDIMENSIONAL FAILURE RATE ANALYSIS SUMMARY

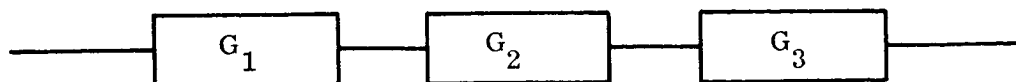
<u>Subassembly</u>	<u>No. of Parts</u>	<u>Nondimensional Failure Rate</u>
<u>Gyro Group</u>		
Gyro	3	.5440
Retorquing Electronics	3	.0822
Sub Total		.6262
<u>Accelerometer Group</u>		
Accelerometer	3	.1511
Retorquing Electronics	3	.1033
Sub Total		.2544
<u>Auxiliary Electronics</u>		
Frequency Countdown	1	.0368
Temperature Control	1	.0168
Crystal Oscillator and Electronics		
Sub Total		.0536
<u>Power Supply</u>	1	.0658
Total		1.0000

- package using current technology. As would be expected, the sensors because of their mechanical nature are most subject to failure. The relative contribution of accelerometer loops in a reliability budget for an extended space mission, however, would be considerably less than that shown in Table V-II. The accelerometers and the temperature controlling of the sensor package would be designed to allow the accelerometers to be turned off except during thrusting periods (including boost, transfer maneuvers, trajectory corrections, orbit keeping etc.). Thus operating time is very small compared to the total mission time. Survival of the boost phase of the mission can be virtually assured by the use of high probable-lifetime components and proper system design and installation. Once in space, thrusting periods are infrequent so that the accelerometers can be shutdown for periods when not needed. Available data indicates that repeated reactivation of the accelerometers does not increase their failure rates above that stated in Table V-II. Thus, the duty cycle of the accelerometers compared to that of the gyros, which must operate over longer periods of time (if not for the entire mission) to maintain the inertial reference, is so small that the reliability of the accelerometer loops have a small effect upon the reliability of the inertial sensor package for extended space missions. Therefore, the most significant modification that can be made to improve reliability is the improvement of gyro loop reliability. Assuming that the most reliable gyros available would be selected for use in extended space missions, further improvements can be achieved only by providing gyro redundancy.

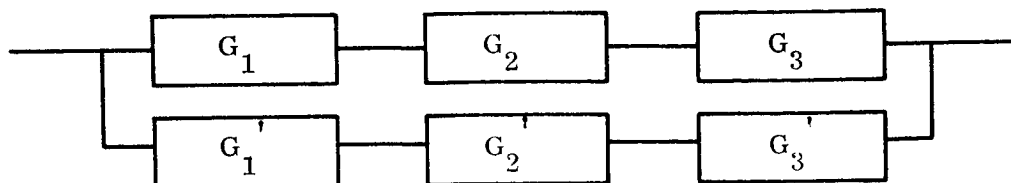
Gyro sensor redundancy can be implemented in several ways. The alternatives considered in this study are shown in Figure V-3. Without redundancy the basic sensor gyro triad can be operationally represented as a serial device; a failure of any one gyro causes a system breakdown. The most obvious approach to sensor redundancy is to provide a second set of three gyros oriented parallel to the first which can be used if a failure occurs in the primary set. The redundant triad could be substituted, either as a complete set (serial-parallel configurations, Figure V-3) or individually (parallel-cross-strapped configurations, Figure V-3) when a failure occurs. For cross-strapped configurations, each gyro in the redundant set provides a backup for a specific gyro in the primary set; therefore, as many as three discrete failures (but only one along each axis of the triad) can be tolerated using a cross-strapped configuration whereas only one can be tolerated in a serial-parallel configuration (substituting on a system basis) before a complete system breakdown occurs. In either the serial-parallel or the cross-strapped arrangements, the redundant sensors can be maintained in either an operative or a standby mode.

Another approach to gyro redundancy is to utilize a single redundant sensor to provide backup for all the gyros in the primary set. In order to accomplish this, the gyro must be oriented so that its sensitive axis does not coincide with that of any gyro in the basis triad (the necessary mathematics to resolve the output of the gyro into the coordinate reference frame of the primary set must be provided in the strap-down navigator). The singular redundant gyro may also be kept in either an operative or standby mode. This approach may be extended even further by using three additional backup sensors each of which is capable of backing up any one of the three sensors of the primary system (Figure V-3).

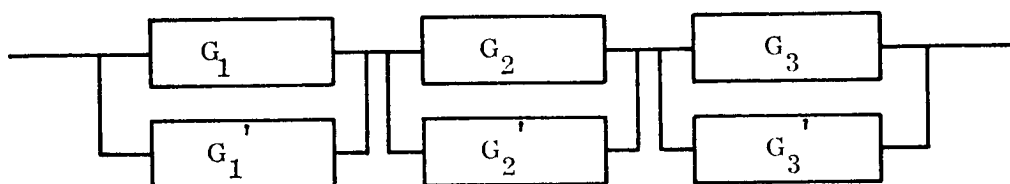
BASIC CONFIGURATION



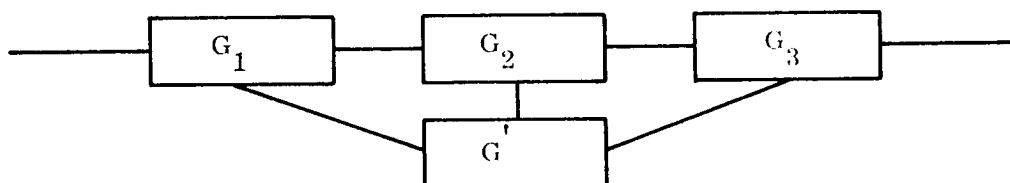
COMPLETE SYSTEM REDUNDANCY SERIAL PARALLEL REDUNDANCY



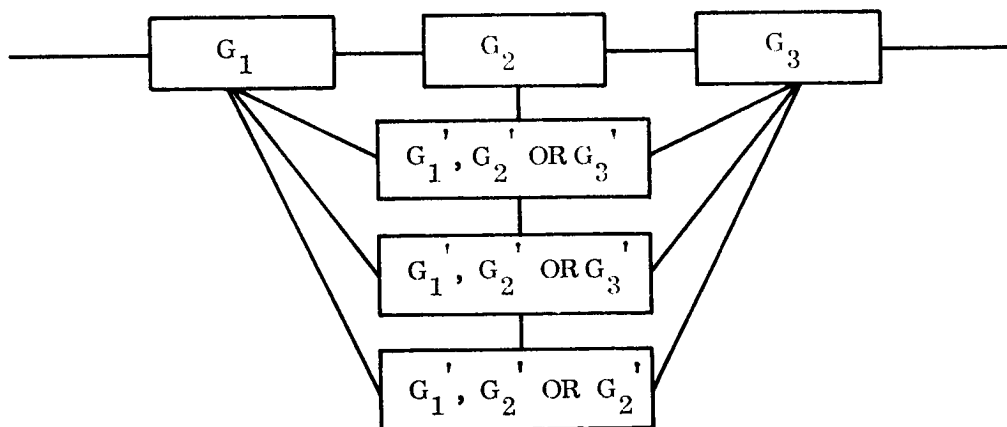
CROSS STRAP - REDUNDANCY



SINGLE GYRO REDUNDANCY



MULTIPLE GYRO REDUNDANCY



66-2226

Figure V-3 Redundant Gyro Configuration Functional Schematic

The improvement in reliability of the gyro sensor loops, considered collectively as a contributing element of overall reliability, has been evaluated parametrically for each of the aforementioned redundant configurations under the following assumptions:

1. The gyros exhibit an exponential failure distribution (i.e., the gyros are operating after run in and before wear exerts an apparent influence on failure rate).
2. The basic gyro and torquing electronic reliability, whether a primary of or redundant sensor, is the same for each element within the configuration.

Figure V-4 presents the probability of success of redundant configurations as a function of the probability of success of a nonredundant triad.

Of the configurations considered, the multiple gyro redundancy mechanization yields the largest increase in gyro system reliability; the standby mode, of course, provides the higher reliability of the two operating modes. For this configuration, three failures of any gyros either in the basic triad or the redundant group can be tolerated.

The completely redundant cross-strapped mechanization yields the next highest increase in gyro system reliability; the standby mode again producing the higher reliability of the two operational modes. For this system up to three failures in the systems, but a maximum of one along any axis of the triad, can be tolerated.

Both the multiple gyro redundancy and the cross-strapped gyro mechanizations are most applicable for strapdown systems. In a gimbaled system, the size and weight penalties that result from implementation of these arrangements are very large because all sensors must be put on the cluster inside the gimbals. Usually a gimbaled inertial unit employs redundancy on a system level as in the serial redundancy mechanization.

Serial system redundancy provides a substantial improvement in overall reliability but not as much as the two previous configurations because the serial system redundancy can only tolerate a single failure. The single gyro redundancy mechanization in fact provides a higher reliability in the operating mode than does the serial system mechanization in the operating mode because there are fewer elements in the single gyro redundant system. In the standby mode, both the single redundant gyro and the system-serial mechanization offer about the same reliability.

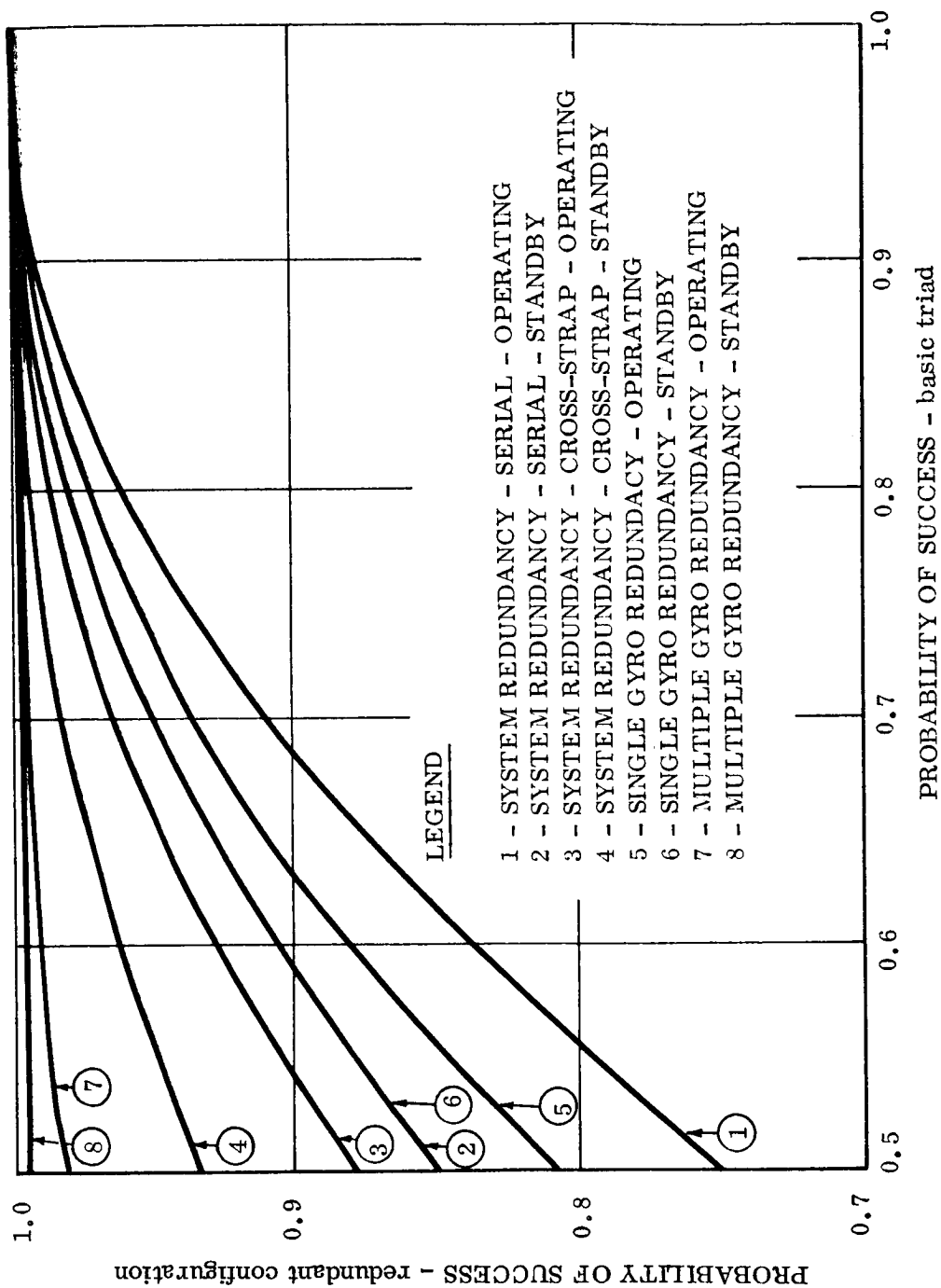


Figure V-4 Effect of Redundancy on Probability of Mission Success

The effect on probability of success (that the gyros operate for the mission duration) using either the single or multiple gyro redundancy approach, the preferred approach for strapdown systems, is extremely large. Figure V-5 depicts probability of success versus time for various mean time between failures. Assuming a triad of gyros of 10,000 hours MTBF and a mission time of a year, the probability of success is about 0.5. Using a single redundant gyro in the standby mode raises the probability of success to 0.85. For three redundancy gyros, the probability of success is 0.994.

Although the multiple redundant gyro system offers the highest reliability of the configurations studied, the singularly redundant gyro offers reliability that is sufficient for many missions plus the advantages in power and weight savings. The three gyros and torquing electronics of the inertial sensor unit typically comprise 25 percent of the total unit weight. To add three additional gyros with matched torquing electronics to this envelope would increase unit weight by 40 to 45 percent allowing for associated increases in structure, insulation, etc. whereas system weight would be increased by 15 to 20 percent if a single gyro torquing electronics were added. The additional power required for thermal control of each additional gyro requirement of the original triad in the standby mode is 1 percent of the basic power. An increase of approximately 10 percent in the maximum power input to the basic unit is required to maintain each additional gyro in an operating mode. Operating all gyros continuously requires increased power over standby conditions and reduces reliability but continuous operation does offer the ability to switch from primary to backup gyros without requiring a period of time for the sensors to reach a condition of stable operation. With power and reliability continuing to remain critical factors for extended duration missions, standby operation appears to be the favorable mode of operation other than during critical phases of the mission such as midcourse corrections and terminal maneuvers.

2. Performance

The performance of the singularly redundant gyro configuration has been studied, both from the standpoint of using the fourth gyro to provide redundant information to improve the accuracy of a properly operating basic triad and from the standpoint of determining the accuracy of the system after the redundant gyro has replaced a failed unit in the primary triad. (The approach applies equally to the multiple redundant gyro system.) As previously pointed out, the redundant sensor must be skewed with respect to each of the primary gyro input axes. Three such configurations illustrated in Figure V-6 were selected for study. The reference configuration on which the performance of all other combinations is based is assumed to be an orthogonal triad with input axes coincident with a body reference coordinate frame. The first redundant configuration places the fourth gyro on a diagonal of the basic system. The second redundant configuration utilizes gyros positioned along diagonals in each quadrant of the reference coordinate system so that no sensor axis is coincident with the body reference

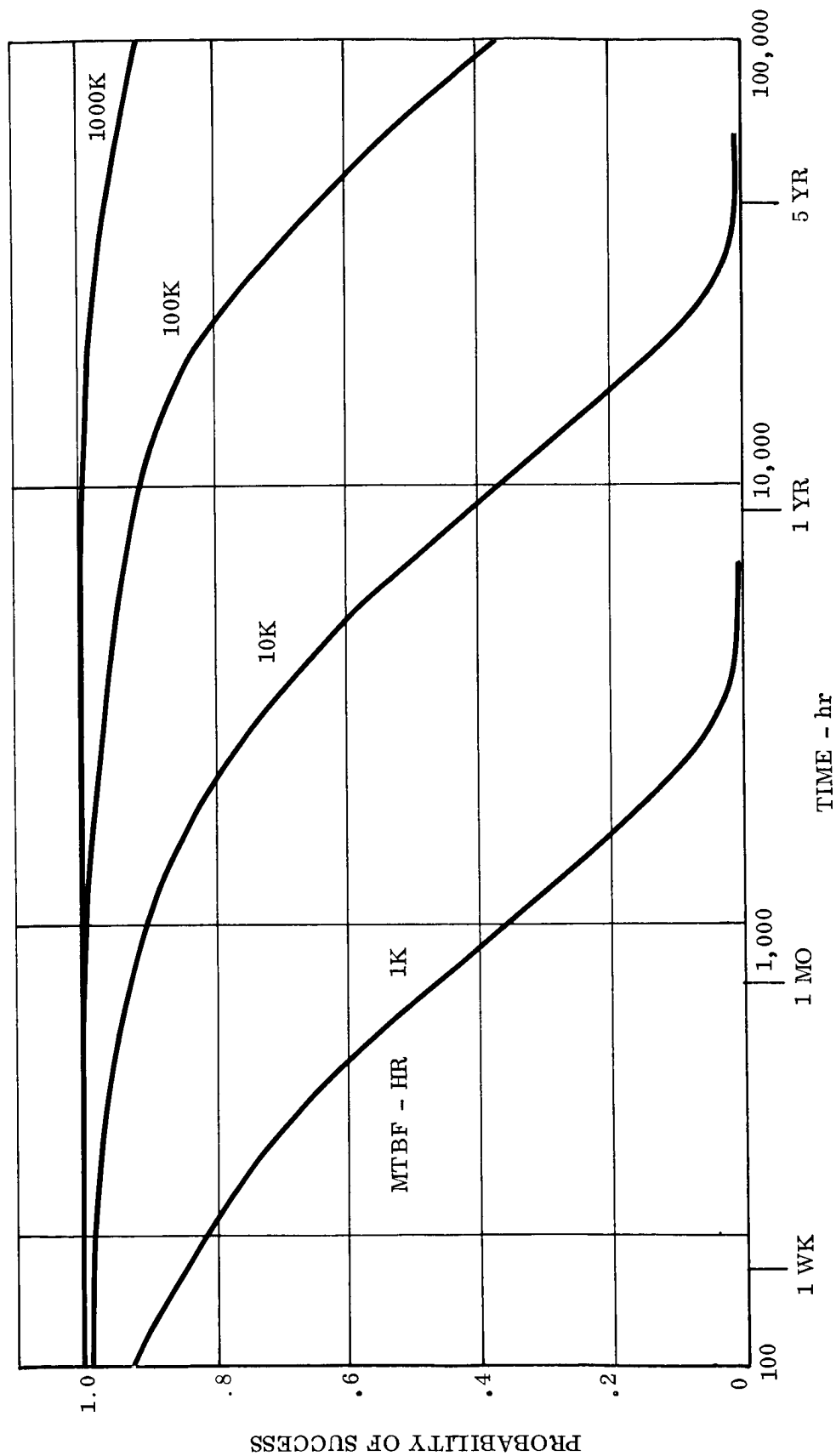


Figure V-5 Effect of MTBF on Probability of Success

CONFIG- URATION NO.	GYRO PLACEMENT	COMPUTED BODY RATES ω_1	AVERAGE BODY RATES ω_1	ERROR VECTOR - 4 GYROS OPERATING EQUAL GYROS		ERROR VECTOR - 3 GYROS OPERATING SKEW GYROS RESCALED	
				SKEW GYROS RESCALED		EQUAL GYROS	
1		$\omega_x = \omega_x$ $\omega_y = \omega_y$ $\omega_z = \omega_z$ $\omega_x = \sqrt{3}\omega_R - \omega_y - \omega_z$ $\omega_y = \sqrt{3}\omega_R - \omega_x - \omega_z$ $\omega_z = \sqrt{3}\omega_R - \omega_x - \omega_y$	$\bar{\omega}_x = \frac{1}{2}(\omega_x + \sqrt{3}\omega_R - \omega_y - \omega_z)$ $\bar{\omega}_y = \frac{1}{2}(\omega_y + \sqrt{3}\omega_R - \omega_x - \omega_z)$ $\bar{\omega}_z = \frac{1}{2}(\omega_z + \sqrt{3}\omega_R - \omega_x - \omega_y)$	$(4.5B^2 + 1.5SF^2)^{1/2}$	$(9B^2 + 3SF^2)^{1/2}$	$(7B^2 + 3SF^2)^{1/2}$	$(13B^2 + 5SF^2)^{1/2}$
2		$\omega_x = \frac{\sqrt{3}}{2}(\omega_a - \omega_d) = \frac{\sqrt{3}}{2}(\omega_b - \omega_c)$ $\omega_y = \frac{\sqrt{3}}{2}(\omega_a - \omega_b) = \frac{\sqrt{3}}{2}(\omega_d - \omega_c)$ $\omega_z = \frac{\sqrt{3}}{2}(\omega_a + \omega_c) = \frac{\sqrt{3}}{2}(\omega_b + \omega_d)$	$\bar{\omega}_x = \frac{\sqrt{3}}{4}(\omega_a + \omega_b - \omega_c - \omega_d)$ $\bar{\omega}_y = \frac{\sqrt{3}}{4}(\omega_a - \omega_b - \omega_c + \omega_d)$ $\bar{\omega}_z = \frac{\sqrt{3}}{4}(\omega_a + \omega_b + \omega_c + \omega_d)$	$(2.25B^2 + .75SF^2)^{1/2}$	$(6.75B^2 + 2.25SF^2)^{1/2}$	$(4.5B^2 + 1.5SF^2)^{1/2}$	$(13.5B^2 + 4.5SF^2)^{1/2}$
3		$\omega_x = \omega_a - \omega_d = \omega_b - \omega_c$ $\omega_y = \omega_a - \omega_b = \omega_d - \omega_c$ $\omega_z = \frac{1}{\sqrt{2}}(\omega_a + \omega_c) = \frac{1}{\sqrt{2}}(\omega_b + \omega_d)$	$\bar{\omega}_x = \frac{1}{2}(\omega_a + \omega_b - \omega_c - \omega_d)$ $\bar{\omega}_y = \frac{1}{2}(\omega_a - \omega_b - \omega_c + \omega_d)$ $\bar{\omega}_z = \frac{1}{2\sqrt{2}}(\omega_a + \omega_b + \omega_c + \omega_d)$	$(2.5B^2 + .625SF^2)^{1/2}$	$(10B^2 + 2.5SF^2)^{1/2}$	$(5B^2 + 1.25SF^2)^{1/2}$	$(20B^2 + 5SF^2)^{1/2}$

Figure V-6 Redundant Gyro Equations and Sensor Arrangements

coordinate axes. The third configuration is similar to the second except that the gyro input axes are placed along equally spaced elements of a right circular cone.

With each of the above configurations the angular rate about any one of the body reference axes can be calculated with the output of any of the three gyros. Geometrical expressions for translating sensed gyro rates to computed body axis rates for each of the above redundant configurations are shown in Figure V-6. The redundant data provided by a fourth gyro permits body angular rates to be calculated by means of two alternate expressions for each assignment if all gyros are operating. Thus, performance improvements attained by averaging the two pieces of redundant data made available by operating all four gyros simultaneously should be achieved by averaging. The computer requirements for performing this averaging sequence are shown in Figure V-6 and are small. Averaging, of course, cannot be performed when one gyro has failed. When a gyro has failed the alternate calculation of rate still exists.

Performance analyses have shown that modest accuracy improvements can be achieved by using a fourth gyro to provide redundant sensor information. The qualitative measure of system accuracy used in these studies for both redundant information and replacement modes of operation is the root-sum-square (RSS) value of the errors appearing on each of the reference coordinate axes. The apparent errors on the coordinate axes are comprised of individual sensor errors which are combined geometrically in accordance with the previously discussed rate expressions shown in Figure V-6. Non-thrusting orbital motion has been assumed so that only the bias (B), scale factor (SF) and input axis (which can be treated as a scale factor error) error terms can be considered. Appropriate expressions for the resultant system error vector are presented in Figure V-6.

The performance of the redundant configuration is affected by the manner in which the maximum angular rate environment for a particular mission occurs. For example, all gyros could be scaled the same to meet a rate environment specified such that "the instantaneous rate about an arbitrary axis shall not exceed a specified value". If, however, the rate environment is specified such that maximum rates about each coordinate reference axis can be imposed simultaneously, one or more of the gyros (as appropriate) used in the reference basic triad capable of following the motion must be rescaled in order to follow the larger resultant angular motion which exists about axes that are not principal body axes. A given strapdown gyro can be rescaled to follow higher angular rates but usually only with an appropriate growth of the instrument errors.

Expressions for the system error vector for both maximum rate specifications are presented in Figure V-6 for both redundant information and replacement modes of operation.

Table V-III summarizes a comparison of the performance of normal and appropriately rescaled redundant gyro systems with the performance achieved by the reference triad considering bias errors only. The performance figure of merit is the performance of the noted configuration divided by the performance of the basic triad. The performance figure of merit operating under each of the four conditions is strongly affected by the geometry of the sensor arrangement and the angular rate specification. (None of these arrangements are proposed to be optimum. They are simply cases that have been selected to study the variations in performance.)

TABLE V-III
REDUNDANT SENSOR PERFORMANCE SUMMARY

Configuration	CONFIGURATION ERROR BASIC TRIAD ERROR			
	REDUNDANT OPERATION		REPLACEMENT OPERATION	
	Normal*** Gyro Scaling	Appropriate** Gyro Rescaled	Normal*** Gyro Scaling	Appropriate** Gyro Rescaled
Basic Triad	1.00	NA*	---	---
#1	1.224	1.732	1.523	2.08
#2	.866	1.502	1.223	2.110
#3	.912	1.825	1.292	2.585

* Rescaling not required

** Maximum angular rate components about all three axes simultaneously

*** Maximum angular rate about any arbitrary body axis

3. Failure Detection

Implicit in the concept of redundancy is the ability to sense and isolate component failures. Gyro failures may be categorized into two types:

1. Sudden, catastrophic failures rendering the sensor completely inoperative.
2. Partial failures, either sudden or gradual, which degrade the performance of the unit to an unacceptable level.

Complete or sudden failure of the gyro can usually be traced to a mechanical or electrical breakdown within the gyro or its torquing electronics. Experience with gyro failures indicates that this type of failure can be effectively detected by monitoring critical parameters, such as wheel speed (by means of a Spin Motor Rotation Detection device) or the torquing electronics output pulse train, in serene environments. With this type of monitoring technique, the identity of the failed unit is determined directly. The computer switching logic required to monitor and mathematically implement the substitution of the redundant unit into the configuration is very small as compared to the requirements of the total system. Catastrophic failures by their nature usually are impossible to detect before they happen so that some means of reinitializing the inertial attitude reference must be provided. External data is needed to update attitude errors accrued during periods when the gyro system is inoperative. This data can be provided by stellar measurements.

Partial gyro failures are more difficult to isolate than complete failures. A method of determining if a partial failure has occurred is to compare the two alternate methods of computing angular rates (Figure V-6) by periodically running all redundant gyros along with the basic triad. If the computed rates do not agree within a predetermined tolerance, it can be assumed that a failure has occurred. The technique, to this point, does not require the use of any information external to the system. However, due to the cross-coupling between the body rate equations, it is impossible to isolate the failure without the use of additional data. Consequently, if a failure has been detected, external information must be used to complete the diagnosis. Stellar trimming or similar procedure for updating gyro bias is one technique to provide this information. If the gyro drift error established by two successive stellar measurements exceeds a pre-established schedule, this can be interpreted as a probable failure of that unit and the appropriate substitution can be made and the system reinitialized.

It should be noted also that partial gyro failures through performance degradation of the basic triad can be ascertained directly from information derived from stellar measurements if they are periodically performed as a matter of course throughout the mission. This prospect offers the advantage of eliminating the need to periodically activate the redundant gyros.

VI. COMPUTATIONAL REQUIREMENTS STUDY

In conjunction with the development of analytic models of the computational errors associated with strapdown navigation systems, a digital computer program has been developed which employs these error models to evaluate the effect of the computational process upon attitude, velocity and position accuracy throughout the mission. The previous section and the appendices of this volume describe these computational error models and the second volume of this report describes the digital program and its use. This section evaluates the computational requirements of a restrained strapdown navigation system for a translunar mission and phases thereof. The translunar mission consists of the following phases: boost, injection into a parking orbit, coast and injection onto the translunar trajectory. These phases of the mission apply equally as well to many other space missions. Similarly, they share assumed flight environments encompassing a wide range of launch vehicles.

The first part of this section discusses the error sources and tradeoffs that exist between the sensors and computational processes in the presence of a dynamic environment. Both the sensor and computational processes must be considered simultaneously in a system design process as they process the same data in a serial fashion. The next part defines the flight environments assumed for this study. The final section presents a parametric evaluation of the computational error in terms of computational and computer characteristics. The results presented should be viewed as an example and a guideline rather than as a broad, generalized projection of future computer requirements because of the strong, critical interaction that exists between the vehicle vibratory environment, the structural characteristics of the sensor package mounting shelf, the sensor loop frequency response characteristics and the computational process.

A. System Error Analysis

A strapdown navigator during thrusting phases of flight requires the coordinated operation of gyro and accelerometer sensors in conjunction with a computational process to accomplish the navigation function. As usually mechanized, the computational process for a restrained sensor system is

$$\bar{V}^I = \left[\int \begin{bmatrix} T_b^I \\ \omega \end{bmatrix} dt \right] \cdot \int F^{-b} dt - \int g^{-I} dt$$

which is intended to approximate

$$\bar{V}^I = \int \left(F \begin{bmatrix} -I \\ -g \end{bmatrix} \right) dt$$

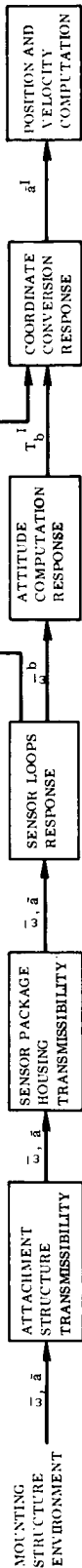
In these equations \bar{V} represents velocity, T_b^I the attitude of the vehicle relative to the inertial computational frame, $[\omega]$ is the rate matrix describing the inertial attitude of the vehicle, \bar{F} is specific force and \bar{g} is gravitational acceleration. The sequential coupling of the sensors and computational process in implementing this navigation process is shown functionally in the top section of Figure VI-1. The bottom section of the same figure displays the coupling between the flight environment and the errors in the navigation process.

The objective of navigation system performance design is to achieve a given level of performance for a specified flight environment within one or more other system constraints, i. e., reliability, cost, weight, power, etc. Sometimes the converse problem is posed: optimize performance for specified reliability, weight, power, etc. In achieving this objective, the entire navigation process must be simultaneously considered and analyzed. An error allocation or budget must be formulated considering the relative significance of individual error sources upon both total mission performance and the physical characteristics of the system. The evaluation of navigation performance requirements (sensors plus computational) requires a specification of the flight environment, the desired system performance and the determination of the weighting factors between component performance requirements and the total system's physical characteristics.

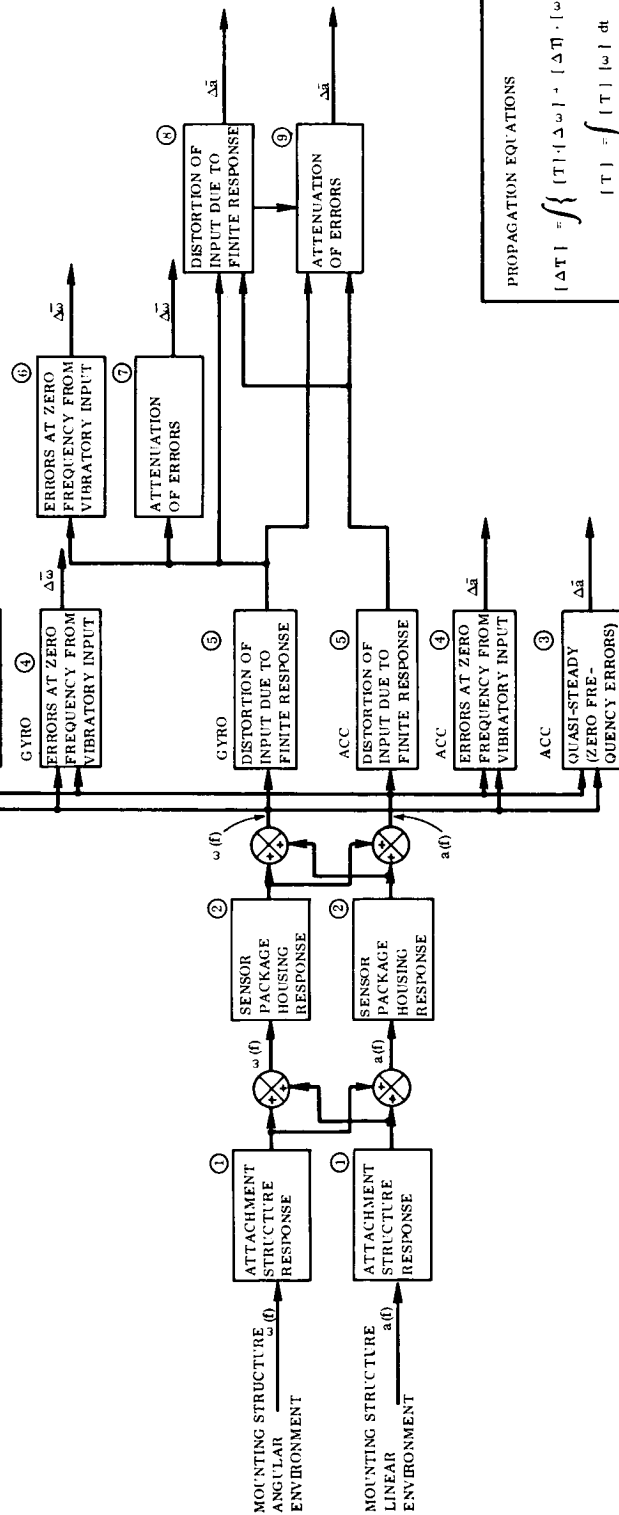
In a subsequent section the computational requirements versus accuracy for an assumed flight environment and sensor characteristics are parametrically presented. In order to place the assumptions in **proper perspective** all the navigation system error sources and their interactions are summarized in the following paragraphs.

With reference to Figure VI-1, the flight environment to which the system is subjected is usually specified at the mounting structure to which the inertial sensor package is attached. The environment consists of: (1) zero or low frequency angular motions associated with vehicle control and its flexible bending modes, (2) linear acceleration associated with the main propulsion unit, and (3) both linear and angular vibratory motion distributed over the frequency spectrum, arising principally from the main propulsion unit. The task of the navigation system is to sense the angular and linear motion applied to it and to compute its attitude, velocity and position. By reason of its mechanical attachment to the vehicle, these data are also an excellent estimate of vehicle conditions. In Figure VI-1, the angular and linear flight environments are transferred to the sensors through the sensor package attachment structure and the sensor housing structure itself (Boxes 1 & 2). The mechanical design of the sensor package attachment and housing structure therefore are an integral part of the performance analysis and design of the system. The attachment structure may be hard or soft (shock mounts or a vibration isolation system), while the sensor housing should be stiff. A rigid sensor housing is desired

NAVIGATION SYSTEM INFORMATION FLOW



NAVIGATION SYSTEM INFORMATION ERROR MODEL



PROPAGATION EQUATIONS

$$[\Delta T] = \int \{ [T] \cdot [\Delta \omega] + [\Delta T] \cdot [\omega] \} dt$$

$$[T] = \int [T] \cdot [\omega] dt$$

$$\Delta \dot{V} = \int \{ [T] \cdot \Delta \dot{a} + [\Delta T] \cdot \dot{a} \} dt$$

$$\Delta \dot{P} = \int \Delta \dot{V} dt$$

87-104

Figure VI-1 Navigation System Information Error Model

to preserve the mechanical alignment between sensor input axes and the sensor package reference orthogonal coordinate frame to which all data is resolved prior to computing attitude and resolving accelerometer data into the inertial computational frame. It is functionally indicated in this figure that the attachment and housing structures can translate a linear environment into both linear and angular motion as seen by the sensors: Similarly angular motion can be translated into both linear and angular motion.

In addition to the typically treated sensor errors - the zero frequency quasi-steady errors of bias, scale factor, rectification, etc., denoted in boxes labeled 3 and 4, there exists an additional group of errors that arise through the distortion of the true signal by the sensor due to its finite frequency response, both phase and amplitude (Box 5). These errors arise in the presence of correlated angular and linear motion input to more than one inertial sensor. Examples are: (1) unmatched phase response between the gyro triad that result in an unbounded attitude drift rate for sinusoidal inputs having components on more than one gyro input axis and (2) unmatched frequency response (both amplitude and phase) between the gyros and accelerometers, that result in unbounded velocity drift rate. These errors cannot, however, be considered alone; these errors can be amplified or attenuated by the attitude and coordinate conversion process (Boxes 7 and 9) depending upon the frequency of the output signal and the frequency of the computation. Ref 12 describes these errors, their models and the characteristics of the interaction in detail.

In Box 6, the attitude computational errors of truncation and roundoff are represented. As described in Section IV, these errors are affected by the computer and computational characteristics and the angular motion passed onto the computational process by the gyros. Of predominant importance is the gyro loop's amplitude ratio (a function of frequency) as it defines the frequency range of the significant motions to be followed by the computational process. In Box 8, the distortion of the angular motion caused by a finite coordinate transformation frequency in resolving the accelerometer outputs into the inertial frame is functionally represented. This error is associated with the uncertainty in knowledge of the orientation of the accelerometer input axes between attitude computational interval and occurs because

$$\int \left[T_b^I \right] \cdot [\omega] dt \cdot \int \bar{f}^b dt$$

is used to approximate

$$\int \left\{ \int \left[T_b^I \right] \cdot [\omega] dt \cdot \bar{f}^b \right\} dt$$

in the navigation process. The size effect error described in Section IV is typical of this class of error.

The effect of each of these classes of errors can be appropriately modeled in terms of an error rate ($\Delta\omega$) or error acceleration ($\Delta\alpha$) in the sensor or vehicle frame. The computational error models have been previously presented in this report; Reference 12 summarizes the sensor, coupled sensor and coupled computer-sensor errors. To evaluate the effect of these errors on system performance (attitude, velocity and position) a linearized set of navigation or propagation equations can be employed; the enclosed box of Figure VI-1 represents one type of linearized propagation equations.

With a system performance model formulated as above, the design of the system for a particular mission or missions can be accomplished in performing such an analysis. The following areas may warrant tradeoff studies: 1) attachment structure resonance frequency, sensor loop bandwidth and computational frequency; 2) dynamic and quasi-steady error allocations, and 3) allocation of errors between the various dynamic errors and between the various quasi-steady errors.

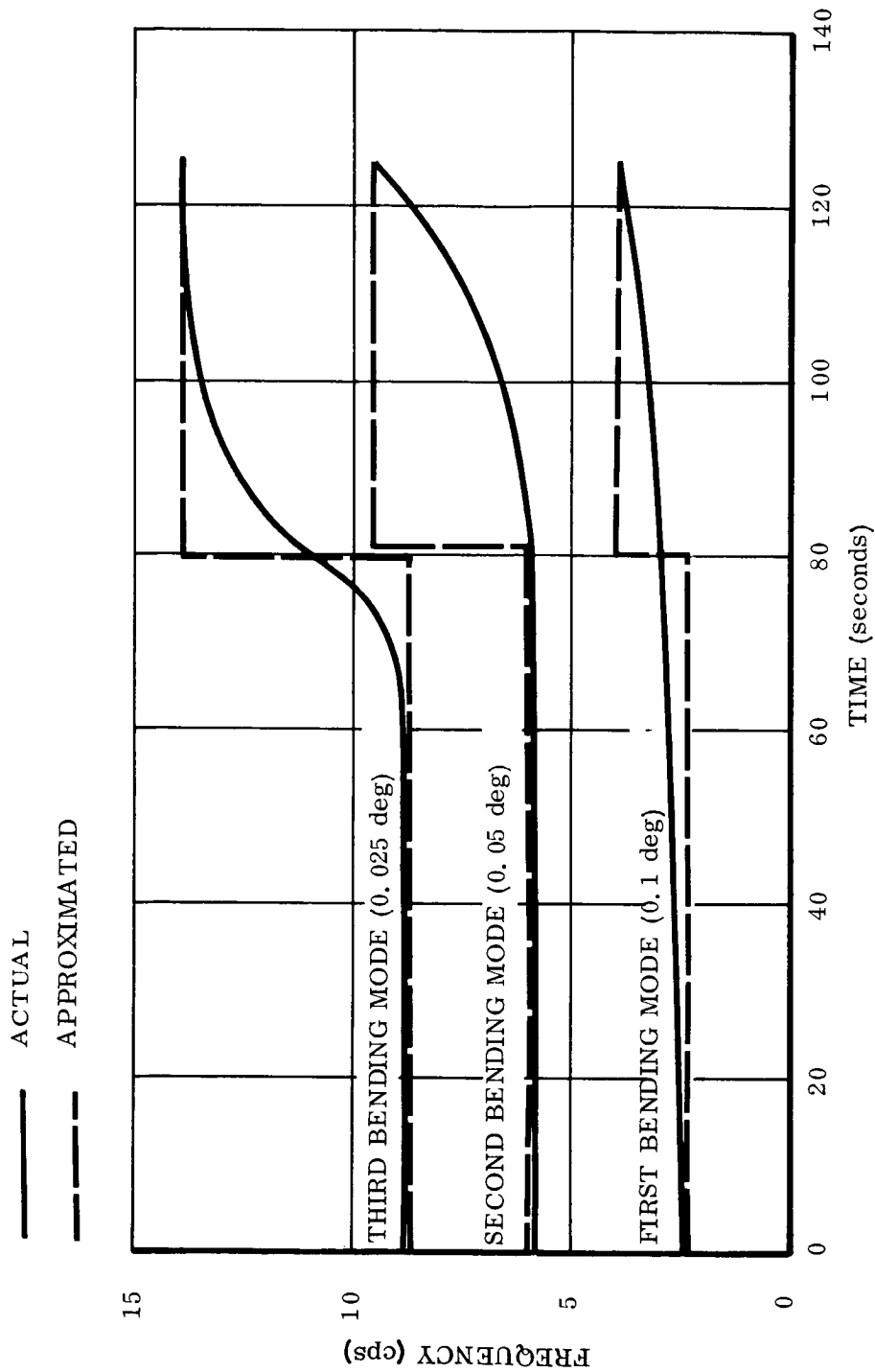
B. Flight Environments

The flight environments employed in the computational requirements study are presented in this section. The mission selected for analysis was that of a boost and injection in a circular (108) n mi) parking orbit, a coast phase of one period and then an injection onto a translunar trajectory. The flight environment employed was that of an Atlas-Centaur which is also typical of an Atlas-Agena and a Thor-Delta environment.

Figure VI-2 presents the atmospheric angular induced motion for the first three vehicle bending modes lasting for the first 140 seconds of flight. The dashed lines are the approximations employed in the analysis in order to reduce the amount of data into the digital evaluation program.

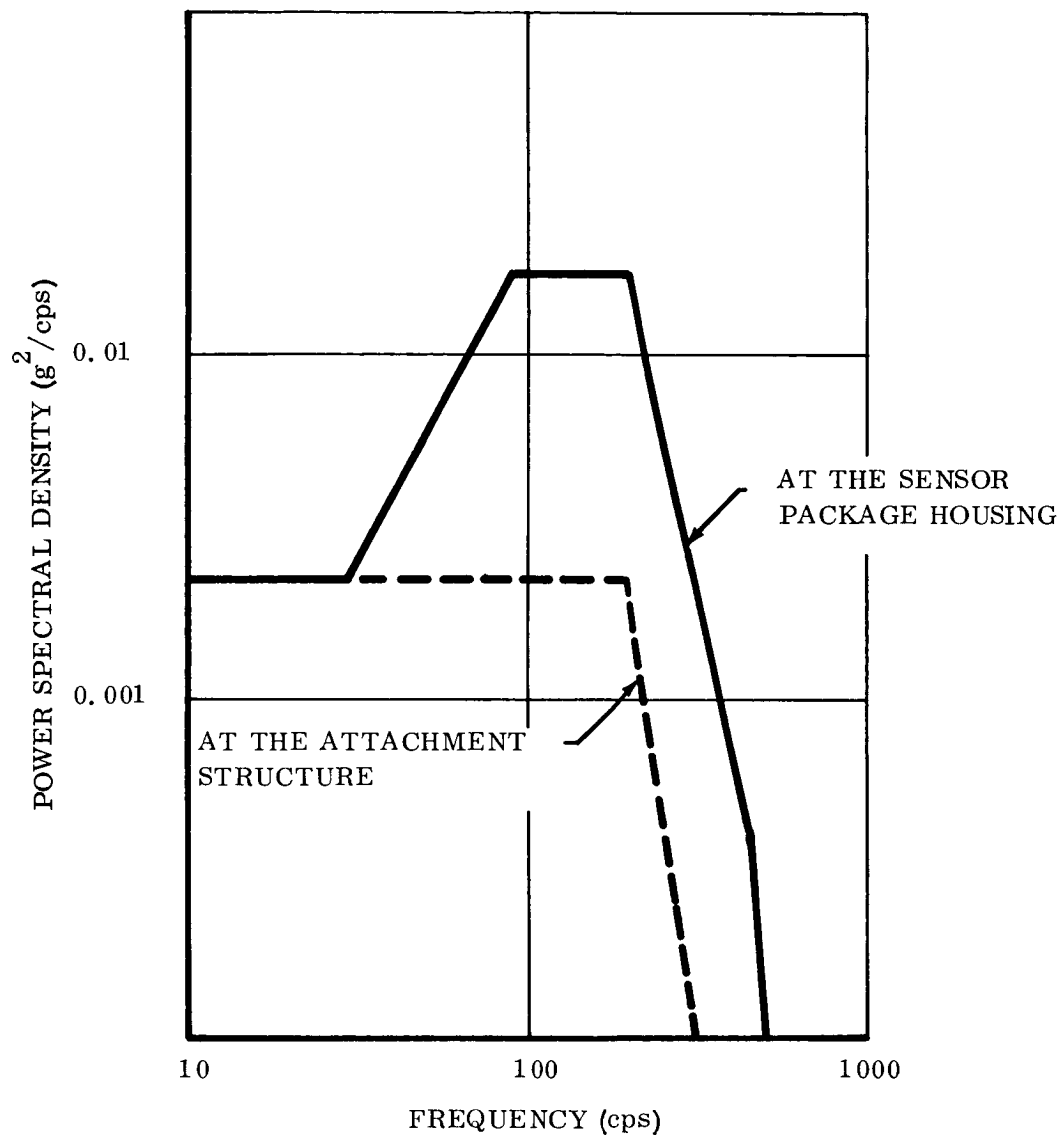
In addition to these atmospheric induced motions, a control system limit cycle of 2 deg/sec at 2 cps about each of the vehicle axes was assumed during all phases of power flight. During the free flight portion of the mission, a control limit cycle of 1 degree amplitude with a period of 200 seconds is assumed.

Figure VI-3 presents the linear vibratory input envelope at the Centaur mounting shelf measured during the flight of AC-2. The solid line represents the estimated amplification of the environment by a sensor package attachment structure characterized by a structural resonance at 200 cps with an amplification factor of 3. Associated with this linear environment is the estimated induced angular



67-184

Figure VI-2 Atmospheric Induced Angular Motion



67-183

Figure VI-3 Linear Power Spectral Density

environment presented in Figure VI-4 for a non-cg mounted sensor package of the size and shape of the LEM Abort Sensor Assembly. This estimated linear induced angular environment represents the path in Figure VI-1 from block 1 associated with the linear environment to the environment summer in the angular environment line. These estimates of induced angular motion were based upon planar or two-dimensional models; a three dimensional model to evaluate the possibility of introducing coning motion is not available.

These environments form the basis for evaluating the effect of different strap-down computational processes upon navigational accuracy presented in the following section. It was assumed that the band width of the gyros were significantly wide to pass all of the vibrating motion shown in Figure VI-4 onto the computer.

C. Analysis Results

Using the program described in Volume II, four computational and computer configurations were analyzed; the attitude errors and their effect upon navigational accuracy were established. These studies were performed for the trajectory and flight environment described in Appendix E of Volume II. The computer and computational configurations investigated are shown in Table VI-I.

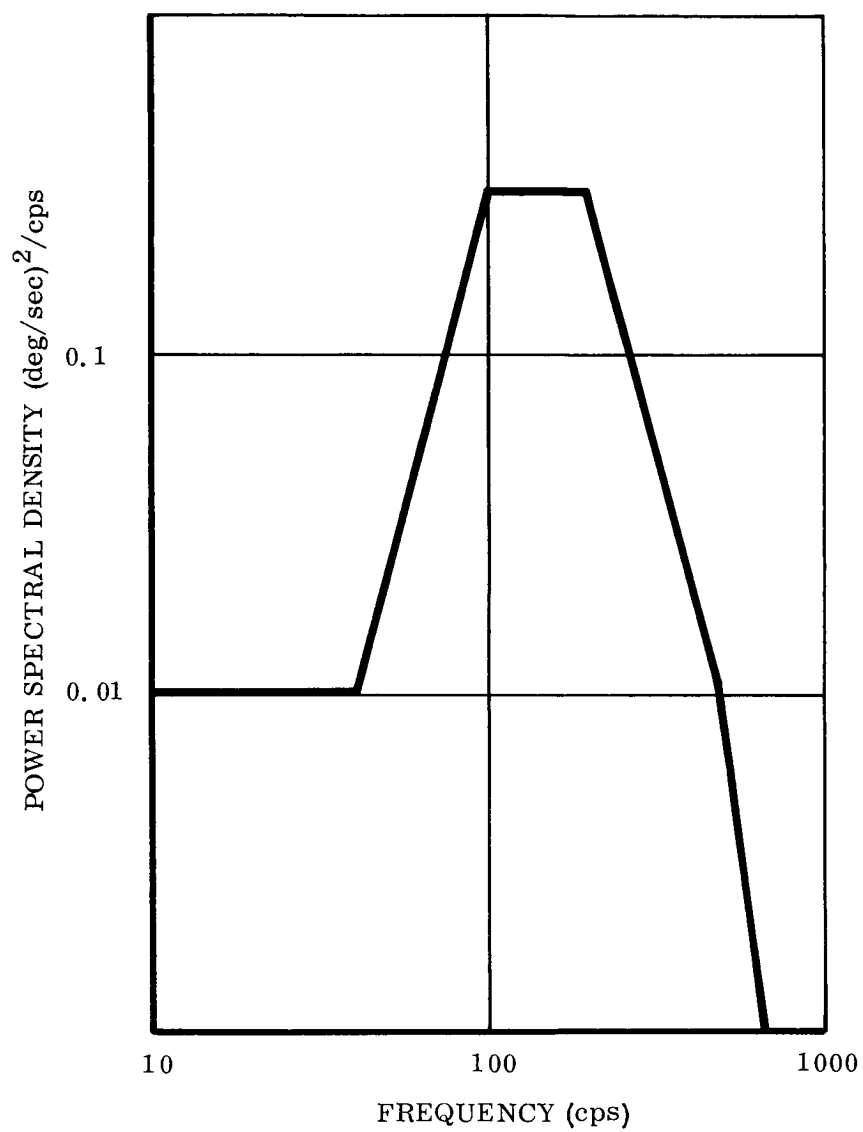
TABLE VI-I

SUMMARY OF COMPUTATIONAL CHARACTERISTICS FOR SIMULATION RUNS

Configuration Number	Word Length (bits)	Attitude Integration Scheme (order)	Attitude Frequency (cps)	Coordinate Conversion Scheme (order)	Coordinate Conversion Frequency (cps)
1	35	1st	200	2nd	200
2	27	1st	100	4th	50
3	30	2nd	100	2nd	100
4	27	2nd	50	4th	25

Because the computational errors are independent, the various processes analyzed and their associated errors can be permuted into many different combinations. In this section the various errors will be discussed in three groups:

- 1) Roundoff associated with computer word length used in the attitude process;
- 2) Truncation associated with the integration scheme and frequency used in the attitude process; and



67-185

Figure VI-4 Angular Power Spectral Density

- 3) Coordinate conversion associated with the scheme and frequency used to resolve the accelerometer data into the inertial computational frame.

The truncation errors are associated with the attitude computational process following the motions described by the constant pitch rate of the vehicle and the sinusoidal and vibratory motions described in the previous figures. Table VI-II presents the legend employed in Table VI-III through VI-VI wherein the navigational errors due to initial conditions and the computational errors are presented for the four configurations analyzed. Initial condition errors of 20, 20 and 10 meters for downrange, crossrange and altitude and 20, 10 and 10 arcseconds for azimuth, in-plane and out of plane vertical alignment were assumed. The errors were evaluated at five points within the trajectory; segment (1) at 80 seconds at which the atmospheric induced motions were changed; segment (2) at 140 seconds corresponding to the termination of the first stage; segment (3) at 560 seconds corresponding to the termination of the second stage and injection into a 108 n mi circular orbit; segment (4) at 5900 seconds with the completion of one orbit; and segment (5) at 6065 seconds after a ΔV of 10,000 ft/second was applied tangential to the orbit. In these tables the attitude error (DELR), the downrange error (DELRD), the crossrange error (DELCR), the velocity magnitude error (DELV) and the in-plane (DELGAM) and out-of-plane (DELP) velocity errors are shown.

In order to graphically examine the variations in performance with different computational characteristics, the total position and velocity errors at 560 seconds are presented in Figure VI-5 through 7 for truncation, roundoff and coordinate conversion, respectively. In these figures, the actual data points obtained from the simulation are circled; the dash lines connecting these points and extrapolating beyond are based upon the analytical models presented in Section IV.

In Figure VI-5, the truncation error for the first order integration process is presented as a function of computational frequency. The curve presented represents the root sum square of the errors due to the constant rate, the sinusoidal and random environments. For the angular environments considered, the truncation error for the second order process is negligible as indicated in Tables VI-5 and 6. (Similarly the errors for any higher order integration scheme would also be negligible.) In the first order data presented, the truncation error decreases then increases as the computational frequency is increased. This behavior is the result of the interaction of the sinusoidal and random environments. For the sinusoidal motion, the computational error decreases as computational frequency is increased. For the vibratory input, the analytic model developed provides an optimistic estimate of the error; in fact, the model's characteristics are such that the vibratory motion at frequencies beyond the computational frequency yield no error at all. For this reason, the computational error using this model is a function of only the environment at frequencies below that of the computer. Therefore, with reference to

TABLE VI-II
DEFINITION OF ERROR SOURCES

ES	ERROR DEFINITION
2	INITIAL RADIAL POSITION
3	INITIAL DOWNRANGE POSITION
4	INITIAL CROSSRANGE POSITION
5	INITIAL RADIAL VELOCITY
6	INITIAL DOWNRANGE VELOCITY
7	INITIAL CROSSRANGE VELOCITY
8	AZIMUTH ALIGNMENT
9	INPLANE VERTICAL MISALIGNMENT ANGLE
10	OUT OF PLANE VERTICAL MISALIGNMENT ANGLE
11	CONSTANT RATE TRUNCATION
12	SINUSOIDAL RATE TRUNCATION (X BODY AXIS)
13	SINUSOIDAL RATE TRUNCATION (Y BODY AXIS)
14	SINUSOIDAL RATE TRUNCATION (Z BODY AXIS)
15	ROUND OFF (X BODY AXIS)
16	ROUND OFF (Y BODY AXIS)
17	ROUND OFF (Z BODY AXIS)
18	CONING TRUNCATION (X BODY AXIS)
19	CONING TRUNCATION (Y BODY AXIS)
20	CONING TRUNCATION (Z BODY AXIS)
21	VIBRATORY TRUNCATION (X BODY AXIS)
22	VIBRATORY TRUNCATION (Y BODY AXIS)
23	VIBRATORY TRUNCATION (Z BODY AXIS)
24	GYRO QUANTIZATION (X BODY AXIS)
25	GYRO QUANTIZATION (Y BODY AXIS)
26	GYRO QUANTIZATION (Z BODY AXIS)
27	SIZE EFFECT

TABLE VI-III
ERROR SUMMARY FOR CONFIGURATION 1

ERROR SUMMARY FOLLOWS							
FLIGHT SEGMENT 1							
ES	DELRA(M)	DELDL(M)	DELCR(M)	DELVEL(M/S)	DELGM(URAD)	DELPST(URAD)	DELTIME(MSEC)
2	10.1	-0.1	-0.0	C.00	-2.3	0.	0.
3	0.1	19.9	0.1	-C.00	-1.2	0.	0.
4	0.1	-0.0	19.9	-C.00	0.0	-2.6	C.
5	0.	-0.	0.	-C.00	0.0	0.	0.
6	-0.0	-0.0	-0.0	-C.00	0.	0.	0.
7	0.	-0.	0.	-C.00	0.0	0.	0.
8	0.0	-0.0	0.5	-C.00	-0.1	43.9	C.
9	0.0	0.0	-2.5	C.00	0.1	-62.7	0.
10	-0.3	2.2	-0.1	C.04	48.3	0.	0.
11	-0.2	0.2	0.1	C.01	12.9	0.	0.
12	-0.0	-0.0	0.2	-C.00	-0.0	12.7	0.
13	-0.1	0.0	-2.8	C.00	0.1	-115.8	0.
14	-0.7	2.6	-0.1	C.07	97.8	0.	0.
15	0.	-0.	0.	-C.00	0.1	0.	0.
16	0.	-0.	0.	-C.00	0.0	0.	0.
17	0.0	0.0	0.0	0.00	0.2	0.	0.
18	0.	-0.	0.	-C.00	0.0	0.	0.
19	0.	-0.	0.	-C.00	0.0	0.	0.
20	0.	-0.	0.	-C.00	0.0	0.	C.
21	0.1	-0.0	1.5	-C.00	-0.1	104.6	C.
22	-0.0	0.0	-7.9	C.00	0.4	-338.4	0.
23	-2.1	7.6	-0.0	C.20	285.5	0.	0.
24	0.	-0.	0.	-C.00	0.0	0.	0.
25	0.	-0.	0.	-C.00	0.0	0.	0.
26	C.	-0.	0.	-C.00	0.0	0.	0.
27	0.2	0.0	-0.1	C.00	-4.4	0.	0.
RSS	10.3	21.6	21.8	C.21	306.0	380.6	0.

TABLE VI-III (Continued)

ES	FLIGHT SEGMENT 2	DELRA (M)	DELDL (M)	DELCR (M)	DELVEL (M/S)	DEL GAM (URAD)	DEL PSI (URAD)	DEL TIME (MSEC)
2	10.2	-0.2	0.1	0.00	-1.4	0.	0.	0.
3	0.4	19.7	0.1	-0.00	-0.5	0.	0.	0.
4	0.1	-0.0	19.7	-0.00	0.0	-1.5	0.	0.
5	-0.0	-0.0	-0.0	0.	0.0	0.	0.	0.
6	-0.0	-0.0	-0.0	-0.00	0.0	0.	0.	0.
7	-0.0	-0.0	-0.0	0.	0.0	0.	0.	0.
8	0.1	-0.0	7.2	-0.00	-0.1	76.8	0.	0.
9	-0.2	0.0	-7.4	0.00	0.1	-40.5	0.	0.
10	-3.5	7.3	-0.1	0.07	50.3	0.	0.	0.
11	-1.7	2.0	0.1	0.02	27.9	0.	0.	0.
12	0.0	-0.0	2.7	-0.00	-0.1	33.4	0.	0.
13	-0.4	0.0	-20.5	0.00	0.2	-225.9	0.	0.
14	-14.4	16.7	0.1	0.19	246.8	0.	0.	0.
15	-0.0	-0.0	-0.0	0.	0.0	0.	0.	0.
16	-0.0	-0.0	-0.0	-0.00	0.0	0.	0.	0.
17	-0.1	0.0	0.0	0.00	0.4	0.	0.	0.
18	-0.0	-0.0	-0.0	0.	0.0	0.	0.	0.
19	-0.0	-0.0	-0.0	0.	0.0	0.	0.	0.
20	-0.0	-0.0	-0.0	-0.00	-0.2	274.4	0.	0.
21	0.1	-0.1	22.8	-0.00	0.4	-517.7	0.	0.
22	-0.3	0.1	-53.3	0.50	578.9	0.	0.	0.
23	-36.4	44.9	0.2	0.	0.0	0.	0.	0.
24	-0.0	-0.0	-0.0	0.	0.0	0.	0.	0.
25	-0.0	-0.0	-0.0	0.	0.0	0.	0.	0.
26	-0.0	-0.0	-0.0	0.	0.0	0.	0.	0.
27	1.0	0.6	-0.1	0.02	-3.3	0.	0.	0.
RSS	40.7	52.4	65.4	0.54	632.0	634.8	0.	0.

TABLE VI-III (Continued)

FLIGHT SEGMENT 3		DELRA(M)	DELR(M)	DELCR(M)	DELVEL (M/S)	CELGAM(URAD)	DELPSI(URAD)	DELTIME(MSEC)
ES								
2	14.3	-4.7	-0.2	-C.00	-2.3	0.	0.	0.
3	5.6	14.5	0.1	-C.02	0.1	0.	0.	0.
4	-0.2	-0.1	15.6	-0.00	0.0	-1.9	0.	0.
5	-0.0	-0.0	-0.0	-0.00	0.0	0.	0.	0.
6	-0.0	-0.1	-0.0	-C.00	0.0	0.	0.	0.
7	-0.0	-0.0	-0.0	-C.00	0.0	0.	0.	0.
8	-0.4	-0.1	188.2	-0.00	0.1	87.7	0.	0.
9	-0.6	0.1	-60.7	-0.00	0.1	-13.8	0.	0.
10	-78.1	89.7	0.1	C.22	45.0	0.	0.	0.
11	-55.1	47.8	-0.2	C.13	32.6	0.	0.	0.
12	-0.5	-0.3	123.6	-0.00	0.1	82.2	0.	0.
13	-0.6	0.5	-655.5	0.00	0.1	-341.3	0.	0.
14	-661.6	499.8	-0.6	1.56	448.2	0.	0.	0.
15	-0.0	-0.0	0.4	-C.00	0.0	0.	0.	0.
16	-0.3	-0.1	-0.7	-C.00	0.1	0.	0.	0.
17	-1.7	0.8	0.1	C.00	1.1	0.	0.	0.
18	-0.0	-0.0	-0.0	-C.00	0.0	0.	0.	0.
19	-0.0	-0.0	-0.0	-0.00	0.0	0.	0.	0.
20	-0.0	-0.0	-0.0	-0.00	0.0	0.	0.	0.
21	0.7	-1.8	1017.8	-C.01	0.2	674.9	0.	0.
22	-0.5	0.6	-1976.8	C.01	0.8	-1328.7	0.	0.
23	-2018.5	1365.9	-0.4	4.92	1625.6	0.	0.	0.
24	-0.0	-0.0	-0.0	-0.00	0.0	0.	0.	0.
25	-0.0	-0.0	-0.0	-C.00	0.0	0.	0.	0.
26	-0.0	-0.0	-0.0	-C.00	0.0	0.	0.	0.
27	12.3	6.4	-0.2	C.02	-4.1	0.	0.	0.
RSS	2126.4	1458.1	2329.8	5.17	1687.2	1533.7	0.	0.

TABLE VI-III (Continued)

FLIGHT SEGMENT 4								
FS	DELRA(M)	DELDL(M)	DELCR(M)	CELVEL(M/S)	DELGA(M/URAD)	DELPSI(URAD)	DELTIME(MSEC)	
2	14.3	0.	-0.2	-C.00	-1.5	-0.0	0.5	
3	5.6	0.	0.1	-0.02	-2.1	0.0	3.0	
4	-0.2	-0.	15.6	-C.00	0.0	-1.9	-0.0	
5	-0.0	0.	-0.0	-C.00	0.0	-0.0	0.0	
6	-0.0	0.	-0.0	-C.00	0.1	-0.0	-C.0	
7	-0.0	0.	-0.0	-C.00	0.0	-0.0	0.0	
8	-0.4	0.	188.2	-C.00	0.1	87.7	-0.0	
9	-0.6	-0.	-60.7	-C.00	0.1	-13.8	-0.0	
10	-78.2	0.	0.1	C.22	31.4	0.0	-5.3	
11	-55.1	0.	-0.2	0.13	25.4	-0.0	-4.6	
12	-0.5	0.	123.6	-C.00	0.1	82.2	0.0	
13	-0.6	-0.	-655.6	C.00	0.0	-341.3	0.0	
14	-662.2	0.	-0.6	1.56	372.3	-0.0	-62.6	
15	-0.0	0.	0.4	-C.00	0.0	0.0	0.0	
16	-0.3	0.	-0.7	-C.00	C.1	-0.0	0.1	
17	-1.7	0.	0.1	C.00	1.0	0.0	-0.1	
18	-0.0	0.	-0.0	-C.00	0.0	-0.0	0.0	
19	-0.0	0.	-0.0	-0.00	0.0	-0.0	0.0	
20	-0.0	0.	-0.0	-C.00	0.0	-0.0	0.0	
21	0.7	0.	1017.8	-C.01	0.5	674.9	0.1	
22	-0.5	-0.	-1976.9	C.01	0.7	-1328.7	-0.3	
23	-2020.0	0.	-0.4	4.92	1418.1	-0.0	-219.2	
24	-0.0	0.	-0.0	-C.00	0.0	-0.0	0.0	
25	-0.0	0.	-0.0	-C.00	0.0	-0.0	C.0	
26	-0.0	0.	-0.0	-C.00	0.0	-0.0	0.0	
27	12.3	0.	-0.2	0.02	-5.0	-0.0	0.7	
RSS	2128.0	0.	2330.0	5.17	1466.7	1533.7	228.1	

TABLE VI-III (Continued)

FLIGHT SEGMENT 5								
ES	DELRA(M)	DELD(R)(M)	DELCR(M)	DELVEL(M/S)	DELGAM(URAD)	DELPSI(URAD)	DELTIME(MSEC)	
2	16.2	-4.2	-0.1	-C.00	-1.7	0.	0.4	
3	7.8	-4.5	-0.1	-0.02	-1.7	0.	3.0	
4	-0.3	0.1	12.8	-C.00	0.0	-1.7	-0.1	
5	-0.1	-0.0	-0.0	-C.00	0.0	0.	0.	
6	-0.1	-0.0	-0.1	-C.00	0.0	0.	-0.1	
7	-0.1	-0.0	-0.0	-C.00	0.0	0.	0.	
8	-0.7	-0.1	317.7	-C.00	0.1	86.8	-0.1	
9	-0.5	-0.0	-75.8	-C.00	0.1	-6.7	-0.1	
10	-120.5	66.1	0.2	0.27	39.0	0.	-5.4	
11	-95.0	46.2	-0.3	C.20	37.2	0.	-4.6	
12	-7.0	2.6	257.5	C.02	8.4	97.3	0.	
13	-5.9	2.4	-1195.6	C.02	7.5	-390.5	0.	
14	-1234.3	575.1	-0.7	2.39	512.7	0.	-62.6	
15	-3.8	1.6	0.6	0.01	4.9	0.	0.	
16	-5.5	1.7	-1.1	C.01	6.8	0.	0.1	
17	-9.3	3.5	0.1	C.03	9.5	0.	-0.1	
18	-2.2	1.0	-0.1	0.01	2.7	0.	0.	
19	-2.2	1.0	-0.1	0.01	2.7	0.	0.	
20	-2.2	1.0	-0.1	C.01	2.7	0.	0.	
21	-6.7	0.3	2115.7	C.02	9.3	799.0	0.1	
22	-7.7	3.6	-4310.8	0.04	9.5	-1847.2	-0.3	
23	-4398.8	1987.2	-0.5	8.90	2195.6	0.	-219.2	
24	-2.2	1.0	-0.1	C.01	2.7	0.	0.	
25	-2.2	1.0	-0.1	C.01	2.7	0.	0.	
26	-2.2	1.0	-0.1	0.01	2.7	0.	0.	
27	19.4	-1.3	-0.1	C.02	-4.5	0.	0.7	
SS	4571.4	2070.3	4966.0	9.22	2255.4	2054.3	228.1	

TABLE VI-IV

ERROR SUMMARY FOR CONFIGURATION 2

ERROR SUMMARY FOLLOWS

FLIGHT SEGMENT 1

ES	DELRA (M)	DELDOR (M)	DELCR (M)	DELVEL (M/S)	DELGAU (URAD)	DELPST (URAD)	DELTIME (MSEC)
2	10.1	-0.1	-0.0	C.00	-2.3	0.	0.
3	0.1	19.9	0.1	-0.00	-1.2	0.	0.
4	0.1	-0.0	19.9	-C.00	0.0	-2.6	0.
5	0.	-0.	0.	-C.00	0.0	0.	0.
6	-0.0	-0.0	-0.0	-C.00	0.	0.	0.
7	0.	-0.	0.	-0.00	0.0	0.	0.
8	0.0	-0.0	0.5	-C.00	-0.1	43.9	0.
9	0.0	0.0	-2.5	C.00	0.1	-62.7	0.
10	-0.3	2.2	-0.1	C.04	48.3	0.	0.
11	-0.2	0.5	0.1	0.02	25.7	0.	0.
12	-0.0	-0.0	0.3	-C.00	-C.0	25.5	0.
13	-0.1	0.0	-5.3	C.00	0.4	-231.1	0.
14	-1.3	5.2	-0.1	C.13	195.1	0.	0.
15	-0.0	-0.0	0.1	-0.00	-0.0	7.9	0.
16	0.1	0.0	-0.7	-C.00	0.2	-25.4	0.
17	-0.2	0.6	0.0	C.01	21.7	0.	0.
18	0.	-0.	0.	-C.00	0.0	0.	0.
19	0.	-0.	0.	-0.00	0.0	0.	0.
20	0.	-0.	0.	-C.00	0.0	0.	0.
21	-0.1	-0.0	0.8	-C.00	-0.1	59.2	0.
22	-0.3	0.0	-4.6	C.00	0.3	-191.4	0.
23	-1.1	4.3	-0.1	0.11	161.6	0.	0.
24	0.	-0.	0.	-C.00	0.0	0.	0.
25	0.	-0.	0.	-C.00	0.0	0.	0.
26	0.	-0.	0.	-C.00	0.0	0.	0.
27	0.1	0.0	-0.0	0.00	-0.5	0.	0.
KSS	10.2	21.1	21.3	C.18	260.1	317.5	0.

TABLE VI-IV (Continued)

ES	FLIGHT SEGMENT 2	DELRA(M)	DELDOR(M)	DELCR(M)	DELVEL(M/S)	DELGM(URAD)	DELPST(URAD)	DELTIME(MSEC)
2	10.2	-0.2	0.1	0.00	-1.4	0.	0.	0.
3	0.4	19.7	0.1	-0.00	-0.5	0.	0.	0.
4	0.1	-0.0	19.7	-0.00	0.0	-1.5	0.	0.
5	-0.0	-0.0	-0.0	C.	0.0	0.	0.	0.
6	-0.0	-0.0	-0.0	-0.00	0.0	0.	0.	0.
7	-0.0	-0.0	-0.0	0.	0.0	0.	0.	0.
8	0.1	-0.0	7.2	-0.00	-0.1	76.8	0.	0.
9	-0.2	0.0	-7.4	C.00	0.1	-40.5	0.	0.
10	-3.5	7.3	-0.1	0.07	50.3	0.	0.	0.
11	-3.6	4.0	-0.1	0.05	55.7	0.	0.	0.
12	0.0	-0.0	5.6	-0.00	-0.1	66.8	0.	0.
13	0.2	0.0	-41.0	C.00	0.5	-450.4	0.	0.
14	-28.9	33.3	-0.2	C.38	492.2	0.	0.	0.
15	0.0	-0.0	1.6	-0.00	-0.1	20.7	0.	0.
16	-0.0	0.0	-3.8	-0.00	0.2	-39.0	0.	0.
17	-2.8	3.4	0.1	C.04	43.7	0.	0.	0.
18	-0.0	-0.0	-0.0	0.	0.0	0.	0.	0.
19	-0.0	-0.0	-0.0	C.	0.0	0.	0.	0.
20	-0.0	-0.0	-0.0	C.	0.0	0.	0.	0.
21	-0.0	-0.0	12.8	-0.00	-0.1	155.2	0.	0.
22	-0.3	0.0	-30.3	C.00	0.3	-292.9	0.	0.
23	-20.9	25.4	0.0	C.28	327.5	0.	0.	0.
24	-0.0	-0.0	-0.0	C.	0.0	0.	0.	0.
25	-0.0	-0.0	-0.0	C.	0.0	0.	0.	0.
26	-0.0	-0.0	-0.0	0.	0.0	0.	0.	0.
27	0.1	0.1	-0.0	C.01	-0.6	0.	0.	0.
RSS	37.5	47.2	57.5	C.48	597.6	571.5	0.	0.

TABLE VI-IV (Continued)

FLIGHT SEGMENT	3	DELRA(M)	DELOR(M)	DELCR(M)	DELVEL(M/S)	DELGAM(URAD)	DELPSI(URAD)	DELTIME(INSEC)
ES								
2	14.3	-4.7	-0.2	-C.00	-2.3	0.	0.	0.
3	5.6	14.5	0.1	-C.02	0.1	0.	0.	0.
4	-0.2	-0.1	15.6	-C.00	0.0	-1.9	0.	0.
5	-0.0	-0.0	-0.0	-C.00	0.0	0.	0.	0.
6	-0.0	-0.1	-0.0	-C.00	0.0	0.	0.	0.
7	-0.0	-0.0	-0.0	-C.00	0.0	0.	0.	0.
8	-0.4	-0.1	188.2	-C.00	0.1	87.7	0.	0.
9	-0.6	0.1	-60.7	-C.00	0.1	-13.8	0.	0.
10	-78.1	89.7	0.1	C.22	45.0	0.	0.	0.
11	-111.0	96.1	-0.2	C.27	65.3	0.	0.	0.
12	-0.3	-0.5	247.8	-C.00	0.2	164.3	0.	0.
13	-0.3	0.7	-1306.4	0.00	0.2	-679.8	0.	0.
14	-1320.2	997.0	-0.6	3.12	894.1	0.	0.	0.
15	0.4	-0.6	76.2	-C.00	0.0	50.9	0.	0.
16	0.4	-0.2	-149.0	-C.00	0.1	-100.1	0.	0.
17	-151.9	102.6	-0.5	0.37	122.7	0.	0.	0.
18	-0.0	-0.0	-0.0	-C.00	0.0	0.	0.	0.
19	-0.0	-0.0	-0.0	-C.00	0.0	0.	0.	0.
20	-0.0	-0.0	-0.0	-C.00	0.0	0.	0.	0.
21	-0.3	-0.8	576.2	-C.00	0.3	381.8	0.	0.
22	-0.7	0.6	-1118.0	C.00	C.2	-751.7	0.	0.
23	-1142.0	772.7	-0.9	2.78	919.8	0.	0.	0.
24	-0.0	-0.0	-0.0	-C.00	0.0	0.	0.	0.
25	-0.0	-0.0	-0.0	-C.00	0.0	0.	0.	0.
26	-0.0	-0.0	-0.0	-C.00	0.0	0.	0.	0.
27	2.1	1.5	0.0	C.00	-0.8	0.	0.	0.
RSS	1757.5	1272.5	1848.6	4.21	1291.0	1104.7	0.	0.

TABLE VI-IV (Continued)

FLIGHT SEGMENT 4								
ES	DELRA(M)	DELDRA(M)	DELCRA(M)	DELVEL(M/S)	DELGAM(URAD)	DELPST(URAD)	DELTIME(MSEC)	
2	14.3	0.	-0.2	-C.00	-1.5	-0.0	0.5	
3	5.6	0.	0.1	-C.02	-2.1	0.0	3.0	
4	-0.2	-0.	15.6	-C.00	0.0	-1.9	-0.0	
5	-0.0	0.	-0.0	-0.00	0.0	-0.0	0.0	
6	-0.0	0.	-0.0	-C.00	0.1	-0.0	-0.0	
7	-0.0	0.	-0.0	-C.00	0.0	-0.0	0.0	
8	-0.4	0.	188.2	-C.00	0.1	87.7	-0.0	
9	-0.6	-0.	-60.7	-C.00	0.1	-13.8	-0.0	
10	-78.2	0.	0.1	C.22	31.4	0.0	-5.3	
11	-111.1	0.	-0.2	C.27	50.7	-0.0	-9.2	
12	-0.3	0.	247.8	-C.00	0.3	164.3	0.0	
13	-0.3	-0.	-1306.5	0.00	0.1	-679.8	-0.1	
14	-1321.2	0.	-0.6	3.13	742.6	-0.0	-125.0	
15	0.4	0.	76.2	-C.00	0.1	50.9	0.0	
16	0.4	-0.	-149.0	-0.00	0.1	-100.1	0.0	
17	-152.0	0.	-0.5	C.37	107.1	-0.0	-16.5	
18	-0.0	0.	-0.0	-C.00	0.0	-0.0	0.0	
19	-0.0	0.	-0.0	-C.00	0.0	-0.0	0.0	
20	-0.0	0.	-0.0	-C.00	0.0	-0.0	0.0	
21	-0.3	0.	576.2	-C.00	0.4	381.8	0.1	
22	-0.7	-0.	-1118.1	C.00	0.1	-751.7	-0.1	
23	-1142.8	0.	-0.9	2.78	802.4	-0.0	-124.0	
24	-0.0	0.	-0.0	-0.00	0.0	-0.0	0.0	
25	-0.0	0.	-0.0	-C.00	0.0	-0.0	0.0	
26	-0.0	0.	-0.0	-C.00	0.0	-0.0	0.0	
27	2.1	0.	0.0	C.00	-1.0	0.0	C.2	
RSS	1758.8	0.	1848.7	4.21	1100.1	1104.7	177.1	

TABLE VI-IV (Continued)

FLIGHT SEGMENT 5		DELRA(M)	DELDL(M)	DELCR(M)	DELVEL (M/S)	DELGAM (URAD)	DELPSI (URAD)	DELTIME (MSEC)
ES								
2	16.2	-4.2	-0.1	-0.1	-C.00	-1.7	0.	0.4
3	7.8	-4.5	-0.1	0.	-0.02	-1.7	0.	3.0
4	-0.3	0.1	12.8	0.	-0.00	0.0	-1.7	-0.1
5	-0.1	-0.0	-0.0	-0.0	-C.00	0.0	0.	0.
6	-0.1	-0.0	-0.1	-0.0	-C.00	0.0	0.	-0.1
7	-0.1	-0.0	-0.0	-0.0	-C.00	0.0	0.	0.
8	-0.7	-0.1	317.7	0.1	-0.00	0.1	86.8	-0.1
9	-0.5	-0.0	-75.8	0.1	-C.00	0.1	-6.7	-0.1
10	-120.5	66.1	0.2	0.2	C.27	39.0	0.	-5.4
11	-271.5	130.2	-0.3	-0.3	C.73	186.4	0.	-9.2
12	-6.6	2.1	515.1	0.02	0.02	8.2	194.5	0.
13	-6.4	3.5	-2381.5	C.03	C.03	8.6	-777.6	-0.1
14	-2461.0	1147.0	-0.7	4.77	4.77	1020.4	0.	-125.0
15	-6.6	2.6	159.0	C.03	C.03	9.3	60.3	0.
16	-5.9	2.2	-324.9	0.02	0.02	8.2	-139.3	0.
17	-382.1	172.8	-0.5	C.88	C.88	235.8	0.	-16.5
18	-2.2	1.0	-0.1	C.01	C.01	2.7	0.	0.
19	-2.2	1.0	-0.1	C.01	C.01	2.7	0.	0.
20	-2.2	1.0	-0.1	C.01	C.01	2.7	0.	0.
21	-7.3	1.5	1197.3	C.02	C.02	8.9	451.9	0.1
22	-6.1	3.2	-2438.3	C.03	C.03	7.6	-1044.9	-0.2
23	-2489.3	1124.9	-1.0	5.04	5.04	1243.5	0.	-124.0
24	-2.2	1.0	-0.1	0.01	0.01	2.7	0.	0.
25	-2.2	1.0	-0.1	C.01	C.01	2.7	0.	0.
26	-2.2	1.0	-0.1	C.01	C.01	2.7	0.	0.
27	3.5	-0.3	-0.0	C.00	C.00	-0.9	0.	0.1
RSS	3533.8	1622.5	3681.4	7.04	7.04	1637.0	1403.3	177.2

TABLE VI-V
ERROR SUMMARY FOR CONFIGURATION 3

ERROR SUMMARY FOLLOWS									
FLIGHT SEGMENT 1									
ES	DELRA(M)	DELDL(M)	DELCR(M)	DELVEL(M/S)	DELGM(URAD)	DELPST(URAD)	DELTIME(MSEC)		
2	10.1	-0.1	-0.0	0.00	-2.3	0.	0.		
3	0.1	19.9	0.1	-0.00	-1.2	0.	0.		
4	0.1	-0.0	19.9	-0.00	0.0	-2.6	0.		
5	0.	-0.	0.	-0.00	0.0	0.	0.		
6	-0.0	-0.0	-0.0	-0.00	0.	0.	0.		
7	0.	-0.	0.	-0.00	0.0	0.	0.		
8	0.0	-0.0	0.5	-0.00	-0.1	43.9	0.		
9	0.0	0.0	-2.5	0.00	0.1	-62.7	0.		
10	-0.3	2.2	-0.1	0.04	48.3	0.	0.		
11	0.0	0.0	0.0	0.00	0.1	0.	0.		
12	0.	-0.	0.	-0.00	0.0	0.	0.		
13	0.	-0.	0.	-0.00	0.1	0.	0.		
14	0.	-0.	0.	-0.00	0.0	0.	0.		
15	-0.0	-0.0	-0.0	-0.00	0.	0.	0.		
16	0.1	-0.0	-0.1	-0.00	0.1	-3.2	0.		
17	0.0	0.1	0.0	0.00	2.9	0.	0.		
18	0.	-0.	0.	-0.00	0.0	0.	0.		
19	0.	-0.	0.	-0.00	0.0	0.	0.		
20	0.	-0.	0.	-0.00	0.0	0.	0.		
21	0.	-0.	0.	-0.00	0.0	0.	0.		
22	0.	-0.	0.	-0.00	0.1	0.	0.		
23	0.	-0.	0.	-0.00	0.0	0.	0.		
24	0.	-0.	0.	-0.00	0.0	0.	0.		
25	0.	-0.	0.	-0.00	0.0	0.	0.		
26	0.	-0.	0.	-0.00	0.0	0.	0.		
27	1.0	0.1	-0.1	0.02	-17.7	0.	0.		
RSS	10.1	20.0	20.0	0.05	51.6	76.6	0.		

TABLE VI-V (Continued)

FLIGHT SEGMENT 2		DELDR(M)	DELCR(M)	DELVEL (M/S)	DELGM(URAD)	DELPSI(URAD)	DELTIME(MSEC)
ES	DELRA(M)						
2	10.2	-0.2	0.1	C.00	-1.4	0.	0.
3	0.4	19.7	0.1	-0.00	-0.5	0.	0.
4	0.1	-0.0	19.7	-C.00	0.0	-1.5	0.
5	-0.0	-0.0	-0.0	C.	0.0	0.	0.
6	-0.0	-0.0	-0.0	-C.00	0.0	0.	0.
7	-0.0	-0.0	-0.0	C.	0.0	0.	0.
8	0.1	-0.0	7.2	-C.00	-0.1	76.8	0.
9	-0.2	0.0	-7.4	C.00	0.1	-40.5	0.
10	-3.5	7.3	-0.1	0.07	50.3	0.	0.
11	0.0	0.0	0.0	0.00	0.1	0.	0.
12	-0.0	-0.0	-0.0	C.	0.0	0.	0.
13	-0.0	-0.0	-0.0	-C.00	0.0	0.	0.
14	-0.0	-0.0	-0.0	0.	0.0	0.	0.
15	0.0	-0.0	0.2	-0.00	0.0	2.3	0.
16	0.1	-0.0	-0.5	-C.00	0.1	-4.9	0.
17	-0.3	0.4	0.0	C.00	5.6	0.	0.
18	-0.0	-0.0	-0.0	0.	0.0	0.	0.
19	-0.0	-0.0	-0.0	C.	0.0	0.	0.
20	-0.0	-0.0	-0.0	C.	0.0	0.	0.
21	-0.0	-0.0	-0.0	C.	0.0	0.	0.
22	-0.0	-0.0	-0.0	-C.00	0.0	0.	0.
23	-0.0	-0.0	-0.0	-0.00	0.0	0.	0.
24	-0.0	-0.0	-0.0	C.	0.0	0.	0.
25	-0.0	-0.0	-0.0	0.	0.0	0.	0.
26	-0.0	-0.0	-0.0	0.	0.0	0.	0.
27	3.8	2.4	0.0	0.09	-13.4	0.	0.
RSS	11.4	21.2	22.2	C.12	52.4	87.0	0.

TABLE VI-V (Continued)

FLIGHT SEGMENT		3	DELOR (M)	DELCR (M)	DELVEL (M/S)	DEL GAM (URAD)	DEL PSI (URAD)	DEL TIME (MSEC)
ES	DELRA (M)							
2	14.3	-4.7	-0.2	-0.00	-2.3	0.	0.	0.
3	5.6	14.5	0.1	-0.02	0.1	0.	0.	0.
4	-0.2	-0.1	15.6	-0.00	0.0	-1.9	0.	0.
5	-0.0	-0.0	-0.0	-0.00	0.0	0.	0.	0.
6	-0.0	-0.1	-0.0	-0.00	0.0	0.	0.	0.
7	-0.0	-0.0	-0.0	-0.00	0.0	0.	0.	0.
8	-0.4	-0.1	188.2	-0.00	0.1	87.7	0.	0.
9	-0.6	0.1	-60.7	-0.00	0.1	-13.8	0.	0.
10	-78.1	89.7	0.1	0.22	45.0	0.	0.	0.
11	-0.1	0.1	-0.0	0.00	0.2	0.	0.	0.
12	-0.0	-0.0	-0.0	-0.00	0.0	0.	0.	0.
13	-0.0	-0.0	-0.1	-0.00	0.0	0.	0.	0.
14	-0.0	-0.1	-0.0	-0.00	0.1	0.	0.	0.
15	-0.6	-0.2	9.0	-0.00	0.2	6.3	0.	0.
16	-0.1	-0.1	-18.6	-0.00	0.2	-12.5	0.	0.
17	-19.2	12.5	-0.7	0.05	15.4	0.	0.	0.
18	-0.0	-0.0	-0.0	-0.00	0.0	0.	0.	0.
19	-0.0	-0.0	-0.0	-0.00	0.0	0.	0.	0.
20	-0.0	-0.0	-0.0	-0.00	0.0	0.	0.	0.
21	-0.0	-0.0	-0.0	-0.00	0.0	0.	0.	0.
22	-0.0	-0.0	-0.1	-0.00	0.0	0.	0.	0.
23	-0.0	-0.1	-0.0	-0.00	0.1	0.	0.	0.
24	-0.0	-0.0	-0.0	-0.00	0.0	0.	0.	0.
25	-0.0	-0.0	-0.0	-0.00	0.0	0.	0.	0.
26	-0.0	-0.0	-0.0	-0.00	0.0	0.	0.	0.
27	48.7	25.6	0.1	0.07	-16.4	0.	0.	0.
RSS	95.3	95.3	199.4	0.23	50.4	89.9	0.	0.

TABLE VI-V (Continued)

FLIGHT SEGMENT 4								
ES	DELRA (M)	DELDL (M)	DELCR (M)	DELVEL (M/S)	DELGA (URAD)	DELPSI (URAD)	DELTIME (MSEC)	
2	14.3	0.	-0.2	-0.00	-1.5	-0.0	0.3	0.0
3	5.6	0.	0.1	-0.02	-2.1	0.0	3.0	3.0
4	-0.2	-0.	15.6	-0.00	0.0	-1.9	-0.0	-0.0
5	-0.0	0.	-0.0	-0.00	0.0	0.0	0.0	0.0
6	-0.0	0.	-0.0	-0.00	0.1	-0.0	-0.0	-0.0
7	-0.0	0.	-0.0	-0.00	0.0	-0.0	0.0	0.0
8	-0.4	0.	188.2	-0.00	0.1	87.7	-0.0	-0.0
9	-0.6	-0.	-60.7	0.22	31.4	-13.8	-0.0	-5.3
10	-78.2	0.	0.1	0.00	0.2	0.0	-0.0	-0.0
11	-0.1	0.	-0.0	0.00	0.0	-0.0	0.0	0.0
12	-0.0	0.	-0.0	-0.00	0.0	-0.0	0.0	0.0
13	-0.0	0.	-0.1	-0.00	0.0	-0.0	0.0	0.0
14	-0.0	0.	-0.0	-0.00	0.1	-0.0	0.1	0.1
15	-0.6	0.	9.0	-0.00	0.2	6.3	0.0	0.0
16	-0.1	-0.	-18.6	0.00	0.2	-12.5	0.1	0.1
17	-19.2	0.	-0.7	0.05	13.5	-0.0	-2.1	-2.1
18	-0.0	0.	-0.0	-0.00	0.0	-0.0	0.0	0.0
19	-0.0	0.	-0.0	-0.00	0.0	-0.0	0.0	0.0
20	-0.0	0.	-0.0	-0.00	0.0	-0.0	0.0	0.0
21	-0.0	0.	-0.0	-0.00	0.0	-0.0	0.0	0.0
22	-0.0	0.	-0.1	-0.00	0.0	-0.0	0.0	0.0
23	-0.0	0.	-0.0	-0.00	0.1	-0.0	0.1	0.1
24	-0.0	0.	-0.0	-0.00	0.0	-0.0	0.0	0.0
25	-0.0	0.	-0.0	-0.00	0.0	-0.0	0.0	0.0
26	-0.0	0.	-0.0	-0.00	0.0	-0.0	0.0	0.0
27	48.7	0.	0.1	0.07	-20.3	0.0	2.8	2.8
RSS	95.4	0.	199.4	0.23	39.8	89.9	7.1	7.1

TABLE VI-V (Continued)

FLIGHT SEGMENT 5							
ES	DELRA(M)	DELDL(M)	DELCR(M)	DELVEL (M/S)	DELGAM(URAD)	DELPSI(URAD)	DELTIME(MSEC)
2	16.2	-4.2	-0.1	-6.00	-1.7	0.	0.4
3	7.8	-4.5	-0.1	-0.02	-1.7	0.	3.0
4	-0.3	0.1	12.8	-0.00	0.0	-1.7	-0.1
5	-0.1	-0.0	-0.0	-0.00	0.0	0.	0.
6	-0.1	-0.1	-0.1	-0.00	0.0	0.	-0.1
7	-0.1	-0.0	-0.0	-0.00	0.0	0.	0.
8	-0.7	-0.1	317.7	-0.00	0.1	86.8	-0.1
9	-0.5	-0.0	-75.8	-0.00	0.1	-6.7	-0.1
10	-120.5	66.1	0.2	6.27	39.0	0.	-5.4
11	-0.8	0.4	-0.1	0.00	0.7	0.	-0.1
12	-3.8	1.6	0.1	0.01	4.9	0.	0.
13	-4.9	2.2	-0.1	0.02	6.5	0.	0.
14	-2.5	0.6	-0.1	6.00	2.9	0.	0.
15	-6.1	2.2	19.2	0.02	7.3	7.5	0.
16	-6.7	2.1	-40.7	0.02	8.8	-17.4	0.
17	-44.0	19.6	-0.7	0.09	23.9	0.	-2.1
18	-2.2	1.0	-0.1	6.01	2.7	0.	0.
19	-2.2	1.0	-0.1	6.01	2.7	0.	0.
20	-2.2	1.0	-0.1	6.01	2.7	0.	0.
21	-3.8	1.6	0.1	6.01	4.9	0.	0.
22	-5.0	2.2	-0.1	6.02	6.5	0.	0.
23	-2.5	0.6	-0.1	6.00	2.9	0.	0.
24	-2.2	1.0	-0.1	6.01	2.7	0.	0.
25	-2.2	1.0	-0.1	6.01	2.7	0.	0.
26	-2.2	1.0	-0.1	6.01	2.7	0.	0.
27	77.5	-5.4	0.2	6.07	-17.9	0.	2.8
SS	151.6	69.6	329.9	0.30	52.4	89.1	7.1

TABLE VI-VI

ERROR SUMMARY FOR CONFIGURATION 4

ERROR SUMMARY FOLLOWS

FLIGHT SEGMENT 1

ES	DELRA(M)	DELDL(M)	DELCR(M)	CELVEL(M/S)	DELGAW(URAD)	DELPST(URAD)	DELTIME(MSEC)
2	10.1	-0.1	-0.0	C.00	-2.3	0.	0.
3	0.1	19.9	0.1	-0.00	-1.2	0.	0.
4	0.1	-0.0	19.9	-0.00	0.0	-2.6	0.
5	0.	0.	0.	-0.00	0.0	0.	0.
6	-0.0	-0.0	-0.0	-0.00	0.	0.	0.
7	0.	0.	0.	-0.00	0.0	0.	0.
8	0.0	-0.0	0.5	-0.00	-0.1	43.9	0.
9	0.0	0.0	-2.5	C.00	0.1	-62.7	0.
10	-0.3	2.2	-0.1	C.04	48.3	0.	0.
11	0.0	0.0	0.0	0.00	0.2	0.	0.
12	0.	0.	0.	-0.00	0.0	0.	0.
13	0.	0.	0.	-0.00	0.1	0.	0.
14	0.	0.	0.	-0.00	0.0	0.	0.
15	0.0	-0.0	0.0	-0.00	-0.0	3.9	0.
16	0.0	0.0	-0.3	-0.00	0.2	-12.7	0.
17	-0.1	0.3	0.0	C.01	10.9	0.	0.
18	0.	0.	0.	-0.00	0.0	0.	0.
19	0.	0.	0.	-0.00	0.0	0.	0.
20	0.	0.	0.	-0.00	0.0	0.	0.
21	0.	0.	0.	-0.00	0.0	0.	0.
22	0.	0.	0.	-0.00	0.0	0.	0.
23	0.	0.	0.	-0.00	0.1	0.	0.
24	0.	0.	0.	-0.00	0.0	0.	0.
25	0.	0.	0.	-0.00	0.0	0.	0.
26	0.	0.	0.	-0.00	0.0	0.	0.
27	0.6	0.1	-0.3	0.01	-8.7	0.	0.
RSS	10.1	20.0	20.0	C.04	50.3	77.7	0.

TABLE VI-VI (Continued)

FLIGHT SEGMENT 2		DELRA(M)	DELDL(M)	DELCR(M)	DELVEL(M/S)	DELGAM(URAD)	DELPSI(URAD)	DELTIME(MSEC)
ES								
2		10.2	-0.2	0.1	0.00	-1.4	0.	0.
3		0.4	19.7	0.1	-0.00	-0.5	0.	0.
4		0.1	-0.0	19.7	-0.00	0.0	-1.5	0.
5		-0.0	-0.0	-0.0	0.	0.0	0.	0.
6		-0.0	-0.0	-0.0	-0.00	0.0	0.	0.
7		-0.0	-0.0	-0.0	0.	0.0	0.	0.
8		0.1	-0.0	7.2	-0.00	-0.1	76.8	0.
9		-0.2	0.0	-7.4	0.00	0.1	-40.5	0.
10		-3.5	7.3	-0.1	0.07	50.3	0.	0.
11		-0.1	0.0	0.0	0.00	0.3	0.	0.
12		-0.0	-0.0	-0.0	0.	0.0	0.	0.
13		-0.0	-0.0	-0.0	-0.00	0.0	0.	0.
14		-0.0	-0.0	-0.0	-0.00	0.0	0.	0.
15		0.1	-0.0	0.9	-0.00	-0.1	10.3	0.
16		0.1	-0.0	-2.1	-0.00	0.1	-19.4	0.
17		-1.3	1.7	-0.0	0.02	21.9	0.	0.
18		-0.0	-0.0	-0.0	0.	0.0	0.	0.
19		-0.0	-0.0	-0.0	0.	0.0	0.	0.
20		-0.0	-0.0	-0.0	0.	0.0	0.	0.
21		-0.0	-0.0	-0.0	0.	0.0	0.	0.
22		-0.0	-0.0	-0.0	-0.00	0.0	0.	0.
23		-0.0	-0.0	-0.0	0.	0.0	0.	0.
24		-0.0	-0.0	-0.0	0.	0.0	0.	0.
25		-0.0	-0.0	-0.0	0.	0.0	0.	0.
26		-0.0	-0.0	-0.0	0.	0.0	0.	0.
27		2.6	2.2	-0.2	0.09	-9.9	0.	0.
RSS		11.2	21.2	22.3	0.11	55.8	89.6	0.

TABLE VI-VI (Continued)

FLIGHT SEGMENT 3							
ES	DELRA (M)	DELDL (M)	DELCR (M)	DELVEL (M/S)	DELGAM (URAD)	CELPSI (URAD)	DELTIME (MSEC)
2	14.3	-4.7	-0.2	-0.00	-2.3	0.	0.
3	5.6	14.5	0.1	-0.02	0.1	0.	0.
4	-0.2	-0.1	15.6	-0.00	0.0	-1.9	0.
5	-0.0	-0.0	-0.0	-0.00	0.0	0.	0.
6	-0.0	-0.1	-0.0	-0.00	0.0	0.	0.
7	-0.0	-0.0	-0.0	-0.00	0.0	0.	0.
8	-0.4	-0.1	188.2	-0.00	0.1	87.7	0.
9	-0.6	0.1	-60.7	-0.00	0.1	-13.8	0.
10	-78.1	89.7	0.1	0.22	45.0	0.	0.
11	-0.8	0.5	0.3	0.00	0.4	0.	0.
12	-0.0	-0.0	-0.0	-0.00	0.0	0.	0.
13	-0.0	-0.0	-0.1	-0.00	0.0	0.	0.
14	-0.0	-0.1	-0.0	-0.00	0.1	0.	0.
15	0.5	-0.6	38.0	-0.00	0.0	25.5	0.
16	-0.7	0.1	-74.3	-0.00	0.2	-50.0	0.
17	-76.3	51.2	-0.4	0.18	61.4	0.	0.
18	-0.0	-0.0	-0.0	-0.00	0.0	0.	0.
19	-0.0	-0.0	-0.0	-0.00	0.0	0.	0.
20	-0.0	-0.0	-0.0	-0.00	0.0	0.	0.
21	-0.0	-0.0	-0.0	-0.00	0.0	0.	0.
22	-0.0	-0.0	-0.1	-0.00	0.0	0.	0.
23	-0.0	-0.1	-0.0	-0.00	0.1	0.	0.
24	-0.0	-0.0	-0.0	-0.00	0.0	0.	0.
25	-0.0	-0.0	-0.0	-0.00	0.0	0.	0.
26	-0.0	-0.0	-0.0	-0.00	0.0	0.	0.
27	40.4	24.6	-0.2	0.06	-13.6	0.	0.
RSS	117.4	107.2	215.2	0.29	77.4	105.1	0.

TABLE VI-VI (Continued)

FLIGHT SEGMENT 4							
ES	DELRA(M)	DELOR(M)	DELCR(M)	DELVEL (M/S)	DELGAM(URAD)	DELPSI(URAD)	DELTIME(MSEC)
2	14.3	0.	-0.2	-C.00	-1.5	-0.0	0.5
3	5.6	0.	0.1	-0.02	-2.1	0.0	3.0
4	-0.2	-0.	15.6	-0.00	0.0	-1.9	-0.0
5	-0.0	0.	-0.0	-0.00	C.0	-0.0	0.0
6	-0.0	0.	-0.0	-C.00	0.1	-0.0	-0.0
7	-0.0	0.	-0.0	-C.00	0.0	-0.0	0.0
8	-0.4	0.	188.2	-C.00	0.1	87.7	-0.0
9	-0.6	-0.	-60.7	-C.00	0.1	-13.8	-0.0
10	-78.2	0.	0.1	C.22	31.4	0.0	-5.3
11	-0.8	0.	0.3	C.00	0.3	0.0	-0.1
12	-0.0	0.	-0.0	-0.00	0.0	-0.0	0.0
13	-0.0	0.	-0.1	-0.00	0.0	-0.0	0.0
14	-0.0	0.	-0.0	-C.00	0.1	-0.0	0.1
15	0.5	0.	38.0	-C.00	0.1	25.5	0.0
16	-0.7	-0.	-74.3	-0.00	0.2	-50.0	0.0
17	-76.3	0.	-0.4	C.18	53.7	-0.0	-8.3
18	-0.0	0.	-0.0	-C.00	0.0	-0.0	0.0
19	-0.0	0.	-0.0	-C.00	0.0	-0.0	0.0
20	-0.0	0.	-0.0	-C.00	0.0	-0.0	0.0
21	-0.0	0.	-0.0	-C.00	0.0	-0.0	0.0
22	-0.0	0.	-0.1	-C.00	0.0	-0.0	0.0
23	-0.0	0.	-0.0	-0.00	0.1	-0.0	0.1
24	-0.0	0.	-0.0	-C.00	0.0	-0.0	0.0
25	-0.0	0.	-0.0	-C.00	0.0	-0.0	0.0
26	-0.0	0.	-0.0	-C.00	0.0	-0.0	0.0
27	40.3	0.	-0.2	0.06	-17.4	-0.0	2.5
RSS	117.5	0.	215.2	0.29	64.6	105.1	10.6

TABLE VI-VI (Continued)

FLIGHT SEGMENT 5		DELDR(M)	DELCR(M)	CCELVEL(M/S)	DELGAM(URAD)	DELPSI(URAD)	DELTIME(MSEC)
ES	DELRA(M)						
2	16.2	-4.2	-0.1	-C.00	-1.7	0.	0.4
3	7.8	-4.5	-0.1	-0.02	-1.7	0.	3.0
4	-0.3	0.1	12.8	-C.00	0.0	-1.7	-0.1
5	-0.1	-0.0	-0.0	-C.00	0.0	0.	0.
6	-0.1	-0.0	-0.1	-C.00	0.0	0.	-0.1
7	-0.1	-0.0	-0.0	-C.00	0.0	0.	0.
8	-0.7	-0.1	317.7	-C.00	0.1	86.8	-0.1
9	-0.5	-0.0	-75.8	-C.00	0.1	-6.7	-0.1
10	-120.5	66.1	0.2	C.27	39.0	0.	-5.4
11	-2.2	1.0	0.2	0.01	1.6	0.	-0.1
12	-3.8	1.6	0.1	C.01	4.9	0.	0.
13	-5.0	2.2	-0.1	C.02	6.5	0.	0.
14	-2.5	0.6	-0.1	C.00	2.9	0.	0.
15	-6.5	2.5	79.4	C.03	9.5	30.1	0.
16	-6.9	2.2	-162.4	C.02	8.2	-69.6	0.
17	-169.5	76.3	-0.4	C.35	87.3	0.	-8.3
18	-2.2	1.0	-0.1	C.01	2.7	0.	0.
19	-2.2	1.0	-0.1	0.01	2.7	0.	0.
20	-2.2	1.0	-0.1	C.01	2.7	0.	0.
21	-3.8	1.6	0.1	C.01	4.9	0.	0.
22	-4.9	2.2	-0.2	C.02	6.4	0.	0.
23	-2.5	0.6	-0.1	0.00	2.9	0.	0.
24	-2.2	1.0	-0.1	C.01	2.7	0.	0.
25	-2.2	1.0	-0.1	C.01	2.7	0.	0.
26	-2.2	1.0	-0.1	C.01	2.7	0.	0.
27	65.1	-4.0	-0.3	C.06	-15.3	0.	2.5
RSS	219.2	101.4	373.5	C.45	98.6	115.5	10.6

NOTE
EQUIVALENT ERROR DUE TO
0.1 deg/hr GYRO DRIFT:
280 METERS
1.5 METERS/SEC

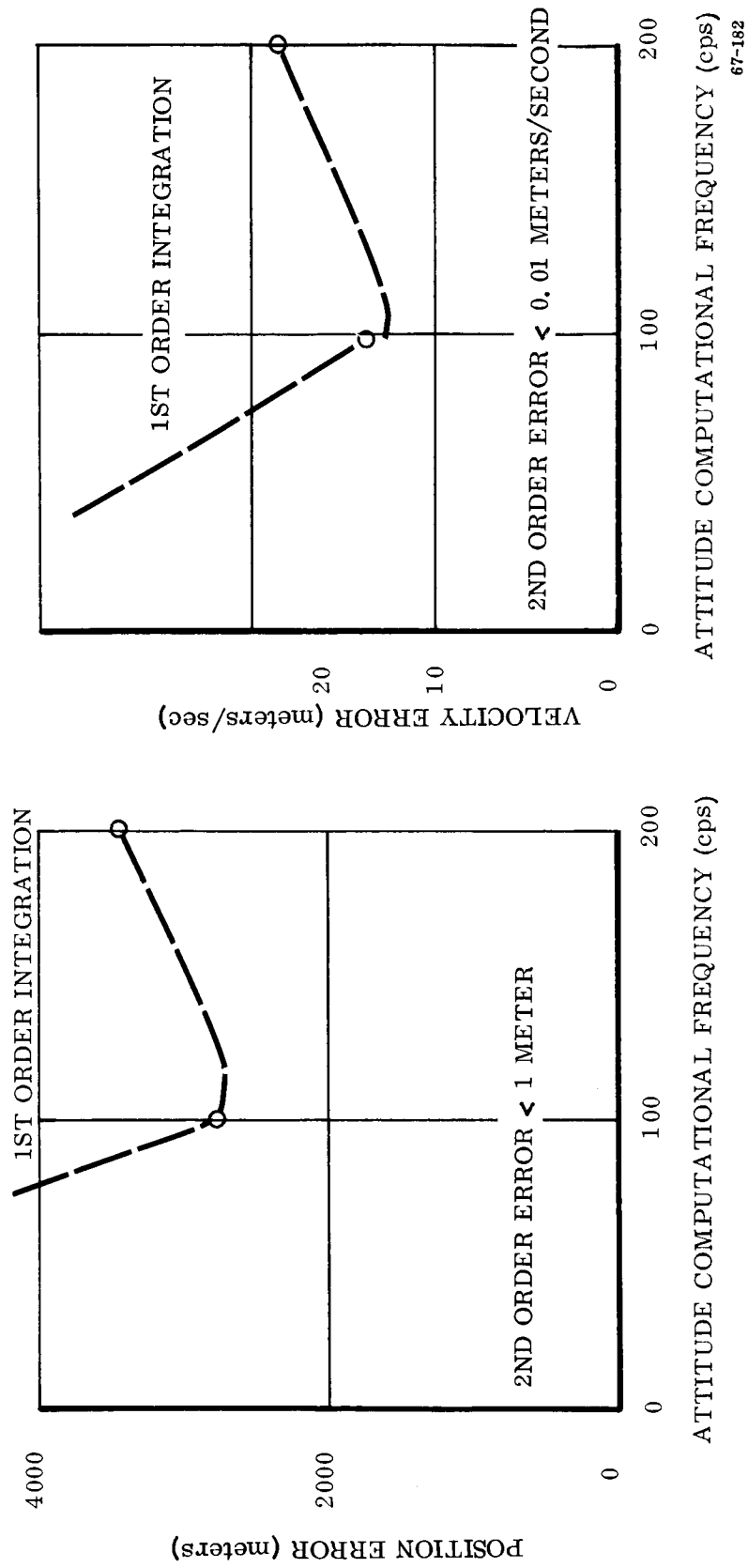


Figure VI-5 Injection Errors Due to Attitude Computation Truncation Errors

NOTE

EQUIVALENT ERROR DUE TO 0.1 deg/hr

GYRODRIFT: 284 meters

1.5 meters/second

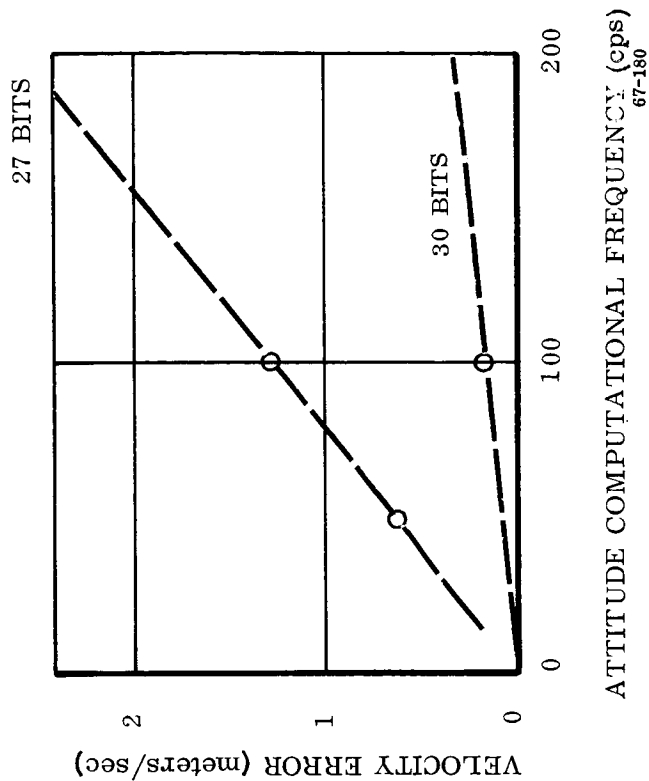
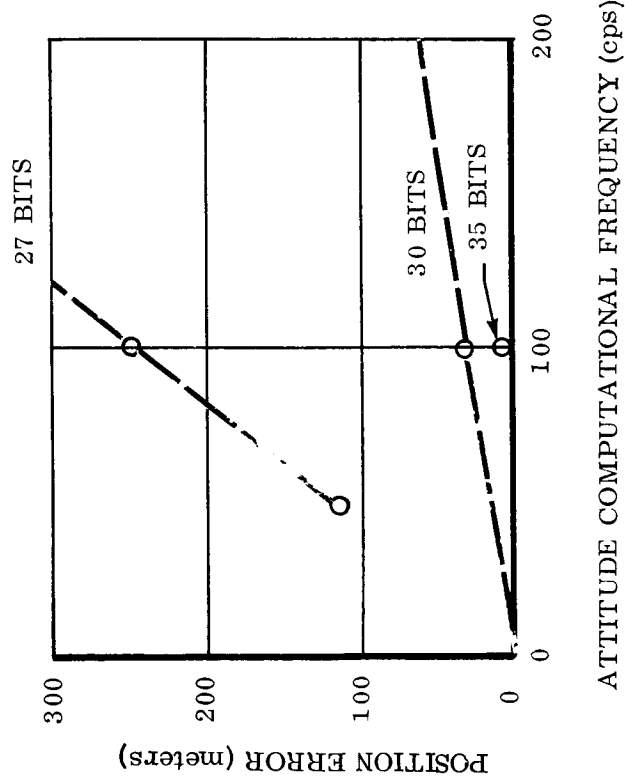
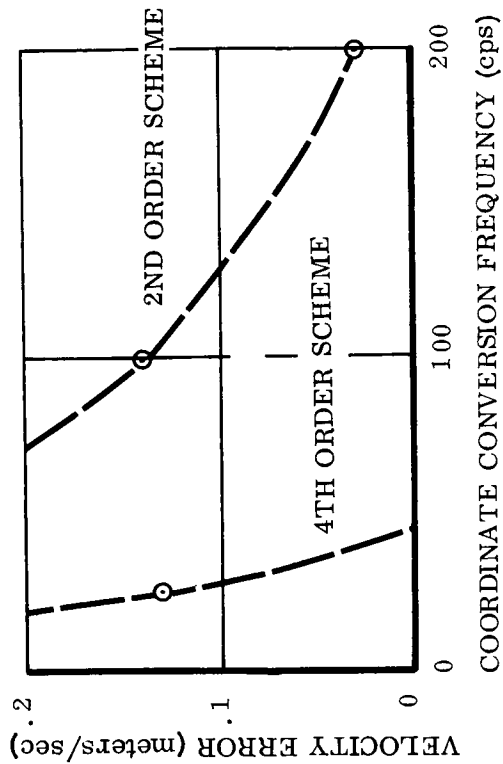


Figure VI-6 Injection Errors Due to Attitude Computation Round Off Errors



67-181

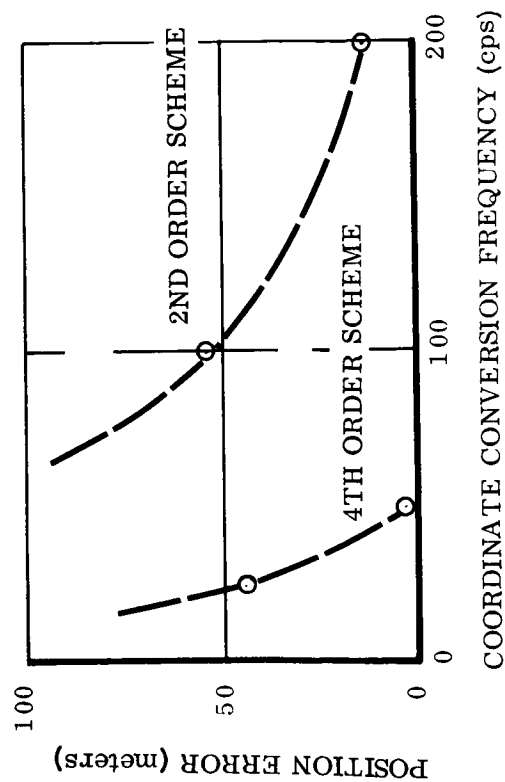


Figure VI-7 Coordinate Conversion Computational Error

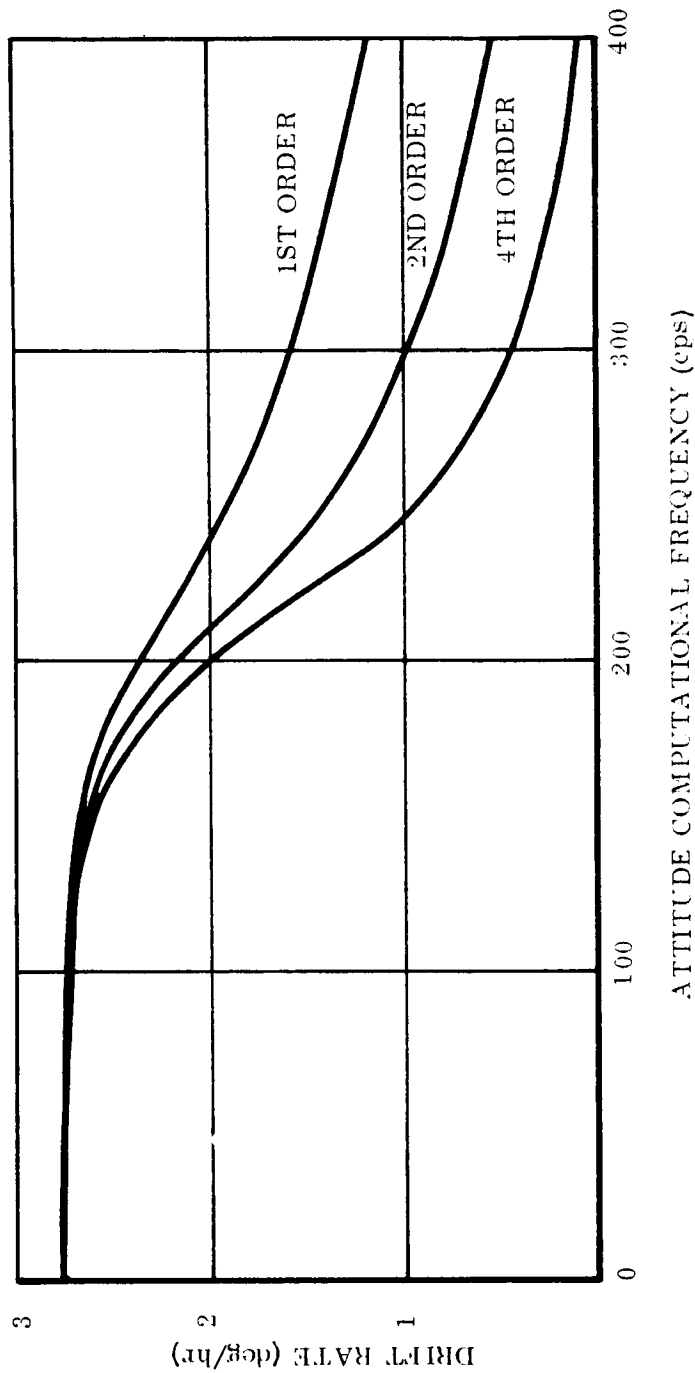
Figure VI-4, the computational error for the first order scheme with this model increases as the computational frequency is increased. This model, although inappropriate for the assumed environment below frequencies of 400 to 500 cps, does however set an upper bound on accuracy (a lower bound on error) as it is as shown in Section IV to be an optimistic estimate of the error.

In this evaluation of the attitude process truncation error, no coning motion was assumed. Coning motion was not assumed because if it occurs, it most probably occurs at the resonance of the sensor package mounting structure or shelf. To determine whether the motion at resonance is correlated to produce coning requires actual testing of the structure loaded and stressed as it would be in flight. Complex three dimensional analyses may indicate the potential existence of coning motion, but testing is required for complete verification. To demonstrate the effect that coning motion could have upon the computational process requirements, it was assumed that coning was associated with the vibratory environment in this region of 100 to 200 cps, the resonance frequency range of the assumed mounting shelf and attachment structure. The resulting error as a function of computational frequency and integration scheme is shown in Figure VI-8. For computational frequencies below 100 cps, the shown drift rate would cause navigational errors of 7 kilometers and 39 meters per second. It is seen in this figure that if this coning motion did exist, computational frequencies of 400 cps using a fourth order integration would be required to achieve acceptable accuracy; integration frequencies appreciably higher would be required for lower order integration schemes.

In Figure VI-6, the roundoff error associated with the word length used in the attitude process is presented. The navigation error shown behaves as predicted; it is proportional to computer frequency and is inversely proportional to word length. The word length required depends entirely upon the frequency of the integration process necessary to maintain the round off error at an acceptable level.

In Figure IV-7, the size effect error associated with resolving the accelerometer data into the inertial frame is presented for both the second and fourth order processes. The navigational errors are inversely proportional to the fourth and the second power of the coordinate conversion frequency for the fourth and second order schemes, respectively.

For the assumed environments, a satisfactory computational process would consist of a second order attitude integration scheme at a computational frequency of 50 cps. This would allow a fourth order coordinate conversion process to be performed at a frequency of 25 cps. To balance the round off error with that of the data processing scheme error, 32 bits of precision would be required in performing the attitude computational process. Assuming gyros whose maximum torquing



67-186

Figure VI-8 Attitude Computation Truncation Errors (For Postulated Coning Motion)

angular velocity is 10 degrees per second, a 24 bit (including sign) word length computer would be required. This computational system would yield navigational accuracies on the order of 75 meters and 0.2 meters per second. If the characteristics of the mounting shelf and the sensor package mounting structure are such that coning will be encountered, the bandwidth of the sensors and the attitude computational frequency must be sufficient to follow the motion. If the coning frequency occurs at high frequencies, the computational requirements can be substantially changed as typified by the example and the errors displayed in Figure VI-8.

SECTION VII

LIST OF SYMBOLS

$[T_a^b]$	3 x 3 direction cosine transformation matrix from coordinate system (a) to coordinate system (b)
t	time
ω	angular rate
$[\Omega]$	the skew symmetric angular rate matrix
\bar{F}	specific force
\bar{V}	velocity
R	position
g	gravitation induced acceleration
Δt	integration time interval
α_{ij}	direction cosine element of the i^{th} row and j^{th} column
$\Delta\alpha_{ij}$	the error in the α_{ij} element
\dot{C}	rate of change of the norm of the attitude error matrix
f	frequency in cycles per second
Q	quantization level
ϕ	power spectra density of angular or linear environments
β	maximum angular amplitude of sinusoidal oscillations
f_c	computational frequency in computational cycles per second
G	transfer function

VIII. REFERENCES

1. "Inertial Guidance, Navigation and Control Systems"; Duncan, R. C. and Gunnerson, A. S., Jr.; NASA Manned Spacraft Center, Houston Texas; Journal of Spacecraft and Rockets; November-December 1964.
2. "Preliminary Analysis and Evaluation of Analytic Platform Systems-FY63"; Alongi, R. E.; Systems Analysis Branch Army Inertial Guidance and Control Laboratory, Redstone Arsenal, Alabama; Rpt. No. RG-TR-63-23; August 21, 1963.
3. "A Body Bound Inertial Navigation System Using Electrostatically Supported Pendulous Gyro Accelerometers"; Gentry, C. D., Navigation and Guidance Division, Avionics Laboratory, WPAFB, and Johnson, F. V., General Electric Co.; Transaction of the Eighth Symposium on Ballistic Missile and Space Technology; October 16-18, 1963, Secret.
4. "The Present and Future Roles of Strapped-Down Inertial Systems"; Powell, J. C. 1 Honeywell Inc.; Transactions of the Eighth Symposium on Ballistic Missile and Space Technology; October 16-18, 1963.
5. "Strapped-Down Inertial Guidance"; Quasies, G. R; Honeywell Inc.; Space/Aeronautics; August 1963.
6. "Navigation and Guidance Systems Employing Gimballess IMU"; Bumstead, R. W. and Vander Velde, W. E.; MIT; AIPA Guidance and Control Conference; August 12-14, 1963.
7. "Theoretical Analysis of Gimballess Inertial Reference Equipment"; Weener, T. F.; Doctoral Thesis; MIT; March 1962.
8. "Strapped-Down Navigation"; Bessen, A. S. and Levine, J.; Sperry Rand Ford Instrument Co.; Data Systems Engineering; April 1964.
9. "A Solution for the Problems of the No-Gimbal Inertial Navigator Concept"; Turley, A. R.; Avionics Laboratory, WPAFB; AFAL-TR-64-307; January 1965.
10. "Vehicle-Fixed Component Inertial Guidance System Study"; Broxmeyer, C. and Wishner, H; Raytheon Company; NAVWEPS Report 8668, NOTSTP 3715; December 1964.
11. Haystings, Cecil, Approximations for Digital Computing, Princeton University, Press, 1955.
12. "Test Equipment Definition Study for NASA/ERC"; United Aircraft Corporate Systems Center; Report SCR 325; January 1967.

APPENDIX A

STRAPDOWN INERTIAL SENSORS AND SENSOR LOOPS

A. Introduction

The primary purpose of an inertial navigation system is to compute with respect to inertial space the velocity, position and orientation of the carrier vehicle. The information necessary to perform these functions for a strapdown navigator is obtained from measurements of the linear and angular motions of the vehicle by inertial sensors rigidly attached to the vehicle. The strapdown computational process is a function of the type and format of this sensor information. Therefore, a certain degree of understanding of the sensors as mechanized in strapdown inertial navigators is a prerequisite to the development of the computational requirements.

B. Inertial Sensors

For the purpose of developing the requirements for and analyzing the computational process, strapdown mechanizations may be classified by the type of information appearing at the sensor-computer interface. Such a classification results in two distinct classes of strapdown systems based entirely upon the data obtained from the sensors.

The first system employs sensors whose sensitive or input axes are maintained fixed relative to the vehicle; these sensors are called restrained sensors. The outputs for restrained gyros are the components of the angular rate of the vehicle or its integral relative to inertial space along the gyro input axes. The outputs for restrained accelerometers are the integral of specific force along their input axes. Since the attitude information to be derived from the gyros is vehicle angular orientation with respect to inertial space, this class of mechanization requires that the gyro data be used in the numerical integration of the equations expressing the angular rates of change of the desired attitude parameters. Specific gyro mechanizations that have received attention and fall into this category are rate, rate integrating, single axis platforms, paired pendulous integrating gyro accelerometers and, because of the similarity of output, displaced, paired accelerometers. Restrained accelerometers that have been considered are: force or torque rebalanced pendulous accelerometers, restrained pendulous integrating gyro accelerometers and a concept under development wherein the force required to center the sphere of a free gyro is used as a measurement of acceleration.

The second class of systems employs sensors whose sensitive axes are free of the vehicle's orientation; these sensors are called free sensors. The output of free gyros are trigonometric functions of the angular orientation of the vehicle relative to the gyro rotor (the model of inertial space). This class of gyro provides the required vehicle

attitude through the solution of a set of transcendental and matrix equations without integration of the angular rate equations. To date, only one type of gyro mechanization falls into this category, namely, the free gyro with different types of suspension: cryogenic, magnetic, or electrostatic. The free pendulous gyro accelerometer sensor, because of its pendulousity along the spin axis of the rotor, provides specific force information through a measurement of its precession rate relative to inertial space.

C. Sensor Loop Mechanizations and Characteristics

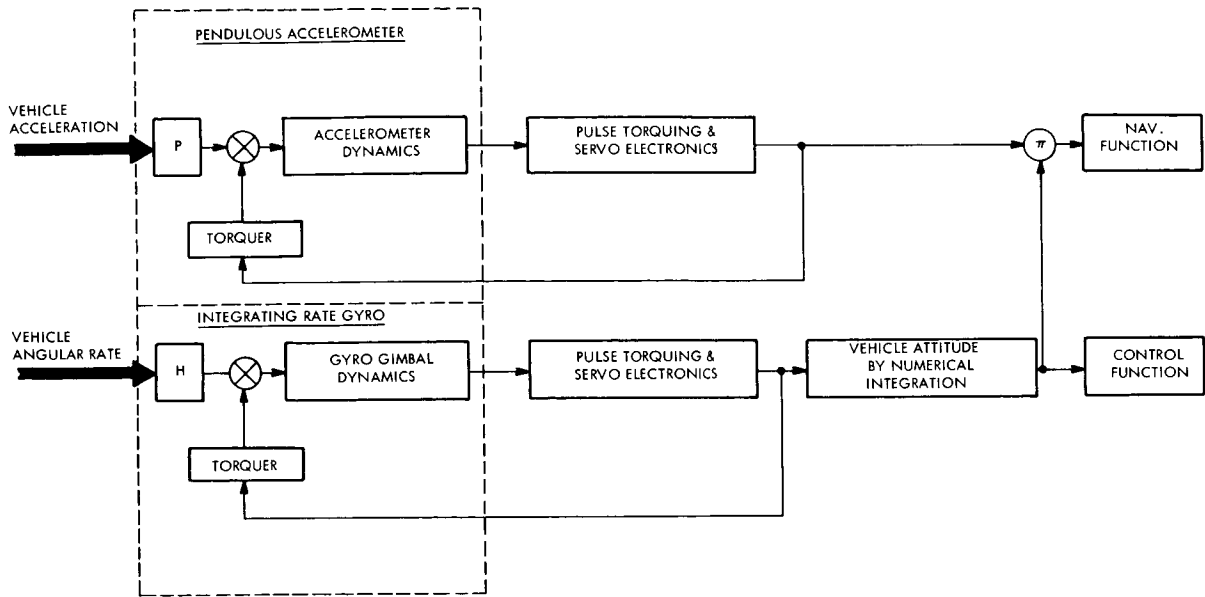
Each of the sensor loop configurations listed in the previous section have certain key requirements that must be satisfied in order to obtain a precise strapdown inertial navigator. These requirements are summarized in Table A-I. Figures A-1 through A-5 present the functional block diagrams of each of these sensor configurations as they would be employed in a strapdown navigation system.

TABLE A-I
KEY REQUIREMENTS FOR DIFFERENT STRAPDOWN
SENSOR CONFIGURATIONS

<u>Sensor Configurations</u>	<u>Key Requirements*</u>
Pulse Torqued Gyros (Figure A-1)	Wide dynamic range and a high degree of linearity
Single Axis Platform (Figure A-2)	Accurate angular encoder under extreme dynamic conditions
Paired PIGA's (Figure A-3)	Accurate angular encoder under extreme dynamic conditions
Paired Rebalanced Accelerometers (Figure A-4)	Structural stability between accelerometers mounted many feet apart
Free Gyro (Figure A-5)	Critical sphere pattern and accurate optical pickoff under extreme dynamic conditions

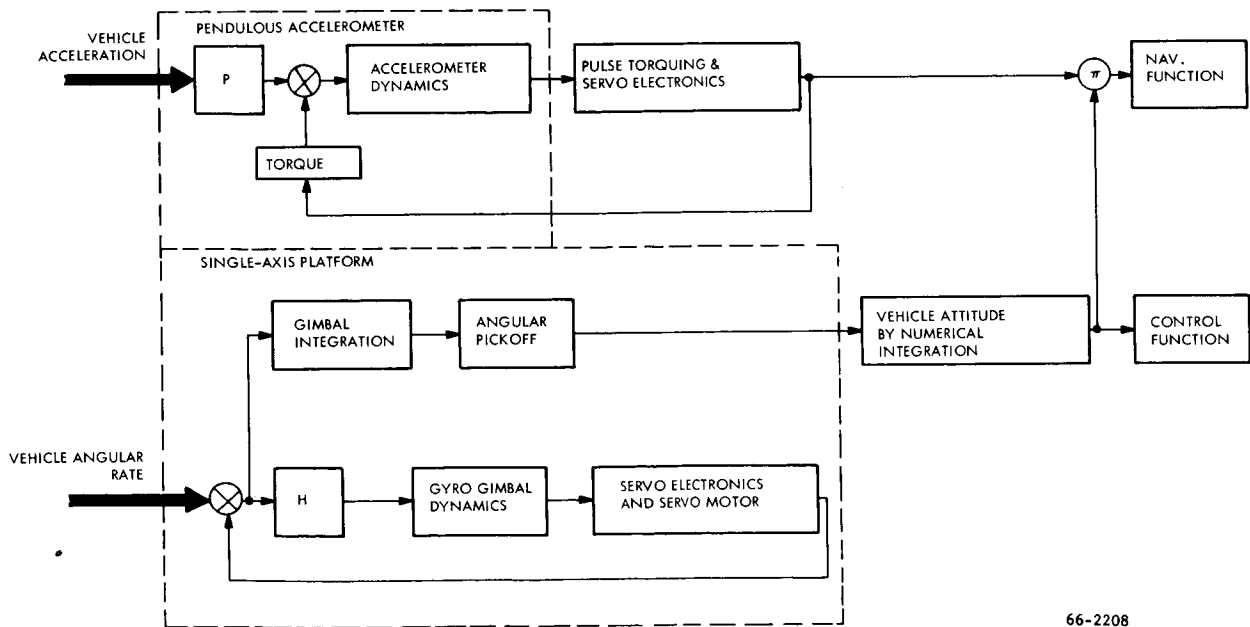
* - all require high data resolution (low quantization)

- all but free gyro require sufficient bandwidth in the sensor loop to follow significant vehicle motion
- all require accurate alignment or knowledge of the orientation of the sensitive (input) sensor axis



66-2207

Figure A-1 Functional Operation of Pulse-Torque-Rebalance Strapdown IMS



66-2208

Figure A-2 Functional Operation of Single-Axis Platform Strapdown IMS

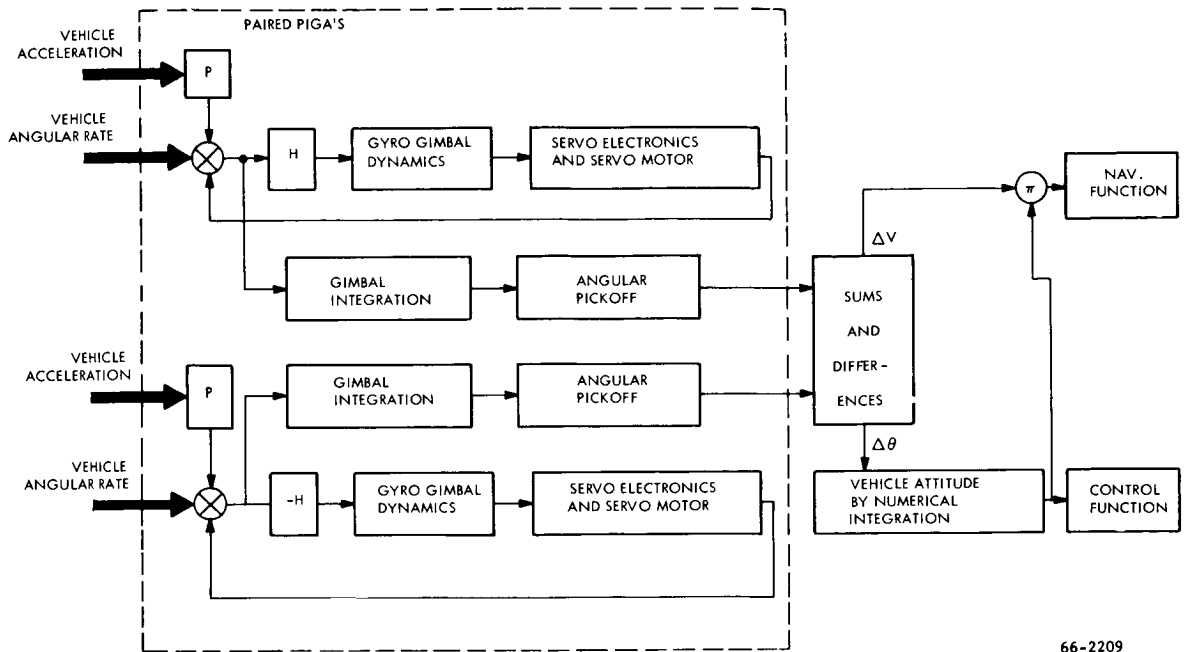


Figure A-3 Functional Operation of a Paired PIGA Strapdown IMS

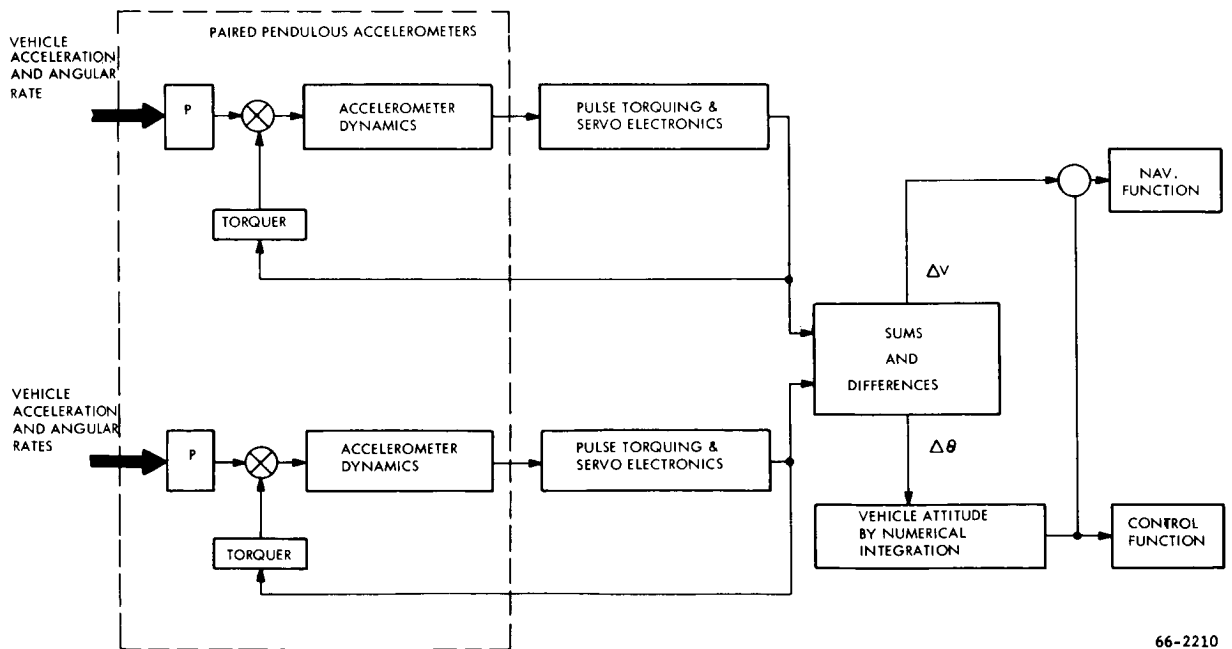
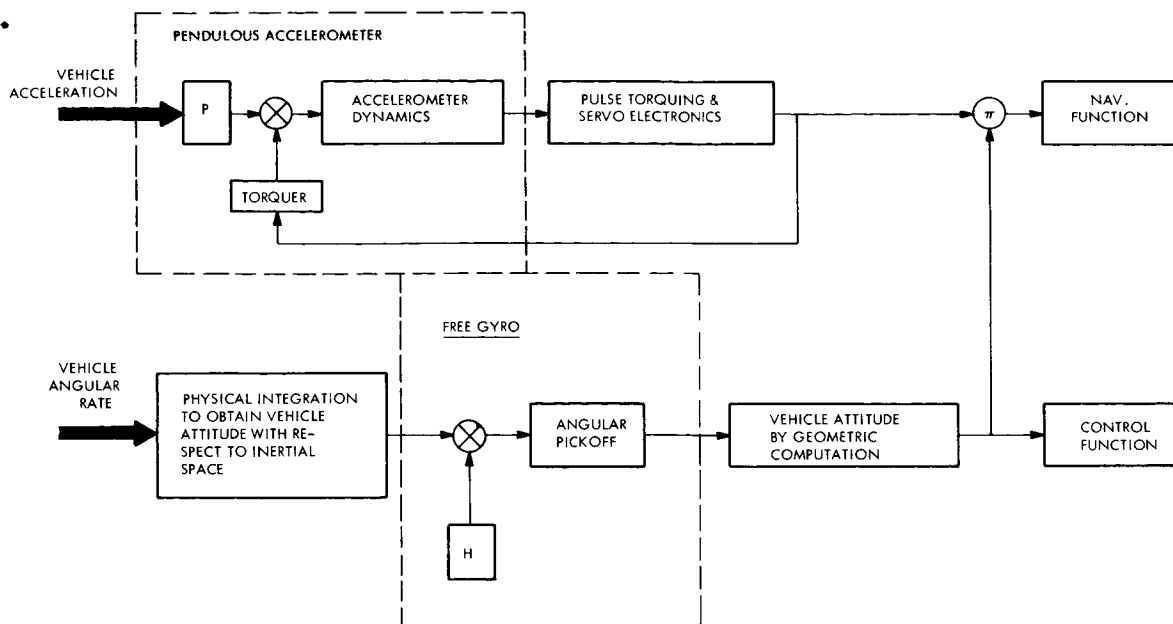


Figure A-4 Functional Operation of a Paired Pulse-Torque-Rebalanced Accelerometer Strapdown IMS



66-2206

Figure A-5 Functional Operation of Free Gyro Strapdown IMS

1. Angular Rate Measuring Sensor Loop Configurations

The two primary requirements for a strapdown rate sensing device are: (1) a high degree of linearity over the dynamic range between the random drift rate of the sensor up to the maximum angular rate of the vehicle (a dynamic range of six to eight decades) and (2) a high information resolution or a low quantization level. In addition, the sensor loop must have a bandwidth sufficient to follow all significant vehicle motions.

The first four sensor configurations presented in Table A-I are basically rate measurers that attempt to satisfy the primary requirements by different approaches.

In the rate integrating gyro mechanization (Figure A-1) the pick-off on the gyro output axis is proportional to the applied rate. This rate signal is used by the torque rebalancing electronics to generate a current proportional to the sensed input that retorques the float, thus nulling the sensed input and holding the input axis of the sensor tightly fixed with respect to the vehicle. Rate integrating gyros mechanized as described above are used in place of rate gyros simply because the latter have not demonstrated the required accuracy. To make a precise measurement of the input signal in the rate integrating gyro servo loop and to convert an analog signal to digital information (for computational purposes), the retorquing signal is broken into a series of pulses.

In such a pulse-rebalancing scheme, each pulse represents the integral of rate (the magnitude of the current times the time duration of the applied pulse) and is termed the sensor's resolution or quantization level. Either current magnitude or its applied time duration can be controlled as a function of the magnitude of the input rate. Usually current is held constant because it is easier and more accurate to control and measure time.

Several methods of pulse rebalancing have been conceived; they are termed binary, ternary and pulse-width-modulated pulse torquing. Binary torquing is a scheme in which alternate positive and negative pulses of equivalent weight represent a zero input. For any other input there is a net difference between the sum of positive and the sum of negative pulses over a finite time period. The net difference represents the angular rotation that has occurred during that time period. Ternary torquing (a pulse-on-demand scheme) consists of applying constant weight pulses (either positive or negative) only as required. In the binary and ternary schemes, the current switching points are fixed such that the quantization level (the value of each pulse) is a function of the switching frequency whose upper limit is presently limited by the impedance of the gyro torquer. A third scheme is one in which pulsing is continuous (similar to binary), but the width or time duration of the positive and negative pulses is controlled as a function of the sensed input. This scheme has the advantage of the binary torquing scheme (constant power input to the gyro), but also permits much smaller quantization levels (a fraction of an arc-second) for the same retorquing current switching frequency as binary or ternary because of the allowed variability in the pulse width thus making the quantization level independent of the switching frequency.

In order to avoid the problem of nonlinearity in torquing a gyro over a wide dynamic range (about seven decades), the gyro can be mounted on a single-axis platform such that its sensitive axis is isolated from the high vehicle angular rates. This mechanization is schematically represented in Figure A-2. Any sensed input by the gyro is used to rotate the platform about its gimbal axis which is parallel to the input axis of the gyro. Angular information (the integral of rate) is derived from a pick-off mounted on the gimbal axis. Either an incremental encoder with a "counter" or a total angle encoder with a subtraction of sequential readings can be used to generate incremental angular changes. The quantization error is now associated with the encoder rather than with a gyro retorquing servo loop. Both optical and electrical encoders have been applied to this application.

The gyro sensors used in these two schemes rely upon the angular momentum vector of a spinning body as the physical inertial reference. Three other sensor mechanizations can also be used to measure angular rate: vibrating momentum (tuning-fork), nuclear, and laser gyros. The vibrating momentum gyro's major problem is achieving a good null stability; the laser gyro requires much additional research work to increase its ability to detect differences in frequency using small optical path lengths; while nuclear gyros require improvements in many areas, readouts being one.

In a mechanization using six pendulous integrating gyro accelerometers (PIGA), each system measurement axis consists of two PIGA's whose input axes are anti-parallel. The PIGA's are packaged as close together as possible so the two sensors are essentially making measurements at the same point. Linear velocity and angular displacement data as shown in Figure A-3 are derived by adding and subtracting the outputs of the angular encoders of the two paired sensors. Any angular rotation of the float about the gyro output axis due to either sensed linear acceleration or angular rate is again used to control rotations about a gimbal axis so as to null out the output axis error. Again the quantization error is associated with the angular pickoff.

Another mechanization that also uses paired accelerometers employs force or torque restrained devices whose input axes are parallel but separated by a large and precisely known distance. The sums and differences of the output of each pair as shown in Figure A-4 provide a measure of the incremental angular change about an axis perpendicular to the plane of paired input axes and a measure of the linear velocity change in the plane of the paired input axes. The quantization error is associated with the sensors' retorquing or forcing loops which are similar to those previously described in the rate gyro scheme. This scheme requires that the sensors be linearly but rigidly displaced by a large amount. For many applications, the accelerometer bias and the stability of the displacement are so poor that the required displacement must be greater than the diameter of the vehicle to determine angular rates to the level of accuracy required.

2. Free Gyros

A free gyro maintains an inertial physical reference stabilized with respect to inertial space; direct observation of this reference yields the vehicle attitude. The inertial reference is usually the angular momentum vector of a rotating sphere suspended in an evacuated spherical container. After a spin-up, torquing is terminated and the sphere is allowed to coast. The suspension scheme for the rotating sphere (cryogenic, magnetic, or electrostatic) is not critical to the concept of the sensor configuration; it is only important with respect to performance. Attitude of the vehicle relative to the angular momentum vector can be computed by inscribing a pattern on the rotor such that the timing of series of lines crossing under an optical pick-off is a function of the angle between the pick-off and the spin vector of the rotor; from this the "direction cosine" or attitude of the spin axis relative to the pick-off can be computed (Figure A-5). A minimum of two pick-offs are required to define the orientation of the spin vector to the vehicle. Two free gyros whose spin axes are nominally perpendicular are sufficient to define an inertial reference from which vehicle attitude can be computed.

3. Accelerometers

The accelerometers usually considered for use with either a free gyro configuration or the restrained rate measuring gyros are the forced or torque-rebalanced class. Their rebalancing process and electronics are identical to those employed with torque-rebalanced gyros. Some consideration has been given to the use of a free gyro as an accelerometer by (1) measuring the force necessary to center the spinning sphere (force-rebalancing) or (2) unbalancing the accelerometer along the spin axis and measuring its precession rate relative to other balanced free gyros.

APPENDIX B

KINEMATIC EQUATIONS AND ALGORITHMS

A. Introduction

The function of an inertial navigator is to indicate attitude, velocity and position of a vehicle with respect to a selected reference frame using information obtained from onboard instruments. To perform this function, a solution of a set of three first order nonlinear differential equations must be mechanized in a digital computer to obtain position. A restrained gyro mechanization requires an additional set of differential equations to compute attitude. These equations can be solved by many different numerical integration algorithms of varying degrees of complexity and accuracy. The schemes evaluated in this study are presented in this appendix.

The measurements of linear and angular motions of the vehicle relative to inertial space are obtained in vehicle coordinates for a strapdown navigator because the inertial sensor's readouts are rigidly attached to the vehicle. This necessitates that (1) the gyro outputs be used to compute the attitude of the vehicle relative to the computational frame, and (2) the computed attitude be used to resolve the accelerometer outputs into the computational frame where they are doubly integrated along with a gravitational model to yield vehicle position. The kinematic equations, expressed in vector-matrix notation, that must be solved are:

$$\frac{d}{dt} [T_S^I(t)] = [T_S^I(t)] \cdot [\Omega(t)] \quad (B-1)$$

$$\bar{F}^I(t) = [T_S^I(t)] \cdot \bar{F}^S(t) \quad (B-2)$$

$$\bar{V}^I(t) = \bar{V}_0^I + \int_0^t \left\{ \bar{F}^I(t) - \bar{g}^I(\bar{R}) \right\} dt \quad (B-3)$$

$$\bar{R}^I(t) = R_0^I + \int_0^t \bar{V}^I(t) dt \quad (B-4)$$

For simplicity, these equations have been expressed in an inertial computation frame; a 3×3 matrix, $[T_S^I(t)]$ is used to define the orientation of the vehicle or sensor readout frame relative to the computational frame. The elements of the skew matrix, Ω , are the components of the angular rate of vehicle sensor readout frame relative to the inertial frame. The functional mechanization for the solution of these equations is shown in Figure B-1. In this figure, the gyro data processing function for restrained

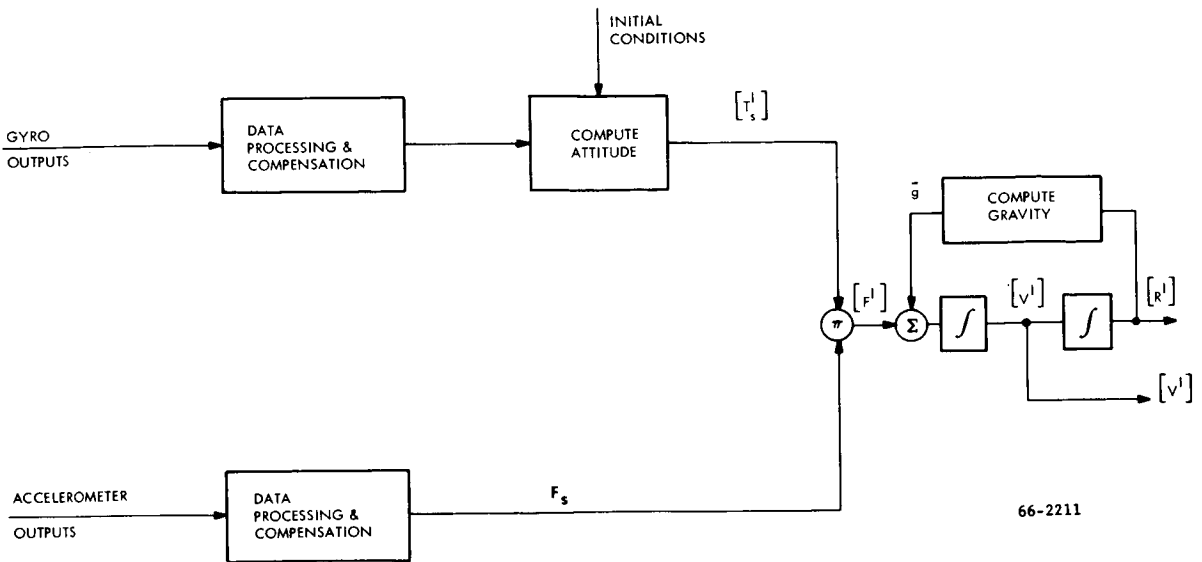


Figure B-1 Functional Mechanization for the Solution to the Navigation Equations

gyros would consist of extracting angular rates (as required by equation B-1) from the integral of rate (available from the gyros). In a free gyro mechanization it would be a synchronization of the outputs from the multiple pickoffs of these gyros. The accelerometer data processing would consist of extracting specific force from its integral for both restrained and free accelerometers. For all sensors, compensation for deterministic errors would be applied.

Although these navigation equations have been expressed in an inertial frame, considerations of computational simplicity with respect to a specific mission may suggest a different computational frame. Satellite navigation for instance may well be best accomplished in a rotating frame. However, such considerations do not affect the computational requirements because such a frame differs from the inertial frame by at most a transformation matrix whose time dependency is computable.

The following section describes the integration schemes, sensor data processing schemes and attitude parameters that have been investigated in this study. In the presentation of the various integration schemes, the required inertial measurements of angular rate and specific force will be assumed to be available; the following section describing sensor data processing schemes will describe the techniques for obtaining rate and specific force from their respective integrals that is in actuality the output of the inertial sensors.

B. Integration Algorithms

The solution of equations B-1 through B-4 requires the numerical integration of a set of first order, nonlinear differential equations because no general closed form solution to these equations is available. Many numerical difference schemes can be used; rectangular, second order Runge-Kutta and fourth order Runge-Kutta algorithms were considered in this study.

The difference equations for each of these schemes for computing attitude in a restrained gyro system by solving equation B-1 can be expressed for one integration step as:

$$[T_b^c]_{n+1} = [T_b^c]_n \cdot \left\{ [1] + [G] \right\} \quad (B-5)$$

where $[G]$ is a weighted average of the angular rate components at various points within the integration step coupled with higher order corrections for the Runge-Kutta procedures; $[T_b^c]$ denotes the direction cosine matrix defining the orientation of the vehicle body relative to the inertial computational frame.

With time as the independent integration parameter, Δt is defined to be integration step size. Ω_1 , Ω_2 , and Ω_3 denote in the following equations, the angular rate matrices at the beginning, at the midpoint and at the end of the integration interval. When mechanized within the computer using a matrix multiply subroutine, equation (B-5) takes on the following forms for each of the three integration schemes considered:

(1) Rectangular (Euler)

$$[T_b^c]_{n+1} = [T_b^c]_n \left\{ [1] + [\Omega_3] \Delta t \right\} \quad (B-6)$$

(2) Second Order Runge-Kutta

$$[T_b^c]_{n+1} = [T_b^c]_n + \frac{1}{2} \left\{ [K_1] + [K_2] \right\} \quad (B-7)$$

where

$$[K_1] = [T_b^c]_n \cdot [\Omega_1] \Delta t$$

$$[K_2] = \left\{ [T_b^c]_n + [K_1] \right\} \cdot [\Omega_3] \Delta t$$

(3) Fourth Order Runge-Kutta

$$[T_b^c]_{n+1} = [T_b^c]_n + 1/6 \left\{ [M_1] + 2[M_2] + 2[M_3] + [M_4] \right\} \quad (B-8)$$

where

$$[M_1] = [T_b^c]_n \cdot [\Omega_1] \Delta t$$

$$[M_2] = \left\{ [T_b^c]_n + \frac{1}{2} [M_1] \right\} \cdot [\Omega_2] \Delta t$$

$$[M_3] = \left\{ [T_b^c]_n + \frac{1}{2} [M_2] \right\} \cdot [\Omega_2] \Delta t$$

$$[M_4] = \left\{ [T_b^c]_n + [M_3] \right\} \cdot [\Omega_3] \Delta t$$

These equations state the numerical procedure used for each integration step. The inputs to each step are the last calculated orientation, available either as an initial condition or from the previous computation, and the angular matrices at the specified times, $[\Omega_i]$, that must be available or derived from the output of the triad of gyros.

The six differential equations defining the position and velocity of the vehicle with respect to the computational coordinate frame are presented as equations B-3 and B-4. Beginning with the integral of specific force in the computational frame ($\Delta \bar{V}^c$) and using fourth order Runge-Kutta as the integration algorithm, the numerical procedure for solving these equations for one integration step, Δt , is:

$$\bar{V}_{n+1}^c = \bar{V}_n^c + \Delta \bar{V}_{n+\frac{\Delta t}{2}}^c + \Delta \bar{V}_{n+\Delta t}^c \quad (B-9)$$

$$- \frac{1}{6} \Delta t [g^I(\bar{R}_n) + 2\bar{g}^I(\bar{C}_1) + 2\bar{g}^I(\bar{C}_2) + \bar{g}^I(\bar{C}_3)]$$

$$\bar{R}_{n+1}^I = \bar{R}_n^I + \bar{V}_n^I \Delta t + \frac{1}{6} \Delta t [5\Delta \bar{V}_{n+\frac{\Delta t}{2}}^I + \Delta \bar{V}_{n+\Delta t}^I$$

$$- \Delta t \left\{ \bar{g}^I(\bar{C}_1) + \bar{g}^I(\bar{C}_2) + \bar{g}^I(\bar{C}_3) \right\}]$$

where $\Delta \bar{V}_{n+\frac{\Delta t}{2}}^I$ and $\Delta \bar{V}_{n+\Delta t}^I$ are the integral of specific force over the first half and second half of the integration step, respectively; \bar{C}_j is an intermediate position vector defined by

$$\bar{C}_1 = \bar{R}_n^I + \frac{1}{2} \Delta t \bar{V}_n^I$$

$$\bar{C}_2 = \bar{R}_n^I + \frac{1}{2} \Delta t \left[\bar{V}_n^I + \Delta \bar{V}_{n+\frac{\Delta t}{2}}^I - \frac{1}{2} \Delta t \bar{g}^I (\bar{C}_1) \right]$$

$$\bar{C}_3 = \bar{R}_n^I + \Delta t \left[\bar{V}_n^I + \Delta \bar{V}_{n+\frac{\Delta t}{2}}^I - \frac{1}{2} \Delta t \bar{g}^I (\bar{C}_2) \right]$$

The general form for the potential used in computing gravitational forces, g^c , within the Earth's sphere of influence is

$$U = \mu/R \left[1 - \sum_{n=2}^{\infty} J_n \left(\frac{R_e}{R} \right)^n P_n^{(0)}(\sin \theta) + \sum_{n=2}^{\infty} \sum_{m=1}^n J_n^{(m)}(\sin \theta) \cos \left[m(\lambda - \lambda_n^{(m)}) \right] \right] \quad (B-10)$$

where

U is the potential function,

μ is the product of Earth mass and the universal gravitational constant,

R_e is the Earth's equatorial radius,

R is the geocentric radius,

λ is east longitude with respect to Greenwich,

θ is geocentric latitude,

$P_n^{(m)}$ are Legendre Polynomials,

$J_{n(m)}$ are zonal (latitude dependent) harmonic constants,

J_n are tesseral (longitude and latitude dependent) harmonic constants,

$\lambda_n^{(m)}$ are longitude constants of the $J_n^{(m)}$.

This expression is normally differentiated with respect to the directions of the chosen coordinate system to yield the gravitational force per unit mass on a vehicle at the location θ, λ, R . Recent fits to ground observational data of orbiting satellites

have refined the knowledge of the constants up to the fourth order. The second oblateness harmonic, J_2 , is necessary in all but the crudest navigation systems, since it can cause perturbations from the spherical case of several miles over a fraction of an orbit. The higher order terms are necessary for more accurate systems. Reference B-1 shows short term perturbations of over a mile within one orbit due to the $J_2^{(2)}$ and $J_3^{(3)}$ tesseral terms.

Consideration has been given to multi-step integration schemes of the predictor type, such as the Adams-Bashforth and Milne schemes, or corrector types, such as Adams-Moulton, Milne-Simpson, and Milne-Hamming. However, these multiple step schemes have some characteristics that must be carefully evaluated in trade-off studies from the system standpoint before applying them in space navigation systems. The corrector forms are most accurate, but must be used in conjunction with a predictor method. Care must be taken in selecting a method, since some of them, though accurate in minimizing local truncation error, are somewhat unstable to the propagation of computational errors (Reference B-2). Single step methods, on the other hand are stable; the Runge-Kutta algorithm "displays a most interesting ability to follow a solution without increasing its error" (Reference B-3). The one-step methods are considerably less complex and require less computer storage. They are self-starting and adaptable to changing integration step sizes, whereas the multiple step methods require a starting procedure (usually with a one-step method) for initiation.

For some applications it may be desirable to use an incremental Digital Differential Analyzer (DDA) rather than a whole number, general purpose digital data processor (DDP). In utilizing a DDA, angle (or velocity in the case of accelerometers) is logically used as the independent integration parameter rather than time. Each sensor pulse, or a fixed number of pulses, is allowed to accumulate until a specified level is reached, at which time an integration step is performed. Because the multiplications in the angular motion difference equations are between direction cosines and the incremental angular change, only additions or subtractions are needed because the angular change is always constant. DDA's readily lend themselves to rectangular integration processes although second order schemes such as modified Euler integration (second order Runge-Kutta) can be implemented without undue computer complexity.

C. Sensor Data Processing Techniques

1. Restrained Gyros

The integration of the angular equations of motion requires rate information while the gyro pulse data represents the integral of angular velocity. The output of the gyros must, in effect, be differentiated with respect to time to establish compatibility between the gyro outputs and the integration process. If the gyro output data are

treated as incremental angular rotations and this angular change is assigned vector properties, the accuracy of the rate extraction process ($\bar{\omega} = \bar{\Delta\theta}/\Delta t$) and hence that of the solution of equation (B-1) is limited to second order, independent of the use of higher order integration schemes. This has been sometimes construed to be a fundamental accuracy limitation of strapdown systems associated with the commutative error of assigning vector properties to incremental rotations.

The incremental outputs of the gyro, however, are not angular rotations in the true sense, but more correctly the integral of the angular rate components as a function of time and these integrated quantities are correct at the data sampling instants to within the accuracy of the integrating sensor. Thus, an inverse estimation process that derives the angular rate components (whose integrals best fit the data) can be used to provide rate data of higher order accuracy at specified points in time for use in higher order numerical integration algorithms.

a. Development of Angular Rate Extraction Process

The output of an integrating rate gyro, if assigned vector properties gives rise to a set of computed direction cosines which, by the mean value theory, lead the true set of direction cosines by some phase angle often termed the third order commutativity error. A more accurate processing scheme consists of (1) fitting an n^{th} order polynomial to the gyro outputs over an interval of time using multiple samples of the gyro output during that interval and then (2) extracting the rate information from the polynomial which can be differentiated analytically. The following analysis demonstrates that errors arising from the use of a second order polynomial when implemented with fourth order Runge-Kutta are of fifth order, consistent with the accuracy of the fourth order Runge-Kutta integration scheme. The same procedure may be extended to any order integration algorithm.

The fourth order Runge-Kutta integration of the angular rate equations (equation B-8) may be rewritten for each integration interval as

$$\begin{aligned}
 [T]_{n+1} = [T]_n + \frac{1}{6} [T]_n \bigg\{ & ([\Omega_1] + 4 [\Omega_2] + [\Omega_3]) \Delta t \quad (B-11) \\
 & + ([\Omega_1] \cdot [\Omega_2] + [\Omega_2] \cdot [\Omega_2] + [\Omega_2] \cdot [\Omega_3]) \Delta t^2 \\
 & + \frac{1}{2} ([\Omega_1] \cdot [\Omega_2] \cdot [\Omega_2] + [\Omega_2] \cdot [\Omega_2] \cdot [\Omega_3]) \Delta t^3 \\
 & + \frac{1}{4} ([\Omega_1] \cdot [\Omega_2] \cdot [\Omega_2] \cdot [\Omega_3]) \Delta t^4 \bigg\}
 \end{aligned}$$

The above equation requires values of the angular rate matrix at the beginning, midpoint, and end of each integration interval, $[\Omega_1]$, $[\Omega_2]$, and $[\Omega_3]$, respectively.

The required rate estimates are obtained from the following gyro data processing scheme which assumes that (1) the frequency of angular motion to be followed by the integration scheme is lower than that of the attitude computational frequency and (2) that the integral of angular rate component along each body axis over any integration interval can be represented as a polynomial expanded in powers of time about the beginning of the integration interval (t_0) (for convenience, $t_0 = 0$):

$$\theta = \int_0^t \omega dt = \alpha t + \beta t^2 \quad (\text{B-12})$$

During each integration interval, the value of θ is obtained twice from the sensor, first at the midpoint ($\Delta t/2$), again at the end of the interval (Δt)

$$\theta_2 = \int_0^{\Delta t/2} \omega dt$$

$$\theta_3 = \int_0^{\Delta t} \omega dt$$

such that the coefficients of the polynomial in Equation (B-12) may be evaluated in terms of θ_2 and θ_3 :

$$\alpha = \frac{1}{\Delta t} (4\theta_2 - \theta_3) \quad \beta = \frac{1}{(\Delta t)^2} (2\theta_3 - 4\theta_2) \quad (\text{B-13})$$

Estimates of components of angular rate denoted by ω' (where ω denotes the true rates components) at any time within the interval can then be obtained by substituting these coefficients into the derivative of the θ polynomial (equation B-12):

$$\omega'(t) = \alpha + 2\beta t = \frac{1}{\Delta t} (4\theta_2 - \theta_3) + \frac{4t}{\Delta t^2} (\theta_3 - 2\theta_2) \quad (\text{B-14})$$

For convenience define

$$\Delta\theta_2 = \theta_2 \text{ and } \Delta\theta_3 = \theta_3 - \Delta\theta_2 \quad (\text{B-15})$$

Substituting these values into Equation (B-14) and evaluating that equation at times 0, $\Delta t/2$, and Δt as required by the fourth order Runge-Kutta integration scheme (equation B-11) yields the estimated rates at these times along the body axes:

$$\omega'_i(t=0) = \omega'_{1i} = \frac{1}{\Delta t} (3 \Delta \theta_{2i} - \Delta \theta_{3i}) \quad (\text{B-16})$$

$$\omega'_i(t=\frac{\Delta t}{2}) = \omega'_{2i} = \frac{1}{\Delta t} (\Delta \theta_{2i} + \Delta \theta_{3i})$$

$$\omega'_i(t=\Delta t) = \omega'_{3i} = \frac{1}{\Delta t} (3 \Delta \theta_{3i} - \Delta \theta_{2i})$$

i = x, y, or z body axis

b. Evaluation of the Gyro Data Processing Error

The accuracy of the gyro data processing scheme (Equation B-16) may be determined by expressing the angular rate component along a body axis as a polynomial expansion in time to any desired degree of accuracy:

$$\omega_i = a_0 + a_1 t + a_2 t^2 + a_3 t^3 + a_4 t^4 + \dots \quad (\text{B-17})$$

This expression may then be integrated to obtain $\Delta \theta_2$ and $\Delta \theta_3$ thus simulating the outputs of a perfect gyro loop:

$$\Delta \theta_{i+1} = \int_{t_i}^{t_{i+1}} \omega dt = a_0 (t_{i+1} - t_i) + \frac{a_1}{2} (t_{i+1}^2 - t_i^2) + \dots \quad (\text{B-18})$$

and the results substituted into Equation B-16 to obtain the estimates of angular rate, ω' that the computational scheme would compute:

$$\omega'_1 = a_0 + a_1 t_1 + a_2 (t_1^2 - \frac{1}{6} \Delta t^2) + a_3 (t_1^3 - \frac{1}{2} t_1 \Delta t^2 - \frac{3}{16} \Delta t^3) \quad (\text{B-19})$$

$$+ a_4 (t_1^4 - t_1^2 \Delta t^2 - \frac{3}{4} t_1 \Delta t^3 - \frac{7}{40} \Delta t^4) + \dots$$

$$\omega'_2 = a_0 + a_1 (t_1 + \frac{\Delta t}{2}) + a_2 (t_1^2 + t_1 \Delta t + \frac{1}{3} \Delta t^2) + a_3 (t_1^3 + \frac{3}{2} t_1^2 \Delta t + t_1 \Delta t^2 + \frac{1}{4} \Delta t^3) + a_4 (t_1^4 + 2 t_1^3 \Delta t + 2 t_1^2 \Delta t^2 + t_1 \Delta t^3 + \frac{1}{5} \Delta t^4) + \dots$$

$$\omega'_3 = a_0 + a_1 (t_1 + \Delta t) + a_2 (t_1^2 + 2 t_1 \Delta t + \frac{5}{6} \Delta t^2) + a_3 (t_1^3 + 3 t_1^2 \Delta t + \frac{5}{2} t_1 \Delta t^2 + \frac{11}{16} \Delta t^3) + a_4 (t_1^4 + 4 t_1^3 \Delta t + 5 t_1^2 \Delta t^2 + \frac{11}{4} t_1 \Delta t^3 + \frac{23}{40} \Delta t^4) + \dots$$

The true values of angular rate, ω_1 , ω_2 , and ω_3 , are available from Equation (B-17) by substituting $t = t_1$, $t_1 + \Delta t/2$, and $t_1 + \Delta t$, respectively. If the error in the estimated values of rate (ω') is defined to be the estimated value minus the true value ($\omega' - \omega$), the errors in each of the estimates $\epsilon = (\omega' - \omega)$, at the beginning, midpoint, and end of the integration interval are

$$\epsilon_1 = -\Delta t^2 (\frac{1}{6} a_2 + \frac{1}{2} a_3 t_1 + a_4 t_1^2 + \dots) - \Delta t^3 (\frac{3}{16} a_3 + \frac{3}{4} a_4 t_1) \quad (\text{B-20})$$

$$+ \dots - \Delta t^4 (\frac{7}{40} a_4 + \dots) + \dots$$

$$\epsilon_2 = \Delta t^2 (\frac{1}{12} a_2 + \frac{1}{4} a_3 t_1 + \frac{1}{2} a_4 t_1^2 + \dots) + \Delta t^3 (\frac{1}{8} a_3 + \frac{1}{2} a_4 t_1 + \dots) + \Delta t^4 (\frac{11}{80} a_4 + \dots) + \dots$$

$$\epsilon_3 = -\Delta t^2 (\frac{1}{6} a_2 + \frac{1}{2} a_3 t_1 + a_4 t_1^2 + \dots) - \Delta t^3 (\frac{5}{16} a_3 + \frac{5}{4} a_4 t_1 + \dots) + \Delta t^4 (\frac{17}{40} a_4 + \dots) + \dots$$

These equations show the error in approximating ω about any axis at any of the three required times in the integration interval is proportional to the second and higher powers of the integration interval. This is to be expected since only a two-term polynomial (Equation B-12) is used to extract rate from its integral.

c. Evaluation of the Effect of the Gyro Data Processing Error Upon the Accuracy of Fourth Order Runge-Kutta Integration

Although the error in the rate estimation presented in the previous section is not fourth order, the third and fourth order terms cancel when they are substituted into the fourth order Runge-Kutta integration process, thus preserving the fourth order accuracy of integration process. This favorable cancellation occurs because the value of the integral of rate obtained from the gyro is not changed by the errors in the rate approximations as may be seen by examining the cancellation, term by term, in the following analysis. For convenience of analysis, Equation (B-11) may be rewritten as

$$[T]_{n+1} = [T]_n + \frac{1}{6} [T] [A + B + C + D] \quad (B-21)$$

where

$$A = ([\Omega_1] + 4 [\Omega_2] + [\Omega_3]) \Delta t$$

$$B = ([\Omega_1] \cdot [\Omega_2] + [\Omega_2] \cdot [\Omega_2] + [\Omega_2] \cdot [\Omega_3]) \Delta t^2$$

$$C = \frac{1}{2} ([\Omega_1] \cdot [\Omega_2] \cdot [\Omega_2] + [\Omega_2] \cdot [\Omega_2] \cdot [\Omega_3]) \Delta t^3$$

$$D = \frac{1}{4} ([\Omega_1] \cdot [\Omega_2] \cdot [\Omega_2] \cdot [\Omega_3]) \Delta t^4$$

The error in the A summation of rate matrices times the integration interval of Equation B-21) is:

$$\begin{aligned} E_A &= \Delta t ([\Omega'_1] + 4 [\Omega'_2] + [\Omega'_3] - [\Omega_1] - 4 [\Omega_2] - [\Omega_3]) \\ &= \Delta t ([\epsilon_1] + 4 [\epsilon_2] + [\epsilon_3]) \end{aligned} \quad (B-22)$$

Since the rate matrices are skew-symmetric, the error in the rate matrices are likewise skew-symmetric. The error in the A summation can thus be analyzed one axis or one element at a time using Equation (B-20).

$$E_{Ai} = \Delta t \epsilon_{1i} + 4 \Delta t \epsilon_{2i} + \Delta t \epsilon_{3i} \quad (B-23)$$

where

i = X, Y, or Z body axis

Substituting Equation (B-20) into (B-23) and collecting terms demonstrates that the error in the A summation is proportional to the fifth power of the integration interval

$$E_{Ai} = O(\Delta t^5)$$

After the matrix multiplication indicated in the B summation is performed, the diagonal elements of the resulting matrix are composed of the summation of the products of the rate along the same body axis at different times (the subscripts i and j denote different body axes; the subscripts 1, 2 and 3 denote different times):

$$B_{nn} = -\Delta t^2 \left\{ (\omega_{i1} \omega_{i2} + \omega_{i2} \omega_{i2} + \omega_{i2} \omega_{i3}) + (\omega_{j1} \omega_{j2} + \omega_{j2} \omega_{j2} + \omega_{j2} \omega_{j3}) \right\} \quad (B-24)$$

While the off-diagonal elements are the summation of the products of rate about different body axes at different times:

$$B_{mn} = \Delta t^2 \left\{ \omega_{i1} \omega_{j2} + \omega_{i2} \omega_{j2} + \omega_{i2} \omega_{j3} \right\} \quad (B-25)$$

where

n and m = 1, 2, or 3 and are the usual row and column specification of the elements of the rate matrix with $m \neq n$

and

i and j = x, y, or z with $i \neq j$.

The error in the B matrix is now easily analyzed element by element in terms of the functional form of each element (of the rate matrix). Since the diagonal elements

are composed of two similar groupings of terms, only one need be considered. From Equation (B-24) the B summation diagonal error (E_{BD}) can be expressed as:

$$\begin{aligned} E_{BD} &= \Delta t^2 \omega_{i2}^1 \left\{ \omega'_{i1} + \omega'_{i2} + \omega'_{i3} \right\} - \Delta t \omega_{i2} \left\{ \omega_{i1} + \omega_{i2} + \omega_{i3} \right\} \\ &= \Delta t^2 \left[\omega_{i2} \left\{ \epsilon_{i1} + \epsilon_{i2} + \epsilon_{i3} \right\} + \epsilon_{i2} \left\{ \omega_{i1} + \omega_{i2} + \omega_{i3} \right\} \right. \\ &\quad \left. + \epsilon_{i2} \left\{ \epsilon_{i1} + \epsilon_{i2} + \epsilon_{i3} \right\} \right] \end{aligned} \quad (B-26)$$

The error in the last term is immediately seen to be of $O(\Delta t^6)$. Substituting Equation (B-17) for the rate and Equation (B-20) for the errors into the first two terms of the above equation and collecting terms, the error in these terms is demonstrated also to be of $O(\Delta t^6)$.

The error in the off-diagonal elements (Equation B-25) can be also expressed as:

$$\begin{aligned} E_{BOD} &= \Delta t^2 \left\{ (\omega'_{i1} + \omega'_{i2}) \omega'_{j2} + \omega'_{i2} \omega'_{j3} - (\omega_{i1} + \omega_{i2}) \omega_{j2} + \omega_{i2} \omega_{j3} \right\} \\ &= \Delta t^2 \left\{ \omega_{j2} (\epsilon_{i1} + \epsilon_{i2}) + \epsilon_{j2} (\omega_{i1} + \omega_{i2}) + \epsilon_{i2} \omega_{j3} \right. \\ &\quad \left. + \omega_{i2} \epsilon_{j3} + \epsilon_{j2} (\epsilon_{i1} + \epsilon_{i2}) + \epsilon_{i2} \epsilon_{j3} \right\} \end{aligned} \quad (B-27)$$

The error in the last two terms is of $O(\Delta t^6)$; when the true rate from Equation (B-17) and the errors in estimated rate from Equation (B-20) are substituted into this equation, the error in the first four terms of Equation (B-27) is shown to be of $O(\Delta t^5)$.

No further detailed analysis is necessary to establish that the error in the C and D terms is at most fifth order since the error in approximating each $[\Omega]$ is proportional to the second power of the integration interval, and the C term is multiplied by Δt^3 and the D term by Δt^4 . The errors in these terms are at most $O(\Delta t^5)$ and $O(\Delta t^6)$, respectively.

2. Restrained Accelerometers

In a strapdown system, the accelerometers are fixed in the rotating vehicle frame and must be resolved into the computational frame using the results of the attitude computations. One method by which this transfer of data can be accomplished is

$$\Delta \bar{V}^c = [T_b^c] \cdot \Delta \bar{V}^b \quad (B-28)$$

This procedure, however, has the disadvantage of introducing a phase angle error similar to that for the comparable gyro data processing scheme. A more accurate procedure, suitable for the use with higher order integration of the position tracking equations, involves three steps: first, the estimation of specific force (in a manner similar to the gyro data processing) at the beginning, midpoint and end of an interval obtained from the integral of specific force; second, the resolution of the specific force into the computational frame using the computed transformation matrices at each of these times; third, the integration of specific force in the computational frame over this interval. The entire data processing scheme can be summarized in the following equation:

$$\Delta \bar{V}_j^c = \frac{1}{6} \left\{ (3 [T_b^c]_1 + 4 [T_b^c]_2 - [T_b^c]_3) \cdot \Delta \bar{V}_2^b + (3 [T_b^c]_3 + 4 [T_b^c]_2 - [T_b^c]_1) \cdot \Delta \bar{V}_3^b \right\} \quad (B-29)$$

when the subscripts 1, 2, and 3 refer to the beginning, mid-point, and the end, respectively, of the time interval of interest; ΔV_2 and ΔV_3 denote the accelerometer outputs over the first and second half of the time interval respectively.

Using this accelerometer data processing scheme, the rate at which the accelerometer data can be transferred to the computational frame is one-half the attitude matrix computation frequency. Employing this scheme with 4th order Runge-Kutta integration, the position-tracking computations must be carried out at multiples of four times the attitude computation integration interval; the transfer of data to the computational coordinates system requires two attitude computation intervals to obtain one velocity increment and the 4th order Runge-Kutta integration scheme requires two of these velocity increments (Equation B-9). If it is desired to increase the position-tracking integration interval beyond that of four intervals, the velocity increments are resolved into the computational frame every two attitude computation intervals and then summed for the appropriate length of time in the computational frame.

3. Free Accelerometers

The outputs of free pendulous gyro accelerometers are the unit vectors describing the orientation of the spin axes of the instruments in the body frame. These vectors must then be resolved into the inertial frame using the transformation matrix $[T_s^I(t)]$ derived from the gyro data and their derivatives obtained. The components of specific force are extracted after this transformation and differentiation process. The transfer of the data to the inertial frame presents no particular problems, simply a matrix times a vector process. The extraction of specific force however is more complicated as it requires that the set of linear differential equations (presented in Table B-I) be

TABLE B-I

FREE PENDULOUS GYRO ACCELEROMETER
COORDINATE TRANSFORMATION PROCESS

EQUATION OF MOTION FOR SPIN AXIS IN INERTIAL SPACE

$$\frac{d\bar{a}^I}{dt} = \frac{P}{H} \bar{a}^I \times \bar{F}^I$$

$$\frac{d\bar{b}^I}{dt} = \frac{P}{H} \bar{b}^I \times \bar{F}^I$$

P - PENDULOUS MOMENT
H - ANGULAR MOMENTUM
F - SPECIFIC FORCE
 \bar{a} , \bar{b} - SPIN AXIS UNIT VECTORS

SPECIFIC FORCE SOLUTION

- ATTITUDE COMPUTATIONS YIELDS $\left[T_b^I(t) \right] \left\{ \begin{array}{l} \bar{a}^I(t), \bar{b}^I(t) \end{array} \right\}$
- FPGA OUTPUTS YIELDS $\bar{a}^b(t), \bar{b}^b(t)$
- $$\begin{bmatrix} F_\ell \\ F_m \\ F_n \end{bmatrix} (t) = \frac{P}{H} \cdot \begin{bmatrix} 0 & -an & am \\ an & 0 & -a\ell \\ -am & a\ell & 0 \\ 0 & -bn & bm \\ bn & 0 & -b\ell \\ -bm & b\ell & 0 \end{bmatrix}^{-1} (t) \cdot \frac{d}{dt} \begin{bmatrix} a\ell \\ am \\ an \\ b\ell \\ bm \\ bn \end{bmatrix}$$
- YIELDS SPECIFIC FORCE IN THE INERTIAL FRAME

solved. This set of equations, however, is degenerate and their solution requires either a best fit procedure based on a least squares or similar criteria (Reference B-4) or logic to choose from among the equations an independent set of three that can be directly solved at the possible expense of accuracy. After specific force is obtained, it must be integrated so as to yield the information required by the position tracking equations.

D. Attitude Parameters for a Restrained Gyro Attitude Reference System

In a restrained gyro system, the angular relationship of the vehicle to the non-rotating computational frame must be computed from the gyro outputs. The angular orientation of the rotating frame with respect to the inertial computational frame can be expressed by many different classes of parameters. Three classes of predominant interest are

- (1) a three attitude parameter set: three Euler angles representing successive rotations about three body-fixed axes in a specified sequence,
- (2) four attitude parameter sets: quaternions, Cayley-Klein parameters or four Euler angles, and
- (3) a nine parameter set: direction cosines relating each of the vehicle axes to the three computational axes.

All three of these schemes involve the solution of first order non-linear differential equations to describe vehicle angular motion.

Euler angles have been used extensively to analyze and describe aircraft angular motion. A typical set of equations for an x-y-z rotation sequence is shown in Table B-II. The principal advantage of Euler angles is the ease by which one can relate the mathematics to the actual physical orientation; i.e., pitch, roll, and yaw angles. Although only three parameters and, thus, three integrations are necessary, the required sine and cosine functions and the nine conversion equations to obtain $[T_S^I(t)]$ make the solution of these equations more difficult and time consuming than the other two methods for any difference scheme of third order accuracy or better. Also, there is a singular point analogous to the gimbal "lock" problem on an electro-mechanical three-gimbal platform; when the second of the three sequential angles approaches ninety degrees, the other two axes of rotation become near collinear and the rate of change of these two Euler angles becomes indeterminate. Logic is necessary to prevent this singularity by either changing to a different angle sequence or adding a fourth angle to the sequence (analogous to a four-gimbal platform) along with logic to account for redundancy of information. This leads to the more general class of four-parameter or quaternion description of orientation, described below.

TABLE B-II

ANGULAR EQUATIONS OF MOTION FOR THREE CLASSES OF PARAMETERS

1. Euler Angle Method; integrate the following three differential equations:

$$\dot{\phi} = \sec \theta (\omega_x \cos \psi - \omega_y \sin \psi)$$

$$\dot{\theta} = \omega_x \sin \psi + \omega_y \cos \psi$$

$$\dot{\psi} = \omega_z + \tan \theta (\omega_y \sin \psi - \omega_x \cos \psi)$$

Where ϕ, θ, ψ are Euler angles about the body x, y, z axes. (The above equations define a ϕ - θ - ψ sequence). ω_i ($i = x, y, z$) are the measured body rates. Logic must be included to switch variables when θ approaches $\pm \pi/2$. Also required are the nine equations to obtain $[T_a^c]$:

$$[T_s^I(t)] = \begin{bmatrix} \cos \theta \cos \phi & \sin \psi \sin \phi - \sin \theta \cos \psi \cos \phi & \cos \psi \cos \phi + \sin \theta \cos \phi \sin \psi \\ \sin \theta & \cos \psi \cos \theta & -\sin \psi \cos \theta \\ -\cos \theta \sin \phi & \sin \psi \cos \phi + \cos \psi \sin \theta \sin \phi & \cos \psi \cos \phi - \sin \psi \sin \theta \sin \phi \end{bmatrix}$$

2. Direction Cosine Method, integrate the following nine differential equations:

$$\frac{d}{dt} [T_s^I(t)] = [T_s^I(t)] \cdot [\Omega]$$

where

$$[\Omega] = \begin{bmatrix} 0 & -\omega_z & \omega_y \\ \omega_z & 0 & -\omega_x \\ -\omega_y & \omega_x & 0 \end{bmatrix}$$

no logic or additional equations are necessary

TABLE B-II (continued)

ANGULAR EQUATIONS OF MOTION FOR THREE CLASSES OF PARAMETERS

3. Quaternion Method, integrate the following four differential equations:

$$\dot{q}_0 = -1/2 (q_1 \omega_x + q_2 \omega_y + q_3 \omega_z)$$

$$\dot{q}_1 = 1/2 (q_0 \omega_x + q_3 \omega_y - q_2 \omega_z)$$

$$\dot{q}_2 = 1/2 (-q_3 \omega_x + q_0 \omega_y + q_1 \omega_z)$$

$$\dot{q}_3 = 1/2 (q_2 \omega_x - q_1 \omega_y + q_0 \omega_z)$$

where q_0 , q_1 , q_2 , and q_3 are the quaternions.

Also required are the nine equations to obtain $[T_a^c]$

$$[T_s^I(t)] = \left[\begin{array}{c|c|c} q_0^2 + q_1^2 - q_2^2 - q_3^2 & 2(q_1 q_2 - q_0 q_3) & 2(q_0 q_2 + q_1 q_3) \\ 2(q_0 q_3 + q_1 q_2) & q_0^2 - q_1^2 + q_2^2 - q_3^2 & 2(q_2 q_3 - q_0 q_1) \\ 2(q_1 q_3 - q_0 q_2) & 2(q_3 q_2 + q_1 q_0) & q_0^2 - q_1^2 - q_2^2 + q_3^2 \end{array} \right]$$

Direction cosines are a straightforward method of describing orientation of one axis frame with respect to another. Solution of the difference equations involves only multiplications and additions, and the resulting nine numbers can be used directly as elements of $[T_s^I(t)]$ in resolving the sensed acceleration vector into the computational frame (Table B-II). There is no singularity point or region prone to computational errors as is the case with Euler angles. However, since only four of the nine cosine numbers are independent parameters, computational errors in the integration of all nine lead to non-orthogonality of the matrix $[T_s^I(t)]$. For short-term applications, such as boost and injection of a missile or satellite, no correction is necessary for this non-orthogonality. The error in solution of Equation (B-1) is no worse than if the matrix $[T_s^I(t)]$ were orthogonalized regularly during the computations. When the

matrix $[T_S^I(t)]$ is re-aligned in long-term applications, such as by stellar observations or orbital gyro-compassing with a vertical sensor, logic should be included to insure that the sum of the squares of each row and column of $[T_S^I(t)]$ equal unity. This is normally considered part of the alignment computation.

The quaternion method of describing angular orientation is based upon Euler's theorem that any real rotation can be expressed as a single rotation through some angle about a fixed axis. The four variables consist of a scalar, representing the magnitude of the angle, and a unit vector, representing the axis of rotation. It has been shown that geometric derivation of the Euler parameters and a derivation from a complex-number approach (Cayley-Klein parameters) both lead to the same set of equations describing the rates of change of the four variables as a function of the angular velocity components (Reference B-5). Solution of these equations requires only multiplications and additions, as in the case of direction cosines, and only four integrations. One of the four parameters is not independent, subject to the unit vector condition of the direction of rotation. Thus, similar orthogonalization considerations exist as in the direction cosine case, although with somewhat less logic when it is desired to re-align the attitude computations. Fewer instructions are required to implement the solution of quaternion differential equations of angular motion than the direction cosine equations. However, nine additional equations are necessary to convert the four quaternion parameters into the matrix $[T_S^I(t)]$ for use in Equation (B-2). Table B-II gives a typical set of quaternion equations which would be implemented in the computer. Overall requirements differ only slightly between four- or nine-parameter systems from the standpoint of computational requirements.

E. References

- B-1 Guttman, Peter T., "The Influence of Tesseral Harmonics on Nearly Circular Polar and Equatorial Orbits," AIAA Paper No. 64-397, June 29, 1964
- B-2 Pitkin, Edward T., "Integration and Optimization of Sustained Thrust Rocket Orbits," UCLA PhD. Thesis, 1964 pp. 200-2-5
- B-3 Schlesinger, S., "Integration Methods for Differential Equations," Journal of Astronautical Science, 4, pp. 53-57 (Winter 1959)
- B-4 Frame, J. S., "Matrix Functions and Applications," Part I IEEE Spectrum, March 1964 pp. 208-220
- B-5 Robinson, Alfred G., "On the Use of Quaternions in Simulation of Rigid Body Motion," WADC Technical Report 58-17, Dec. 1958

APPENDIX C

CLOSED FORM SOLUTIONS FOR ANGULAR MOTIONS

The attitude computations of a strapdown system (using direction cosines as parameters) consist of solving the first order, nonlinear, matrix differential equation:

$$\frac{d}{dt} [T_s^I(t)] = [T_s^I(t)] \cdot [\Omega] \quad (C-1)$$

Because there is no known general solution to this equation, it must be numerically integrated in real-time by using the data supplied by the gyros. However, analytic solutions can be obtained for special classes of motions. Solutions have been obtained and are presented herein for rotations about an axis with a fixed spatial orientation and for a class of motions termed coning in which equal rate amplitude sinusoidal oscillations ninety degrees out-of-phase appear along a pair of orthogonal axes with an arbitrary constant rate along the third axis of the triad. These solutions provide the essential means, the absolute reference, for evaluating the functional characteristics and the magnitude of the errors incurred in the solution of equation (C-1) by open loop numerical integration.

A. Solution for Rotations About a Stationary Axis

A solution can be obtained by means of a matrix algebra method applied to the set of simultaneous linear differential equations with constant coefficients. This matrix solution has two unique advantages in using it as the reference model for an error evaluation of the numerical integration processes:

1. It requires only a single formal integration of a scalar quantity, the magnitude of the angular rate vector, as opposed to nine direction cosines and reduces the digital simulation running time and cost.
2. It provides a unified solution to the problem valid for any angular rate vector whose magnitude function is at least piecewise integrable with respect to time over the interval of interest and whose spatial orientation is time invariant.

In the presentation of the solution upper case letters will be reserved to represent matrices and scalar quantities will be represented by lower case letters. The symbol I will be used for the identity matrix.

The restriction of a fixed spatial orientation of the axis of rotation (defined, with respect to the body axes, by its direction cosines: l_1, l_2, l_3) reduces the general expression for $[\Omega]$ to:

$$[\Omega] = \begin{bmatrix} 0 & -l_3 & l_2 \\ l_3 & 0 & -l_1 \\ -l_2 & l_1 & 0 \end{bmatrix} \quad \omega(t) = L \omega(t) \quad (C-2)$$

when $\omega(t)$ is a scalar function of time. Using equation (C-2), equation (C-1) may be rewritten as:

$$d/dt \ T = T \ L \omega(t) \quad (C-3)$$

Defining θ such that:

$$d\theta/dt = \omega(t) \quad (C-4)$$

the independent variable, t , in equation (C-3) may be replaced with θ .

$$d/d\theta (T) = T \cdot L \quad (C-5)$$

Equation (C-5) is easily solved for T by analogy with the solution of an ordinary differential equation of the same form (by assuming a matrix power series solution in t and solving for the coefficients):

$$T(t) = K e^{L\theta(t)} \quad (C-6)$$

where:

$$\theta(t) = \int_0^t \omega(\tau) d\tau \quad (C-7)$$

The solution for $T(t)$ is now complete although not in a very useful form for evaluation. The remainder of this section will be concerned with developing an expression for the solution as a function of the initial conditions, L , and $\theta(t)$. The

steps will consist of: first, defining the matrix exponential appearing in equation (C-6) in terms of scalar exponentials; then, the matrix K will be defined in terms of the initial conditions; and finally, the result will be reduced to the form specified above.

The exponential of a matrix appearing in equation (C-6) is defined in terms of the series expansion for the exponential function, hence:

$$e^{L\theta(t)} = \sum_{i=0}^{\infty} \frac{[L\theta(t)]^i}{i!} \quad (C-8)$$

At this point it is convenient to define matrices \mathcal{L}_j , one associated with each eigenvalue of L, λ_j , having the following properties:

$$\mathcal{L}_i \mathcal{L}_j = \delta_{ij} \mathcal{L}_j \text{ which implies } \mathcal{L}_j^n = \mathcal{L}_j \quad (C-9a)$$

$$\sum_j \mathcal{L}_j = I \quad (C-9b)$$

$$\sum_j \lambda_j \mathcal{L}_j = L \quad (C-9c)$$

where δ_{ij} is the Kronecker delta. The matrices \mathcal{L}_i are called the constituent idempotents of the matrix L. The development of the definition of the idempotent matrices is presented in Reference C-1. *

Using equation (C-9c), equation (C-8) may be rewritten as:

$$e^{L\theta(t)} = \sum_{i=0}^{\infty} \frac{\theta^i(t)}{i!} \left(\sum_{j=1}^3 \lambda_j \mathcal{L}_j \right)^i \quad (C-10)$$

and using the orthogonality properties of the \mathcal{L}_j 's, (equation C-9a), this becomes

$$e^{L\theta(t)} = \sum_{i=0}^{\infty} \frac{\theta^i(t)}{i!} \left(\sum_{j=1}^3 \lambda_j^i \mathcal{L}_j \right) \quad (C-11)$$

*Reference C-1 Frame, J.S., "Matrix Functions and Applications," Part II IEEE Spectrum, April 1964 pp 102-108.

Since the summation over j is finite, the order of the summations may be interchanged to give:

$$e^{L\theta(t)} = \sum_{j=1}^3 \mathcal{L}_j \sum_{i=0}^{\infty} \frac{\theta^i(t) \lambda_j^i}{i!} \quad (C-12)$$

The second summation is merely a power series expansion for the exponential function, hence this expression may be rewritten as:

$$e^{L\theta(t)} = \sum_{j=1}^3 \mathcal{L}_j e^{\lambda_j \theta(t)} \quad (C-13)$$

Equation (C-6) may now be rewritten using the expression for the exponential of a matrix (equation C-13).

$$T(t) = K \sum_{j=1}^3 \mathcal{L}_j e^{\lambda_j \theta(t)} \quad (C-14)$$

From equation (C-7) it is seen that $\theta(t)|_{t=0} = 0$ and inserting this in the expression for $T(t)$ (equation C-14), one obtains:

$$T(0) = K \sum_{j=1}^3 \mathcal{L}_j \quad (C-15)$$

Using equation (C-9b)

$$T(0) = K$$

The solution to $T(t)$ has now been reduced to a summation of products of scalar exponentials with the constituent idempotents of L and the matrix K defined.

$$T(t) = T(0) \sum_{j=1}^3 \mathcal{L}_j e^{\lambda_j \theta(t)} \quad (C-16)$$

The eigenvalues, λ_j , of the matrix L are computed from the defining relation for the eigenvalues of a square matrix:

$$LX = \lambda X$$

which may be rewritten as:

$$(L - I\lambda)X = 0$$

Since this homogeneous equation possesses nontrivial solutions ($X \neq 0$) if and only if the determinant of the coefficient matrix vanishes, the eigenvalues may be determined from the characteristic equation:

$$|(L - I\lambda)| = 0 = \lambda (\lambda^2 + 1_1^2 + 1_2^2 + 1_3^2)$$

Using the fact that $\sum_{i=1}^3 1_i^2 = 1$ the eigenvalues of L are

$$\lambda_1 = 0 \quad \lambda_2 = i \quad \text{and} \quad \lambda_3 = -i \quad (\text{C-17})$$

Since the eigenvalues of L , independent of the orientation of the axis of rotation, are all distinct, the constituent idempotents associated with each eigenvalue may be computed from:

$$\mathcal{L}_j = \prod_{\substack{k=1 \\ k \neq j}}^3 \frac{(L - \lambda_k I)}{\lambda_j - \lambda_k} \quad (\text{C-18})$$

The derivation of equation C-18 is presented in Reference C-1*. The constituent idempotents associated with each eigenvalue (equation C-18) of L are therefore

$$\lambda_1 = 0; \quad \mathcal{L}_1 = L^2 + I \quad (\text{C-19a})$$

$$\lambda_2 = i; \quad \mathcal{L}_2 = -\frac{1}{2}(L^2 + iL) \quad (\text{C-19b})$$

$$\lambda_3 = -i; \quad \mathcal{L}_3 = -\frac{1}{2}(L^2 - iL) \quad (\text{C-19c})$$

*Reference C-1 Frame, J.S., "Matrix Functions and Applications," Part II
IEEE Spectrum, April 1964 pp 102-108.

Inserting equations (C-19a, b, c) into equation (C-16) we may write the solution in a more useful form:

$$T(t) = T(0) \left[(L^2 + I) - \frac{1}{2}(L^2 + iL) e^{i\theta(t)} - \frac{1}{2}(L^2 - iL) e^{-i\theta(t)} \right]$$

which upon rearranging terms becomes:

$$T(t) = T(0) \left[I + L^2 (1 - \cos \theta(t)) + L \sin \theta(t) \right] \quad (C-20)$$

As an example of the use of equation (C-20) consider a constant rate of rotation, α , about the z-body axis with the body axes initially coincident with the inertial axes. For this case,

$$\omega(t) = \alpha$$

$$l_1 = 0, l_2 = 0, l_3 = 1$$

$$T(0) = I$$

Inserting these values into equation (C-20) using equations (C-2) and (C-7) and collecting terms,

$$T(t) = \begin{bmatrix} \cos(\alpha t) & -\sin(\alpha t) & 0 \\ \sin(\alpha t) & \cos(\alpha t) & 0 \\ 0 & 0 & 1 \end{bmatrix}$$

B. Solution for Coning Motion

Coning motion can be described by an angular rate vector with sinusoidal components of the same frequency and some phase difference along two axes of an orthogonal triad and an arbitrary constant rate along the third axis. "Classical" coning motion results when the constant rate component is specified in terms of the amplitude and frequency of the sinusoidal components such that the triad of body axes returns to its initial orientation after each cycle of the sinusoidal motion. This motion has an important part in studies of attitude computational errors due to multiple axis motions of the flight vehicle. The results contained in this section provide a continuous truth model for digital simulations of this motion.

The motion considered consists of equal sinusoidal amplitudes with a ninety degree phase difference. It may be described by an angular rate vector as follows:

$$\omega = \begin{bmatrix} \alpha \sin \beta t \\ \alpha \cos \beta t \\ \gamma \end{bmatrix}$$

It should be stated at this point that the particular order of the components of the rate vector is arbitrary and any permutation of the components is also amenable to solution in a manner identical to that to be developed.

In forming the product $[T][\Omega]$ of equation (C-1) one finds that the rows of $[T]$ are independent and all have the same form; therefore, it is only necessary to solve the equation for a typical row as the solution for the other rows will be of the same form. for the i^{th} row therefore:

$$\dot{T}_{i1} = T_{i2} \gamma - T_{i3} \alpha \cos \beta t \quad (\text{C-21a})$$

$$\dot{T}_{i2} = -T_{i1} \gamma + T_{i3} \alpha \sin \beta t \quad (\text{C-21b})$$

$$\dot{T}_{i3} = T_{i1} \alpha \cos \beta t - T_{i2} \alpha \sin \beta t \quad (\text{C-21c})$$

Starting with equation (C-21c), differentiating once with respect to time and inserting (C-21a) and (C-21b), one obtains

$$\ddot{T}_{i3} = -T_{i3} \alpha^2 + \alpha (\gamma - \beta) [T_{i1} \sin \beta t + T_{i2} \cos \beta t] \quad (\text{C-22})$$

Differentiating again, using (C-21a) and (C-21b), and collecting terms, one obtains

$$\ddot{\ddot{T}}_{i3} + [\alpha^2 + (\gamma - \beta)^2] T_{i3} = 0 \quad (\text{C-23})$$

The characteristic equation associated with equation (C-23),

$$\lambda^3 + \lambda [\alpha^2 + (\gamma - \beta)^2] = 0$$

has three roots,

$$\lambda_1 = 0 \quad \lambda_{2,3} = \pm i \sqrt{\alpha^2 + (\gamma - \beta)^2} = \pm i \xi$$

which yields a general solution of the form:

$$T_{i3} = A + B \cos \xi t + C \sin \xi t \quad (C-24)$$

where the coefficients A, B and C are evaluated from the initial conditions.

Having obtained the solution for T_{i3} , we now turn to the solutions for T_{i1} and T_{i2} . Differentiating equation (C-21a) once and inserting the expressions for T_{i2} (equation C-21b), T_{i3} and T_{i3} , one obtains for T_{i1} after collecting terms:

$$\begin{aligned} \ddot{T}_{i1} + \gamma^2 T_{i1} = & A (\beta + \gamma) \alpha \sin \beta t \\ & + B (\alpha/2) (\beta + \gamma + \xi) \sin (\beta + \xi)t \\ & + B (\alpha/2) (\beta + \gamma - \xi) \sin (\beta - \xi)t \\ & - C (\alpha/2) (\beta + \gamma + \xi) \cos (\beta + \xi)t \\ & + C (\alpha/2) (\beta + \gamma - \xi) \cos (\beta - \xi)t \end{aligned} \quad (C-25)$$

Using a similar procedure beginning with equation (C-21b) one obtains for T_{i2}

$$\begin{aligned} \ddot{T}_{i2} + \gamma^2 T_{i2} = & A (\beta + \gamma) \alpha \cos \beta t \\ & + B (\alpha/2) (\beta + \gamma + \xi) \cos (\beta + \xi)t \\ & + B (\alpha/2) (\beta + \gamma - \xi) \cos (\beta - \xi)t \\ & + C (\alpha/2) (\beta + \gamma + \xi) \sin (\beta + \xi)t \\ & - C (\alpha/2) (\beta + \gamma - \xi) \sin (\beta - \xi)t \end{aligned} \quad (C-26)$$

The solutions of the homogeneous part of equations (C-25) and (C-26) are identical, with characteristic equations

$$\lambda^2 + \gamma^2 = 0$$

$$\lambda_{1,2} = \pm i \gamma$$

Hence the general solutions for T_{i1} and T_{i2} are given by:

$$T_{i1} = K_1 \cos \gamma t + L_1 \sin \gamma t \quad (C-27)$$

$$T_{i2} = K_2 \cos \gamma t + L_2 \sin \gamma t \quad (C-28)$$

The particular solution corresponding to the forcing function on the right hand side of the appropriate equation (C-25) and (C-26) must be added to these solutions to produce the complete solutions for T_{i1} and T_{i2} .

The particular solutions to equations (C-25) and (C-26) may be found quite easily using the method of undetermined coefficients. Adding these particular solutions to the general solutions (equations C-27 and C-28) completes the solution for the i^{th} row for the case $\alpha \neq 0$.

$$\begin{aligned} T_{i1} = & K_1 \cos \gamma t + L_1 \sin \gamma t - A \frac{\alpha}{(\beta - \gamma)} \sin \beta t \\ & + \frac{B \alpha (\beta + \gamma + \xi)}{2 (\gamma^2 - (\beta + \xi)^2)} \sin (\beta + \xi)t \\ & + \frac{B \alpha (\beta + \gamma - \xi)}{2 (\gamma^2 - (\beta - \xi)^2)} \sin (\beta - \xi)t \\ & - \frac{C \alpha (\beta + \gamma + \xi)}{2 (\gamma^2 - (\beta + \xi)^2)} \cos (\beta + \xi)t \\ & + \frac{C \alpha (\beta + \gamma - \xi)}{2 (\gamma^2 - (\beta - \xi)^2)} \cos (\beta - \xi)t \end{aligned} \quad (C-29)$$

$$\begin{aligned}
T_{i2} = & K_2 \cos \gamma t + L_2 \sin \gamma t - \frac{A \alpha}{(\beta - \gamma)} \cos \beta t \\
& + \frac{B \alpha (\beta + \gamma + \xi)}{2 (\gamma^2 - (\beta + \xi)^2)} \cos (\beta + \xi)t \\
& + \frac{B \alpha (\beta + \gamma - \xi)}{2 (\gamma^2 - (\beta - \xi)^2)} \cos (\beta - \xi)t \\
& + \frac{C \alpha (\beta + \gamma + \xi)}{2 (\gamma^2 - (\beta + \xi)^2)} \sin (\beta + \xi)t \\
& - \frac{C \alpha (\beta + \gamma - \xi)}{2 (\gamma^2 - (\beta - \xi)^2)} \sin (\beta - \xi)t
\end{aligned} \tag{C-30}$$

$$T_{i3} = A + B \cos \xi t + C \sin \xi t \tag{C-31}$$

Where A, B and C are understood to carry the subscript i and are evaluated by equating the above result to corresponding row in the initial condition matrix $[T_S^I(t=0)]$.

Substitution of equations (C-29), (C-30) and (C-31) back into equation (C-1) yields the additional restriction that

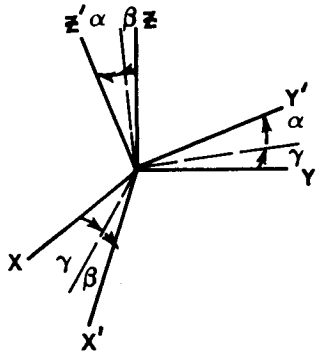
$$K_1 = K_2 = L_1 = L_2 = 0 \quad \text{for} \quad \alpha \neq 0$$

APPENDIX D

DEVELOPMENT OF THE COMPUTATIONAL ATTITUDE ERROR PARAMETER

The attitude computations of a strapdown navigator are used to:

- (1) resolve the output of the accelerometers into the navigation or computational frame and
- (2) to resolve the vehicle attitude commands from the computational frame into the vehicle coordinate system. The attitude error at any time of flight can be described in terms of small angular misalignments of the mathematical vehicle (defined by the computed attitude) relative to the actual vehicle (defined by the reference attitude):

$$\begin{bmatrix} T_{b'}^b \end{bmatrix} = \begin{bmatrix} 1 & -\gamma & \beta \\ \gamma & 1 & -\alpha \\ -\beta & \alpha & 1 \end{bmatrix} \quad \text{D-(1)}$$


where

$$\begin{bmatrix} T_{b'}^I \end{bmatrix} = \begin{bmatrix} T_b^I \end{bmatrix}_{\text{computed}} = \begin{bmatrix} T_b^I \end{bmatrix}_{\text{reference}} \cdot \begin{bmatrix} T_{b'}^b \end{bmatrix} \quad \text{D-(2)}$$

The error of interest is that encountered in transferring a vector from one coordinate frame to another. This error in transferring the vector can be defined in terms of α , β and γ :

$$\begin{bmatrix} \Delta T_b^I \end{bmatrix} = \begin{bmatrix} T_b^I \end{bmatrix}_{\text{computed}} - \begin{bmatrix} T_b^I \end{bmatrix}_{\text{reference}} \quad \text{D-(3)}$$

or using equation (D-(2))

$$\begin{bmatrix} \Delta T_b^I \end{bmatrix} = \begin{bmatrix} T_b^I \end{bmatrix}_{\text{ref}} \cdot \left\{ \begin{bmatrix} T_{b'}^b \end{bmatrix} - \begin{bmatrix} I \end{bmatrix} \right\} = \begin{bmatrix} T_b^I \end{bmatrix}_{\text{ref}} \cdot \begin{bmatrix} 0 & -\gamma & \beta \\ \gamma & 0 & -\alpha \\ -\beta & \alpha & 0 \end{bmatrix} \quad \text{D-(4)}$$

For resolving accelerometer data into the inertial frame, the resulting error vector takes the form

$$\Delta \bar{a}^I = [T_b^I]_{\text{ref}} \cdot \begin{bmatrix} 0 & -\gamma & \beta \\ \gamma & 0 & -\alpha \\ -\beta & \alpha & 0 \end{bmatrix} \cdot [T_I^b]_{\text{ref}} \cdot \bar{a}^I \quad D-(5)$$

For resolving vehicle commands from the computational frame into the vehicle frame, the error takes the form

$$\begin{bmatrix} \Delta \phi \\ \Delta \theta \\ \Delta \psi \end{bmatrix} = \begin{bmatrix} 0 & \gamma & -\beta \\ -\gamma & 0 & \alpha \\ \beta & -\alpha & 0 \end{bmatrix} \cdot [T_I^b]_{\text{ref}} \cdot \overline{\text{Command}}^I \quad D-(6)$$

Thus, the properties of the total attitude error whose components are α , β and γ (the attitude computational errors) are of extreme interest. The remainder of this appendix will show that the norm of the attitude error matrix, Equation (D-3), is proportionate to the root-sum-square of the three attitude error angles. The norm of the attitude error matrix is defined by

$$\text{Norm} = \sqrt{\sum_i \sum_j [\Delta \cos(i, j)]^2} \quad \begin{array}{l} i = E, N, U \\ j = x, y, z \end{array}$$

where

$$\Delta \cos(i, j) = \cos(i, j)_{\text{computed}} - \cos(i, j)_{\text{reference}} \quad D-(7)$$

obtained from

$$[\Delta T_b^I] = [T_b^I]_{\text{computed}} - [T_b^I]_{\text{reference}}$$

The substitution of equation (D-4) into (D-7) yields

$$\text{Norm} = \text{Root-sum-square} \left\{ \left[T_b^I \right]_{\text{ref}} \cdot \begin{bmatrix} 0 & -\gamma & \beta \\ \gamma & 0 & -\alpha \\ -\beta & \alpha & 0 \end{bmatrix} \right\} \quad (\text{D-8})$$

Carrying out the multiplication within the brackets and performing the squaring and then the summing of the squared elements yields

$$\begin{aligned} \text{Norm} &= \left\{ \gamma^2 \left[\bar{y}^I \cdot \bar{y}^I + \bar{x}^I \cdot \bar{x}^I \right] + \beta^2 \left[\bar{z}^I \cdot \bar{z}^I + \bar{x}^I \cdot \bar{x}^I \right] \right. \\ &\quad + \alpha^2 \left[\bar{z}^I \cdot \bar{z}^I + \bar{y}^I \cdot \bar{y}^I \right] - 2\gamma\beta(\bar{y}^I \cdot \bar{z}^I) - 2\alpha\gamma(\bar{x}^I \cdot \bar{z}^I) \\ &\quad \left. - 2\alpha\beta(\bar{x}^I \cdot \bar{y}^I) \right\}^{1/2} \\ &= \sqrt{2} (\alpha^2 + \beta^2 + \gamma^2)^{1/2} \end{aligned} \quad (\text{D-9})$$

Thus the norm of the attitude error matrix defines the total angular error of the computational process.

APPENDIX E

ANALYSIS OF CONING MOTION

A. Introduction

Coning motion, in which two axes of an orthogonal triad experience phase shifted sinusoidal motion at the same frequency is an extremely important class of multiple-axis motion in the performance evaluation of inertial systems. This motion has been observed in single axis vibratory tests of gyros, on centrifuge testing devices, in gimballed inertial navigators because of their gimballed degrees of freedom, and may well be applicable to a strapdown system due to vehicle coning motions about pitch, roll or yaw axes or vibratory modes of the structural member to which the strapdown inertial measurement unit is mounted. An important characteristic of this motion is the coupling of the sinusoidal rates about the two axes through the mechanical restraint of the sensors relative to the vehicle that produces a constant rate along the third orthogonal axis. This property of the motion could lead to unbounded errors in the attitude reference if the sinusoidal motion is above the bandwidth of the gyros or the computational process.

The present appendix extends the analysis of this motion on a linearized basis to a more general case than that contained in Appendix C using an approach similar to the quaternion method for the solution of the angular equations of motion.

B. Analysis

A rigid body possessing an arbitrary angular motion about a fixed point may, at anytime, be returned to the position it occupied at time zero by a simple rotation. That such a rotation about an axis fixed in space exists is ensured by Euler's theorem of kinematics. The angular components of this rotation to return the body to its initial orientation about each of the body axes $\Phi = (\phi_x, \phi_y, \phi_z)$, are defined by the expression developed in Reference E-1:

$$\phi_i = \int_0^t \omega_i d\tau + A_i \pm 2n\pi \quad (E-1)$$

where ω_i is the time varying angular rate about the i^{th} body axis; A_i is the area traced out by this body axis on the surface of a unit sphere centered at the fixed point (assumed coincident with the origin of the body coordinate system). This area is defined by the curve produced by the motion of the i^{th} body axis from time zero to the present and is closed by the rotation Φ that returns the body to its original orientation. A_i is the solid

*Goodman, L. E. & A. R. Robinson, "Effects of Finite Rotations on Gyroscopic Devices," Journal of Applied Mechanics. June 1958 pp 210-213

angle defined by the motion of the i^{th} body axis and Φ . This solid angle provides a means of evaluating the output of a gyro that has its input axis parallel to the i^{th} body axis

$$\int_0^t \omega_i d\tau.$$

The solid angle A_i must be evaluated as a function of the history of the body motions. With reference to Figure E-1, which illustrates the geometry of the problem assuming that at time zero the body frame and the inertial frame were coincident, the area A_z (the same equations can be developed for A_x and A_y) may be written as:

$$\begin{aligned} A_z &= \oint_c dA_z \\ A_z &= \int_{\theta_0}^{\theta(t)} \int_0^{\beta(\theta)} \sin \beta d\beta d\theta \end{aligned} \quad (\text{E-2})$$

Defining, l_1, l_2, l_3 as the direction cosines of the axis of the rotation Φ with respect to both the body axis and inertial axis. (The direction cosines l_1, l_2, l_3 are the components of the normalized eigenvector corresponding to the unit eigenvalue of the matrix describing the rotation Φ .) An expression for β as a function of the rotation Φ may be obtained by applying the law of cosines to the spherical triangle formed by the intersection of the axis of Φ , Z and z with the unit sphere.

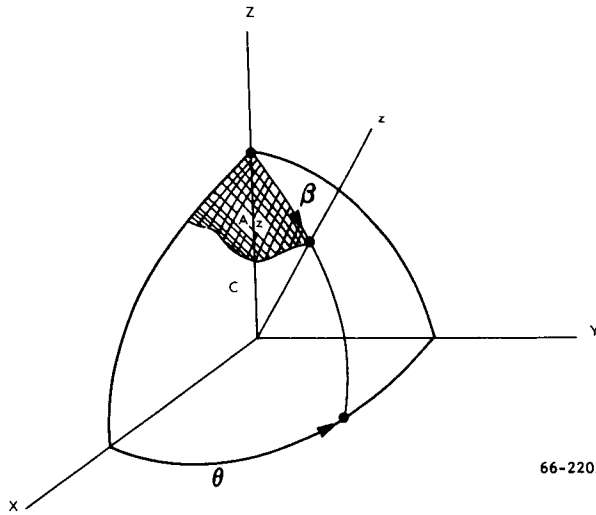
$$\cos \beta = \cos \Phi + l_3^2 (1 - \cos \Phi) \quad (\text{E-3})$$

For small angles this may be approximated by

$$\begin{aligned} \beta &= (l_1^2 + l_2^2)^{1/2} \Phi \\ \beta &= (\phi_x^2 + \phi_y^2)^{1/2} \end{aligned} \quad (\text{E-4})$$

Using the small angle approximation, the expression for A_z may be written as

$$A_z = \frac{1}{2} \int_{\theta_0}^{\theta(t)} \beta^2(\theta) d\theta \quad (\text{E-5})$$



66-2205

Figure E-1 Geometry of the Solid Angle

which, by the two dimensional Green's theorem, is equivalent to :

$$A_z = \frac{1}{2} \int_0^t \left(\phi_x \frac{d\phi_y}{d\tau} - \phi_y \frac{d\phi_x}{d\tau} \right) d\tau \quad (E-6)$$

This expression and equation E-1 provide a convenient means of obtaining the gyro output as a function of time, t , from a knowledge of $\Phi(t)$, where $\Phi(t)$ is simply the rotation necessary to return the body frame to coincidence with the inertial frame at time (t) :

$$\int_0^t \omega_z d\tau = \phi_z - \frac{1}{2} \int_0^t \left(\phi_x \frac{d\phi_y}{d\tau} - \phi_y \frac{d\phi_x}{d\tau} \right) d\tau \quad (E-7)$$

Differentiating, an expression for rate that would be sensed by the z gyro is obtained

$$\omega_z = \frac{d}{dt} \phi_z - \frac{1}{2} \phi_x \frac{d\phi_y}{dt} + \frac{1}{2} \phi_y \frac{d\phi_x}{dt} \quad (E-8)$$

Similarly for ω_x and ω_y :

$$\omega_x = \frac{d}{dt} \phi_x - \frac{1}{2} \phi_y \frac{d\phi_z}{dt} + \frac{1}{2} \phi_z \frac{d\phi_y}{dt} \quad (E-9)$$

$$\omega_y = \frac{d}{dt} \phi_y - \frac{1}{2} \phi_z \frac{d\phi_x}{dt} + \frac{1}{2} \phi_x \frac{d\phi_z}{dt}$$

C. Generalized Coning Motion

A rotation Φ of the form

$$\Phi = (\alpha_x \sin \omega_2 t, \alpha_y \sin (\omega_1 t - \psi), 0)$$

corresponds to a general form of coning motion. This is shown by using equation E-8 and E-9 to determine the rates along each body axis:

$$\omega = \left(\frac{d}{dt} \phi_x, \frac{d}{dt} \phi_y, \frac{1}{2} \left[\phi_x \frac{d\phi_y}{dt} - \phi_y \frac{d\phi_x}{dt} \right] \right) \quad (E-10)$$

$$\omega = (\beta_x \cos \omega_2 t, \beta_y \cos (\omega_1 t - \psi), \omega_z)$$

The resulting rate vector consisting of phase shifted sinusoids along two of the body axes, is immediately recognized as a general form of coning motion with the z gyro coning. The rate sensed by the coning gyro is:

$$\begin{aligned} \omega_z^c = & -\frac{1}{2} \alpha_x \alpha_y \omega_1 \cos (\omega_1 t - \psi) \sin \omega_2 t \\ & + \frac{1}{2} \alpha_x \alpha_y \omega_2 \sin (\omega_1 t - \psi) \cos \omega_2 t \end{aligned}$$

$$\begin{aligned} \omega_z^c = & \frac{1}{4} \alpha_x \alpha_y [(\omega_2 - \omega_1) \sin ((\omega_1 + \omega_2) t - \psi) \\ & + (\omega_2 + \omega_1) \sin ((\omega_1 - \omega_2) t - \psi)] \end{aligned} \quad (E-11)$$

This rate produced by coning motion is of considerable interest as the time average of this rate demonstrates the presence of an unbounded term that introduces an error in the attitude system when the frequency of the sinusoidal motion producing it, is beyond the bandwidth of the gyros or the computational process. The attitude computational process simply does not reconstruct attitude properly as a function of time. The time average is defined by:

$$\langle \omega_z^c \rangle_t = \lim_{T \rightarrow \infty} \frac{1}{T} \int_0^T \omega_z \, d\tau \quad (E-12)$$

Substituting Equation E-10 for ω_z and performing the integration yields:

$$\begin{aligned} \langle \omega_z^c \rangle_t = & \lim_{T \rightarrow \infty} \frac{\alpha_x \alpha_y}{4T} \left\{ \frac{\omega_2 - \omega_1}{\omega_2 + \omega_1} [\cos \psi - \cos ((\omega_1 + \omega_2) T - \psi)] \right. \\ & \left. + \frac{\omega_2 + \omega_1}{\omega_1 - \omega_2} [\cos \psi - \cos ((\omega_1 - \omega_2) T - \psi)] \right\} \end{aligned} \quad (E-13)$$

hence, for $\omega_1 \neq \omega_2$, $\lim_{T \rightarrow \infty} = 0$

and for $\omega_1 = \omega_2$,

$$\begin{aligned} \lim_{T \rightarrow \infty} \int_0^T \omega_z \, d\tau &= \lim_{T \rightarrow \infty} \lim_{\omega_1/\omega_2 \rightarrow 1} \int_0^T \omega_z \, d\tau \\ &= \frac{1}{2} \alpha_x \alpha_y \omega \sin \psi \end{aligned}$$

Therefore, the time average of this "coning rate" may be written as

$$\omega_z^c = \delta \left(k - 1 \right) \frac{1}{2} \alpha_x \alpha_y \omega \sin \psi \quad (\text{E-14})$$

where $k = \frac{\omega_1}{\omega_2}$ and $\delta(k - 1)$ is the Dirac delta function.

Similarly, the gyros may also experience a random spectrum of angular rate whose phase relationship may produce coning motion. It is necessary to evaluate this error (equation E-12) over a spectrum of random angular motions. Such an evaluation may be made by integrating equation E-14 over frequencies above the gyro bandwidth, ω_{bw} , approximating $\frac{1/2 \alpha_x \alpha_y}{\omega}$ by the angular rate power spectral density, $\phi(\omega)$, and assuming that

$$\left\langle \int_{\omega_{bw}}^{\infty} \omega_z^c d\omega \right\rangle_t = \int_{\omega_{bw}}^{\infty} \left\langle \omega_z^c \right\rangle_t d\omega$$

For $\sin \psi = 1$ (a constant ninety degree phase difference at all frequencies)

$$\text{Total drift rate} = \int_{\omega_{bw}}^{\infty} \frac{\phi(\omega)}{\omega} d\omega \quad (\text{E-15})$$

The spacial distribution of these sinusoidal inputs is also of interest and the total error may range from 0 for a random spacial orientation to that expressed in equation (E-15) above for a fixed orientation during a flight. The peculiarities of the spacial distribution are a function of the origin or source of the motion that creates the vibratory modes of the structural member to which the inertial measurement unit is mounted and must be analyzed individually for each vehicle.

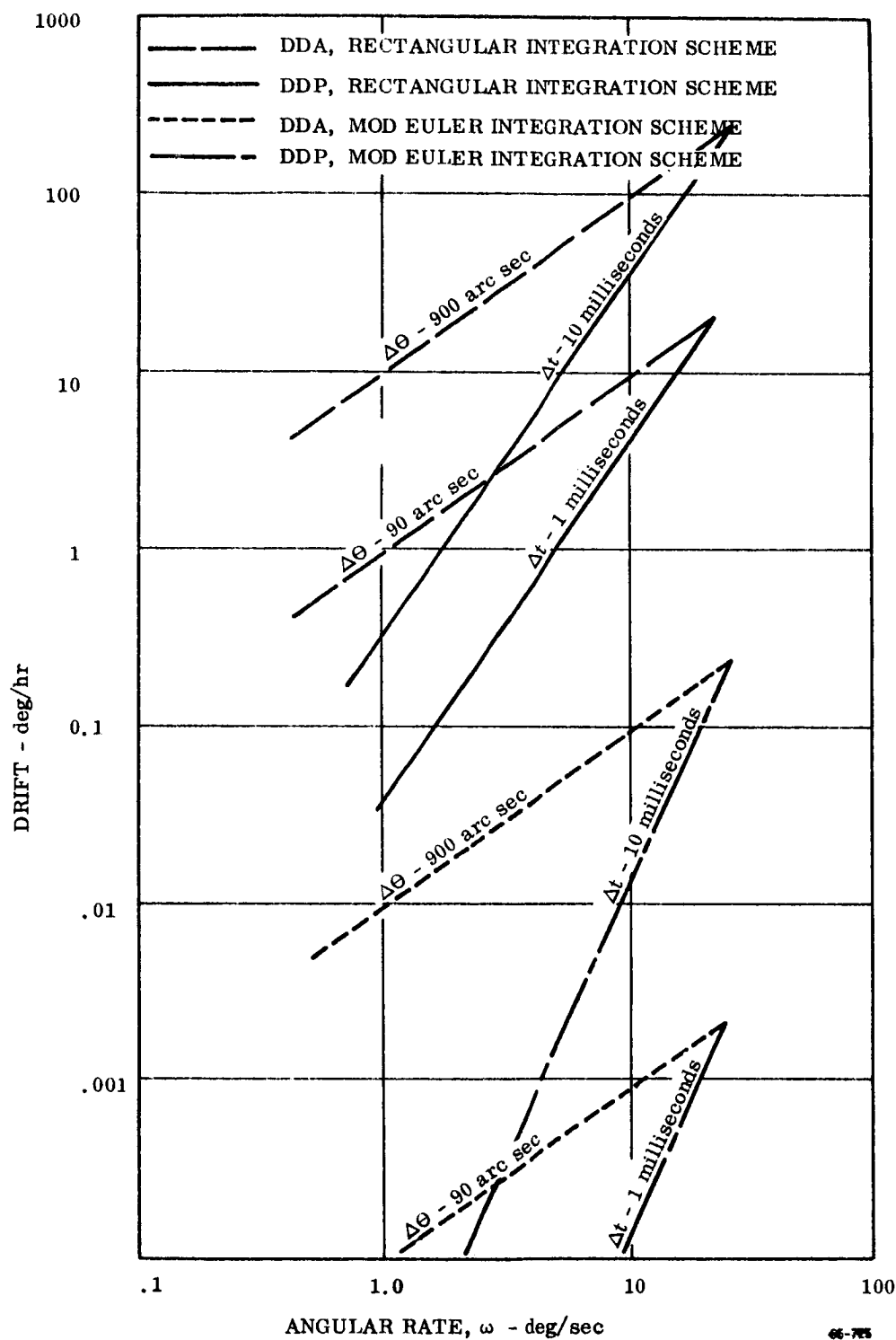


Figure IV-14 Truncation Error Comparison of Incremental (DDA) and Whole Number (DDP) Computers

2. Vibratory Motions

The angular environment in which a strapdown system must operate is composed of discrete motions and a vibratory environment. The vibratory environment consists of sinusoidal and random angular motions. The truncation computational error under a vibratory environment exhibits the same characteristics as observed for discrete motions, namely, higher order integration schemes offer significant improvements with regard to increased accuracy and reduced computational frequency relative to lower order integration schemes.

In analyzing the computational error due to a vibratory environment, the angular motion that the computational process must follow is that passed on to it by the gyro. For example, if the vibratory environment is specified at the strapdown sensor package mounting shelf, the vibratory motion that the computer must process is the specified environment multiplied by the sensor housing transfer function and the gyro transfer function.

Analytic and digital simulation studies have been used to derive the error models for the truncation error under a vibratory environment. The error models obtained by both approaches agree very well. The determination of the truncation error in a vibratory environment lends itself to an analytic evaluation because the attitude computational process possesses the property of superposition that has been verified by digital simulations (see Appendix F.) Therefore, the error models that were derived for the discrete inputs discussed in the previous section can be readily extended to vibratory inputs.

The truncation error for a single sinusoidal input about an axis of rotation fixed with respect to the vehicle can be described (Table IV-I) by:

$$\dot{C} = f_c k_a \beta^b \sin^d \left(\frac{\pi f}{2f_c} \right)$$

where k_a and the exponents of the sinusoidal angular amplitude, and the frequency ratio, b and d , respectively, are dependent upon the order of the integration schemes (Table IV-I); f_c is the number of integrations performed per second; while, f , is the frequency of the sinusoidal input. For multiple sinusoidal input, the total truncation error for any integration scheme is given by

$$\dot{C} = k_a f_c \sum_{\eta=1}^m \beta_n^b \sin^d \left(\frac{\pi f_\eta}{2f_c} \right)$$

Similarly, the truncation error expressed in terms of a total drift rate for a random input described by a power spectral density, $\phi(f)$, can be described by the equations of Table IV-II derived in Appendix F.

These analytic models agree with the results of digital simulation studies, differing essentially by a constant (a factor of 3) for all cases in which the computational frequency was higher than an appreciable portion of the frequency range of the vibratory input ($f_c > .1f_o$) wherein the random input extended over a region of frequency from zero to f_o . This comparison is shown in Figure IV-15 with the analytic models adjusted by a factor of three. When the frequency range of the vibratory input extended beyond that of the computational frequency ($f_o \gg f_c$), the analytic model yielded an optimistic estimate of the error. This region however is usually not of interest in a well designed system. The magnitude of the power spectral density used in this study was $0.55 \text{ (rad/sec)}^2/\text{cps}$, an extremely large value by orders of magnitude, compared to flight environment. A large value was employed to emphasize the truncation error relative to the round-off error.

A similar analytic error model was developed (see Appendix F) for coning motion caused by a vibratory environment. These models are presented in Table IV-III. Digital simulation studies to confirm these models were not performed as it is highly unlikely that coning will occur other than at discrete frequencies associated with the resonance points of mechanical systems.

TABLE IV-II

COMPUTATIONAL TRUNCATION ERROR FOR ANGULAR VIBRATION
MOTION ABOUT AN AXIS OF ROTATION FIXED WITH RESPECT TO THE VEHICLE

Rectangular Integration Scheme

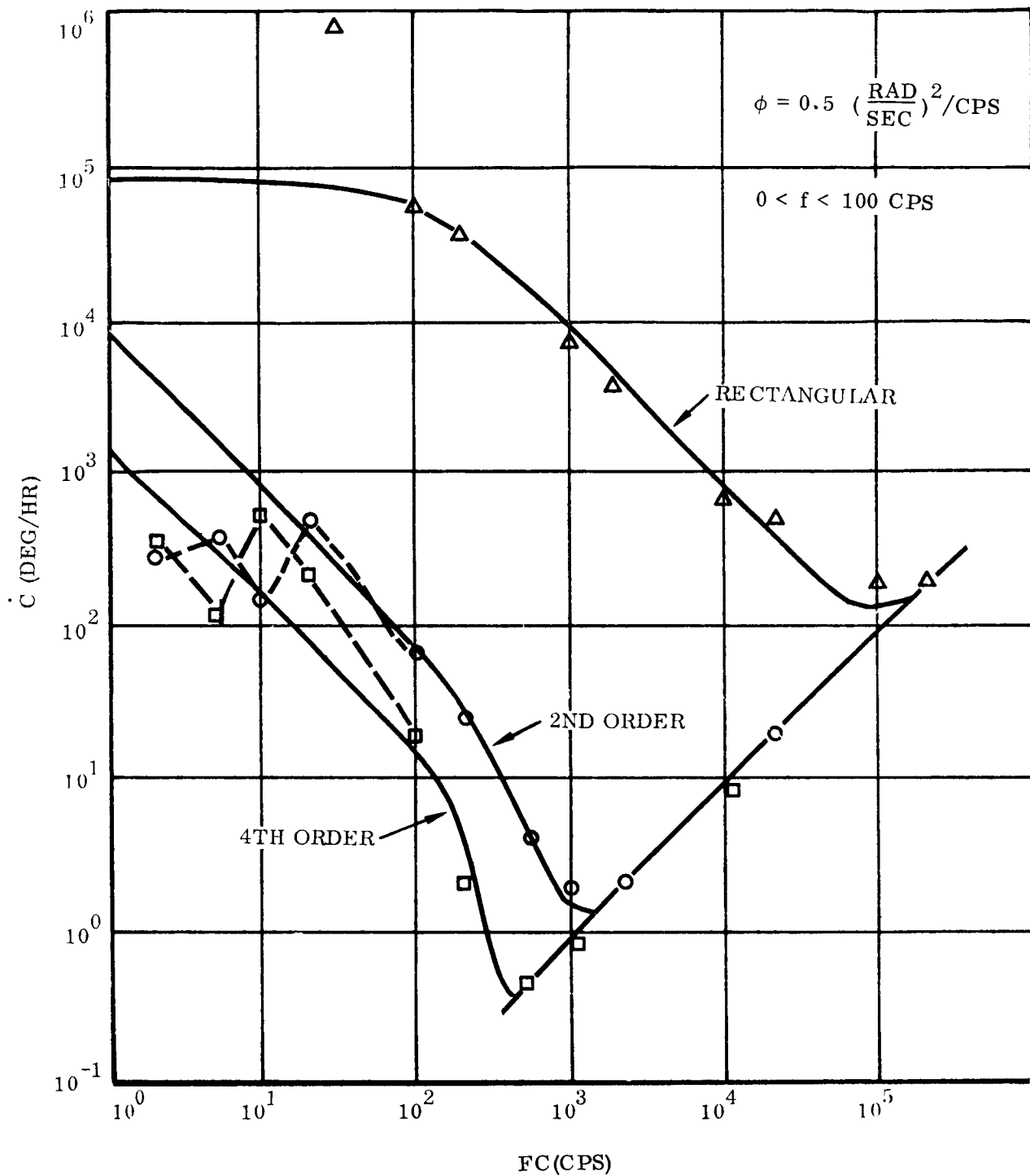
$$\bar{C}_R \left(\frac{\text{deg}}{\text{hr}} \right) = \frac{117}{4\pi} \int_0^{\frac{\pi f_o}{2f_c}} \phi \left(\frac{2f_c \tau}{\pi} \right) \frac{\sin^2 \tau}{\tau^2} d\tau$$

2nd Order Runge Kutta

$$\bar{C}_2 = \frac{0.1}{16\pi^2 f_c} \int_0^{\frac{\pi f_o}{2f_c}} \phi^2 \left(\frac{2f_c \tau}{\pi} \right) \frac{\sin^4 \tau}{\tau^4} d\tau$$

4th Order Runge Kutta

$$\bar{C}_4 = \frac{0.05}{16\pi^2 f_c} \int_0^{\frac{\pi f_o}{2f_c}} \phi^2 \left(\frac{2f_c \tau}{\pi} \right) \frac{\sin^6 \tau}{\tau^4} d\tau$$



67-127

Figure IV-15 Comparison of Adjusted Theoretical and Simulation Results for Single Axis Random Motion

TABLE IV-III
COMPUTATIONAL ERROR FOR RANDOM VIBRATORY CONING MOTION

Integration Scheme	$f_o/f_c < .8$	$f_o/f_c > .8$
Rect	$\bar{C} = \frac{327}{2\pi^2} \frac{1}{f_c} \int_0^f \phi(f) df$	
2nd order RK	$\bar{C} = \frac{408}{2\pi^2} \frac{1}{f_c^2} \int f \phi(f) df$	$\bar{C} = \frac{730}{\pi^2} \int_{.8f_c}^{f_o} \frac{\phi(f)}{f} df$
4th order RK	$\bar{C} = \frac{646}{2\pi^2} \frac{1}{f_c^4} \int f^3 \phi(f) df$	

These analytic models are conservative estimates of the truncation error due to coning produced by a random environment since it assumes that: (1) coning occurs at all frequencies rather than at discrete frequencies that are usually associated with points of resonances of the mounting shelf or the sensor package attachment structure, (2) the amplitude of the variable rate components on each axis are always the maximum values described by the power density spectrum of each frequency, (3) the phase difference between the two variable rate components is ninety degrees so as to produce the maximum error, and (4) the spacial orientation of the input vibration is fixed relative to the vehicle so as to again maximize the error. In actuality, for the computational error estimated for coning motions to have any meaning or validity, each particular vehicle and flight environment must be evaluated individually. Once the environment is known, the analysis is straightforward. If coning does occur at discrete frequencies, the error is computed by summing the errors at all of the coning frequencies. If the coning amplitude is random rather than a continuously maximum value, an average over amplitude and frequency are required. If the phase angle is different than ninety degrees or a variable, a time average of the sine of the phase angle becomes a coefficient of the equations of Table IV-III (Appendix E). Finally, if the spacial orientation of the coning input is random, an integration over orientation is required.

3. Sensor Associated Errors

In the performance evaluation of a restrained gyro strapdown navigator, there are a few sensor loop associated errors that must be analyzed on a system basis. A system type of analysis is required as the sensor loop errors in more than one channel combine to distort and change the type of motion that is passed on to the computer. For example, these errors can change the motion from one of angular rotation about an axis fixed relative to the vehicle to one of angular rotation about an axis that is rotating relative to the vehicle. The attitude computational process, even if it were perfect, cannot undo the error that has been created. Three sensor loop errors of this type have been analyzed: (1) finite gyro bandwidth, (2) unmatched gyro loop frequency response between the three gyro loops, and (3) gyro output axis acceleration sensitivity.

a. Finite Gyro Bandwidth

The finite bandwidth characteristics of the strapdown gyros cause two navigation errors. First is the attenuation, beyond the bandwidth of the gyro, of the angular environment applied to the sensor package. This represents true angular motion of the accelerometer input axes that should be followed by the gyros in order to correctly resolve the accelerometer outputs into the inertial frame. Second is the error introduced if vehicle coning motion occurs at frequencies beyond the bandwidth of the gyro; the two sinusoidal or variable rate components will be attenuated by the gyro loops and not seen by the computer while the constant rate component

(zero frequency) will be passed on to the computer. This results in a drift rate of the attitude reference equal to the value of the constant rate component. The errors for each of these cases are derived in Appendix G.

The mean square error in the system's knowledge of the orientation of the accelerometers' input axes due to the attenuation of the magnitude of the angular motion by the finite bandwidth of the gyro loops is

$$\overline{\epsilon_o^2} = \frac{1}{2\pi} \int_{-\infty}^{\infty} [1 - G_g(j\omega)]^2 \frac{|G_s(j\omega)|^2}{(j\omega)^2} \phi(j\omega) d\omega$$

where G_s is the structural transfer function between the gyros and the sensor package's mounting surface on the vehicle, ϕ is the random angular rate power spectral density at the mounting surface and G_g is the gyro loop transfer function.

This mean square angular error contributes an error in the transformation of the accelerometer outputs from the vehicle to the inertial computational frame. For a strapdown system this error has components along the roll vehicle axis of magnitude

$$\Delta F = F \cdot (\overline{\epsilon_\theta})^2$$

where F is the applied specific force and ΔF is the resulting error.

The total drift rate due to coning motion beyond the bandwidth of the gyro is the second error that must be considered. If coning occurs for all frequencies, the error induced can be described by:

$$\omega \text{ (drift rate)} = \frac{1}{\beta \pi^2} \int_0^{\infty} [1 - G_g(j\omega)]^2 |G_s(j\omega)|^2 \phi(\omega) \ln \omega d\omega$$

b. Unmatched Gyro Loop Frequency Response

For a triad of restrained gyros whose transfer functions differ slightly, the application of a sinusoidal angular rate whose axis of rotation is fixed relative to the sensor package and is noncollinear with the gyro input axes, creates a distortion of the true angular motion. The processing of this distorted motion by even a perfect attitude computation yields an erroneous knowledge of attitude (Appendix G).

The effect of differences in amplitude response between the gyro loops is to change the magnitude and spacial orientation of the applied rate. However, the true and distorted motion cause the body to return to its initial orientation periodically so the error introduced into the knowledge of attitude is also periodic and bounded.

The effect of differences in phase response causes an error that is characterized by two parts of different behavior. First, there is a term that introduces a periodic, but bounded, error in the knowledge of attitude. It is identical in behavior to that which occurs for amplitude response differences. Secondly, there is the creation of an error rate vector of constant magnitude whose axis of rotation rotates relative to the sensor at a constant frequency equal to the frequency of the applied sinusoidal rate. This erroneous rotating rate vector causes an unbounded attitude error whose rate of growth is proportional to the phase differences between the loops and the amplitude of the sinusoidal rates that are passed onto the computer (Appendix G).

c. Gyro Output Axis Acceleration Sensitivity

Single-degree-of-freedom gyros not only measure angular rate about the input axis, but they are also sensitive to accelerations about the output axes. If angular accelerations are applied about the output axis of a gyro, an erroneous rate signal will be created that will be processed by the attitude computations. For a strapdown IMU that is subjected to a sinusoidal angular rate about an axis parallel to the input axis of one gyro and the output axis of another gyro, the combined outputs lead to a divergent error in the knowledge of attitude even with a perfect attitude computational process. This drift rate in the knowledge of attitude is proportional to both the output axis inertia to angular momentum ratio (I_o/H) and the square of the amplitude of the applied sinusoidal rate (α); it is independent of the frequency of the input motion up to the bandwidth of the gyro (the error model is derived in Appendix G):

$$W \text{ (deg/hr)} = 30.8 \frac{I_o}{H} [\alpha \text{ (deg/sec)}]^2$$

Beyond the bandwidth of the gyros, this error falls off rapidly due to the loop's normal attenuation of high frequency signals. This error in gimbaled platform systems is termed output axis coupling. The same name can be carried over into the strapdown navigator. The error arises because the signal from the gyro whose output axis is parallel to the sinusoidal rate lags the signal output of the gyro whose input axis is parallel to the sinusoidal rate by ninety degrees at all frequencies and, therefore, produces a pseudo coning type of motion. The combined effect of the two signals is to create an angular rate error vector whose magnitude varies with time and whose axis of rotation rotates with respect to the sensor package at the same frequency as the applied sinusoid.

B. Free Gyro Attitude Reference System

The computational process for determining attitude using two free gyros, each possessing a minimum of two readouts, consists of measuring the orientation of the spin axes of the gyros relative to the vehicle and the formation of the matrix relationship between the spin axes coordinate frame and the vehicle. Initial alignment of the spin axes with respect to the desired inertial reference allows the navigation system to determine the orientation of the vehicle relative to inertial space. An example of this computational process is presented in Table III-III.

Each time that attitude is desired, the orientation of the spin axes in the vehicle frame is measured anew; therefore, the computation error is associated with each individual determination of attitude and is not cumulative with time. The computation errors for free gyro systems are those associated with the reduction of the optical readout data, which are measurements of lapsed time between crossings of lines inscribed on the rotor under the optical readout. When great circles are scribed upon the rotor, the reduction of the readout data involves square root and trigonometric functions. The magnitude of the error in these computations is influenced by the approximations used for the square root and transcendental functions and computer word length. The latter may be eliminated by using scribe lines that yield output time intervals that are already trigonometric functions of the vehicle-spin vector orientation but at the expense of more difficulty in the fabrication of the rotor.

The accuracy in computing trigonometric functions depends upon the form of the numerical trigonometric approximation, the number of terms used in the numerical approximation and the computer word length used to implement the numerical process. Chebyshev approximations of trigonometric functions readily lend themselves to rapid and accurate computations in digital computers and are widely used in the aerospace field. Typical approximations of trigonometric and inverse trigonometric functions are approximated by a truncated series expansion. The most commonly used functions are the sine expansion for computing trigonometric functions and the arctangent for computing inverse trigonometric functions. (The arctangent function is included because such a function is necessary if Euler attitude angles are to be derived from free gyros). The Chebyshev approximations provide adequate accuracy for a minimum number of computer operations. The form of the expansions are (Reference 11):

$$\begin{aligned}\arctan X &= C_1 X + C_3 x^3 + C_5 x^5 + \dots && ; -1 \leq x \leq 1 \\ \sin \frac{\pi}{2} X &= C_1 X + C_3 x^3 + C_5 x^5 + \dots && , -1 \leq x \leq 1\end{aligned}$$

Figure IV-16 presents the typical behavior of the error in terms of the argument and tabulates the maximum error as a function of the number of terms in the series. The number of zero crossings for the arctangent function error is one more than the number of terms in the series; for the sine function error the number of zero crossings is equal to the number of terms in the expansion.

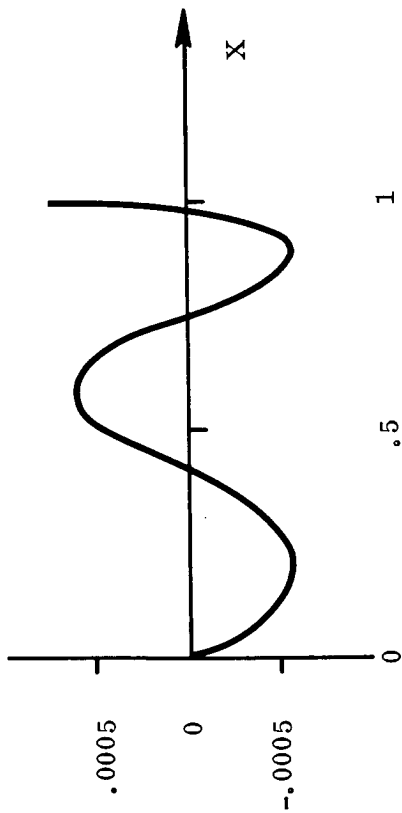
In order to maintain the inherent accuracy of the trigonometric approximations, a sufficient word length must be employed. The choice of word length must ensure that the cumulative round-off error in the calculations is less than the approximation error. The minimum round-off error that can be expected after a series of calculations is equal to the value of the least significant bit used in the calculations. Usually the round-off error is larger than this with the error depending upon the number of operations and the numbers operated upon. To evaluate the error due to word length, digital simulations were employed. Figure IV-17 depicts the average error for a four term arctangent approximation (in the regions of maximum error) as a function of word length. Also shown in this figure is the error predicted by assuming that the error is equal to the least significant bit employed in the computations. It is seen for a four term expansion, that four additional bits are required beyond the number indicated by employing the value of the least significant bit itself as an error guide.

Also required in the free gyro computations is a square root process. For typical digital computers, the square root is an available instruction. The usual error encountered in forming the square root is $2^{-(n+1)}/\sqrt{X}$ where X is the number whose square root is to be obtained and where n is the value of the least significant bit of the number used. If a square root instruction is not available, it must be solved by a computational subroutine. An example of such a process is the Newton-Raphson iterative method. Figure IV-18 defines the numerical process and presents the error as a function of word length; the maximum error occurs for values of numbers near zero. Table IV-IV tabulates the number of iterations required to converge to the region of the word length error as a function of the magnitude of the number whose square root is desired. It is seen that the number of iterations is inversely proportional to the magnitude of the numbers for the range presented. More iterations are required for lower numbers because the Newton-Raphson method is based upon the secant approximating the tangent.

Additional computational errors in the solution of the free gyro attitude equations arise when single sets of optical pickoff data are too noisy to permit accurate determination of attitude; thus, several sets of measurements must be taken and smoothed. This requires solution of the equations over a finite time period, which introduces errors due to vehicle motion. These errors can be reduced by fitting a polynomial to the angular data over the selected smoothing integral. A higher order polynomial would reduce the errors at the expense of increased computer complexity.

ARC TANGENT FUNCTION

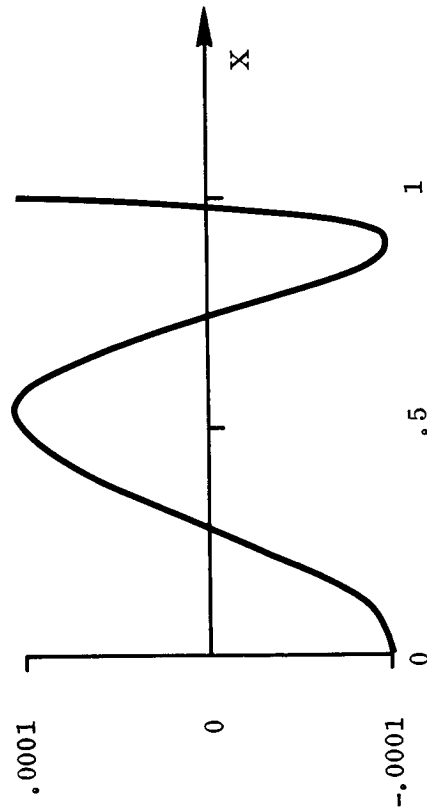
APPROXIMATION - TRUE VALUE



NUMBER OF TERMS	MAXIMUM ERROR
3	6×10^{-4}
4	8×10^{-5}
5	1×10^{-5}
6	2×10^{-6}
7	2×10^{-7}
8	4×10^{-8}

IV-33

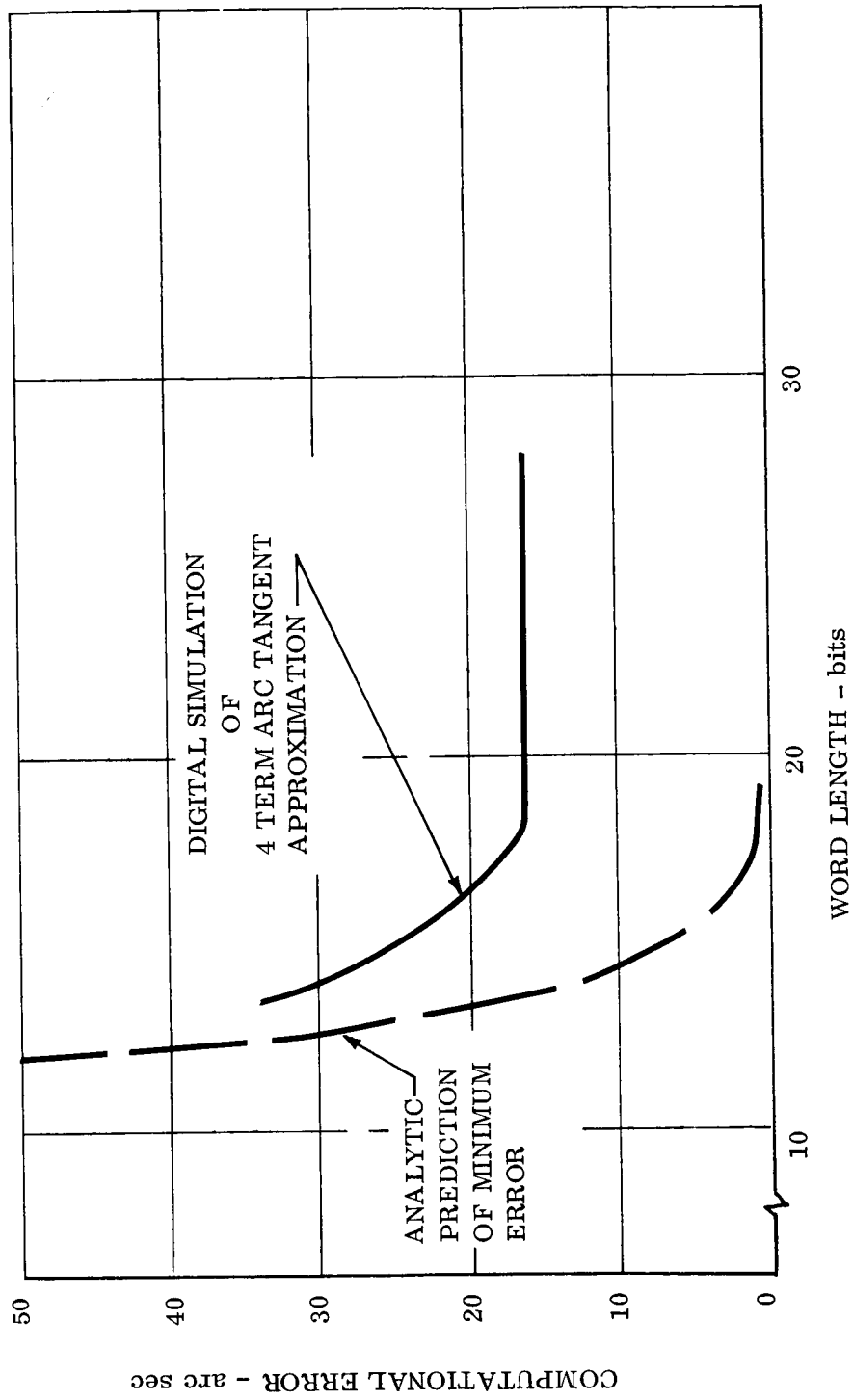
(APPROXIMATION - TRUE VALUE)/TRUE VALUE



NUMBER OF TERMS	MAXIMUM ERROR
3	10^{-4}
4	10^{-6}
5	5×10^{-9}

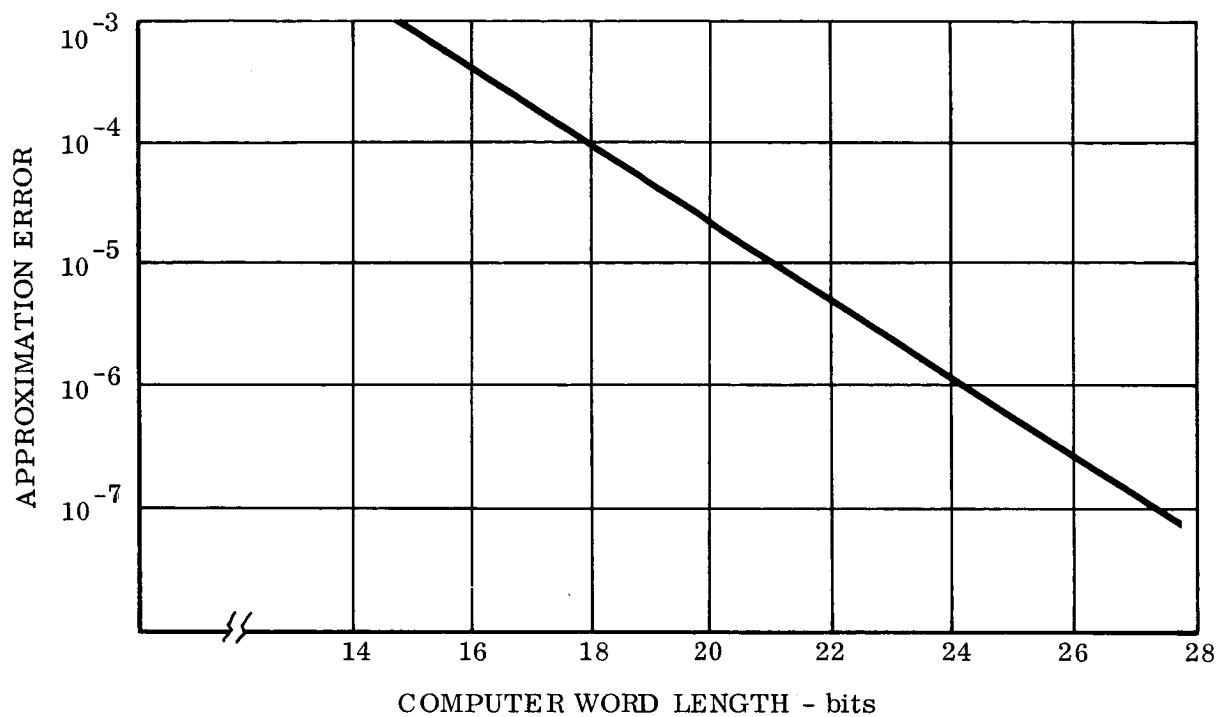
66-2223

Figure IV-16 Error Characteristics of Trigonometric Approximations



66-2221

Figure IV -17 Effect of Word Length on Trigonometric Computational Errors



66-719

NEWTON RAPHSON ITERATIVE EQ: $\sqrt{X} = Y_N = 1/2 (Y_{N-1} + X/Y_{N-1})$
 $Y_0 = (X + 1)/2$

Figure IV-18 Computer Square Root Routine Errors vs Computer Word Length

The solution of the free gyro equations involves a matrix inversion for the final solution $[T_{\text{body}}^{\text{inertial}}(t)]$. As shown in Table III-III, the inversion would be of the time variant matrix $[T_{\text{spin vector}}^b(t)]$. Considerations of solution time would force a compromise of accuracy if this inversion were to be made at the solution rate necessary for resolving accelerometer data. However, by utilizing the fact that the body to inertial matrix transformation is orthogonal and its inverse is equal to its transpose, the final equation of Table III-III can be rewritten as

$$[T_{\text{body}}^{\text{inertial}}(t)] = \left[[T_{\text{spin vector}}^b(t)] [T_{\text{spin vector}}^I(t=0)]^{-1} \right]^T$$

so that only the inverse of the constant matrix $[T_{\text{spin vector}}^I(t=0)]$ need be taken,

which can be done each time that the gyro alignment is obtained either at prelaunch or in flight by stellar measurements.

TABLE IV-IV
NUMBER OF ITERATIONS FOR CONVERGENCE

X		Error For 22 Bits
.1	5	.41 x 10 ⁻⁵
.2	4	.27 x 10 ⁻⁵
.3	4	.26 x 10 ⁻⁵
.4	4	.12 x 10 ⁻⁵
.5	3	.11 x 10 ⁻⁵
.6	3	.24 x 10 ⁻⁵
.7	3	.15 x 10 ⁻⁵
.8	3	.18 x 10 ⁻⁵
.9	2	.15 x 10 ⁻⁵
1.0	1	.1 x 10 ⁻⁵

C. Free Accelerometer Reference System

The motion of a free pendulous gyro accelerometer's input axis is caused by the linear acceleration applied to the vehicle that acts upon the pendulous moment along the spin axis and thus causes the input axes to precess with respect to inertial space. The applied acceleration during thrusting phases of flight can be divided into a constant thrust component and linear random and sinusoidal vibrations. The computational frequency or accelerometer transfer rate is governed by the magnitude and frequency content of the linear vibrations; the constant thrust component of acceleration causes a very smooth and easily followed precession rate. Any significant linear vibration at frequencies beyond that of the accelerometer data transfer rate results in an angular uncertainty in the knowledge of the accelerometer input axis and thus an improper resolution of the main thrust acceleration into the inertial computational frame.

The coordinate transformation error is an unbounded position and velocity error growing with time for it acts as uncertainty in knowledge of the accelerometer input axis just as if it were an electrical or mechanical uncertainty within the sensor itself. It should be treated as such in the analysis of the system's errors.

The motion of the spin and hence the input axes of a free pendulous gyro accelerometer is described, with respect to inertial space, by the following vector equation

$$\frac{d}{dt} (\bar{S}) = \frac{P}{H} (\bar{S} \times \bar{F})$$

where the spin axes precess at a given rate for each unit of applied specific force, F . The magnitude of the accelerometer "scale factor" is determined by the magnitude of the pendulous moment (P) and the magnitude of the angular momentum, H .

The mean square angular motion of the input axis in the presence of a linear ergodic vibratory environment is defined by

$$\overline{\Theta^2} = \frac{1}{2\pi^2} \int_{f_a}^{f_b} \left(\frac{P}{H} \right)^2 \frac{\phi(f)}{f^2} df$$

where ϕ is the linear power spectral density expressed in units of S^2/cps . Because the coordinate transformation is performed at a finite rate, the motion of the input axis will not be precisely followed. The mean square angular error is thus the difference between the actual motion described by the above equation and the motion followed by the coordinate transformation process. With the transfer function of the transformation process indicated by G , the error in knowledge of the orientation of the input axis is

$$\overline{\epsilon_{\theta}^2} = \frac{1}{2\pi^2} \int_{f_a}^{f_b} [1-G(f)]^2 \left(\frac{P}{H}\right)^2 \frac{\phi(f)}{f^2} df$$

For a linear vibratory input which has a significant amplitude that extends over a frequency band that is significantly wider than the accelerometer data transfer frequency, f_c , the above equation can be approximated by

$$\overline{\epsilon_{\theta}^2} = \frac{1}{2\pi^2} \int_{f_c}^{f_b} \left(\frac{P}{N}\right)^2 \frac{\phi(f)}{f^2} df$$

in which the transfer function G is assumed to be unity out to the frequency with which the transformation is performed, and is zero at all frequencies beyond this value.

With the specification of the power spectral density of the linear environment for each mission, the mean uncertainty in input axis orientation can be evaluated and the resulting error in the measurement of acceleration computed. If the error is unacceptably large or unnecessarily low, the transformation frequency or the accelerometer scale factor, (P/H) , should be suitably modified within the limits permitted by the state-of-the-art.

The transformation frequency requirements dictated by this analysis are independent of whether the gyros are free or restrained. If free gyros are employed as the attitude reference, the acceleration transformation frequency requirements dictate the minimum attitude computational frequency. If restrained gyros are employed as the attitude reference, the transformation frequency requirements dictate not only the minimum attitude computation frequency, but also the minimum acceptable bandwidth of the gyros. This arises because the attitude computations can only follow the output of the gyros and thus cannot operate upon the signal attenuated by the bandwidth limitations of the gyro. All that increased attitude computational frequency will provide with gyros of finite bandwidth is a minimization of the error in handling the signal passed by the gyro.

D. Restrained Accelerometer Reference System

The computational process for the restrained accelerometer system in a manner similar to free accelerometer systems also creates an uncertainty in accelerometer input axis orientation due to the finite coordinate transformation rate in the presence

of a vibratory environment. The environment of concern for restrained accelerometers is angular rather than linear. The restrained accelerometers also have an additional error, termed "size effect." It occurs because the accelerometers are really velocity meters integrating specific force in the rotating coordinate frame. Thus, any centrifugal and tangential accelerations caused by rotations of the sensor package about a point not coincident with the center of the sensor will result in an equivalent bias error unless the accelerometer data is resolved into the computational frame at a rate significantly faster than the angular oscillations.

1. Uncertainty in Accelerometer Input Axis Orientation

The means square angular motion of the accelerometer's input axis in the presence of the random ergodic angular environment, ϕ , is defined by

$$\overline{\Theta^2} = \frac{1}{2\pi^2} \int_a^{f_b} \frac{\phi(f)^2}{f^2} df$$

Because the coordinate transformation is performed at a finite rate, the motion of the input axis will not be precisely followed. With the coordinate transformation transfer function symbolized by G , the mean square angular error is thus defined by

$$\epsilon_{\Theta}^2 = \frac{1}{2\pi^2} \int_a^{f_b} [1-G(f)]^2 \frac{\phi(f)^2}{f^2} df$$

For an angular vibratory input of significant amplitude extending over a frequency band beyond the computational frequency, the above equation can be approximated by

$$\epsilon_{\Theta}^2 = \frac{1}{2\pi^2} \int_{f_c}^{f_b} \frac{\phi(f)^2}{f^2} df$$

In a manner similar to the free accelerometer, the mean angular error and its effect on system accuracy can be evaluated and gyro bandwidth and computational requirements selected so as to achieve an acceptable level of error in the overall system error budget.

2. Size Effect

The "size effect" error arises because the accelerometers cannot be mounted in the vehicle such that their center of mass coincides with the vehicle's center of mass or bending nodal points. The accelerometer in a strapdown system will, therefore, sense and integrate in the rotating frame the centripetal and tangential accelerations due to vehicle rotations. These unwanted measurements are cyclic and would be exactly removed at the end of each period of oscillation if the accelerometers' outputs were continuously resolved and summed in the computational frame. Because the accelerometer outputs (the increments of velocity) are summed for a finite time in the body frame before the data are transferred to the computational frame, the effects of centripetal and tangential accelerations are not exactly cancelled when summed in the computational frame.

Digital simulations have been conducted to determine the error for the strapdown system in transferring the accelerometer data from the body frame to the inertial computational frame in the presence of angular rotations about a point that is not coincident with the sensors. A sinusoidal oscillation about an axis parallel to one body axis and perpendicular to the input axis of two accelerometers was chosen as the vehicle motion in order to determine the effect of (1) the amplitude and frequency of motion, (2) the effect of the data transfer frequency to the inertial frame, and (3) the effect of accelerometer data processing schemes.

If the accelerometer data is resolved into the computational frame at a frequency that is less than the angular motion, the "size effect" error is equal to the centrifugal acceleration produced by the angular motions. This can be seen by examining the sensor outputs in the vehicle frame where the X axis in the following equations is parallel to this moment arm between the sensor package and the axis of rotation:

$$\Delta V_x^b \Big/_{t_j}^{t_{j+1}} = -R \Theta_m^2 \omega_f^2 \left(\frac{t}{2} + \frac{\sin 2\omega_f t}{4\omega_f} \right) \Big/_{t_j}^{t_{j+1}}$$

$$\Delta V_y^b \Big/_{t_j}^{t_{j+1}} = R \Theta_m \omega_f \cos \omega_f t \Big/_{t_j}^{t_{j+1}}$$

It is observed from the above equations that a term in the ΔV_x^b equation is unbounded; as the time difference between t_j and $t_j + 1$ increases the remaining terms are oscillatory. In the limit, if the accelerometer outputs are never resolved into the inertial frame, the average acceleration error is then centrifugal acceleration that can be expressed as

$$\dot{\bar{V}} = \frac{\Delta V}{\Delta t} = -\frac{1}{2} R \Theta_m^2 \omega_f^2$$

For extremely fast data processing, the other limit, the sign of the accelerometer output in the computational frame alternates and the centrifugal and tangential acceleration integrate to zero each cycle.

In Figure IV-19, the data processing error for two schemes is presented for the transfer of accelerometer data to the inertial frame. The abscissa displays the size effect error (\dot{V}) grouped with other terms that permit the data for a variety of motions to be readily correlated; the ordinate is the ratio of the sinusoidal frequency to the data transfer frequency. The two data processing schemes employed to resolve the accelerometer data are derived in Appendix B and are simply: 1) resolving the velocity increment into the inertial frame each data sampling cycle, and 2) using two successive samples of the velocity increments to estimate specific force as a function of time through a polynomial fitting process, coupling this estimate of specific force with time with a knowledge of attitude as a function of time to resolve the data into the computational frame where it is reintegrated to obtain velocity in the inertial frame.

This figure shows three distinct regions of error as a function of frequency rates for both data processing schemes. In the first region, the error is extremely small and is constant, independent of the motion and the data processing scheme. In this region the errors are due to round-off caused by the computer word length. In the second region, which can be termed the truncation region, the errors due to the two schemes diverge, with the higher order data processing scheme having the lower error. In this region for $f/f_c < .5$, empirical expressions describing the error have been developed for each of the data processing schemes:

Second Order Algorithm

$$\dot{V}(\text{ft/sec}^2) = 2.4R(\text{ft})\left(\dot{\theta}\left(\frac{\text{rad}}{\text{sec}}\right)\right)^2\left(\frac{f}{f_c}\right)^2$$

Fourth Order Algorithm

$$\dot{V}(\text{ft/sec}^2) = 12R(\text{ft})\left(\dot{\theta}\left(\frac{\text{rad}}{\text{sec}}\right)\right)^2\left(\frac{f}{f_c}\right)^4$$

In the final region, $f/f_c > .5$, the computations are carried out at less than twice the frequency of the motion and the error becomes independent of the data processing scheme employed. In this region the error is equal to the centrifugal acceleration:

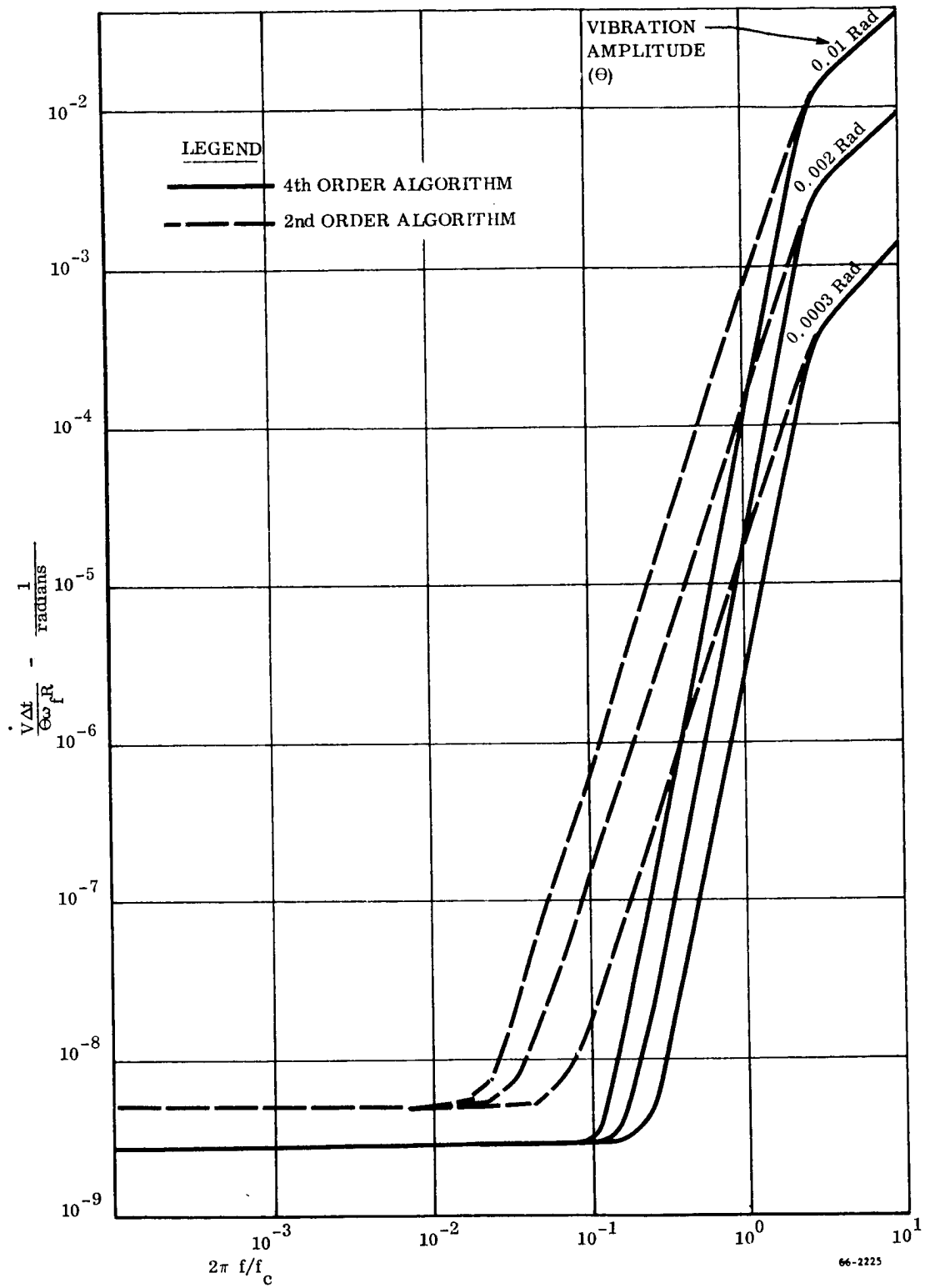


Figure IV-19 Restrained Accelerometer Size Effect Error

$$\dot{V}(\text{ft/sec}^2) = 2\pi^2 R(\text{ft})(\Theta_n(\text{rad}))^2 f^2(\text{cps})$$

These empirical equations can readily be extended to a random environment, for example, the second order schemes, with the assumption

$$\dot{\Theta}_i^2 = A = \frac{\lim}{\Delta f \rightarrow 0} \int_{f_i - \frac{\Delta f}{2}}^{f_i + \frac{\Delta f}{2}} \phi(f) df$$

where $\phi(f)$ is the power spectral density of the angular environment, can be written as

$$\begin{aligned} \dot{V} &= \frac{2.4}{f_c^2} \int_0^{f_o} R(f) A f^2 df, \quad f_o/f_c < .5 \\ &= \frac{1}{2} \int_{f_o}^{\infty} R(f) A df, \quad f_o/f_c > .5 \end{aligned}$$

The radius must be considered a function of frequency because the bending nodal points of the vehicle structure are frequency dependent. If the vehicle were rigid (i. e., no structural flexure) the radius would be a constant and could be removed from under the integral sign. In this form these expressions may be simplified by integrating by parts once:

$$\begin{aligned} V &= \frac{.8R}{f_c^2} \int_0^{f_o} \phi(f) f^3 df, \quad f_o/f_c < .5 \\ &= \frac{1}{2} R \int_{f_o}^{\infty} \phi(f) f df, \quad f_o/f_c > .5 \end{aligned}$$

E. Position Computation

The position computations consist of numerically integrating the incremental velocity outputs of the accelerometers (already resolved into the inertial frame) along with a gravitational acceleration model; a first integration yields velocity, the second yields position. The position computational error since it is an integration process is composed of round-off and truncation errors. These computational errors have been investigated for the fourth order Runge-Kutta integration scheme for different phases of flight: boost and injection, and orbital navigation. In each of these flight phases, the computational error induced by the degree of completeness of the gravitational acceleration model (presented in Appendix B) affects only the round-off error due to the increased number of numerical operations. This variation in round-off error with varying gravitational models, however, is extremely small compared to the round-off error associated with the normal integration operations.

The position computational errors were evaluated with the aid of a digital simulation of the sensors and the integration process. The boost error was computed by constructing a polynomial representation of acceleration during the boost phase that could be integrated in closed form to yield a reference trajectory. This polynomial was then integrated and quantized to synthesize the velocity vector output and entered into the position computations. This information was then processed in the manner described for computing velocity and position as presented in Appendix B. The computed velocity and positions were then compared with the reference value at boost termination. For the orbital phases of flight, a spherical gravitational potential was employed in order to obtain a reference trajectory through a closed-form solution of the equations of motion. The total orbital navigation error was then determined as a function of time in a circular orbit with a 100 nautical mile altitude. The digital simulations yielded the effects of computer word length, integration time interval and total flight time on navigation accuracy.

1. Boost and Injection

The error at injection was determined using 4th order Runge-Kutta integration of the linear equations of motion. Figures IV-20 through IV-22 present (for an injection into a 100 nautical mile orbit) the downrange, altitude and velocity errors, respectively, as a function of the integration time interval and computer word length. For the 20- and 24-bit computer word length data in Figure IV-20, the portions of the curves of negative slope relative to increasing integration time intervals represent computer round-off error associated with computer word length. The remaining portions of each of the error curves for the 20- and 24-bit computers as well as the entire curve for the 28-, 32-, and 35-bit computers are the integration scheme truncation error. These plots demonstrate that precise accuracy can be readily obtained by reducing the integration interval with a corresponding increase in computer word length.

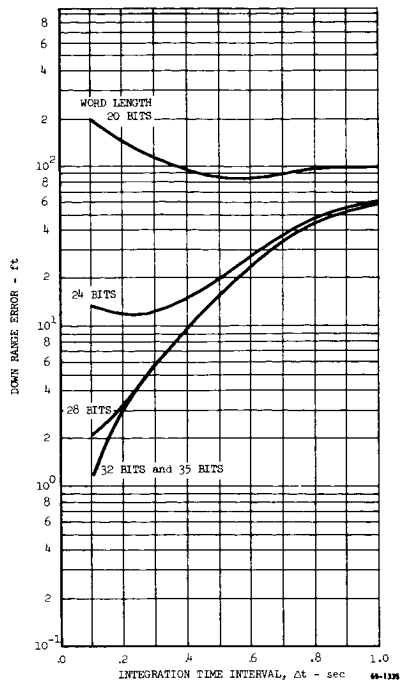


Figure VI-20 Boost Cutoff Injection
Position Computer Error

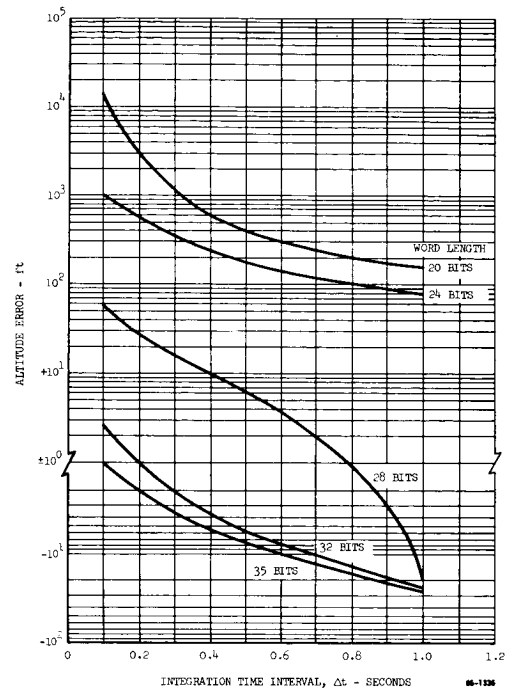


Figure VI-21 Boost Cutoff Injection
Altitude Computer Error

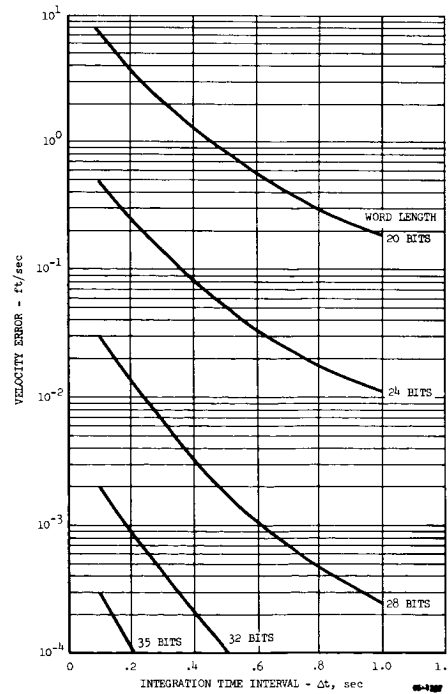


Figure VI-22 Boost Cutoff Velocity Computer Error

In Figure IV-21, the altitude error introduced by the computational process is presented. The positive-valued errors are due to computer round-off, the negative values to a combination of round-off and truncation. It is observed that for a given integration interval, the altitude error decreases with increased computer word length from a round-off error region, passes through zero, and increases negatively into the truncation region as the word length is increased.

In Figure IV-22, the velocity error is shown to continuously decrease with an increasing integration time interval, characteristic of computer round-off indicating that the truncation error associated with the integration of the gravitational-induced acceleration did not enter into the errors of the preceding two figures; the error in these figures was entirely due to round-off plus the truncation error induced by computing position from velocity data, not velocity from acceleration data.

2. Orbital Navigation

The navigation error in orbit due to the computational process was determined for a satellite traveling in a circular orbit about a spherical earth at 100 nautical miles altitude. In addition to investigating the effect of computer integration time interval and word length, the effect and relative importance of the addition and multiplication operations conducted within the computational process were investigated.

The latter investigation was conducted because the multiplication operations are used only to determine incremental changes in position and velocity, the magnitudes of which are small compared to total position and velocity; hence, computational accuracy can be maintained with a smaller computer word length for determining the incremental changes than can be used for summing the changes to the total position and velocity. A computer with a multiplication word length of 22 bits was thus selected for the study since it is capable of representing velocity to better than 0.01 fps and incremental position changes to better than 1 foot assuming a maximum integration interval of one minute. Using a double precision addition operation resulted in a 44-bit representation of total position and velocity.

Figures IV-23 through IV-25 present the position error as a function of the number of orbits traveled and as a function of computer word length and integration time interval. It is seen that when small integration time intervals must be used, a benefit is derived from the double precision add operation on a basically short word length computer.

In each of these figures, the position error is approximately proportional to the number of orbits for the 22/44 and 44/44 computers and approximately proportional to the square of the number of orbits for the 30/30 computer. In the

The truncation errors for these integration schemes were evaluated on a digital computer in which the rate input to a triad of gyros, the integrating gyros themselves, the computer and the numerical computational process were simulated (Figure IV-1). Three particular angular motions from which all vehicle motions can be constructed by judicious summation were investigated: constant and sinusoidal angular rotations about an axis noncollinear with any of the sensor input axes and a special case of multiple axis motion, the classical coning motion. Each of these motions is amenable to a closed form solution (presented in Appendix C), which was used as the reference against which the results of the numerical integration processes were compared and the computational error determined.

Coning motion is characterized by a constant component of angular velocity along an axis in the body frame and sinusoidal out-of-phase components of rate at the same frequency along two axes of the body that are orthogonal to each other and to the aforementioned constant rate component. The motion is termed coning because the body axis containing the constant component of angular rate describes a cone in space, returning each cycle to its initial starting point. This motion, if it occurs or is created by the vehicle or sensor supporting structure is of significant concern in any inertial system either gimballed or strapdown. For a strapdown system, if the attitude computations cannot follow the sinusoidal rate components and properly reconstruct vehicle attitude, the constant rate component along the third body axis (in the limit) becomes the drift rate of the attitude computational error.

As part of these studies three different sets of attitude parameters were evaluated: Euler angles, direction cosines and quaternions. The kinematic angular equations of motion for each of these parametric sets are presented in Appendix B. Cayley-Klein parameters and a four-angle Euler system can also be considered and they have properties similar to quaternions. Studies and digital simulations have been used to investigate the relative merits of each of these sets of attitude parameters. These studies show that there is little difference between quaternions and direction cosines. There is also little difference between both of these attitude parametric sets and the Euler angle set if the latter does not approach the singularity point equivalent to gimbal lock or if four Euler angles and suitable "control" logic for the additional Euler angle are employed. Direction cosines are most widely employed today in strapdown attitude computations because they are well behaved and are required to resolve data between coordinate frames. For this reason the majority of the analyses reported herein were performed using direction cosines as the attitude parameters.

A summary of the results obtained from these digital simulations is presented in Table IV-I in terms of the analytic models that have been derived for the truncation, quantization and round-off errors with time as the integration parameter. The truncation errors are presented for three vehicle motions: constant rates of rotation, sinusoidal oscillations and coning rotations. In order to aid in the visualization of these results, the equations in Table IV-I are plotted in Figures IV-6 through IV-10. The computational error shown in these figures is the derivative of the norm of the attitude error

TABLE IV-I
ATTITUDE COMPUTATIONAL ERROR SUMMARY

Error Source and Angular Motion	Integration Scheme	Error Equations In Terms Of Drift Rate in deg/hr
Truncation (Constant Rates)	Rectangular 2nd Order Runge-Kutta 4th Order Runge-Kutta	$36.5 \omega^2 / f_c$ $0.133 \omega^3 / f_c^2$ $(1.62 \times 10^{-6}) \omega^5 / f_c^4$
Truncation (Sinusoidal Rates)	Rectangular 2nd Order Runge-Kutta 4th Order Runge-Kutta	$117 \beta^2 f_c (\sin \frac{\pi}{2} f / f_c)^2$ $0.0985 \beta^4 f_c (\sin \pi / 2 f / f_c)^4$ $0.0535 \beta^4 f_c (\sin \pi / 2 f / f_c)^6$
Truncation (Coning $f / f_c > 0.8$)	Rectangular 2nd Order Runge-Kutta 4th Order Runge-Kutta	$260 \beta^2 f$
Truncation (Coning $f / f_c < 0.8$)	Rectangular 2nd Order Runge-Kutta 4th Order Runge-Kutta	$327 \beta^2 f^2 / f_c$ $408 \beta^2 f^3 / f_c^2$ $646 \beta^2 f^5 / f_c^4$
Quantization (Coning)	Rectangular 2nd Order Runge-Kutta 4th Order Runge-Kutta	$k \pi Q^2 \beta f^2 / f_c$
Round-off (All Motions)	Rectangular 2nd Order Runge-Kutta 4th Order Runge-Kutta	$(2.1 \times 10^{-5}) 2^{-n} f_c$

SYMBOLS

- ω = Angular velocity in deg/sec
 f_c = Computational frequency in cps
 β = Angular amplitude in deg
 f = Frequency of input motion in cps
 Q = Quantization level in arc seconds
 n = least significant bit of the total direction cosine

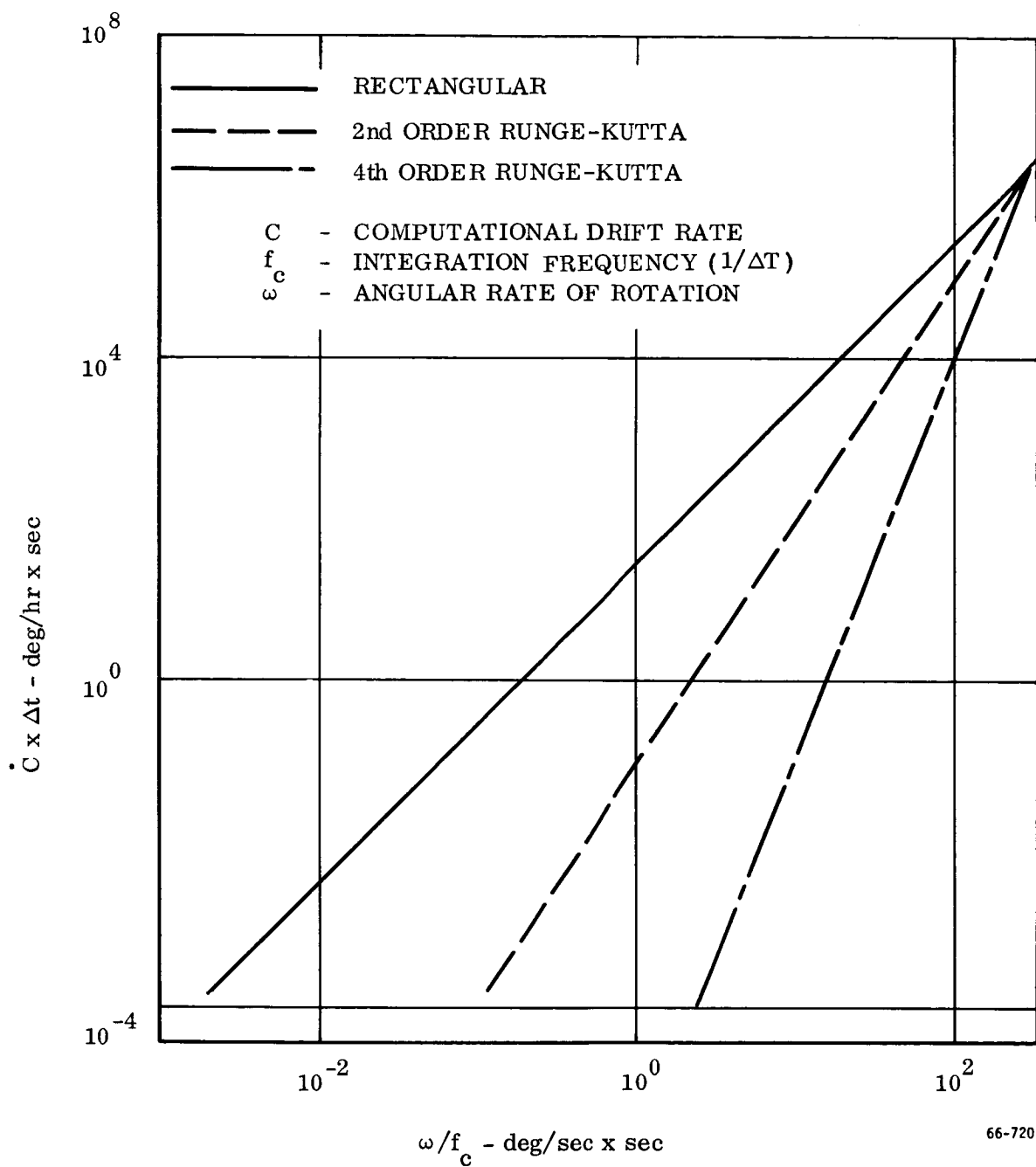


Figure IV-6 Attitude Errors for Constant Rates of Vehicle Rotation

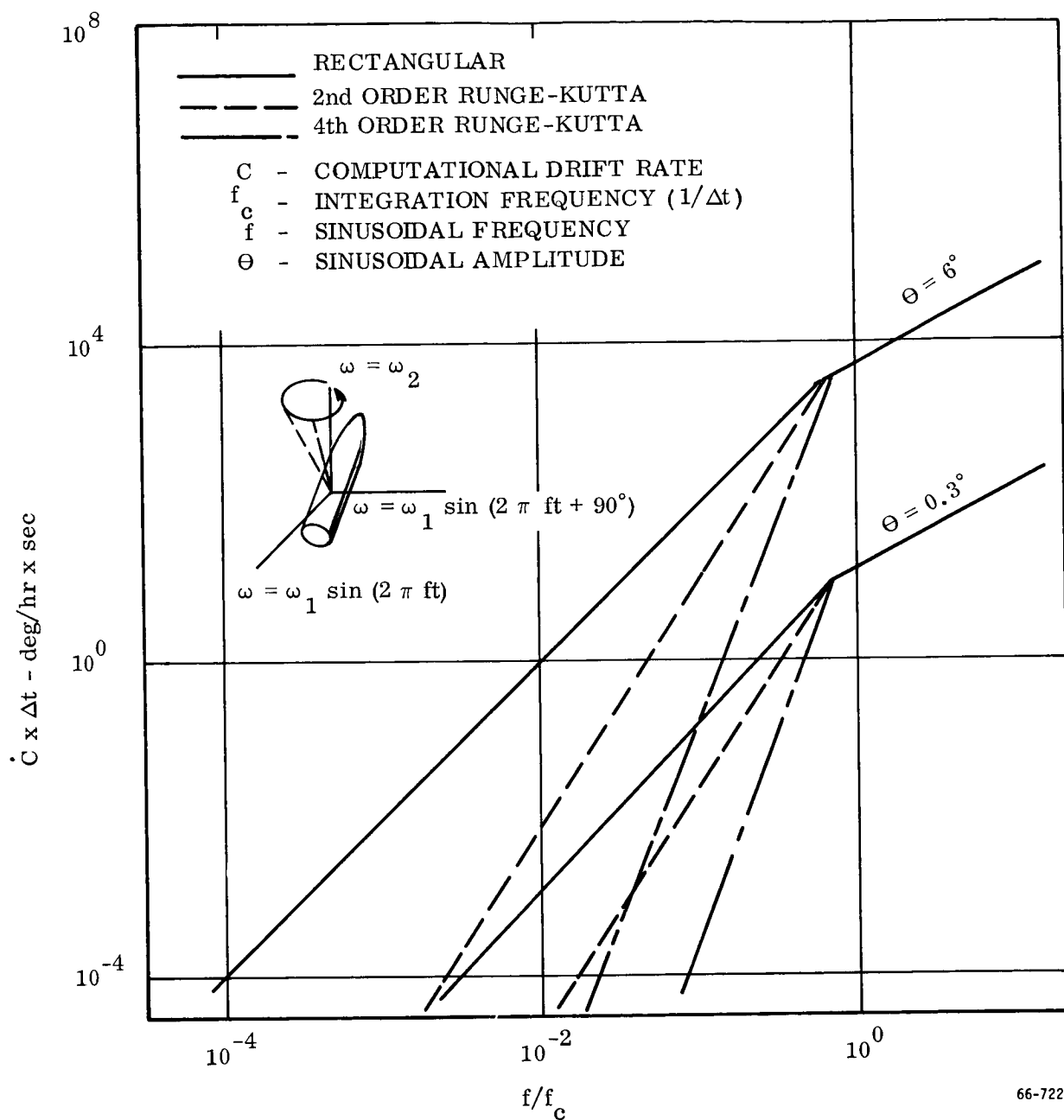


Figure IV-7 Attitude Errors for Two Out-of-Phase Vehicle Sinusoidal Oscillations (Coning)

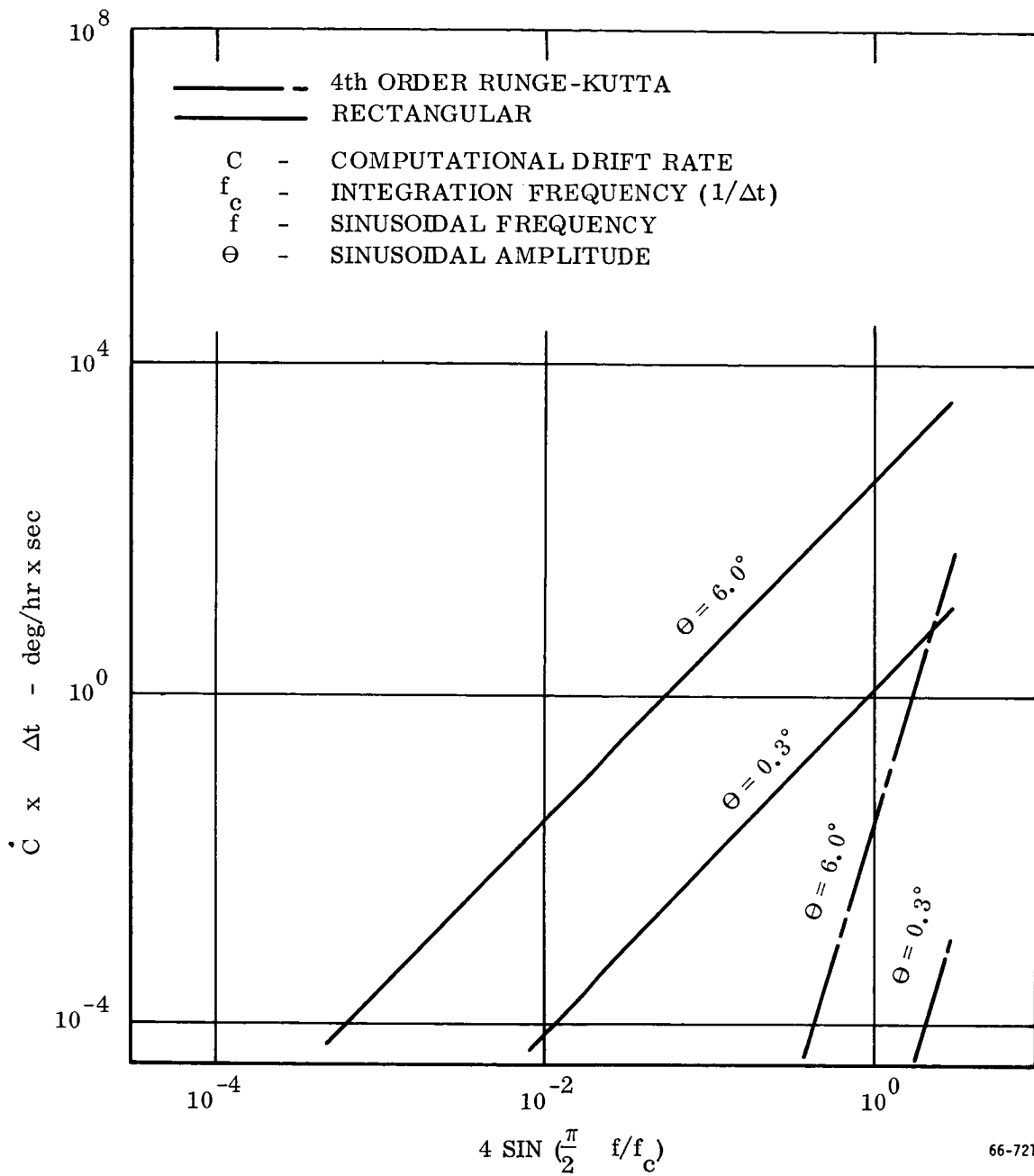
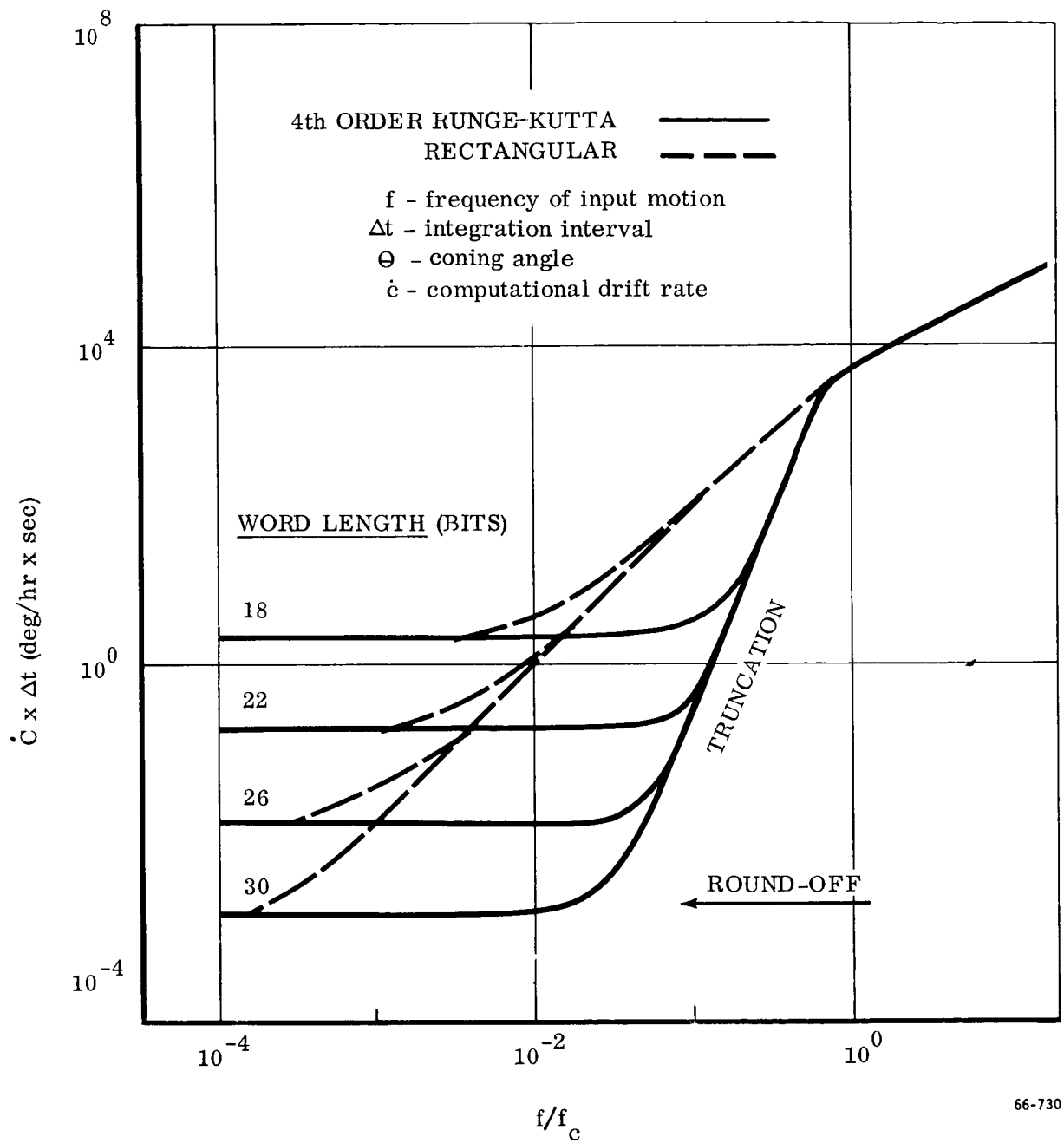
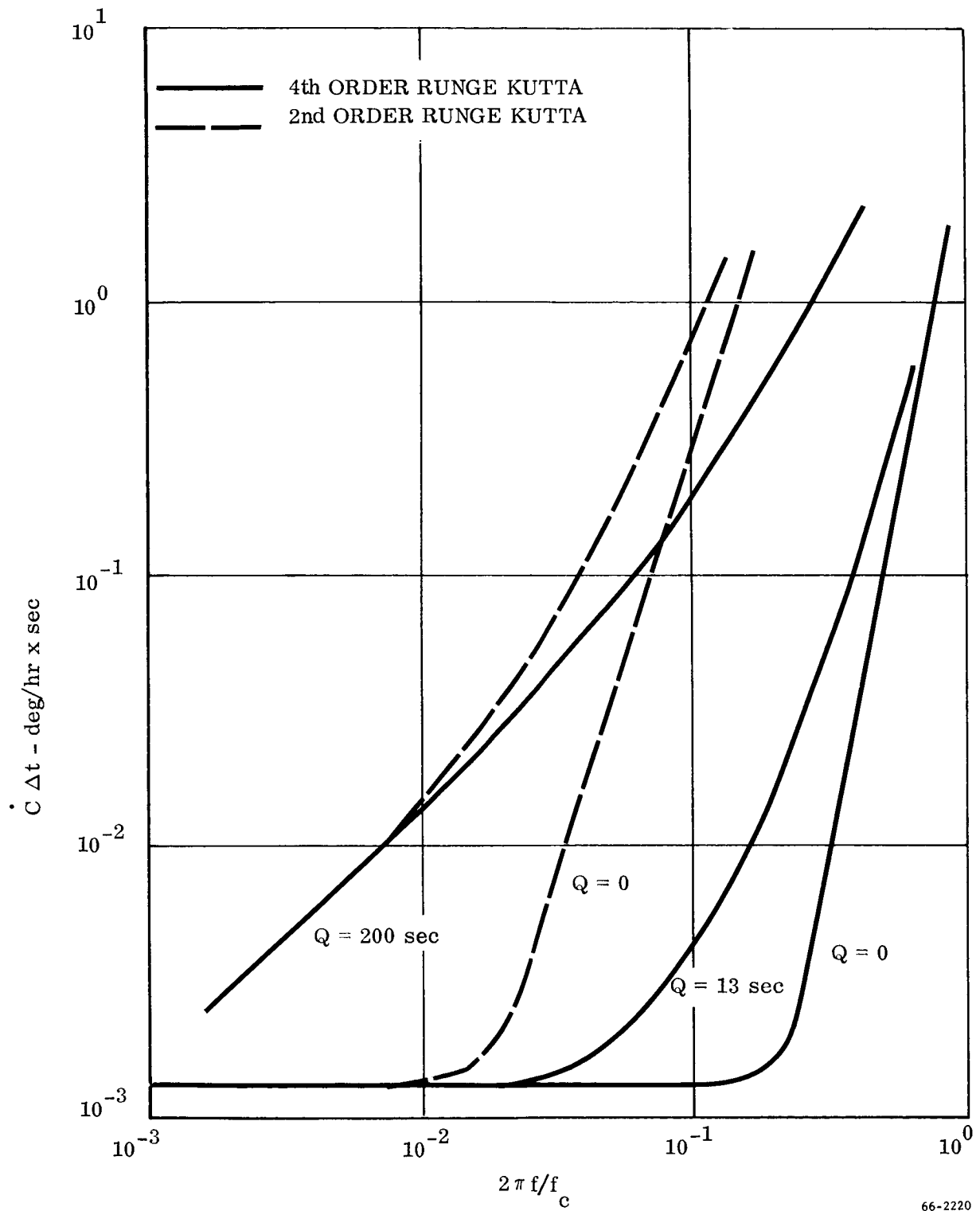


Figure IV-8 Truncation Errors for Sinusoidal Vehicle Oscillations



66-730

Figure IV-9 Combined Truncation and Round-off Error for Coning Rotations



66-2220

Figure IV-10 Effect of Quantization on Computational Error
for Coning Motion ($\Theta = 0.096 \text{ rad}$)

matrix, \dot{C} , in degrees per hour, times the integration step size in seconds. This product is also the computational error per integration step expressed in units of arc-seconds. The abscissa is expressed as a function of the ratio of angular motion frequency to the computational frequency. Note that these figures are log-log plots of the error.

In Figures IV-6 and IV-7 the characteristics of the truncation and bandwidth limited regions are shown for constant and angular rates and coning. When the computational frequency is higher than the angular motion frequency, there are significant differences in the truncation error as the order of the integration process is decreased. As the integration frequency decreases and approaches the angular motion frequency, the errors for various integration schemes approach each other. The error subsequently becomes independent of the integration scheme and enters the bandwidth limited region when the computational frequency is less than the angular motion frequency. In the bandwidth limited region, the error curve presented in these two figures and the error model in Table IV-1 represent the maximum error envelope in this region; the magnitude of the error determined from the digital simulations exhibited a high degree of randomness as a function of frequency ratio in this region, often equal to but never exceeding the presented curve. For coning motion, the bandwidth limited error curve is exactly equal to the constant rate component of the coning motion. In these two figures, the slope of the bandwidth limited error curve is one because the vertical axis indicates the magnitude of the computational drift rate times the magnitude of the integration step size; plotting computational drift rate versus the frequency ratio would reduce the slope of both the truncation and bandwidth limited error curves by one, i. e., a slope of five would become a slope of four and the error curves would have the characteristics presented schematically in Figure IV-4.

These two figures demonstrate the significant improvement in computational accuracy that is obtained in the truncation region using higher order integration schemes. For a fixed angular motion to integration frequency ratio, the accuracy of the higher order integration schemes can be orders of magnitude better than the rectangular integration scheme. Conversely, for a desired level of accuracy, there are significant decreases in computation frequency requirements when higher order integration schemes are employed, again orders of magnitude better. Even though the number of program instructions to be executed per integration step increases with the order of the integration scheme, the total number of instructions that must be executed per second for a given level of accuracy decreases with increasing order of the integration scheme. The number of instructions executed per second, hence the computer's speed requirements, decreases with increasing integration scheme order because the number of integration steps per second required to achieve a given level of accuracy decreases faster than the number of instructions per integration step increases.

In Figure IV-8 the truncation error for different amplitudes and frequencies of sinusoidal input motion are shown for both rectangular and fourth order integration schemes. This figure again demonstrates the significant reduction in truncation error

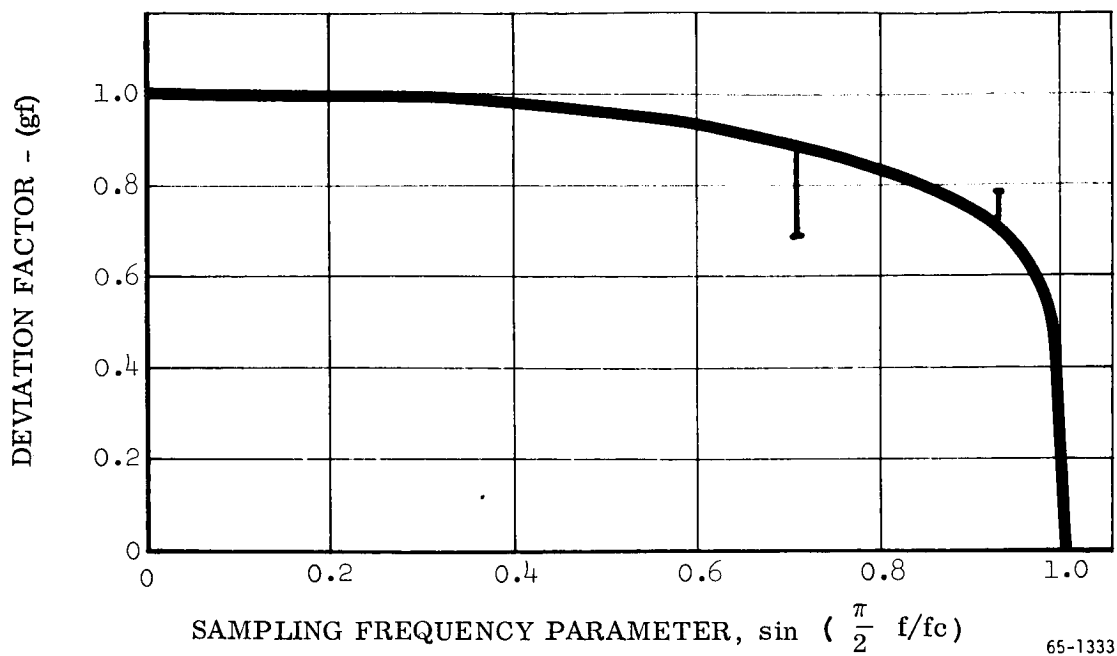
achieved by increasing the order of the integration scheme. The basic difference in the functional behavior of the computational error for sinusoidal motion from that of other motions, is that there is not equivalent bandwidth limited region. As the integration frequency decreases so as to approach the angular motion frequency, the truncation error increases until the integration frequency is less than the angular motion frequency, whereupon the truncation error decreases. This behavior of the truncation error with frequency ratio is observed in Figure IV-8 by noting that the correlation of the error is made upon the sine of the frequency ratio which is periodic. It can be seen that the maximum value for the first derivative of the norm is finite; it occurs at odd multiples of the input motion to the computational frequency ratio; it is less than the maximum value at all other values of the frequency ratio, and is zero at even multiples of the frequency ratio.

The actual truncation errors obtained for sinusoidal environments differ slightly from the error models presented in Table IV-1 and the plots in Figure IV-8. The error models presented are simplifications of more complex models but they are conservative and are of sufficient accuracy for computational design purposes for all missions and flight environments of interest. First, for values of $\sin(\frac{\pi}{2} f/f_c)$ between 0.2 and 1, the truncation error for sinusoidal motions differs by the deviation factor shown in Figure IV-11 for the fourth order scheme. It multiplies the entire error model presented in Table IV-I. A similar factor is obtained for the other integration schemes. Inasmuch as the deviation factor is appreciable only in regions where the computational drift rates are unacceptably high and because the factor represents an attenuation of the computational error, it is sufficient for design purposes to neglect this factor. The second difference is that for the rectangular integration of sinusoidal motions, the higher derivatives of the norm are nonzero. They need only be considered however for: (1) long duration computational intervals during which the attitude matrix is not updated by external means, (2) large angular amplitudes, and (3) for large values of the frequency ratio (f/f_c). For frequency ratios (f/f_c) between zero and unity, the data from the digital simulations has been correlated into an error model for the rectangular integration of sinusoidal motions:

$$\dot{C} = 468 \alpha e^{3.6 \times 10^{-2} \alpha f_c t}; \alpha = \pi^2 \beta^2 \left(\frac{f}{f_c}\right)^2$$

For values of f/f_c less than one, this equation reduces to the error model given in Table IV-I when $\sin(\pi/2 \times f/f_c)$ is approximated by $(\pi/2 \times f/f_c)$. For frequency ratios greater than unity, the data has not been manipulated to yield an error model; the periodicity of the truncation error with frequency ratio described by the error model in Table IV-I is still present along with the exponential growth in the errors with time at any particular frequency ratio.

The above-described exponential growth of the truncation errors with time for sinusoidal environments has not however been observed for the higher order schemes, nor has it been observed for any integration scheme for any other motions.



NOTE: SINGULAR POINTS AT

$$\frac{f}{f_c} = 0.5 \text{ AND } 0.75 \text{ THAT HAVE BEEN OBSERVED.}$$

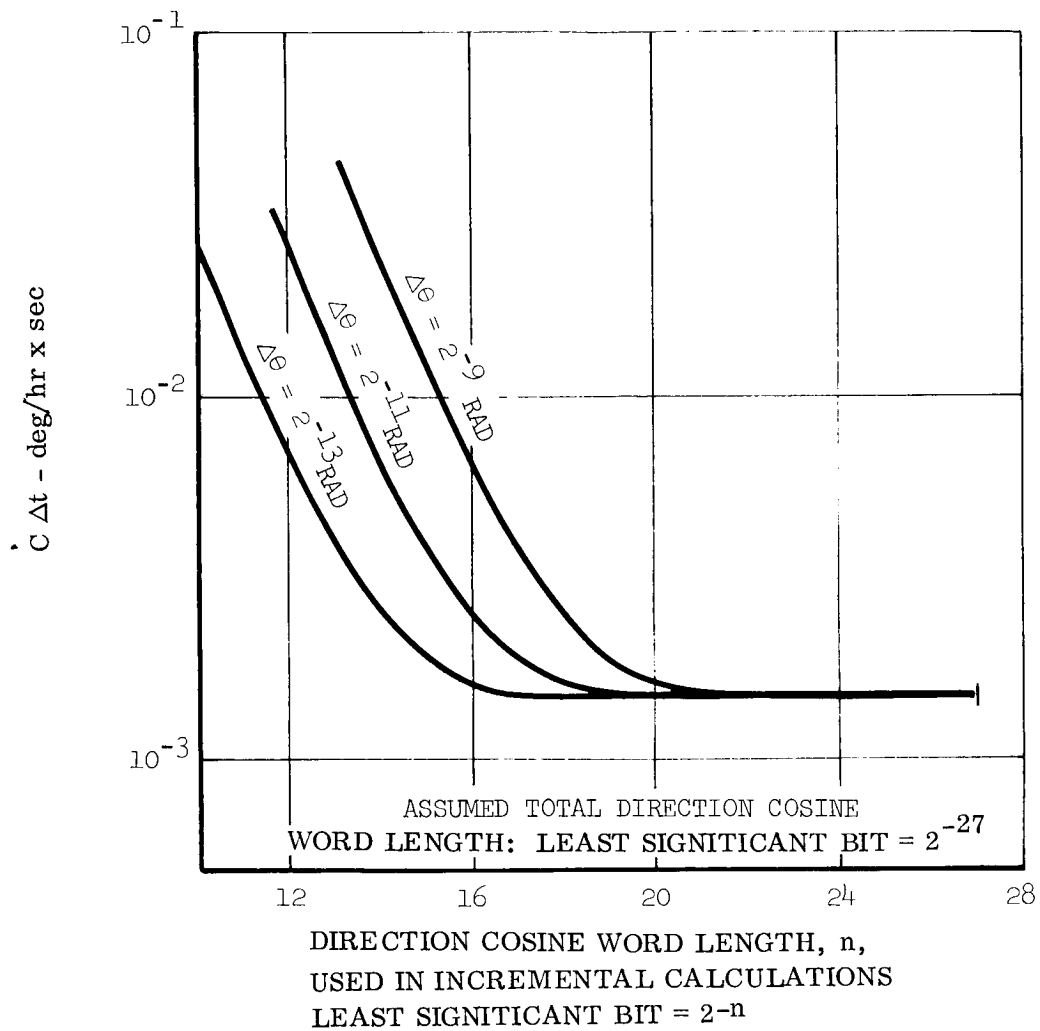
Figure IV-11 Deviation Factors vs. Sampling Frequency Parameter
for Fourth Order Runge Kutta

The effect of computer word length on the computational accuracy is shown in Figure IV-9 along with interrelationships of the round-off and truncation errors for coning motion; the results are identical for all other motions. The word length (n) referred to in this figure and also in Table IV-I is the value of the least significant bit used to represent the total direction cosine value (2^{-n}). The calculations of the incremental changes in direction cosine must be performed with sufficient precision or word length to make the information contained in this bit location (2^{-n}) meaningful. For very small values of the ratio of the angular input to the computational frequency, the round-off error per integration step is a constant that (1) decreases in magnitude linearly with increased word length and (2) is independent of the order of the integration scheme, the type of angular motion and the integration step size.

It is shown in Figure IV-9 that for fixed word length and integration step size, as the frequency ratio is increased the total error for lower order integration schemes breaks away from the round-off error level prior to the higher order schemes and intercepts the truncation error curve at higher levels of truncation error.

The critical items in determining the word length required for the calculation of the incremental changes in direction cosines are (1) the magnitude of the incremental angular rotation at the point of transition from round-off to truncation for the selected value of round-off error and integration scheme and (2) the dynamic range of the sensor. The magnitude of the incremental angular rotation at the transition point governs the number of most significant bits of the total direction cosines required in the incremental calculations; the magnitude of the dynamic range (the maximum to minimum values of the sensor output during the integration interval including compensation for deterministic sensor errors) governs the number of bits required to represent the value of the gyro output ($\Delta\theta$) in the incremental calculations.

The number of bits required to represent the direction cosine in the incremental cosine calculations is theoretically the difference between the number of bits selected to represent the total direction cosines and the magnitude of the maximum angular increment at the point of transition from round-off to truncation. An example of this would be the selection of a least significant bit of the total direction cosine of 2^{-27} and the selection of an integration scheme whose truncation error left the round-off error at a $\Delta\theta$ of 2^{-9} radians. The predicted word length of the direction cosines for the incremental calculations would be 18 bits. Figure IV-12 demonstrates the results of the digital simulation study used to confirm this analysis. These curves are for 2^{-27} accuracy in the total direction cosine and varying $\Delta\theta$ at the error transition point (covering various integration schemes and integration intervals of interest). It is shown in this figure that required direction cosine word length in the incremental calculations is less than the number of bits representing the total direction cosine. These curves become asymptotic to a line having a slope of minus 2 and indeed this asymptote intersects the round-off level (1.5×10^{-3} arc-second) at the predicted values. In practice, an additional bit is required to minimize the error.



65-1345

Figure IV-12 Attitude Round-off Error as a Function of Word Length
for Calculating Incremental Changes in Direction Cosines

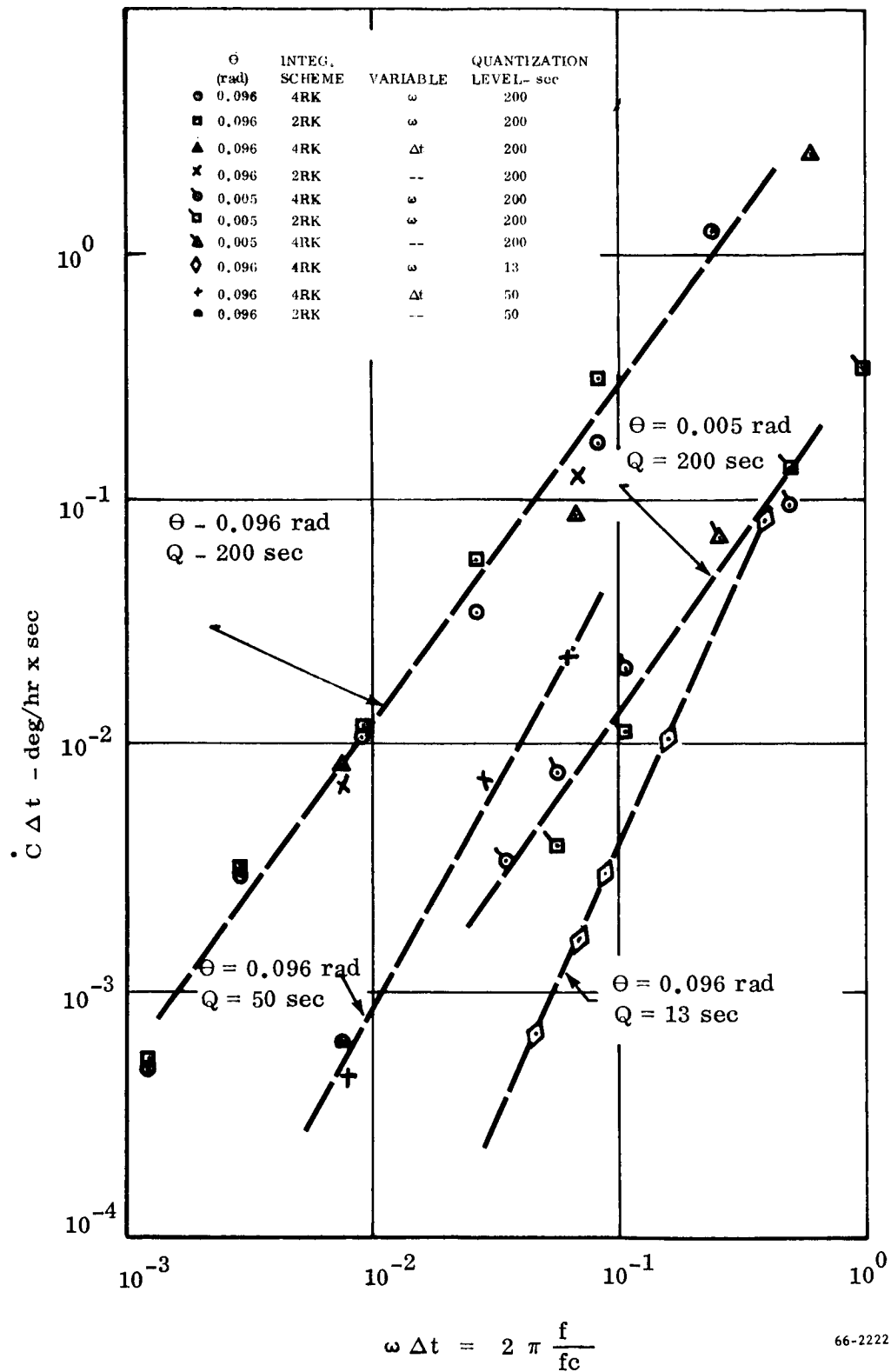
Figure IV-10 now adds the effect of sensor quantization to that of round-off and truncation; second and fourth order integration of a coning environment without quantization and with different levels of quantization are presented. The quantization error is seen to modify the transition region between round-off and truncations. The quantization error is obtained by taking the difference between identical runs with and without quantization. The results of this evaluation procedure are presented in Figure IV-13, which shows the quantization error per integration step, \dot{C} , to be independent of the integration scheme and proportional to the amplitude and the frequency of the motion, the size of the integration interval ($\frac{1}{f_c}$) and the quantization level itself. This error may be expressed as:

$$\dot{C} = k \frac{Q^a}{\Theta} (f/f_c) \left(\frac{1}{2} \Theta^2 \omega \right)$$

The scatter in the data is due to the fact that this error is a small part of the total error. This scatter makes an accurate evaluation of (k) and (a) difficult; a mean value estimate of the exponent (a) is 2. In order to achieve the accuracy benefits of the higher order integration schemes in the truncation region, smaller levels of sensor quantization are required compared to the levels required for lower order schemes. Quantization, however, is not an important error source because pulse torquing schemes capable of quantizing data to an arc sec or less have been developed.

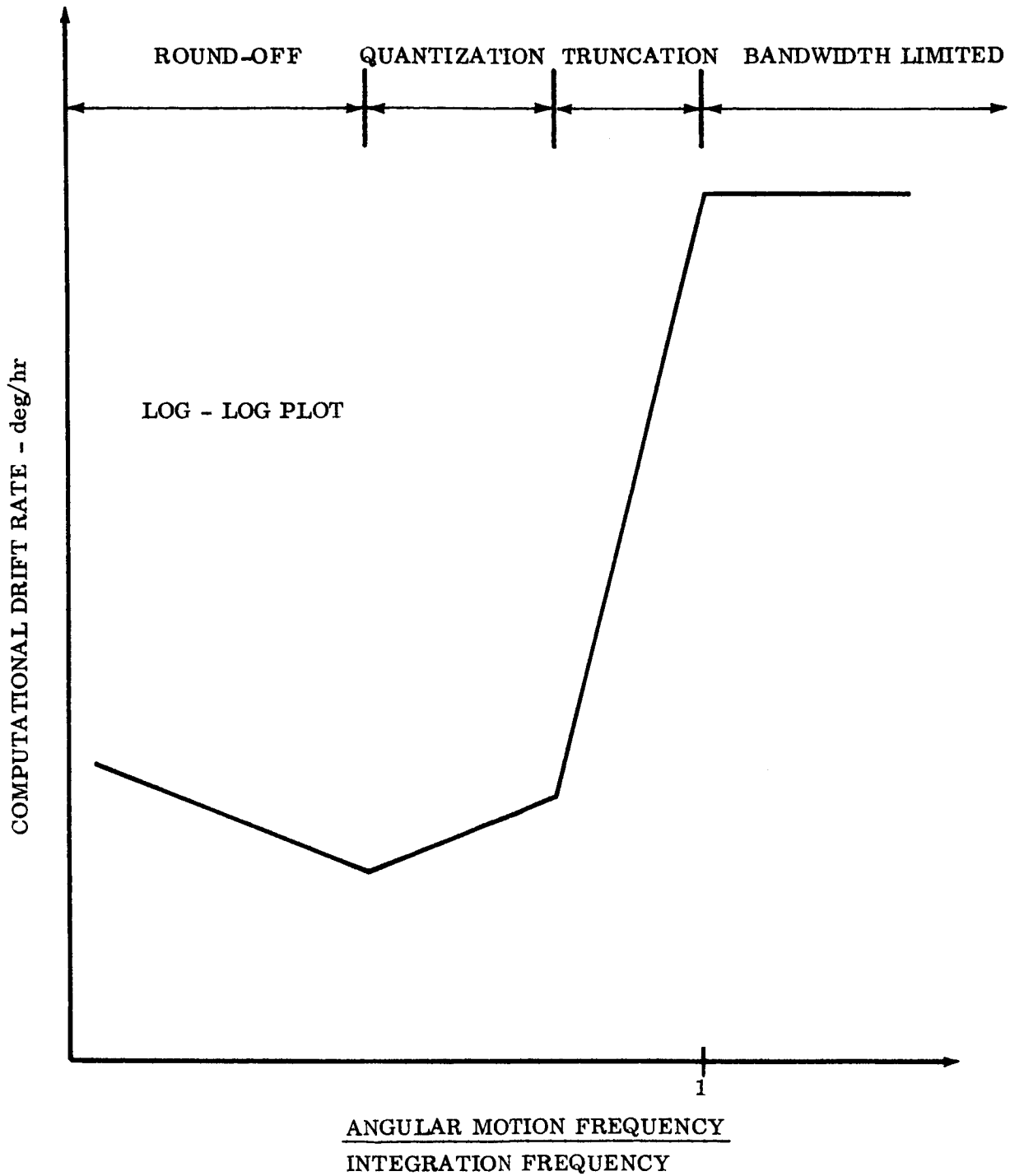
For some applications it may be desirable to use an incremental data processor (DDA) rather than a whole number general purpose computer. In these applications, the angular rotation of the vehicle is logically used as the independent integration parameter rather than time. Each sensor pulse or a fixed number of pulses is allowed to accumulate until a specified level is reached, at which time an integration step is performed. Since the multiplications in the angular motion difference equations are between direction cosines and the incremental angular change, only additions or subtractions need be performed because the angular change is always constant.

Figure IV-14 compares the errors of a DDA approach with that of a whole number computer for both rectangular and second order integration processes. All systems in this figure are sized to handle a maximum rate of 25 degrees per second. At the point of maximum angular rate, the error of the incremental and whole number computational processes are equal. At angular rates below the maximum, the error associated with the whole number computer decreases at a faster rate than that of the incremental computer. This can also be seen in Table IV-I when the integration parameter for rectangular integration of constant rates is changed from (Δt) to ($\omega \Delta t$). Figure IV-14 demonstrates the accuracy improvements to be gained for both the incremental and whole number computational processes with higher order integration schemes. There are no fundamental limitations to prevent the use of higher order integration schemes in a DDA, only hardware limitations when it comes to implementation. The accuracy penalty encountered with a DDA is a computational error that at times other than the maximum rate input will yield larger errors than would occur using time as the independent integration parameter.



66-2222

Figure IV-13 Quantization Error for Coning Motion



66-2218

Figure I-1 Regions of Error for Restrained Gyro Attitude Computations

II. INTRODUCTION

The function of an inertial navigator is to indicate the attitude, the velocity and the position of a vehicle with respect to a selected computational frame using information obtained from on-board inertial instruments. A strapdown navigator is characterized by gyros and accelerometers that are directly attached to the vehicle. The sensor's measurements of linear and angular motion of the vehicle relative to inertial space are expressed in vehicle coordinates. It is necessary in a strapdown navigator that the gyro outputs be used to numerically compute the attitude of the vehicle relative to inertial space and that the computed attitude be used to resolve the accelerometer outputs into the inertial frame where they are doubly integrated along with a gravitational model to yield vehicle position. These strapdown computational functions are schematically shown in Figure II-1. In this same figure, the functional operation of a gimbal navigator is also presented for comparison.

The kinematic equations that must be solved by any inertial guidance system are:

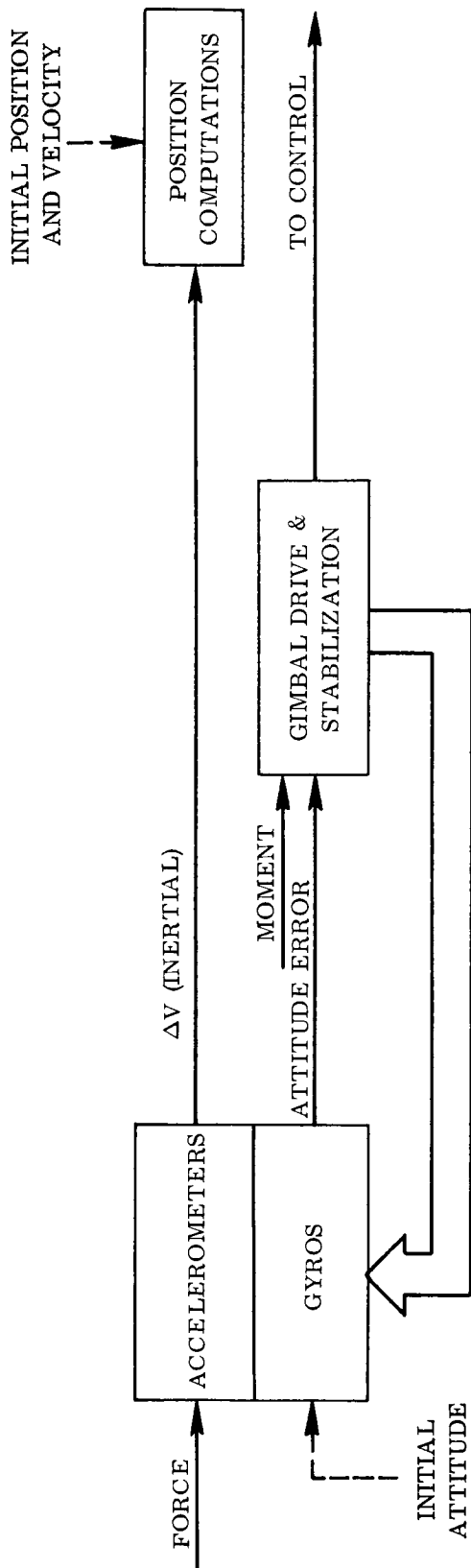
$$\frac{d}{dt} \left[T_s^I(t) \right] = \left[T_s^I(t) \right] \cdot \left[\Omega(t) \right] \quad \text{(Attitude Computations)} \quad \text{(II-1)}$$

$$\frac{I}{F}(t) = \left[T_s^I(t) \right] \cdot \frac{S}{F}(t) \quad \text{(Coordinate Transformation)} \quad \text{(II-2)}$$

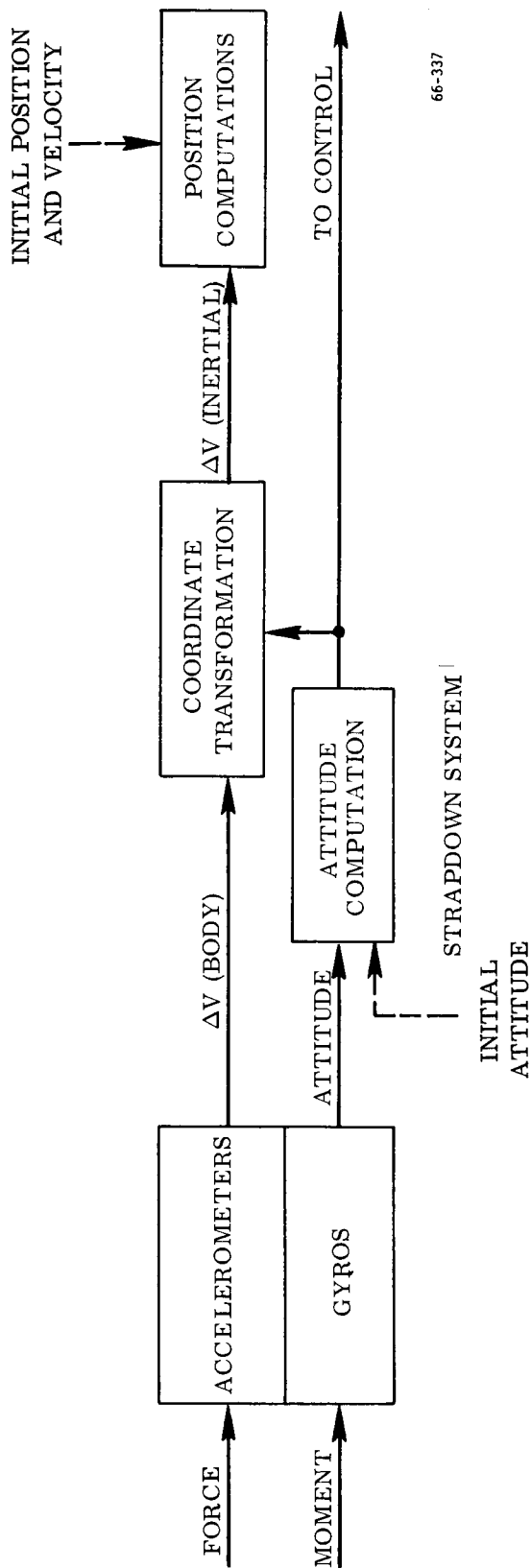
$$\frac{I}{V}(t) = \frac{I}{V}_0 + \int_0^t \left\{ \frac{I}{F}(t) - \frac{I}{g}(\bar{R}) \right\} dt \quad \text{(Velocity and Position)} \quad \text{(II-3)}$$

$$\frac{I}{R}(t) = \frac{I}{R}_0 + \int_0^t \frac{I}{V}(t) dt \quad \text{(Computations)} \quad \text{(II-4)}$$

For simplicity these kinematic equations have been expressed in an inertial computation frame. A 3×3 matrix, $[T_s^I]$, is used to define the orientation of the sensor readout coordinate system relative to the computational inertial frame. The elements of the skew-symmetric matrix, $[\Omega]$, are the components of the angular rate of the vehicle sensor readout frame relative to the inertial frame expressed in the sensor readout frame. F , g , V and R denote, respectively specific force, gravitational acceleration, velocity and position. Section VI presents a list of symbols used in this report.



GIMBAL SYSTEM.



66-337

Figure II-1 Comparison of Strapdown and Gimballed Navigation Systems

For a strapdown navigator, the orientation of the sensor frame relative to the computational frame is nondeterministic and time variant and must therefore be explicitly computed in flight starting with an initial knowledge of attitude. In contrast to a strapdown mechanization, there is a gimballed or platform inertial navigator whose functional mechanization is described in Figure II-1. In the gimballed mechanization, the gyros and accelerometers are mounted on a member, commonly termed a sensor cluster, that is suspended from the vehicle by a gimbal structure. The outputs of the gyros are used as error signals for a gimbal drive or control system to null out all angular motions of the sensor cluster. This control system is designed to isolate the sensor member from all vehicle angular motion thus maintaining the initial attitude of the accelerometers relative to inertial space. This maintains $[T_S^I]$ in equation (II-1) at a predetermined value and results in the accelerometer outputs being directly available in an inertial frame for the position computations.

The significant difference between strapdown and gimballed navigators is the use of gyros in a strapdown system to measure absolute attitude or the absolute change in attitude in contrast to a gimballed system in which the gyros are used as nulling sensors. This results in the replacement of the electromechanical gimbal support and drive system of the gimballed mechanization by a numerical computational process implemented in the digital computer for the strapdown system.

After the accelerometer data of the strapdown navigator are resolved into the computational frame, the position computations for it and a gimballed system are identical. The linear equations of motion including a model of any force fields acting upon the vehicle are numerically integrated, once to obtain velocity and a second time to obtain position.

A. Commonality of Sensor Mechanizations

The design and analysis of the strapdown computational process is greatly simplified by the fact that the computational process can be separated to a large extent from specific sensor mechanizations. The effects of the sensors upon the computational process can be analyzed in terms of the characteristics of the sensor loop output signal.

Basically, there are two classes of strapdown sensor mechanizations. The distinction is made entirely upon the angular orientation relationship maintained between the sensor input axes and the vehicle. One class employs sensors whose

input axes are maintained fixed relative to the vehicle by a rebalancing feedback loop. Typical sensors of this class, which are termed restrained sensors are:

Angular Motion Sensors

Rate or Rate Integrating Gyros

Single Axis Platforms

Restrained Pendulous Integrating
Gyro Accelerometers

"Paired Accelerometers"

Linear Motion Sensors

Force or Torque Rebalanced
Pendulous Accelerometers

Restrained Pendulous Integrating
Gyro Accelerometers

Free Gyro Centering Force
Measurements

The output of a restrained gyro commonly used in strapdown systems is the integral of the component of vehicle angular rate (relative to inertial space) that is projected onto the sensor's input axis. Restrained gyros require the numerical integration of the angular kinematic equation (equation II-1). The output of a restrained accelerometer is the integral of the component of specific force relative to inertial space projected onto the sensor's input axis.

The second class of sensor mechanization employs sensors whose input axes are unrestrained or free of the vehicle. Sensors of this class, which are termed "free sensors", are:

Angular Motion Sensors

Free Gyros

Linear Motion Sensors

Free Pendulous Gyro
Accelerometers

The output of free gyros are trigonometric functions of the angular orientation of the vehicle relative to inertial space and allow a solution to the angular kinematic equations directly without the employment of a numerical integration process. The output of a free pendulous gyro accelerometer is the integral of specific force relative to inertial space but integrated in a rotating sensor frame, namely, the suspended sphere or rotor. The integral is obtained in the vehicle frame and must be resolved into the inertial frame.

These sensor mechanizations are described in References 1 through 4 and briefly discussed in Appendix A. Examples of the data processing equations that can be used to compute attitude for both restrained and free gyros are presented in Appendix B. Similarly, data processing equations required to transfer the accelerometer outputs into the inertial frame for restrained and free accelerometers are also presented in Appendix B. In considering the design of a strapdown navigator for particular mission applications, it is not necessary to use free gyros with free accelerometers nor restrained gyros with restrained accelerometers; any mixture can be employed, depending upon sensor capability and mission requirements.

Within the restrained sensor mechanization class, only four parameters are required to describe or characterize the sensor's data outputs to the computer. These parameters are:

1. Frequency response of the sensor loop, which characterizes the possible frequency content of the sensor output signal that the computational process must follow.
2. Rate or frequency at which data is available to the computer (the sensor output is usually a finite frequency digital output).
3. Resolution or smallest value of the sensor output.
4. Maximum magnitude of the sensor output between sampling times.

For the free sensor mechanization, the following parameters are needed to characterize the signal output:

1. Specific trigonometric outputs of the sensors.
2. Rate or frequency with which the sensor can be meaningfully sampled.
3. Resolution associated with the readout design.

B. Study Objectives and Report Organization

The objective of the study reported upon herein is to define and to develop the techniques for evaluating the computational problems, the computational requirements and the computational accuracy associated with strapdown navigators. Included as areas of concern are the following:

1. Different types of inertial sensor and computer mechanizations.
2. Inertial sensor readout characteristics.
3. Computational requirements to implement sensor utilization techniques by which strapdown mission flexibility, accuracy and reliability can be increased.

The subsequent sections of this report present an analysis of the strapdown computational accuracy as effected by the numerical algorithms, the flight environment and critical computer hardware and inertial sensor characteristics. Section III presents a functional evaluation of the computational requirements and the sensor/computer/flight environment interrelationships. Section IV summarizes the quantitative analyses of the computational errors that have been performed with the aid of detailed digital simulation studies of the strapdown hardware and software. All error sources are evaluated and analytical error models are presented. Section V presents hardware application studies that have been performed in order to improve the mission flexibility, accuracy and reliability of strapdown navigators. Section VI presents the results of the study performed to define the computational requirements in the initial phase of a space mission-launch through transplanetary trajectory injection. Appendices A through G present the detailed analyses and mathematical derivations to supplement the discussion in the main body of this report.

III. FUNCTIONAL EVALUATION OF COMPUTATIONAL REQUIREMENTS

This section establishes, by functional analysis, the significant parameters that must be considered in the design or performance analysis of a strapdown navigator that uses either class of sensor mechanization; free or restrained. The functional analysis is developed by an inspection of the equations that must be solved and a consideration of the forcing functions that create an ideal sensor output. Table III-I defines specific terms that will be frequently used in this and later sections.

The most critical computational problem for strapdown navigators occurs during thrusting phases of flight. The problem is the joint process of maintaining knowledge of the orientation of the accelerometer sensitive axes with respect to inertial space and resolving the outputs of the accelerometers into the inertial computational frame. The process of using the resolved accelerometer data in conjunction with a mathematical gravitational acceleration model to determine velocity and position is at least an order of magnitude less critical with regard to the demands placed upon the computer. The requirements are less severe because the computations are performed in a stabilized frame of reference wherein all that must be followed are the low frequency variations of the position and velocity vectors.

In the following sections the functional requirements for the three computational functions (attitude computation, resolving the accelerometer data into the computational frame, and position evaluation) will be presented in reverse order as each can impose requirements on the preceding computational functions.

A. Position Computations

The basic navigation equations that must be solved to compute inertial position are equations II-3 and II-4. The selection of the coordinate system (linear, spherical, cylindrical, etc.) in which the linear equations of motion are to be integrated for position tracking, dictates the parameters to be used. This selection is not critical to the computational accuracy and is usually made on the basis of convenience. Vehicle position and velocity can be expressed in a number of stationary or rotating coordinate systems. A rotating frame may be useful in certain situations, such as orbiting satellites, to minimize computer round-off error. However, compensation for additional pseudo-specific force terms is necessary to account for the rotation of the computational frame. The center of the coordinate system is often chosen to be at the origin of the primary central force field of interest to simplify the gravity calculation. Trajectory-oriented coordinate systems are sometimes used for powered flight to facilitate implementation of the guidance laws. Selection of a coordinate system and the linear or angular position and velocity parameters which describe the motion of the vehicle's center of mass can also be made to minimize the number of executable computer instructions or program storage requirements. The effect of all these selections on accuracy is of secondary importance and poses no critical computational problems.

TABLE III-I

DEFINITION OF TERMS

<u>Truncation error</u>	-	the error introduced by the inability of a numerical integration process to follow or precisely describe the angular or linear motion of the vehicle as a function of time.
<u>Round-off error</u>	-	the error introduced by the use of a finite computer word length, hence finite precision, to process the sensor data and to perform the numerical computations.
<u>Word length</u>	-	the number of "bits" or characters used to represent a number in the computations using a binary numbering system.
<u>Computational frequency</u>	-	the number of times per second that a "set of equations" describing a complete function, such as attitude or position, is solved.
<u>Integration interval</u>	-	the magnitude or size of the increment across which the integral equations are solved each integration. If time is the independent parameter of integration, the integration interval is the reciprocal of the computational frequency for the integration process.
<u>Sensor sampling frequency</u>	-	the number of times per second that the sensor's outputs are obtained by the computer.
<u>Quantization</u>	-	the resolution or minimum value of the sensor's digital output.
<u>Sensor loop bandwidth</u>	-	the frequency of a sinusoidal input at which the amplitude of the sensor output is 71 per cent (minus 3db) of the amplitude of the input.
<u>Sensor loop phase angle</u>	-	the relative difference in phase between a sinusoidal input to a sensor and the sinusoidal output of the sensor.

Independent of the navigation or computational frame selection, either the accelerometer output data or the gravitational acceleration model, or both, must be resolved between coordinate frames. This requires knowledge of the values of the elements of a three-by-three matrix relating the accelerometer's axes to the computational frame and the elements of another three-by-three matrix relating the gravitational model to the computational frame. For any selected navigation frame, one of these matrices may be assumed to be known as a function of time (many times to reduce the computer program size it is a unit matrix) while the other is obtained using the output of the gyros, or both may be computed from a priori information and gyro outputs. In any case, the problem is identical: the gyro outputs must be used to relate the vehicle orientation to inertial space either explicitly or implicitly independent of whether or not the navigational computational frame is inertial. To simplify the presentations in the following sections, an inertial navigation frame will be assumed. The discussions of the computational functions, problem areas, requirements and characteristics of the error sources are identical for any selected computational frame.

B. Accelerometer Data Coordinate Transformation

The transformation of the accelerometer data into the inertial computational frame can be thought of functionally as the formation of the acceleration vector in inertial space. The accelerometers supply the magnitude and orientation of the acceleration vector relative to a rotating frame while the attitude of this rotating frame relative to inertial space is obtained from the gyro data after suitable processing. From this statement, two fundamental requirements evolve so as to permit the accurate measurement of acceleration in the inertial frame:

1. The time relationship of the accelerometer outputs and the inertial attitude of the accelerometer input axes (as derived from the gyros) to each other must be precisely known.
2. The output of the accelerometers should be resolved into the inertial computational frame at a frequency greater than that associated with the angular motion of the accelerometer input axes relative to inertial space.

In the following subsections, the additional requirements peculiar to the restrained and free accelerometer systems are presented.

1. Restrained Accelerometer System

The computational process for resolving restrained accelerometer outputs into the inertial frame consists of solving the following vector equation:

$$\bar{\mathbf{F}}^{\mathbf{I}}(t) = \left[\mathbf{T}_{\mathbf{S}}^{\mathbf{I}}(t) \right] \cdot \bar{\mathbf{F}}^{\mathbf{S}}(t) \quad (\text{III-1})$$

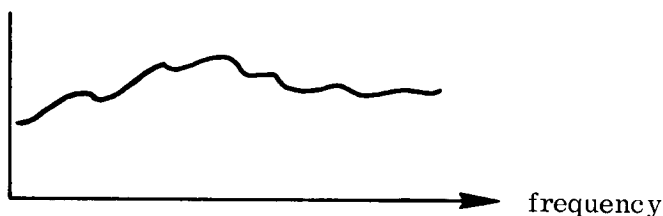
or its equivalent

$$\int \bar{F}^I(t) dt = \int \left\{ \left[\Gamma_S^I(t) \right] \cdot \bar{F}^S(t) \right\} dt \quad (\text{III-2})$$

The motion of the restrained accelerometer's input axes is caused by the angular rate applied to the vehicle and enters into the coordinate transformation process through (T_S^I) in the above equations. This angular motion can be divided into constant angular rates and accelerations, low frequency commanded rotations and limit cycles, and angular sinusoidal and random vibrations. The computational frequency or accelerometer transfer rate that must be employed is governed by the magnitude and frequency content of the angular vibration input and the system accuracy that is desired. Any angular vibration input of significant angular amplitude at frequencies beyond that of the accelerometer data transfer rate results in an angular uncertainty in the knowledge of the accelerometer's input axis and thus an improper resolution of the main thrust acceleration into the inertial computational frame. The following sketches describe this computational error.

INPUT RANDOM
ANGULAR RATE

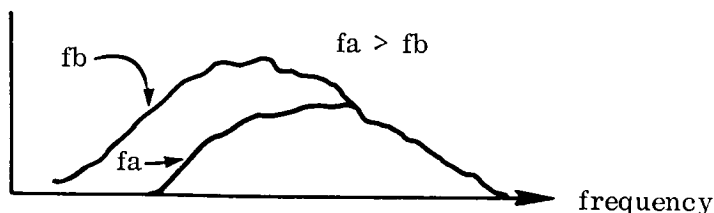
$\frac{(\text{deg/sec})^2}{\text{cps}}$



fa, fb - computational frequency

UNCERTAINTY
IN LOCATION
OF INPUT AXIS

$(\text{deg/sec})^2$



66-727

The first sketch describes the vehicle's and the accelerometer input axes' motion by an angular rate power spectral density. Assuming the existence of perfect knowledge of attitude is continuously available and sampled periodically to resolve the accelerometer data into the computational frame, a finite frequency transformation process would be able to precisely follow the angular motions of the accelerometer input axes below the transformation frequency. At angular frequencies beyond that of the data transformation process, all knowledge of angular motion would be lost; thus, the main thrust vector would be misresolved into the computational frame by an angle equal to the angular motions of the input axes at the higher frequencies. The faster the transformation process, the lower the input axis uncertainty. This is demonstrated in the second sketch wherein f_a denotes a transformation process carried out at a frequency faster than the transformation process implemented at frequency f_b .

Another error that arises for restrained accelerometer mechanizations occurs because they are actually "velocity meters" which yield the integral of specific force in the rotating vehicle frame. What is desired is specific force itself (equation III-1) or its integral (equation III-2) in an inertial frame. It is required that the accelerometer outputs be differentiated in the rotating frame to obtain specific force and that the computed specific force be resolved into the inertial frame and then reintegrated. Methods of differentiating and reintegrating the accelerometer outputs to obtain different degrees of accuracy based upon polynomial fitting are presented in Appendix B.

A common example of the error associated with this problem is termed size effect. Integrating accelerometers when subjected to an angular rotation about any point that is not coincident with the center of the sensing element, will measure and integrate the tangential and centrifugal acceleration induced by the magnitude of the angular rotation and the moment arm between the axis of rotation and the sensor package. As they are instruments integrating in a rotating frame, the sum of their output in the vehicle frame indicates a net linear velocity at the end of each cycle of the angular motion due to the unchanging sign of the centrifugal acceleration. The error can be minimized and made practically negligible by resolving the accelerometer outputs into and then integrating them in the inertial computational frame at a frequency higher than that of the angular motion. Increased accuracy is also achieved by using higher order techniques (presented in Appendix B) to differentiate and reintegrate the accelerometer outputs as described above.

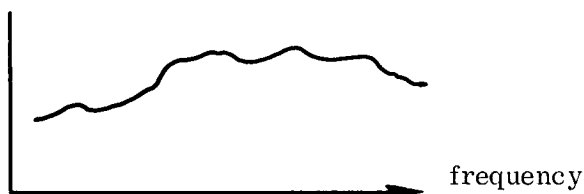
2. Free Accelerometer Systems

Free accelerometers are simply free gyros with an unbalanced pendulous mass along the spin axis. Subjecting such a sensor to a linear acceleration causes the spin axis to precess relative to inertial space. The equations describing the

angular motion of the spin axis are presented in Table III-II. The precession rate is proportional to the magnitude of specific force; the angle through which the spin axis precesses is proportional to the integral of specific force. The computational process for measuring specific force in the inertial frame consists of determining the orientation of the spin axes of two free accelerometers relative to the vehicle and resolving these measurements into the inertial computational frame using the vehicle attitude computed from gyro data. The time differential of the orientation of the spin axes relative to inertial space can be used in conjunction with the kinematic equations presented in Table III-II to obtain specific force as a function of time. The integration of specific force in the inertial frame can then be performed to obtain velocity. The coefficient matrix appearing in front of the time derivative of the spin axes orientation vector simply describes the orientation of the input axes relative to inertial space as a function of time and thus performs the same functional task as does the attitude matrix in equations III-1 and III-2 for restrained accelerometers.

The applied acceleration during thrusting phases of flight that causes precession of the spin axes can be divided into a constant thrust component and linear random and sinusoidal vibrations. The computational frequency or accelerometer transfer rate is governed by the magnitude and frequency content of the linear vibrations; the constant thrust component of acceleration causes a very smooth and easily followed precession rate. Any significant linear vibration at frequencies beyond that of the accelerometer data transfer rate results in an angular uncertainty in the knowledge of the accelerometers' input axis and an improper resolution of the main thrust acceleration into the inertial computational frame. The following sketches describe this computational error.

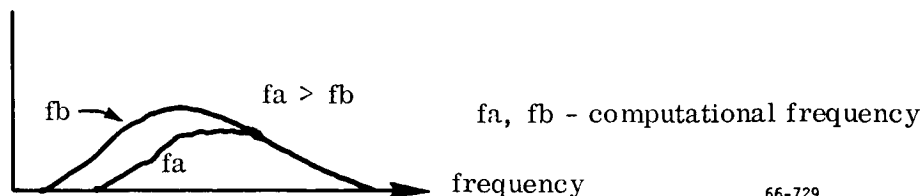
INPUT RANDOM
LINEAR
ACCELERATION
(g^2/cps)



SENSOR
SPIN & INPUT
AXIS MOTION
(deg^2/cps)



UNCERTAINTY
IN LOCATION
OF INPUT AXIS
(deg^2/cps)



66-729

TABLE III-II

FREE PENDULOUS GYRO ACCELEROMETER
COORDINATE TRANSFORMATION PROCESS

EQUATION OF MOTION FOR SPIN AXIS IN INERTIAL SPACE

$$\frac{d\bar{a}^I}{dt} = \frac{\bar{P}}{H} (\bar{a}^I \times \bar{F}^I)$$

$$\frac{d\bar{b}^I}{dt} = \frac{\bar{P}}{H} (\bar{b}^I \times \bar{F}^I)$$

\bar{P} - PENDULOUS MOMENT
 H - ANGULAR MOMENTUM
 \bar{F} - SPECIFIC FORCE
 \bar{a}, \bar{b} - SPIN AXIS UNIT VECTORS

SPECIFIC FORCE SOLUTION

- ATTITUDE COMPUTATIONS YIELDS $\left[T_b^I(t) \right]$
- FPGA OUTPUTS YIELDS $\left. \begin{matrix} \bar{a}^I(t), \bar{b}^I(t) \\ \bar{a}^I(t), \bar{b}^I(t) \end{matrix} \right\}$
- $\left[\begin{matrix} F_\ell \\ F_m \\ F_n \end{matrix} \right] (t) = \frac{\bar{P}}{H} \bullet \left[\begin{matrix} O & -an & am \\ an & O & -a\ell \\ -am & a\ell & O \\ O & -bn & bm \\ bn & O & -b\ell \\ -bm & b\ell & O \end{matrix} \right]^{-1} (t) \bullet \frac{d}{dt} \left[\begin{matrix} a\ell \\ am \\ an \\ b\ell \\ bm \\ bn \end{matrix} \right]$

- YIELDS SPECIFIC FORCE IN THE INERTIAL FRAME

The first sketch describes an input random linear acceleration, defined in terms of a power spectral density, that will cause the free accelerometer's spin axis to precess through the random angular motions whose amplitude is described by a power spectral density as a function of frequency in the second sketch. In exactly an identical manner as described for the restrained accelerometers, angular motions at frequencies beyond the frequency with which the accelerometer data is transformed into the computational frame will cause a computational error. The computational error is the misresolving of the main thrust vector into the computational frame with an angular error equal to the amplitude of the motion at frequencies faster than the accelerometer data transfer frequency. The third sketch describes this angular error for two different data transfer motion frequencies, f_a and f_b , where f_a is greater than f_b . There is also a computational error in following the precession of the spin axis caused by linear vibratory accelerations whose frequencies are below that of the computational frequency. The error is a function of the accuracy with which the orientation of the spin axes are differentiated and then reintegrated in the kinematic equations of Table III-II. Just as in the case of restrained accelerometers, high order, hence more accurate schemes for differentiating and reintegrating these equations can be devised.

The final computational error associated with the free accelerometer system is due to the measurement uncertainty (quantization or resolution) of its body mounted readout system. This resolution error contributes to both an uncertainty in the orientation of the spin axis and also to an uncertainty in the determination of specific force by the time differential of the spin axis orientation relative to inertial space.

C. Attitude Computations

The consideration of the accelerometer coordinate transformation requirements has already placed certain requirements upon the attitude computations during thrusting phases of flight. First, vehicle attitude must be computed and used to resolve the accelerometer data into the computational frame at a frequency that is compatible with the angular motion of the accelerometer input axis and the desired system accuracy. Secondly, the quantization or resolution level of the attitude sensors must be small and preserved by the attitude computations in order to minimize the uncertainty in knowledge of the orientation of the accelerometer input axes relative to inertial space. In the following subsections, the additional requirements peculiar to the free and restrained gyros are discussed.

1. Free Gyro System

The free gyro serves as an inertial reference by providing a physical reference (an angular momentum vector) stabilized with respect to inertial space. Attitude of the vehicle relative to the angular momentum vector is computed by

inscribing a pattern on the sphere, e.g., a great circle, such that the timing of a series of lines crossing under an optical pickoff fixed to the vehicle defines the angle between the spin axis and the pickoff axis. By using a minimum of two pickoffs the attitude of the spin axis relative to the vehicle can be computed. Two free gyros whose spin axes are nonparallel are sufficient to define an inertial reference. A typical computational process is presented in Table III-III. This process requires the solution of transcendental equations, square roots, the product of matrices and a matrix inversion. The computational error associated with this process is the error in approximating the transcendental functions, the accuracy of the square root scheme, and the round-off error in executing these processes. None of these items are a severe limitation to the accuracy of the required transformation matrix because the computational error is not cumulative over the duration of the flight; the computational error in forming the transformation matrix each computational cycle produces an error equivalent to an uncertainty of the orientation of the accelerometer input axes.

2. Restrained Gyro System

The computational process for determining attitude by using restrained gyros requires the numerical integration of the angular rate equations (equation II-1), which use the outputs of gyros which are the integral of the components of angular rate. The computational error associated with any numerical integration process is naturally cumulative. The numerical integration process must be properly designed so as to limit the magnitude of the error to an acceptable level over the duration of the flight. The degree or order of the numerical integration process, the size of the integration step and the computer word length used to implement the procedure must be selected such that the attitude of the vehicle can be computed to the desired degree of accuracy at any point within the mission. Higher order integration schemes, small integration step sizes and longer word lengths are known to yield greater accuracy.

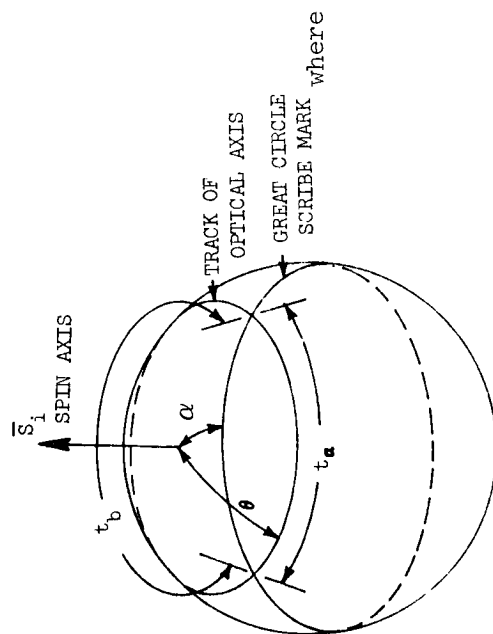
The angular motion that must be followed by the attitude computations is that "passed" by gyros that are characterized by a finite bandwidth. Any significant motion of the vehicle that is not followed or "passed" to the computer by the gyros is classified as a sensor error. Figure III-1 depicts this distinction between the angular motion input to the computer and the sensor error due to finite bandwidth. The largest integration step size permitted is set by the tolerable computational error encountered in either the integration of the angular rate equations or in the computational frequency requirements of the accelerometer data coordinate transformation process previously discussed in Section III B.

One area of extreme importance in the design of the numerical attitude computational process that must be considered when using restrained gyros is the

TABLE III-III

TYPICAL ATTITUDE MATRIX COMPUTATIONAL PROCESS FOR FREE GYROS

Sensor Output: t_{aj} and t_{bj} ; j = optical pickoff, a minimum of 2 are required
 t_a & t_b are time intervals between line crossing under optical pickoff (two crossing per 2π rotation of rotor)



READOUT GEOMETRY

Gyro Data Processing:

$$\cos \theta_j = \sin \beta_j / \sqrt{\sin^2 \beta_j + \tan^2 \alpha}$$

$$\beta_j = \frac{\pi}{2} \left(\frac{t_{aj} - t_{bj}}{t_{aj} + t_{bj}} \right) \quad t_a > t_b$$

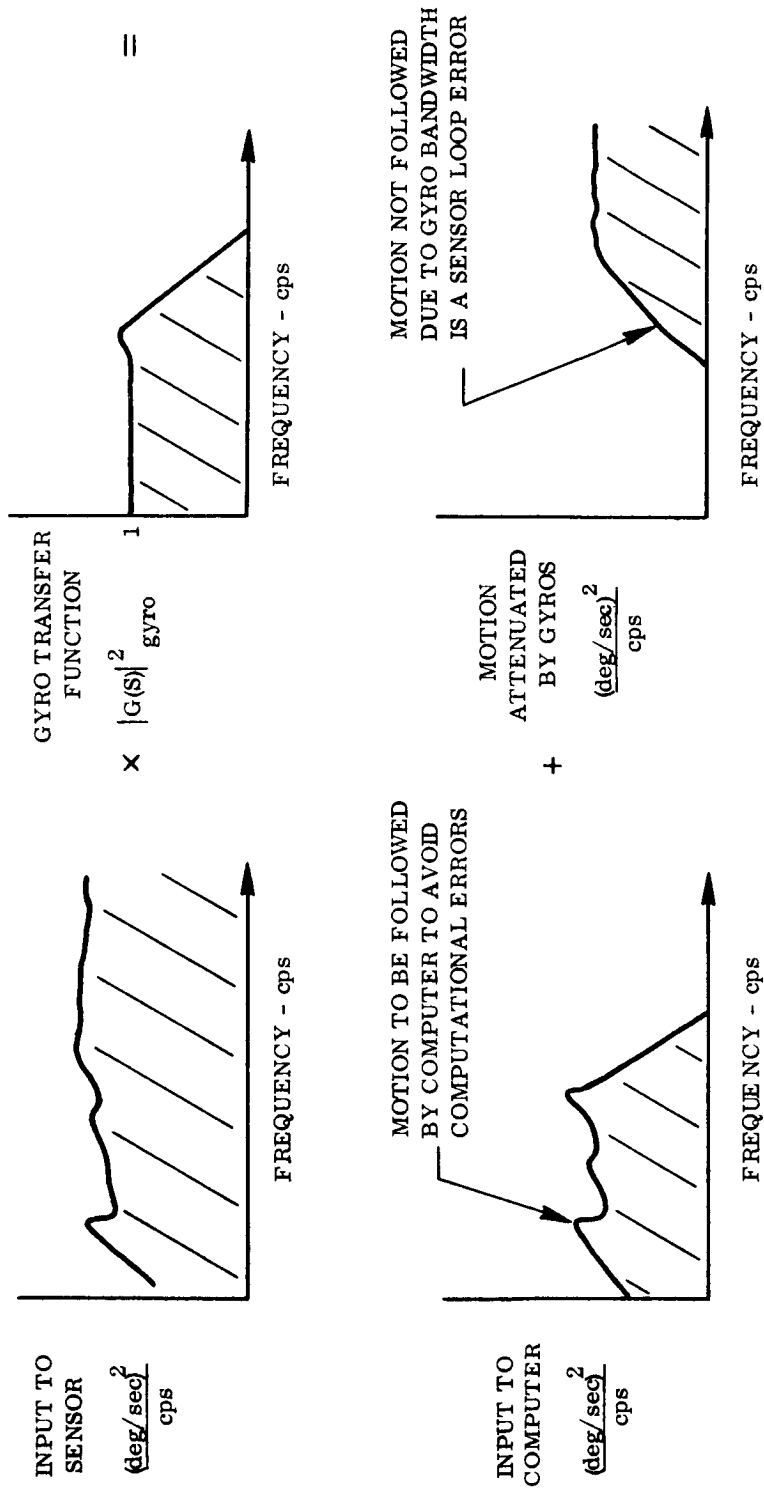
$$\begin{matrix} \text{body} \\ \overline{S}_i(t) = [T_{\text{Optical axes}}^{\text{body}}] \cdot \begin{bmatrix} \cos \theta_j = 1 \\ \cos \theta_j = 2 \\ \cos \theta_j = 3 \end{bmatrix} (t) \end{matrix} \quad ; \quad i = 1^{\text{st}} \text{ or } 2^{\text{nd}} \text{ gyro}$$

Attitude Matrix Computations:

$[T_{\text{sensor spin vector coordinate system}}^{\text{body}}(t)]$

$$= [\overline{S}_{i=1}^b(t), \overline{S}_{i=2}^b(t), \overline{S}_{i=1}^b \times \overline{S}_{i=2}^b]$$

$$[T_{\text{body}}^{\text{inertial}}(t)] = [T_{\text{spin vector}}^{\text{I}}(t=0)] \cdot [T_{\text{spin vectors}}^{\text{b}}(t)]^{-1}$$



64-726

Figure III-1 Restrained Gyro and Attitude Computer Bandwidth Relationship

initial apparent incompatibility between the gyro outputs, the integral of angular rate, and the knowledge of angular rate that is required by the numerical integration process (equation II-1). In order to form a proper interface between the sensors and the integration process, it is necessary (in a restrained gyro system) to extract estimates of angular rate from the integral of angular rate. This extraction of the component of the vehicle rate vector sensed by each gyro must be performed with an accuracy compatible with the accuracy of the intended numerical integration scheme; otherwise, the accuracy of the solution of the angular equations of motion will be limited to the accuracy of the scheme by which rate is extracted from its integral; the lower truncation errors of a higher order integration scheme will not be obtained.

A method for extracting accurate estimates of angular rate consists of: (1) using a number of successive gyro samples within an integration interval to evaluate the coefficients of a polynomial expanded in time that describes the integral of rate components from each gyro, and (2) differentiating the polynomial to obtain angular rate as a function of time over the integration interval. Examples of different rate extraction schemes are presented in Appendix B.

In order to realize the accuracy benefits of high order integration schemes with their lower truncation errors, it is necessary that the error introduced in the integration process by the quantization of the gyro outputs be smaller than the truncation error. The error introduced by quantization is an uncertainty in knowledge of the magnitude of the angular rotation (by the computer) at any instant of time. The largest possible error is equal to the least significant bit of the sampled gyro digital output. This uncertainty is not cumulative with time as the portion of the motion that is less than the quantization level is stored mechanically by the gyro on its output axis, and it becomes the initial conditions for the gyro's integration of rate over the next sampling period. Therefore, the effect of sensor loop quantization is to "phase" or time shift a small portion of the total angular motion. This error is independent of the order of the integration scheme and therefore does not preclude the use of integration schemes higher than rectangular or second order as is often cited in the literature (References 5 through 10). In the implementation of a restrained gyro mechanization the quantization level may be so large as to dominate the truncation error of even a rectangular integration scheme such that the use of higher order schemes are not warranted.

D. Summary of Parameters Affecting Computational Accuracy

The functional analysis presented in the previous section introduced the many parameters that are involved in the design and analysis of the strapdown computational process. The origin of these parameters are the flight environment, the inertial sensors, the computer in which the computational process is implemented

and finally the computational process itself. Table III-IV summarizes these parameters. In order to be able to design or analyze strapdown computational processes and to develop direct and economical techniques for controlling the magnitude of computational error, it is necessary that precise analytic models of the computational errors as a function of all these parameters be available. The analytical models of the computational errors have been derived and are presented and discussed in Section IV.

TABLE III-IV

PARAMETERS AFFECTING STRAPDOWN COMPUTATIONAL ACCURACY

•	Vehicle Angular & Linear Motion
	Amplitude
	Frequency
	Phase
•	Sensor Loop Characteristics
	Bandwidth
	Data Rate
	Quantization
•	Computer Hardware
	Word Length
	Speed
•	Computational Algorithms
	Sensor Data Processing or Filtering [*]
	Order of Numerical Integration Schemes
	Order of Transcendental Approximations
	Frequency of Solution

* Extraction of angular rate or specific force from their respective integrals provided by the inertial sensors

IV. COMPUTATIONAL ERROR ANALYSIS

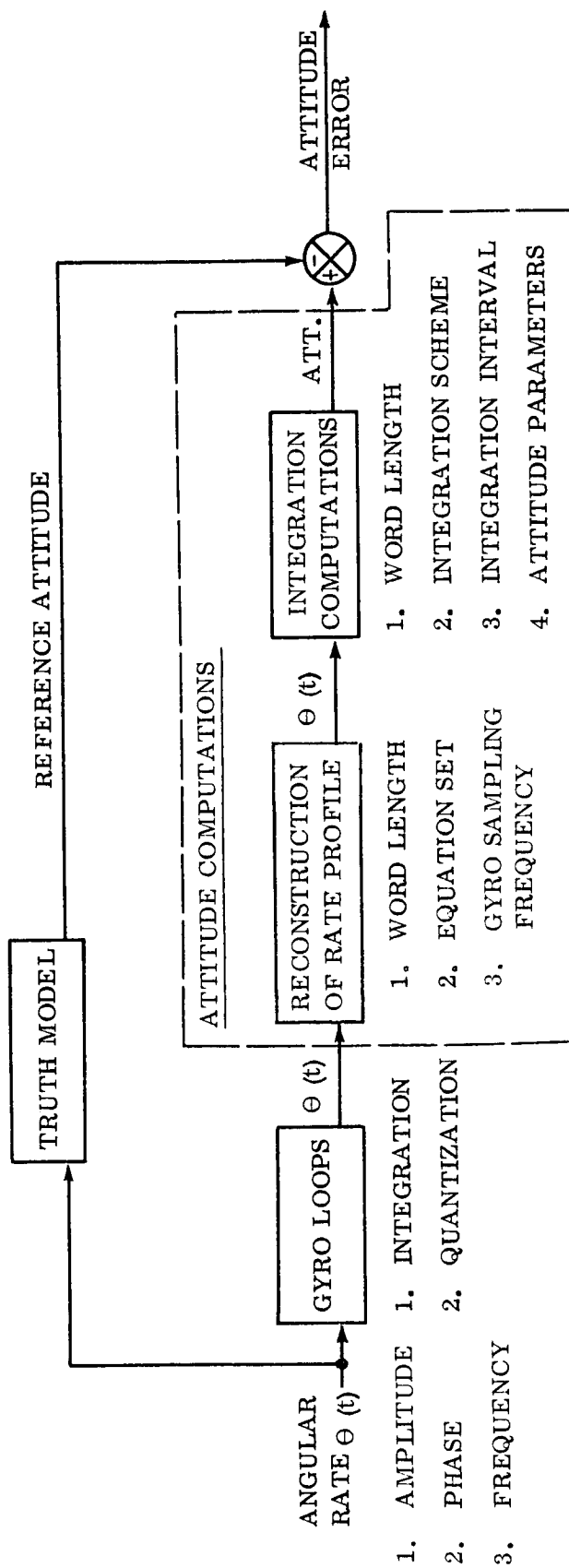
For the design or analysis of strapdown computational processes and to develop techniques for controlling the magnitude of the computational error, it is necessary that analytic models of the computational errors be available. This section summarizes the characteristics of the strapdown error sources and presents the analytic models for each of these errors. These error models immediately imply techniques that can be used to control the magnitude of the computational error. The analytic models were established through the use of large scale digital simulations of inertial sensor loops, airborne digital computers and computational algorithms in a scientific ground computer. An example of the digital simulation program including the programmable variables for analyzing the restrained gyro attitude computational errors is presented in Figure IV-1. With these analytic error models now available, the error models rather than the detailed simulation programs can be used to analyze computational processes or conversely to arrive at a design for any given application. These error models can be formulated and applied in an open loop error analysis technique similar to the technique used throughout industry to evaluate the navigational errors caused by inertial sensors; a rapid method for performing the computational error analysis would then be available for use in system studies and design trade-offs as shown in Figure IV-2.

In the requirements discussion in the preceding section, free gyros were not associated with free accelerometers nor restrained gyros with restrained accelerometers. It is quite reasonable to entertain from the computational viewpoint, the mixture of free and restrained sensors depending upon the mission. Further, it is not necessary to force such a relationship in order to analyze the computational errors. The only tie between the gyros and accelerometers is the speed and accuracy with which the accelerometer data must be resolved from the vehicle frame into the inertial frame; the type of gyro attitude reference is not important. Therefore, in the remainder of this section the computational errors associated with gyros and accelerometers will be summarized separately as will be the computational errors of free and restrained sensors. All the parameters listed in Table III-IV are analyzed and discussed. Further discussions of the errors and their characteristics are presented in the appendices.

A. Restrained Gyro Attitude Reference System

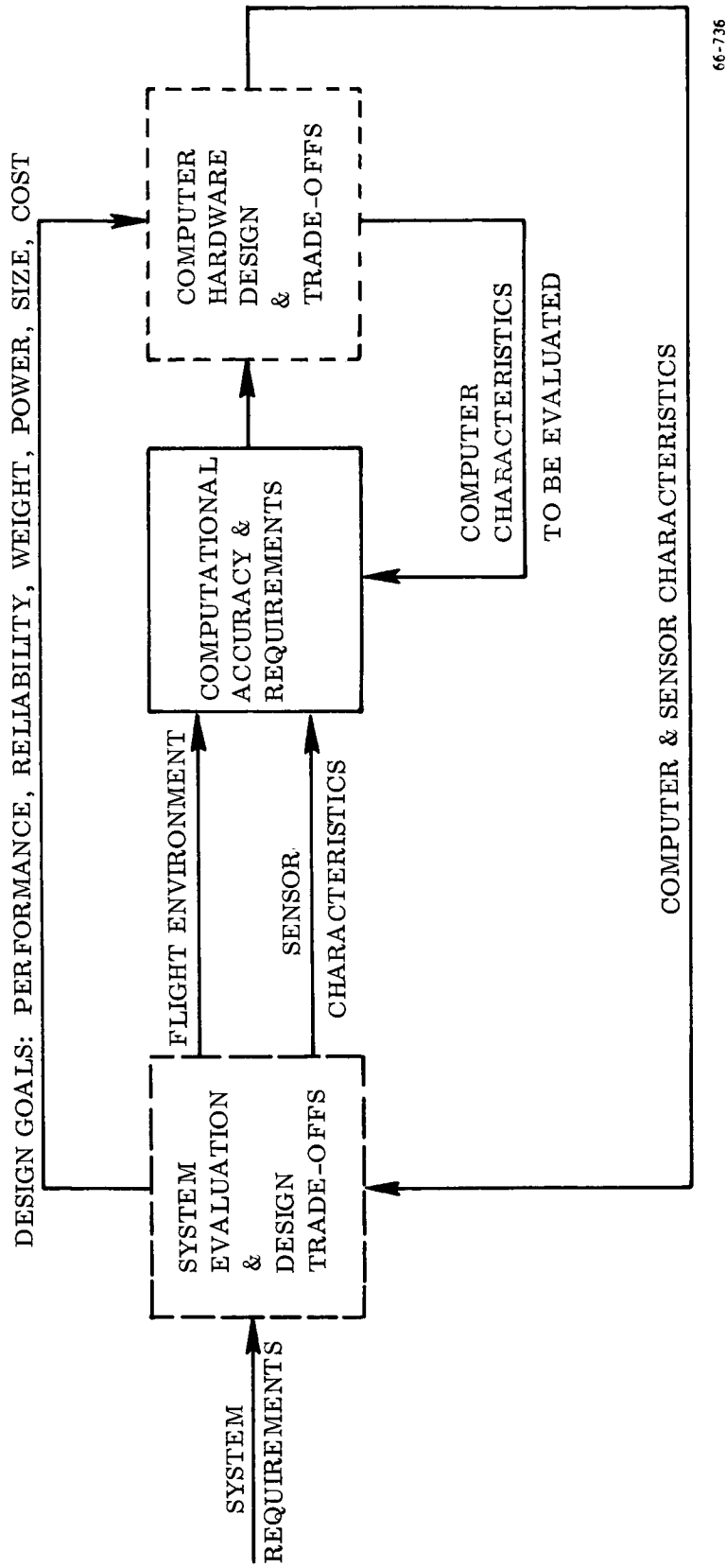
The computational process for determining vehicle attitude from the output of restrained gyros requires the numerical integration of a set of differential equations. The error in this numerical integration process is unbounded, the magnitude of the attitude error increases with time.

The first fundamental result of the digital simulation studies performed is that the attitude error due to the computational process can be described by a single parameter, which is termed the norm. The norm parameter is the root-sum-square of either the error in each element of the transformation matrix between the true inertial frame and the computational inertial frame or the error in each of the three



66-1635

Figure IV-1 Computer Error Analysis Digital Program for Restrained Gyro Attitude Computations



66-736

Figure IV -2 Computational Process Design Procedure

Euler angles that describe the orientation of the computational inertial frame relative to the true inertial frame (Appendix D). The error in orientation between the computational inertial frame and the true inertial frame is obtained by subtracting the strapdown computer vehicle attitude relative to the computational inertial frame from the true vehicle attitude relative to the true inertial frame.

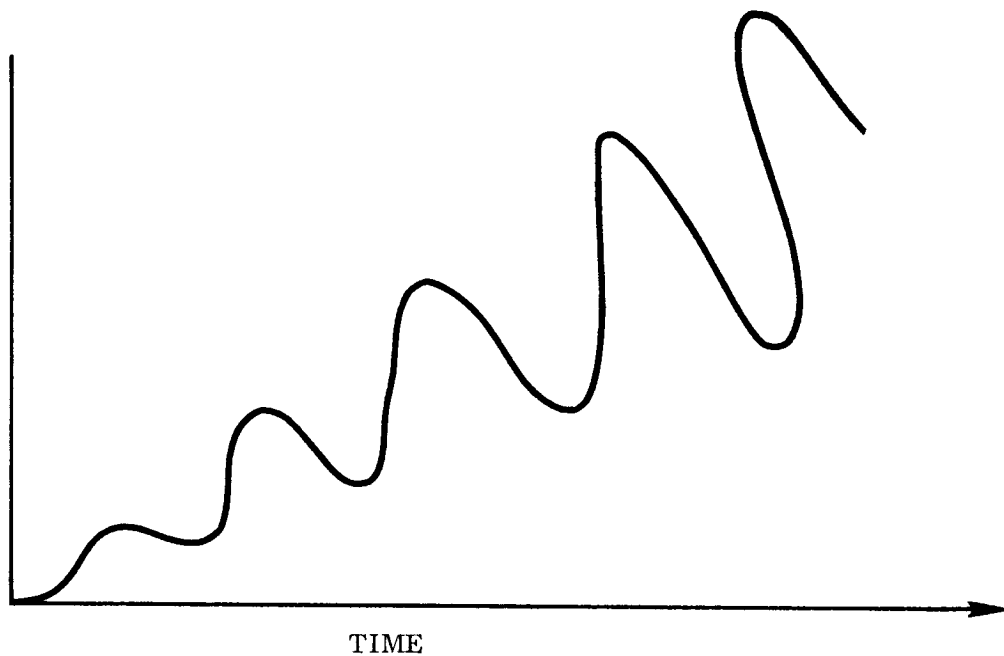
For any input motion and computer characteristics, the error in an element of the direction cosine matrix between the vehicle and inertial space can be described by a ramp plus a sinusoidal oscillation whose amplitude increases as a linear function of time. The frequency of the sinusoidal component of the error is the same as the input motion frequency. This behavior of the error with time is shown in Figure IV-3. Also shown in this figure is the behavior of the norm with time. After an initial transient, the norm of the attitude error matrix is seen to be a linear function increasing with time. A single parameter that describes the norm is therefore its rate of change with time which can be expressed in units of degrees per hour. Analyses have shown that its magnitude and behavior are independent of the orientation of the axis of rotation relative to the gyro input axes and the orientation of the gyros relative to the computational coordinate system.

The second fundamental result of these studies is that there are four regions of computational error that have been termed due to their origin: (1) round-off, (2) quantization, (3) truncation and (4) bandwidth limited. The functional characteristics of each of these regions and their relationship to each other are shown in Figure IV-4. In this figure, the computational error is plotted versus the ratio of angular motion frequency to computer integration frequency on a log-log plot.

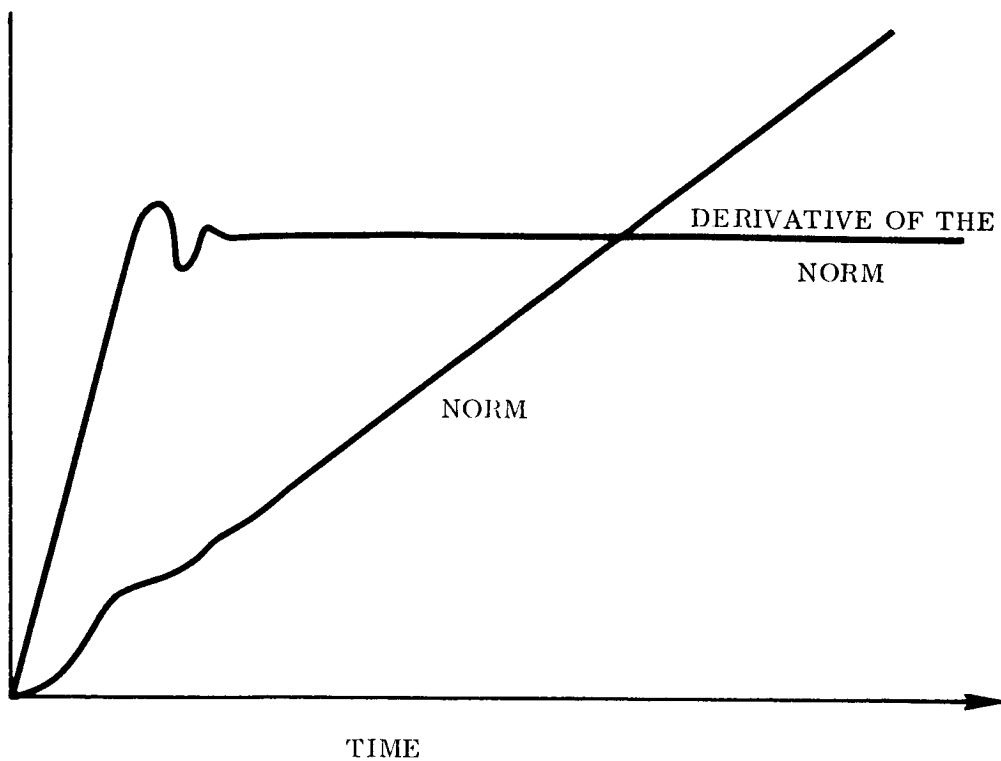
For the case when the frequency of integration is lower than the angular motion that the computer is attempting to follow, the computer is operating in the bandwidth limited region on the extreme righthand side of the curve in Figure IV-4. The error in this region is independent of all computational and computer characteristics. As the computer integration frequency is increased relative to the angular motion frequency, the computational error enters the truncation region.

In the truncation region, the computational error is a function of both the order of the integration scheme (coupled with a rate extraction scheme of suitable accuracy) and the ratio of the angular motion frequency to the integration frequency. Increased integration frequency results in a lower computational error. Increasing the order of the numerical integration scheme also reduces the computational truncation error by increasing the slope of the truncation line, pivoting the line about its point of intersection with the bandwidth limited region. The slope of the truncation line (n) in this figure is equal to the order of the employed integration scheme; e. g., for a fourth order scheme, the slope is 4; for rectangular integration scheme, the slope is unity. As the integration frequency is further increased, the computational error enters the region dominated by the quantization level (pulse weight) of the gyro loop.

TYPICAL ELEMENT
OF THE
ATTITUDE ERROR
MATRIX

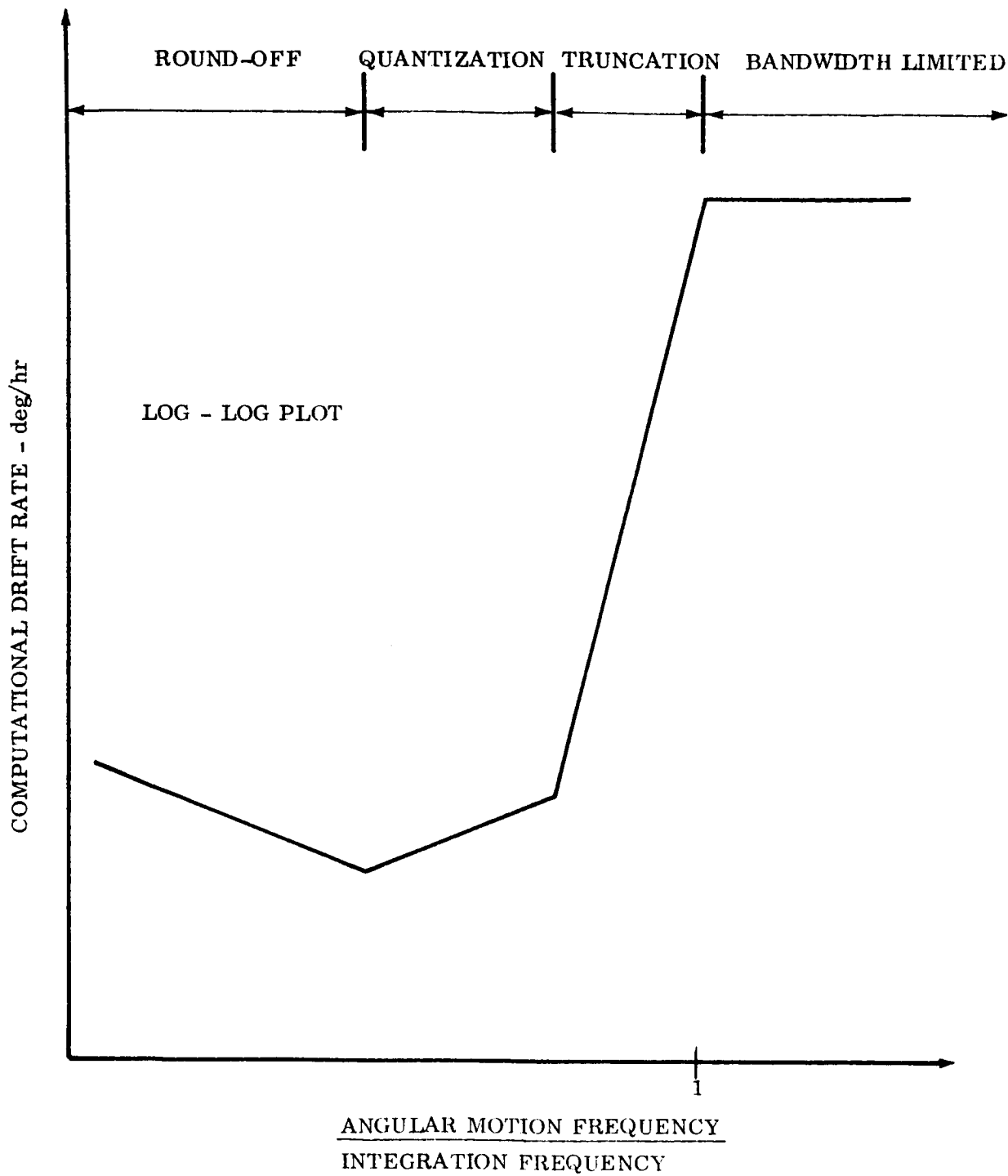


THE NORM OF
THE
ATTITUDE ERROR
MATRIX
&
ITS DERIVATIVE



66-723

Figure IV-3 Characteristics of the Attitude Error Matrix Truncation Error
for Restrained Gyros



66-2218

Figure IV-4 Regions of Error for Restrained Gyro Attitude Computations

In this quantization region, the computational error is a function of the sensor quantization level and the ratio of angular motion frequency to integration frequency. The error is independent of the order of the integration scheme. The slope of the quantization error line relative to the frequency ratio is unity; the magnitude of the quantization error at any frequency ratio is proportional to the square of the sensor quantization level.

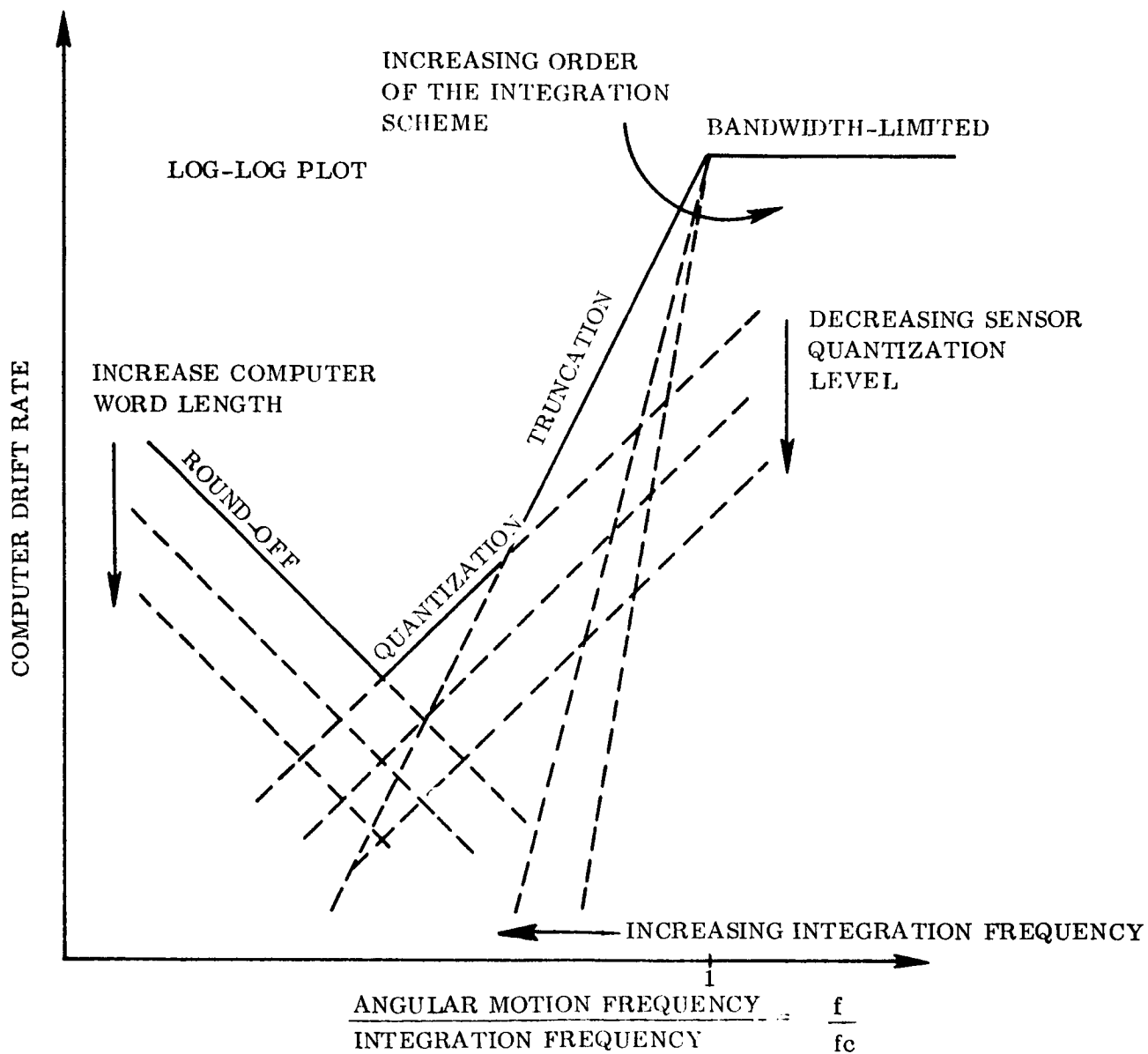
As the integration frequency is increased relative to the frequency of the angular motion, the computational error enters the fourth region round-off. In this region, the computational error is inversely proportional to both the computational integration frequency (a slope of minus one) and the computer word length (the addition of another bit to the computer word length decreases the round-off error by a factor of two).

Figure IV-5 summarizes the four parameters by which the magnitude of the computational error can be controlled: word length, sensor quantization, integration scheme and integration interval. Because the error and the means by which the magnitude can be controlled are independent of each other, all four portions of the error curve versus vehicle angular motion for a particular application can be designed as required and the total curve shaped during the design to obtain the desired computational performance. There are no fundamental limitations that place any accuracy restriction on the computational process; accuracy can only be limited by the state-of-the-art of hardware capability.

In the following subsections, the detailed analytic models of the computational errors are presented for both discrete and random motions. In addition, three error sources are discussed which are associated with a triad of gyros that must be analyzed on a system basis (three sensors plus the computational process). They yield an attitude error even for a perfect computational process because of the computer's processing of erroneous sensor data. The errors considered are: gyro output axis acceleration sensitivity, unmatched gyro loop frequency response and the finite bandwidth of the gyro loop.

1. Discrete Motions

Three self-starting numerical integration schemes of different order accuracy were considered in the analyses directed towards establishment of the characteristics of the computational errors for a restrained gyro attitude system: rectangular, 2nd order Runge-Kutta and 4th order Runge-Kutta. Appendix B presents the numerical difference process for each of these schemes. A first order accurate extraction of rate from the gyro outputs is employed with the first and second order schemes; a second order extraction process presented in Appendix B is used with the fourth order scheme.



06-2219

Figure IV-5 Control of Computational Error